PhD THESIS

Myeloperoxidase-Mediated Alterations of Plasmalogen Homeostasis Induce Blood-Brain Barrier Dysfunction

submitted by

Mag. rer. nat. Andreas Üllen

to obtain the academic degree of

Doctor of Philosophy (Ph.D.)

at the

Medical University of Graz

Institute of Molecular Biology and Biochemistry

under Supervision of Ao.Prof. Dr. Wolfgang Sattler

2011

I. ACKNOWLEDGEMENTS 9

II. ABBREVIATIONS 10

III. ABSTRACT 15

IV. ZUSAMMENFASSUNG 16

V. INTRODUCTION 18

1. The Central Nervous System (CNS) 18

2. The Brain is a Well-Vascularized Structure 19

2.1. Blood Supply to the Brain 20

2.2. Venous Drainage of Cerebral Blood 20

3. Blood-Brain Barrier (BBB) – Multiple Gatekeepers of the CNS 22

3.1. The Architecture of Brain Barriers 23

3.2. The Neurovascular Unit 25

3.2.1. Brain Microvascular Endothelial Cells (BMVEC) - The Anatomic Base of the BBB 25

3.2.2. Astrocytes - Inductors of BBB Integrity 30

3.2.3. Pericytes - Not only a Regulator of Capillary Blood Flow 31

3.2.4. Neurons - Neurovascular Coupling 32

3.2.5. Microglia - Intrinsic Immune Sensors and Effectors 33

4. Blood-Brain Barrier Breakdown – The Vicious Cycle of Neurodegeneration 36

4.1. Neuroinflammation: From Immune Privilege to Neurodegeneration 36

4.2. What are the Triggers of Neuroinflammation? 37

4.3. Neuroinflammation – The Threshold Determines the Outcome 38

4.4. BBB-Dysfunction – Cause, Contributor or Consequence of Neurodegeneration? 39

4.4.1. BBB - Offender of Neuroinflammation 39

4.4.2. BBB - Deterioration of Neuroinflammation 40

4.4.3. BBB - Victim of Neuroinflammation 44

5. Myeloperoxidase (MPO) - Friend and Foe 46

5.1. Phagocytes - Mechanisms of Host-Defense and Tissue-Destruction 46

5.2. Oxidative stress - Multiple Sources for a Variety of Species 47

5.2.1. H_2O_2 - Essential Precursor for the MPO System 48

5.2.2. The MPO-H_2O_2-Halide System - Source of Highly Destructive Oxidants 50

5.3. HOCl-Attack of Biomolecules - Profound Potential to Damage Host Tissue 52

5.3.1. Proteins: Preferred Targets for HOCl-Modification 53
5.3.2. Chlorinated Lipids: Appearance During Neuroinflammation? 54
6. The Crucial Role of Lipids in the CNS **56**
6.1. Plasmalogens - Important Lipids for CNS Function 57
6.2. α-Chloro Fatty Aldehydes - Plasmalogens under HOCl Attack 59

VI. MATERIALS AND METHODS **62**

Materials ***62***

1. Animals Experiments **62**
2. Cell Culture Materials **62**
3. Chemical Synthesis, Derivatization and Standards **62**
4. *In Vitro* Experiments **63**
5. Protein analysis **63**
6. RNA Analysis **65**
7. Buffers **65**

Methods ***67***

1. PREPARATION OF 2-ClHDA, 2-ClHpA AND REAGENT NaOCl **67**
1.1. Synthesis of 2-ClHDA 67
1.2. Synthesis of 2-Chloroheptanal (2-ClHpA) 67
1.3. Determination of NaOCl-Concentration 67
2. IN VITRO BBB MODEL **68**
2.1. Brain Microvascular Endothelial Cells (BMVEC) 68
2.1.1. Isolation and Establishment of Primary Cultures 68
2.1.2. Cultivation of Cells 68
2.1.3. Cell Experiments 69
2.1.4. Counting of BMVEC 69
2.2. Model for In Vitro BBB Function: Electrical Cell-Substrate Impedance Sensing (ECIS) 70
2.3. Analysis of Barrier Architecture: Immunofluorescence of BMVEC 71
2.3.1. Double-Labeling of ZO-1 and VE-cadherin 71
2.3.2. Double-Labeling of F-Actin Cytoskeleton and Nuclei 71
3. PREPARATION OF HUMAN POLYMORPHONUCLEAR LEUKOCYTES **72**
4. ANIMAL MODELS **72**
4.1. Model for In Vivo Neuroinflammation 72
4.1.1. qPCR (performed by S. Waltl) 73

4.1.2. Measurement of MPO Mass in Murine Brain Homogenates 73
4.1.3. Immunohistochemistry and Triple Immunofluorescence in Murine Brain Cryosections 73
4.2. Model for In Vivo BBB Function: In Situ Brain Perfusion 74
5. MODIFICATION EXPERIMENTS 76
5.1. Sn-2-Lyso-Plasmalogen with NaOCl 76
5.2. Murine Brain Lipid Extracts with NaOCl 76
5.3. Cerebrovascular Endothelial Cells 77
5.3.1. NaOCl 77
5.3.2. MPO–H_2O_2–Chloride System 77
5.4. Phloretin 78
5.4.1. NaOCl 78
5.4.2. 2-ClHpA 78
6. IN VITRO ASSAYS 79
6.1. MTT-Test 79
6.2. JC-1 Assay 80
6.3. Measurement of ROS 81
7. DETERMINATION OF 2-ClHDA STABILITY AND METABOLISM 82
7.1. Stability in the Presence of a Mixed Primary Mouse Brain Cell Suspension 82
7.2. Stability in Human Plasma 82
7.3. Stability in Murine Vasculature 83
7.4. Stability in BMVEC Culture 83
7.5. Metabolism of 2-ClHDA by BMVEC 83
7.6. Quantification of 2-ClHA Re-Esterification into the Polar Lipid Fraction 84
8. ANALYTICAL TECHNIQUES 85
8.1. Fourier Transform-Ion Cyclotron Resonance-Mass Spectrometry (FT-ICR-MS) 85
8.2. Synthesis of Stable-Isotope Labeled 2-ClHDA 85
8.3. Pre-Separation of Brain Lipid Extracts by Thin Layer Chromatography 87
8.4. Derivatization 87
8.4.1. Chlorinated- and Non-Chlorinated Fatty Aldehydes 87
8.4.2. Chlorinated Fatty Acids 88
8.4.3. Chlorinated Fatty Alcohols 88
8.4.1. Phloretin 88
8.5. Electron Impact-Gas Chromatography-Mass Spectrometry (EI-GC-MS) 88
8.6. Negative Ion Chemical Ionization-Gas Chromatography-Mass Spectrometry (NICI-GC-MS) 89
8.7. Sodium Dodecylsulfate Polyacrylamide Gel Electrophoresis (SDS-PAGE) and Immunoblotting 90

8. STATISTICAL ANALYSES 90

VI. RESULTS 91

CHAPTER 1 NEUROINFLAMMATION - THE ROLE OF CHLORINATIVE STRESS IN PLASMALOGEN DEFICIENCY ***91***

1. Mouse Brain Plasmalogens are Preferential Lipid Targets for HOCl Modification: *In vitro* evidence **94**

1.1. Phospholipid Composition of Mouse Brain Lipids 94

1.2. Mouse Brain Plasmalogens are the Preferred Lipid Targets for HOCl-Modification 96

2. The Vinyl-Ether Linkage of Plasmalogens is Susceptible to HOCl: Release of alpha-Chloro Fatty Aldehydes **98**

2.1. Plasmalogens Bear a Masked Aldehyde: Vinyl-Ether Linkage between the sn-1 Aliphatic Chain and the Glycerol Backbone 98

2.2. Synthesis of 2-ClHDA and 2-Cl[$^{13}C_8$]HDA 101

2.3. HOCl-Modification of Mouse Brain Plasmalogens Provoke the Formation of alpha-Chloro Fatty Aldehydes and Remnant Lysophospholipids 104

3. Neuroinflammation is Accompanied by Altered Brain Plasmalogen Levels and α-Chloro Fatty Aldehyde Formation **106**

3.1. Systemic LPS Induces Inflammation in Brain Tissue 106

3.2. Brain Plasmalogen Homeostasis is Impaired upon Inflammation 107

3.3. Oxidative Modification of Brain Tissue Plasmalogens 109

3.4. Stability of α-Chloro Fatty Aldehydes in Brain Tissue 112

CHAPTER 2 ALPHA-CHLORO FATTY ALDEHYDES INDUCE BLOOD-BRAIN BARRIER DYSFUNCTION ***113***

1. Neuroinflammation – What happens at the BBB? **116**

1.1. Accumulation of MPO at the Cerebrovasculature 116

1.2. Cerebral Vessels are Attacked by Reactive Intermediates 119

1.3. Activation of Neutrophils Impacts on Barrier Function of BMVEC 120

1.4. Neutrophil-dependent Barrier Dysfunction: Impact of the MPO-H_2O_2-Cl^- System? 121

1.5. BMVEC Contain an Endogenous Pool of Plasmalogens 122

1.6. Endogenous Plasmalogen Pool is Targeted by HOCl 123

1.7. Vascular Stability of α-Chloro Fatty Aldehydes 124

2. Metabolism of α-Chloro Fatty Aldehydes at the Cerebrovasculature **126**

2.1. 2-ClHDA is Taken Up by BMVEC 126

2.2. Functional Aldehyde Group becomes Oxidized and Reduced 127

2.3. Chlorinated Lipids become Esterified into Complex Lipids 130

3. Alpha-Chloro Fatty Aldehydes Impact on BBB-Function 132

3.1. 2-ClHDA is a Powerful Inducer of In Vitro Barrier Dysfunction 132

3.2. Barrier Dysfunction is Accompanied by Reorganization of the Actin-Cytoskeleton 134

3.3. In Vivo Rat Model: BBB-Function is Affected by 2-ClHDA 135

4. BBB-Dysfunction is Based on Cellular Alterations 136

4.1. Cell Viability is Crucial for the Loss of Barrier Integrity 136

4.2. Cytotoxic Properties have Structural Specificity 137

4.3. 2-ClHDA induces Caspase-3 dependent Apoptosis 138

4.4. Mitochondrial Function is Impaired by 2-ClHDA 138

4.5. 2-ClHDA Treatment Leads to Increased Formation of Intracellular ROS in BMVEC 140

4.6. MAPK Signaling is Activated upon 2-ClHDA Treatment 141

4.7. Impact of 2-ClHDA on Junctional Architecture 141

CHAPTER 3 PHARMACOLOGICAL INTERVENTION STRATEGIES TO INTERFERE WITH MPO-MEDIATED BARRIER DYSFUNCTION 144

1. Inhibition of *De Novo* Sphingolipid Synthesis 146

2. Inhibition of MAPK Signaling 147

3. Dietary Benefits of Polyphenols to BMVEC Dysfunction? 148

3.1. Screening for Viability-Promoting Polyphenols 148

3.2. Phloridzin: Structural Homolog of Phloretin 151

3.3. Phloretin Restores Barrier Integrity of 2-ClHDA-treated BMVEC 152

3.4. Phloretin Ameliorates HOCl-Induced Cytotoxicity 152

3.5. Phloretin Reduces Cellular 2-ClHDA Content 154

3.6. α-ClFALDs are Covalently Trapped by Phloretin 155

3.7. Phloretin is a Scavenger for HOCl 156

VII. DISCUSSION 158

1. General Aspects and Rationale of this Project 158

2. Plasmalogen Loss: A Profound Biomarker for Neuroinflammation? 160

3. The Role of Chlorinative Stress in Plasmalogen Deficiency 162

4. LPS-induced Neuroinflammation: The BBB under Chlorinative Attack? 165

5. The Role α-Chloro Fatty Aldehydes in RCS-mediated BBB Dysfunction 168

6. What Are The Key Properties determining the Deleterious Effects of α-ClFALDs towards BMVEC function? 169

6.1. 2-ClHDA: Precursor of a Variety of Chlorinated Effectors 169

6.2. The Role of Signaling in Barrier Dysfunction 170
6.3. The Lipotoxic Potential of Chlorinated Lipids 173
6.4. Barrier Dysfunction: Mitochondrial dysfunction, ROS and Apoptosis 174
7. The Role of Phloretin during LPS-induced Neuroinflammation 175

VIII. CONCLUDING REMARKS 178

IX. SUPPLEMENTARY DATA 182

X. REFERENCES 184

Declaration

I hereby declare that this thesis is my own original work and that I have fully acknowledged by name all of those individuals and organisations that have contributed to the research for this thesis. Due acknowledgement has been made in the text to all other material used. Throughout this thesis and in all related publications I followed the guidelines of "Good Scientific Practice".

Date,

Signature

I. ACKNOWLEDGEMENTS

First of all, I would like to particularly appreciate my supervisor and mentor **Prof. Wolfgang Sattler** for the brilliant guidance and the continuous support during the last four years. Without his enthusiasm and expertise the compilation of this thesis would have been impossible. Wolfgang, I am sure that there will fruitful years follow!

I am grateful to all members of our lab for the friendly atmosphere, the kind help and the nice evenings without doing science. Moreover, I would like to thank **Helga**, **Matthias** and **Doris** for the excellent technical assistance. Thanks to **Christoph**, **Eva**, **Gerald**, **Sabine Waltl**, **Sabine Damm** and **Andrea** for scientific and non-scientific discussions.

I am grateful to my thesis committee member, **Prof. Ernst Malle** and **Prof. Günter Fauler** for scientific- and mass spec-support.

I am thankful to all the collaborators, including **A. Hammer, T. Glasnov, H. Köfeler, E. Painsipp, P. Holzer, O. Kappe, H. J. Leis,** and **R. Saf** who contributed with excellent methods and outstanding knowledge to this project.

I am indebted to the **SFB LIPOTOX** for providing financial support and to **PhD faculty of Medical University Graz** for giving me the opportunity to participate in the PhD program.

Most importantly with gratitude, I want to thank **my family**, especially my parents, and my girlfriend **Bianca**, who shared me for four years with brain lipids, for their unbelievable support and patience.

II. ABBREVIATIONS

2-BrHA	2-bromohexadecanoic acid
2-ClAdA	2-chloroadipic acid
α-ClFALD	α-chloro fatty aldehyde
2-ClHA	2-chlorohexadecanoic acid
2-ClHDA	2-chlorohexadecanal
2-ClHOH	2-chlorohexadecanol
2-ClHpA	2-chloroheptanal
2-ClODA	2-chlorooctadecanal
2-ClODEA	2-chlorooctadecenal
2-IHDA	2-iodohexadecanal
3-ATZ	3-aminotriazole
4-HDDE	4-hydroxydodecadienal
4-HNE	4-hydroxy-2-nonenal
4-HPNE	4-hydroperoxynonenal
4-OHE	4-oxo-2-hexenal
AA	arachidonic acid
ABC	ATP-binding cassette
AD	Alzheimer's disease
ADAPS	dihydroxyacetonephosphate synthase
AEC	3-amino-9-ethylcarbazole
AIDS	acquired immune deficiency syndrome
AJ	adherens junctions
ALDH	aldehyde dehydrogenase
ALS	amyotrophic lateral sclerosis
AMP	adenosine monophosphate
ANOVA	analysis of variance
APO	apolipoprotein
APP	amyloid precursor protein
ATP	adenosine-5'-triphosphate
ATX	autotaxin
Aβ	β-amyloid
BAB	blood-arachnoid barrier
BBB	blood-brain barrier
BCSFB	blood-CSF barrier
BMVE	brain microvascular endothelium
BMVEC	brain microvascular endothelial cells
BSA	bovine serum albumin
carboxy-H_2DCFDA	5-(and-6)-carboxy-2',7'-dichlorodihydrofluorescein diacetate
CD	cluster of differentiation
CDK	cyclin-dependent kinase
CGD	granulomatous disease

CNS	central nervous system
COPD	chronic obstructive pulmonary disease
COX2	cyclooxygenase-2
CP	choroid plexus
CSF	cerebrospinal fluid
Cy	cyanine
Cyp	cytochrome P450
Da	Dalton
DALY	total disability-adjusted life years
DAMP	danger-associated molecular patterns
DAPI	4', 6'-diamidino-2-phenylindole dihydrochloride
DHAPAT	dihydroxyacetonephosphate acyltransferase
DI	direct insertion
dma	dimethyl acetal
DMSO	dimethyl sulfoxide
DNA	deoxyribonucleic acid
DPPC	dipalmitoyl-phosphatidyl choline
EAE	experimental autoimmune encephalomyelitis
EB	Evans blue albumin
ECIS	electric cell-substrate impedance sensing
ECL	enhanced chemiluminescence
EDTA	ethylenediaminetetraacetic acid
EET	epoxyeicosatrienoic acid
EI	electron impact
ELISA	enzyme-linked immunosorbent assay
eNOS	endothelial nitric oxide synthase
ERK	extracellular-signal-regulated kinase
ESI	electrospray ionization
FA	fatty acid
FITC	fluorescein isothiocyanate
fMLP	N-formylmethionyl-leucyl-phenylalanine
FOH	fatty alcohol
FT-ICR	Fourier transform-ion cyclotron resonance
GABA	γ-amino butyric acid
GC	gas chromatography
GD	Gaucher's disease
GPCR	G protein-coupled receptor
GR	glucocorticoid receptor
GSH	glutathione
GTP	guanosine-5'-triphosphat
HBSS	Hank's Buffered Salt Solution
HC	hydrocortisone
HCAEC	human coronary artery endothelial cells
HD	Huntington disease
HDA	hexadecanal

HDL	high density lipoprotein
HETE	hydroxytetraenoic acid
HIV	human immunodeficiency virus
HMG-CoA	3-hydroxy-3-methyl-glutaryl-CoA
HPLC	high-performance liquid chromatography
HRMS	high resolution mass spectrometry
HRP	horseradish peroxidase
HUVEC	human umbilical vein endothelial cells
I.S.	internal standard
Iba	ionized calcium binding adaptor molecule
IC	inhibitory concentration
yah	intercellular adhesion molecule
IFN	interferon
IL	interleukin
iNOS	inducible nitric oxide synthase
ISF	interstitial fluid
JACOP	junction-associated coiled-coil protein
JAM	junction-associated adhesion molecules
JNK	c-Jun N-terminal kinase
LC	lethal concentration
LCAT	lecithincholesterol acyltransferase
LDL	low-density lipoprotein
LFA	lymphocyte function-associated antigen
LOX	lipoxygenase
LPA	lysophosphatidic acid
LPS	lipopolysaccharide
lysoPL	lysophospholipid
M	molecular ion
MCAO	middle cerebral artery occlusion
MAGUK	membrane-associated guanylate kinase
MAPK	mitogen-activated protein kinase
MAPKK	mitogen-activated protein kinase kinase
Met	methionine
MHC	major histocompatibility complex
MMSE	mini–mental state examination
MMP	matrix metalloproteinases
MPG	N-2-mercaptopropionyl glycine
MPO	myeloperoxidase
MPP^+	1-methyl-4-phenylpyridinium ion
MPTP	1-methyl-4-phenyl-1,2,3,6-tetrahydropyridine
MS	multiple sclerosis
MS	mass spectrometry
MSTFA	N-methyl-N-(trimethylsilyl) trifluoroacetamide
MTP	mitochondrial permeability transition pore
MTT	3-(4,5-dimethyl-2-thiazolyl)-2,5-diphenyltetrazolium bromide

NAC	N-acetyl-L-cysteine
NADPH	nicotinamide adenine dinucleotide phosphate
NET	neutrophil extracellular trap
NFκB	nuclear factor κB
NGF	nerve growth factor
NICI	negative ion chemical ionization
NMR	nuclear magnetic resonance
NO	nitric oxide
NO_2Tyr	nitrotyrosine
NOS	nitric oxide synthase
NOX	NAD(P)H oxidase
NTP	nucleoside triphosphate
ODA	octadecanal
ODEA	octadecenal
PAF	platelet activating factor
PAMP	pathogen-associated molecular pattern
PARP	poly (ADP-ribose) polymerase
PAT	palmitoyl acyl transferases
PBS	Phosphate buffered saline
PC	phosphatidylcholine
PCR	polymerase chain reaction
PD	Parkinson' disease
PE	phosphatidylethanolamine
PECAM	platelet endothelial cell adhesion molecule
PFB	pentafluorobenzyl
PFBoyl	pentafluorobenzoyl
PG	prostaglandins
P-gp	P-glycoprotein
PGPC	1-palmitoyl-2-glutaroyl-*sn*-glycero-3-phosphocholine
PHOX	phagocytic NADPH oxidase
PI	phosphatidylinositol
PI3K	phosphatidylinositol-3 kinase
PK	protein kinases
PL	glycerophospholipids
PLA_2	phospholipases A_2
PLTP	phospholipid transfer protein
PMA	phorbol myristate acetate
PMNL	polymorphonuclear leukocytes
PMSF	phenylmethylsulfonyl fluoride
PNS	peripheral nervous system
POVPC	1-palmitoyl-2-(5-oxovaleroyl)-*sn*-glycero-3-phosphocholine
pPC	choline plasmalogen
pPE	Ethanolamine plasmalogen
pPL	plasmalogen
PS	phosphatidylserine

PTK	protein tyrosine kinases
PVDF	polyvinylidene difluoride
RCS	reactive chlorine species
RNS	reactive nitrogen species
ROS	reactive oxygen species
RT	room temperature
SAPK	stress-activated protein kinase
SD	standard deviation
SDS-PAGE	sodium dodecyl sulfate-polyacrylamide gel electrophoresis
SEM	standard error of the mean
SF	sodium fluorescein
SIM	selected ion monitoring mode
siRNA	short interfering RNA
SNCA	α-synuclein
SOD	superoxide dismutase
SPM	synaptosomal plasma membranes
SPTLC	serine-palmitoyltransferase
TBS-T	Tris-buffered saline Tween 20
TBI	traumatic brain injury
TEER	transendothelial electrical resistance
TGFβ	transforming growth factor β
TIC	total ion current
TJ	tight junctions
TLC	thin layer chromatography
TLR	toll-like receptors
TMCS	trimethylchlorosilane
TMS	trimethylsilyl
TNFR	tumor necrosis factor α receptor
TNFα	tumor necrosis factor α
tPA	tissue plasminogen activator
TRITC	rhodamine isothiocyanate
VCAM	vascular cell adhesion molecule
VE-cadherin	vascular endothelial cadherin
VEGF	vascular endothelial growth factor
VLA	very late antigen
vWF	von Willebrand factor
WHO	World Health Organization
ZO	zonula occludens
ZONAB	ZO-1 associated nucleic acid binding protein
$\Delta\psi m$	mitochondrial membrane potential

III. ABSTRACT

Normal brain function depends on a delicately balanced set of remarkably diverse lipids. Consequently, short and long-term alterations in brain lipid composition during acute and chronic neuroinflammatory conditions associated with oxidative stress are casually involved in central nervous system (CNS) disorders (e.g. Alzheimer's disease, multiple sclerosis, Parkinson's disease, stroke or traumatic brain injury). Within the different cerebral lipid subclasses plasmalogens, 1-*O*-alk-1'-enyl-2-acyl-*sn*-glycero-phospholipids, take a central role in CNS function. Plasmalogen deficiency results in severe and long-lasting developmental alterations in the brain and is linked to several neurodegenerative diseases. Among the oxidant systems contributing to the formation of reactive species, myeloperoxidase (MPO) plays a central role. After activation of phagocytes, MPO uses chloride ions and hydrogen peroxide generated from superoxide anion radicals to form hypochlorous acid (HOCl). This potent oxidant targets unsaturated lipids to form a battery of chlorinated lipotoxic compounds. Of note, due to the presence of an *O*-alkenyl-ether group at the *sn*-1 position these ether phospholipids are particularly sensitive towards HOCl-mediated modification. Therefore, the present study aimed at investigating the impact of experimentally induced neuroinflammation on MPO-mediated chlorinative stress on CNS plasmalogens.

By means of an *in vivo* mouse model I could demonstrate that a single dose of peripherally applied endotoxin leads to cerebral plasmalogen loss. These experiments revealed that MPO-derived HOCl modifies a significant proportion of brain plasmalogens leading to the formation of highly reactive α-chloro fatty aldehydes (e.g. 2-ClHDA). Further studies in this murine model identified recruitment of MPO-containing neutrophils to the cerebrovasculature as a likely event contributing to blood-brain barrier (BBB) dysfunction under neuroinflammatory conditions. Using an *in vitro* model of the BBB I could identify molecular mechanisms/signaling pathways leading to 2-ClHDA-induced apoptosis and altered permeability properties. Of note, pharmacological modulation of these pathways resulted in partial restoration of barrier function. Also the use of natural polyphenolic compounds identified candidates with high chemical scavenging potential for MPO-derived HOCl and 2-ClHDA thereby providing significant protection against barrier dysfunction.

In summary, the present study indicates that activation of the innate immune system and plasmalogen modification by MPO-derived HOCl might play a critical role in the setting of neurological disorders. A thorough understanding of the underlying signaling pathways could ultimately impact on targeted pharmacological interventions under conditions where normal function of the BBB is compromised.

IV. ZUSAMMENFASSUNG

Die intakte Funktion des Gehirns ist von einer definierten Lipid-Zusammensetzung abhängig. Aus diesem Grund sind kurz- und langfristige Veränderungen des zerebralen Lipid-Musters als Folge von Entzündung und oxidativem Stress, welche man regelmäßig bei Patienten mit akuten und chronischen neurologischen Erkrankungen (z.B. Alzheimer, Multiple Sklerose, Parkinson, bzw. traumatischen Hirnverletzungen oder Insult) beobachtet, zwangsläufig mit Störungen des zentralen Nervensystems (ZNS) verbunden. Eine zentrale Rolle in der Funktion des ZNS spielen Plasmalogene (1-*O*-Alk-1'-Enyl-2-Acyl-*sn*-Glycerophospholipide). Ein Mangel an dieser Phospholipid-Subklasse geht mit neurodegenerativen Erkrankungen einher und führt zu schweren, lang anhaltenden Entwicklungs-Veränderungen des Gehirns. Unter den zahlreichen Systemen, die zur Bildung von reaktiven Spezies führen, nimmt die Myeloperoxidase (MPO) von Phagozyten eine Sonderstellung ein, da sie aus Wasserstoffperoxid in Gegenwart von Chlorid-Ionen, hypochlorige Säure (HOCl) generiert. Dieses starke Oxidationsmittel hat die pathophysiologische Eigenschaft, aus ungesättigten Lipiden, eine Reihe von chlorierten, lipotoxischen Verbindungen zu bilden. Plasmalogene haben sich als besonders empfindlich gegenüber HOCl-vermittelter Modifikation erwiesen, da sie aufgrund einer *O*-Alkenyl-Ether-Gruppe an der *sn*-1 Position äußerst empfänglich gegenüber Oxidation sind. Ziel dieser Studie war es die Auswirkungen einer experimentell induzierten Neuroinflammation auf die Bildung von HOCl im Gehirn und die daraus resultierenden Veränderungen an der zerebralen Plasmalogen-Zusammensetzung zu untersuchen.

Mit Hilfe eines *in vivo* Mausmodells konnte diese Studie zeigen, dass eine Einzeldosis von peripher appliziertem Endotoxin zu einem Verlust an zerebralen Plasmalogenen führt. Desweiteren ergaben diese Experimente, dass ein erheblicher Teil dieses Verlustes einer HOCl-Modifikation der *O*-Alkenyl-Ether-Gruppe zuzuordnen ist, was zur Bildung von hoch reaktiven, langkettigen, α-chlorierten Aldehyden (z.B. 2-ClHDA) führt. Weitere Studien in diesem Mausmodell konnten zeigen, dass eine im Zuge der Neuroinflammation resultierende Rekrutierung von neutrophilen Granulozyten an das zerebrale Gefäßsystem zu einer Dysfunktion der Blut-Hirn-Schranke (BHS) beitragen kann. Mit Hilfe eines *in vitro* BHS-Modells wurden die molekularen Mechanismen und Signalwege identifiziert, die zu einer 2-ClHDA-induzierten Veränderung der Permeabilität und Zell-Viabilität führen. Durch diese Erkenntnisse war es möglich, bestimmte Signalwege pharmakologisch so zu modulieren, dass die Barriere-Funktion des BHS-Modells partiell wiederhergestellt werden konnte. Außerdem erbrachten weitere Studien den Beweis, dass natürliche Polyphenole durch ihre antioxidativen Eigenschaften einen signifikanten Schutz gegenüber HOCl- und 2-ClHDA-induzierte Barriere-Dysfunktion bieten.

Zusammenfassend konnte die vorliegende Studie zeigen, dass die Aktivierung des angeborenen Immunsystems und eine damit verbundene, HOCl-abhängige Plasmalogen-Modifikation eine entscheidende Rolle im Verlauf von neurologischen Erkrankungen spielt. Ein gründliches Verständnis der zugrunde liegenden Signalwege würde es ermöglichen, in Funktionsstörungen der BHS pharmakologisch gezielt einzugreifen.

V. INTRODUCTION

1. The Central Nervous System (CNS)

The nervous system, along with the endocrine system, controls the maintenance of body homeostasis and monitors the ambience. At the simplest level, it reacts in the way to sustain animal integrity and, at higher levels, it provides interaction with the external environment resulting in complex behavior (Brown A.G. 2001). Anatomically, the nervous system can be divided into the CNS and the peripheral nervous tissue (PNS). The CNS embraces nervous tissue located in brain, brain stem and spinal cord, whereas the PNS is composed by the remnant nervous tissue outside the CNS (Zhang S.X. 1998). In contrast to some invertebrate animals (e.g. cnidarians), equipped with a decentralized nervous system, the brain governs nervous system in all of vertebrate and invertebrate animals (Shepherd 1994). The largest proportion - approx. 77% - of human CNS volume is given by the cerebral cortex, the part playing a key role in consciousness, memory and language followed by the cerebellum (10%), interbrain (4%), midbrain (4%), hindbrain (2%), and spinal cord (2%) (Baars and Gage 2010, Swanson 1995). Based on gross topographical conventions cerebral cortex may be classified into four lobes: Frontal lobe, parietal lobe, occipital lobe, and temporal lobe (Barker et al. 1999).

In preserved nervous tissue gray and white colored areas are found which are also referred to gray and white matter. Gray matter, which is localized at the cortex and in depths of the cerebrum and as well as at the surface of the cerebellum, is mainly composed by neuronal cell bodies, glia cells and capillaries. The white matter, mostly found below the gray matter, predominantly consists of myelinated axons interconnecting neurons in different regions of the cerebral cortex with each other (Purves et al. 2001). There is increasing evidence that volumes of grey and white matter in the cerebral hemispheres are affected by age and several neurological disorders including Alzheimer disease (AD) (***Figure 1***), Huntington disease (HD), multiple sclerosis (MS) and schizophrenia (Hulshoff Pol et al. 2002, Miller et al. 1980, Salat et al. 1999, Sanfilipo et al. 2006, Stoffers et al. 2010).

The subarachnoid space, between the arachnoid layer and the pia, maintains the cerebrospinal fluid (CSF). The function of the CSF and the tissue that secretes it, the choroid plexus (CP), has traditionally

been thought of as both providing physical protection to the brain through buoyancy. However, more recent data suggest, that by joining circulating interstitial fluid (ISF) the CP-CSF system plays active roles in the maintenance of CNS homeostasis e.g. nutrient and ion provision, metabolite removal, and cell intercommunication (Abbott 2004, Johanson et al. 2008, Redzic Z. B. et al. 2005).

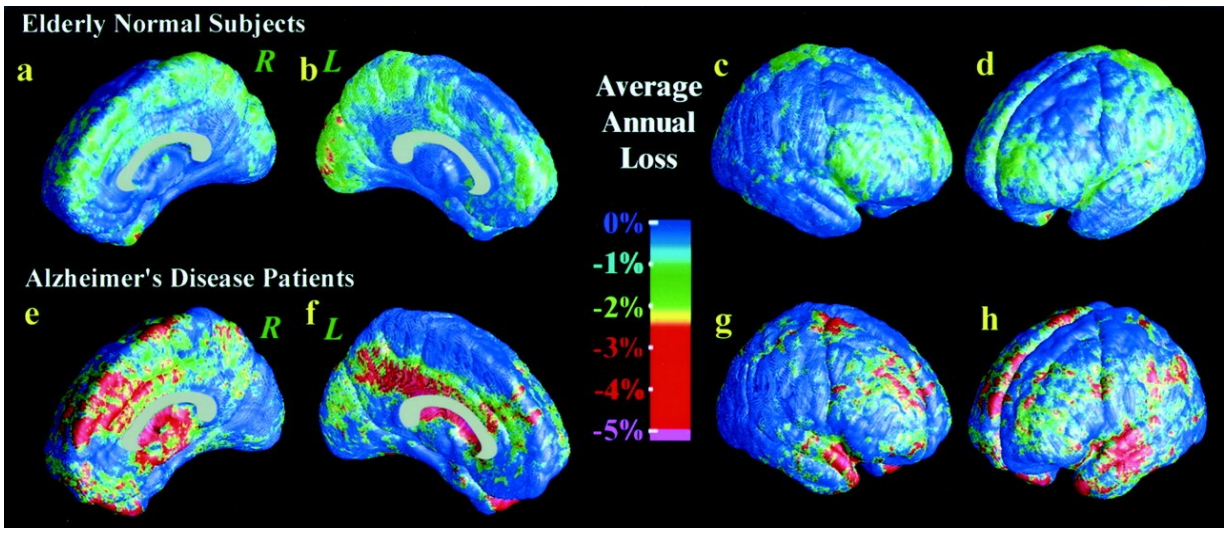

Figure 1: Average gray matter loss rates in healthy aging and AD. The maps show the average local rates of loss for gray matter, in groups of controls (*top*, *a–d*) and patients with AD (*bottom, e–h*). Loss rates are <1% per year in controls. They are significantly higher in AD and strongest in frontal and temporal regions (*g*, *h*) at this stage of AD (as the MMSE score falls from 18 to 13) (Thompson et al. 2003).

2. The Brain is a Well-Vascularized Structure

Although the human brain accounts only for approximately 2% of the body weight it receives about 20% of the total body-circulating blood volume. Upon a brief loss of blood supply, also referred as ischemia, brain functions stop within seconds and damage to neurons may occur within minutes (Girouard and Iadecola 2006, Zlokovic 2008). Therefore, preserving a constant blood supply of about 700 ml/min to the brain is essential for normal brain function because the cerebrovasculature provides brain tissue with oxygen, nutrients, vitamins and other important substances like peptide hormones (Albayrak et al. 2007, Bourre 2006a, b, Poduslo et al. 1994).

2.1. *Blood Supply to the Brain*

The brain receives blood from four large vessels: On the one hand the left and the right internal carotid arteries, which arise at the point where the common carotid arteries bifurcate into the external and internal carotid arteries and on the other hand from the vertebral arteries, which originate directly from the subclavian arteries. The internal carotid arteries divide into the two major cerebral arteries, the anterior and middle cerebral arteries (***Figure 2***). The former supplies blood to many parts of the lateral cerebral cortex, the anterior temporal lobes and the insular cortices while the latter supplies mainly the medial portions of frontal lobes and the medial parietal lobes as well as the corpus callosum. The right and left vertebral arteries fuse on the ventral side of the brainstem forming the basilar artery. The basilar artery branches to form the posterior cerebral artery and to join via the posterior communicating artery the blood supply of the internal carotids in an arterial ring at the base of the brain called the circle of Willis. Together with the anterior communicating artery the circle of Willis is offering the potential to maintain cerebral blood supply in the event of a single arterial occlusion. The posterior cerebral arteries supply blood to the posterior parietal cortex, the occipital lobe and inferior parts of the temporal lobe. Predominantly, the major arteries proceed along the cerebral surface before suddenly diving into the brain ramifying into arterioles and capillaries (Barker et al. 1999, Purves et al. 2001, Zigmond et al. 1999). Brain capillaries connect arterioles and venules, and enable the gas and water exchange as well as the exchange of nutrients, and efflux of waste products between blood and the surrounding brain tissue (Abbott et al. 2006). Due to the unique properties of this microvasculature (*see chapter 3*) to strictly control solute interchange, this physical interface is also referred as BBB (Abbott et al. 2010, Cardoso et al. 2010).

2.2. *Venous Drainage of Cerebral Blood*

The cerebral venous system can be separated into an external and an internal system. At the external system cortical veins drain superficial parts of the cerebral cortex and empty into superior sagittal sinus. This sinus sequentially drains into the transverse sinus, then sigmoid sinus, before emptying into the left or right internal jugular vein. In contrast, at the internal system profound cerebral veins drain the deep structures of the cerebral hemisphere to the great vein of Galen, then into the straight sinus and finally also into internal jugular veins (***Figure 3***). Via anastomosis of left and right

internal jugular veins into the superior vena cava, brain-blood returns to body circulation (Barker et al. 1999, Kilic and Akakin 2008).

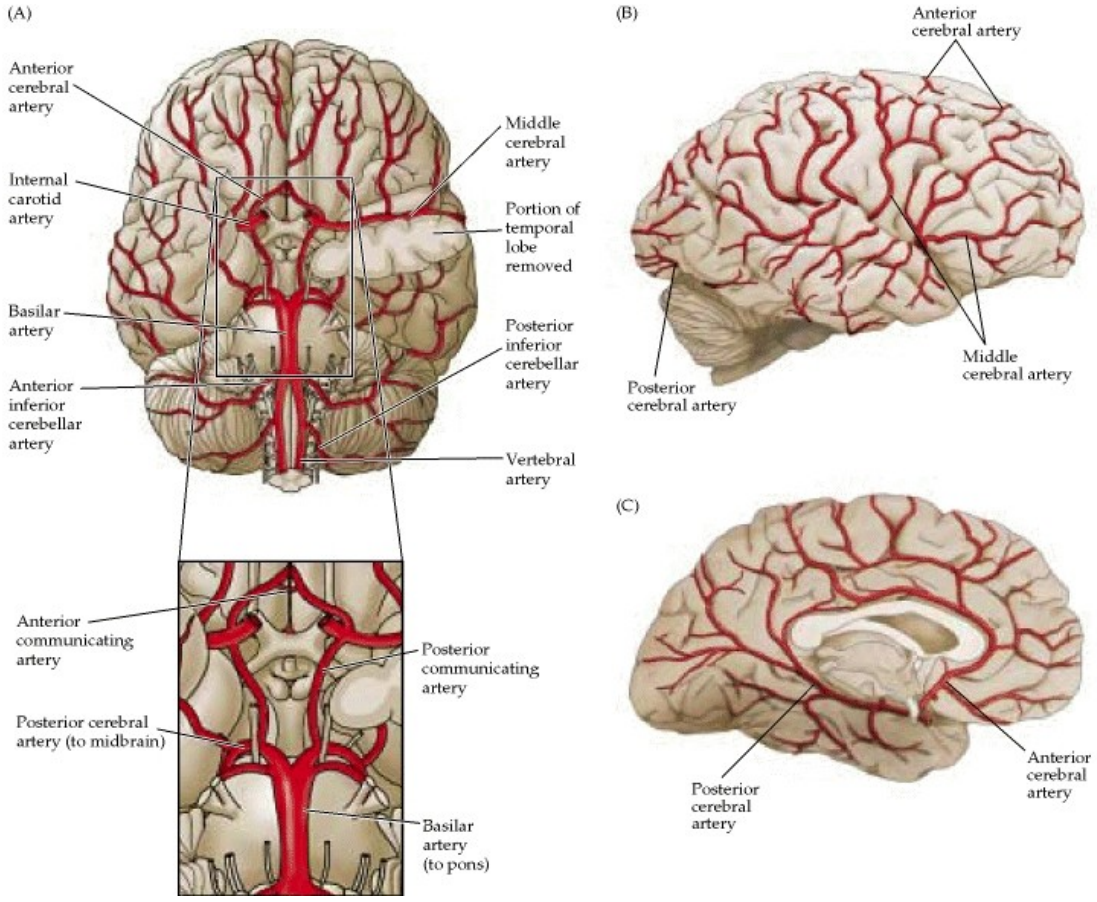

Figure 2: **The major arteries of the brain.** (**A**) Ventral view. The enlargement of the boxed area shows the circle of Willis. (**B**) Lateral and (**C**) midsagittal views showing anterior, middle, and posterior cerebral arteries (Purves et al. 2001).

3. Blood-Brain Barrier (BBB) – Multiple Gatekeepers of the CNS

The CNS represents most probably the most sensitive and critical system in the body of mammalians since neurons communicate using a combination of chemical and electrical signals, and precise regulation of the local ionic microenviroment around synapses and axons is critical for reliable neural signaling. Although nervous tissue shows substantial metabolic demands (approx. 20% of total oxygen consumption in humans) the CNS is extremely sensitive to a broad range of chemical compounds. Many of these substances are consumed in our diet, without any harm to peripheral organs, but in nervous tissue they exhibit toxic properties.

It has been argued, that fundamental aspects like maintenance of CNS homeostasis and protection from blood-borne compounds were chief evolutionary pressures leading to the development of a physical interface between the CNS and the peripheral circulation acting as dynamic regulator of ion milieu, nutrient transport and a barrier to potential harmful compounds (Abbott et al. 2010, Cardoso et al. 2010, Hawkins B. T. and Davis 2005). This interface is not simply constituted by a simple physical barrier (restriction of paracellular flux) but more likely a combination of physical barrier, transport barrier (specific transport of solutes across the barrier) and metabolic barrier (metabolism of compounds by enzymes) that protects the fragile environment of the CNS (Abbott et al. 2010).

The barrier system of the BBB poses severe limitations to the development of new drugs against virtually all CNS disorders including brain tumors, Alzheimer's disease (AD), Parkinson's disease (PD), multiple sclerosis (MS), stroke, schizophrenia, depression, migraine headache, and epilepsy. It had been estimated that essentially 100% of all large molecule drugs such as recombinant proteins and enzymes, monoclonal antibodies (MAb), antisense drugs, and short interfering RNA (siRNA) and approximately 98% of small molecule drugs do not cross the BBB (Pardridge 2005, 2007a, b, Zlokovic 2008). Basically, all drugs presently used in CNS clinical practice are small molecules that feature dual molecular characteristics of lipid solubility and molecular weight (MW) of <400 Da. However, based on experimental and computational approaches the 'Rule of 5' was formulated aimed at predicting the permeation of solutes in pharmacologically significant amounts through biological barriers. Generally, transport of molecules across the BBB is impaired by following characteristics: Molecular weight >500 Da, sum of hydrogen bond donor/acceptor groups >10, substrate for a BBB enzyme system, substrate for BBB active efflux transporter, and avid plasma protein binding of the drug (Lipinski et al. 2001, Pardridge 2002).

The existence of an interface between the blood circulation and the CNS was initially described in the 1880s when Paul Ehrlich discovered that after intravascular injection, certain water soluble dyes were rapidly taken up by all tissues with the exception of brain and spinal cord. Nevertheless, he concluded that this was due to low affinity of nervous tissue to the dye. At the turn of the last century Lewandowsky was the first, who described this interface by using the term bluthirnschranke (blood-brain barrier) based on the observation that neurotoxic compounds affected brain function solely when directly injected into the brain (Dermietzel et al. 2006 , Engelhardt and Sorokin 2009). In the fifties, sixties, and seventies of the last century physiological studies and analysis of the molecular nature of brain barriers (*see chapter 3.2.*) changed the concept from an impermeable barrier to a highly controlled interface (Cardoso et al. 2010, Reese and Karnovsky 1967). At the present time there is an awakened interest of the neuroscience society in the exploration of the BBB since there is a revived appreciation that brain barrier mechanisms play critical roles in brain development and pathophysiology of several neurodevelopmental and neurodegenerative disorders (*see chapter 4.*) as well as in getting therapeutic agents into the CNS for treating such disorders (Pardridge 2007b, Saunders et al. 2008).

3.1. *The Architecture of Brain Barriers*

In contrast to many invertebrate organisms - except some groups e.g. insecta, crustacea and cephalopoda - all vertebrates possess a BBB. As the neural tissue become more centralized, larger, and more complex during the course of evolution the barrier has shifted from a incomplete or leaky BBB, comprised by perivascular glial end-feets, to a highly intricate, tight barrier based on an extensive network of capillaries (Abbott 1987, 2005, Bundgaard and Abbott 2008).

In humans, this microvascular network has a length of approx. 650 km, resulting in a surface area of approx. 20 m^2 for blood-brain exchange of nutrients, waste products etc. It has been estimated that the brain microvasculature is so convoluted that an individual neuron is rarely more than 20 µm distant from a brain capillary, hence, virtually every neuron is perfused by its own capillary (Abbott et al. 2006, Pardridge 2002, Zlokovic 2008). At the entirely differentiated CNS of mammals, homeostasis and protection of nervous tissue are ensured by two other interfaces, namely blood-CSF barrier (BCSFB), and blood-arachnoid barrier (BAB) (Redzic Z. 2011, Saunders et al. 2008).

The BCSFB is localized at the choroid plexuses in the lateral, third and fourth ventricles where epithelial cells, instead of endothelial cells, constitute a barrier between blood and CSF (Brown P. D. et al. 2004). The third interface, provided by the multi-layered avascular arachnoid epithelium, completely envelopes the CNS, where it serves as a seal between the extracellular fluids of the CNS and of the rest of the body (Abbott et al. 2006). Nevertheless, the surface area of either the BCSFB or the BAB is 1000-fold smaller compared to the brain microvascular endothelium (BMVE) of the BBB (Dohrmann 1970, Pardridge 2002).

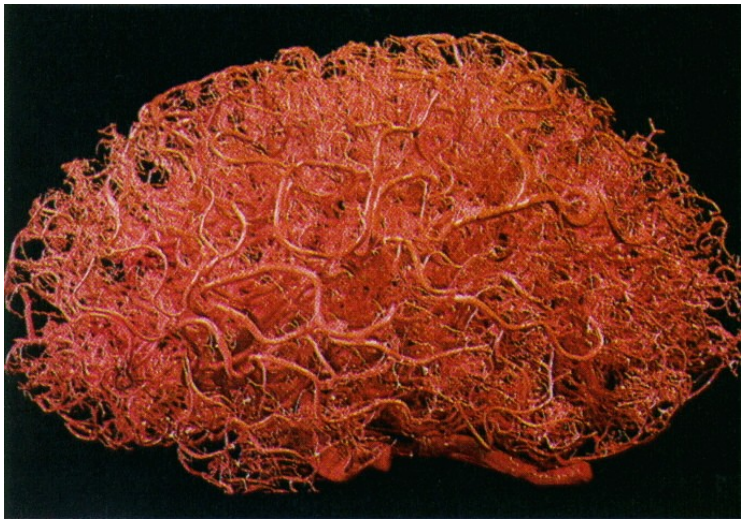

Figure 3: **Human cerebrovasculature.** A plastic emulsion was injected into the brain vessels, and brain parenchymal tissue was dissolved (Zlokovic and Apuzzo 1998).

3.2. *The Neurovascular Unit*

The neuron has traditionally been viewed as the most important cell type within the CNS. However, in recent years there is growing evidence that integrated brain function and dysfunction arise from the complex interaction between a network of several neuronal and non-neuronal cell types, including neurons, astrocytes, oligodendrocytes, pericytes, microglia, and the microvascular endothelial cells. All these cells comprise the cerebrovasculature, forming a functional unit, which is often referred to as a 'neurovascular unit' (Lo et al. 2003, Lok et al. 2007, Zlokovic 2010). The close proximity of participant cell types allows bidirectional-interaction between adjacent cells, directly in a physical manner, or indirectly via paracrine regulation. Therefore, this cellular communication network takes a central role as a regulator of hemodynamic neurovascular coupling, microvascular permeability as well as angiogenic and neurogenic coupling, both in physiological and pathophysiological conditions (del Zoppo 2010, Zlokovic 2008).

3.2.1. Brain Microvascular Endothelial Cells (BMVEC) - The Anatomic Base of the BBB

It has become an accepted model that the brain microvascular endothelium (BMVE) forms the anatomical basis of the BBB since amphibians show high transendothelial electrical resistance (TEER) despite the absence of surrounding astrocytes (Cardoso et al. 2010, Hawkins R. A. et al. 2006). The BMVE is composed of a tightly sealed monolayer (approx. 50-100 times tighter than peripheral microvessels) of BMVEC (***Figure 4 A***), which generally prevents free exchange of compounds between blood and neural tissue. BMVEC differ fundamentally in morphology and physiology from microvascular endothelial cells localized in the periphery, because they show features like small height, increased number of mitochondria, a minute number of caveolae, low pinocytotic activity, high TEER, lack of fenestrations and tight junctions (TJ) between adjacent endothelial cells (Carvey et al. 2009, Wolburg et al. 2009). The tight junctions inhibit paracellular movement ('barrier function'), and divide the membranes of the endothelial cells into two distinct compartments ('fence function'), the luminal (blood side) and abluminal (brain side) face of the plasma membrane. Thus, membrane polarization results in different sets lipid species and proteins (e.g. transporters, enzymes, receptors and adhesion proteins) on the luminal and abluminal side (Betz et al. 1980, Hawkins R. A. et al. 2006, Tewes and Galla 2001).

Interendothelial Junctions. During the pioneering work in the late sixties Reese and co-workers could demonstrate by electron microscopy studies that endothelial junctions occlude the interspaces between blood and brain parenchyma, thereby constituting a structural basis for the BBB (Brightman and Reese 1969, Reese and Karnovsky 1967). The interendothelial space of the cerebrovasculature is characterized by the presence of junctional complexes (***Figure 4 B***) including adherens junctions (AJ) and TJ (Schulze and Firth 1993, Wolburg and Lippoldt 2002). Gap junctions have also been identified but their role in barrier function is still controversial (Nagasawa et al. 2006, Zlokovic 2008).

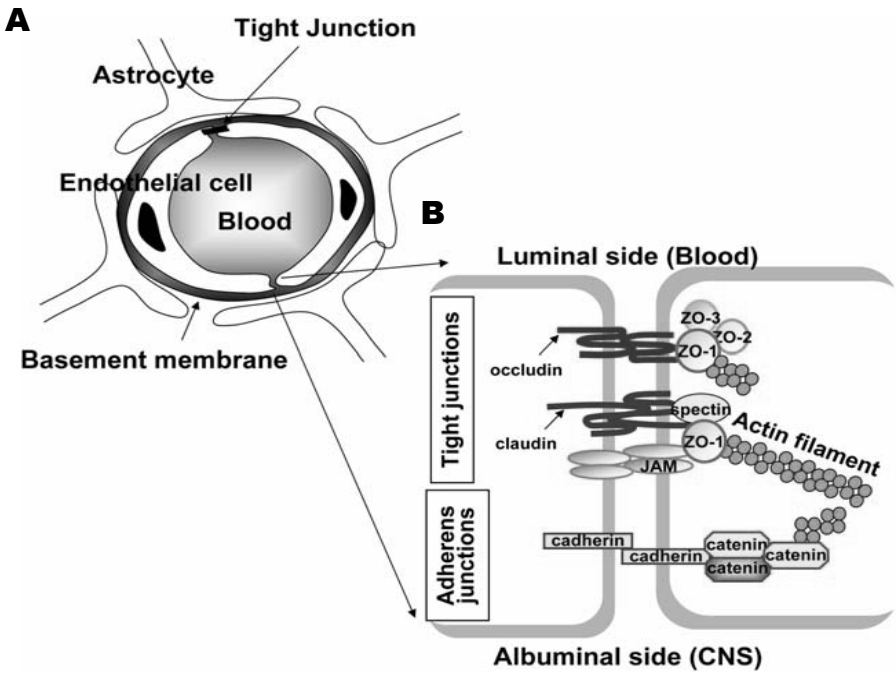

Figure 4: **Simplified schematic illustration of cross-sections of (A) a CNS capillary and (B) the junctional complex between BMVEC.** (A) BMVEC and pericytes are surrounded by a membrane composed of collagen type IV, laminin, fibronectin, and heparin sulfate proteoglycan, which is ensheathed by astrocyte end-foot processes. (B) BMVEC are tightly sealed by AJ and TJ complexes consisting of transmembrane proteins (occluding, claudin, JAMs and VE-cadherin). Accessory proteins (e.g. members of the ZO- and the catenin-family) link junctions to the actin cytoskeleton (Kim et al. 2006).

I. Adherens Junctions (AJ). AJ are specialized cell-cell-junctions, which are ubiquitously found in the vasculature. In general, AJ mediate the adhesion of endothelial cells to each other, they mediate contact inhibition during vascular growth and remodeling as well as the initiation of cell polarity (Hawkins B. T. and Davis 2005). AJ are primarily formed by extracellular domains of the transmembrane glycoprotein vascular endothelial (VE) cadherin (Navarro et al. 1998). The cytoplasmic tail of this protein associates with catenins (α- and β-catenin) and other cytoplasmic proteins like vinculin and α-actinin, thereby linking the junctional complex to the cortical F-actin cytoskeleton (Bazzoni and Dejana 2004). Targeted inactivation or truncation of VE-cadherin was found not to affect the assembly of endothelial cells in vascular plexi, but to induce endothelial apoptosis, thus providing evidence, that VE-cadherin/β-catenin signaling controls endothelial survival (Carmeliet et al. 1999).

A clear role for VE-cadherin in maintaining permeability was established by *in vivo* experiments using anti-VE-cadherin antibodies in mice. This treatment induced hemorrhages by dramatically increasing vascular permeability in several organs but not in brain (Corada et al. 1999). On the other hand, it was shown that permeability-increasing agents like histamine or VEGF induce rapid tyrosine phosphorylation and concomitant cellular redistribution of VE-cadherin and catenins supporting the concept that phosphorylation of VE-cadherin and/or its intracellular partners is involved in regulating the strength of cell-to-cell contacts (Andriopoulou et al. 1999, Fischer et al. 1999). However, it cannot be excluded that phosphorylation of cadherin and catenin may represent a general reaction to stressful agents, which results in increased permeability but may also trigger more complex cell responses and interactions (Bazzoni and Dejana 2004).

II. Tight Junctions (TJ). The most prominent feature of the BBB is the high TEER across the endothelial barrier, established by the presence of TJ. Although TJ are found in endothelia and epithelia of several tissues including brain, lung, heart, liver, placenta etc. (Lievano et al. 2006, Tsukita et al. 2001), barrier tightness varies in a tissue-dependent manner e.g. brain microvascular endothelial junctions impose high TEER of approx. 1500-2000 ohms/cm^2, in comparison, TEER of placenta endothelial cells is only about 20-50 ohms/cm^2. Studies using TJ from different tissues with varying transendothelial and transepithelial electrical resistances demonstrated a correlation between increased organization of cytoplasmic fibrils and decreased permeability (Claude 1978, Huber et al. 2001). Like junctional complexes of AJ, TJ are also composed of integral membrane proteins, first- and second order adapter proteins.

Molecular Architecture. Occludin was the first transmembrane TJ protein, which has been characterized. However, further investigations have identified the existence of 24 members of the claudin family, three of them, claudin-3/5/12, have been reported to be expressed at the BBB (Wolburg et al. 2009). A third class of integral membrane proteins includes the junction-associated adhesion molecules (JAM) 1-3, which can be classified into members of the IgG superfamily (Forster 2008). Regulation of paracellular permeability is ensured by homophilic (occludin, JAMs) or by homo- and heterophilic (claudin-family) interactions of extracellular domains of two adjacent cells (Dejana et al. 2000, Piontek et al. 2008). First order adapter proteins physically interact with the C-terminus of occludin, claudins and JAM and they link junctional complexes to the F-actin cytoskeleton. Adapter proteins of the first order, like ZO proteins (ZO-1/2/3), belong to the family of membrane-associated guanylate kinase (MAGUK) proteins and they serve as recognition proteins for TJ placement as well as signal transducers between TJ and the nucleus (Cardoso et al. 2010, Wolburg et al. 2009). For instance, it has been shown, that during adverse conditions, ZO-1 and ZO-2 shuttle between the junctions and the nucleus, thereby influencing gene expression e.g. blocking cell cycle progression (Balda and Matter 2009, Gonzalez-Mariscal et al. 2009, Tapia et al. 2009). Second order adaptors are based on their indirect association with the integral tight junction proteins and include, for example, cingulin or the cingulin-related junction-associated coiled-coil protein (JACOP). Recent data indicate that these proteins are important for TJ assembly and function most likely through activation of RhoA signaling (Terry et al. 2011, Wolburg et al. 2009).

TJ Deficiency in Animals. In the last ten years several animal models were established aimed at exploring the physiological role of TJ *in vivo*. These studies revealed a surprising complexity of TJ function *in vivo* after genetic modification. For example, mice deficient for claudin-5, died as neonates about 10 h after birth but there were no indications about intracerebral edema or hemorrhage and no obvious abnormalities in TJ formation. However, tracer experiments and magnetic resonance imaging revealed the size-selective opening of the BBB for compounds >800 Da suggesting that each claudin regulates the diffusion of molecules of a certain size (Dermietzel et al. 2006 , Nitta et al. 2003). On the other hand, in occludin$^{-/-}$ mice transepithelial resistance was not affected. Nevertheless, this null mutation resulted in a complex phenotype including histological abnormalities like calcification of brain tissue as well as in morphological- and behavioral differences (Saitou et al. 2000). Deficiency of ZO-1 causes an embryonic lethal phenotype associated with defects in vascular development, impaired formation of vascular trees but abnormal patterns of TJ components were not recognized (Katsuno et al. 2008).

*Mechanisms of Barrier Regulation.*TJ are highly dynamic structures that undergo disintegration and reassembly induced by intracellular mechanisms based on the cross-talk of a complex network of signaling cascades, but we are just at the beginning to understand these processes (Cardoso et al. 2010, Gonzalez-Mariscal et al. 2008). The consequence of TJ complex alteration, modulation of BBB permeability, was shown to occur during a variety of physiological and pathophysiological conditions (*see chapter 4.4.*), including angiogenesis, neurogenesis as well as during acute and chronic neurodegeneration (Hawkins B. T. and Davis 2005, Zlokovic 2008).

During the past two decades extensive research has revealed a large extent of data about the effects of physiological factors (e.g. vasogenic agents, inflammatory- and lipid-mediators) on BBB integrity (Deli et al. 2005). However, signaling routes mainly involve protein kinases, members of mitogen-activated protein kinases (MAPK) pathways, the endothelial nitric oxide synthase (eNOS), and G-proteins, ultimately leading to alterations of TJ complexes and permeability changes (Cardoso et al. 2010). The function of TJ proteins are regulated by transcriptional events, correct subcellular localization, post-translation modification, and protein-protein interaction (Huber et al. 2001).

Glucocorticoids, like hydrocortisone (HC) or dexamethasone, which are commonly known as potent immunosuppressants represent a class of powerful inductors of barrier properties of BMVEC (Dietrich 2004). At the molecular level HC induces expression of occludin and claudin-5 at mRNA and protein levels by activation of the glucocorticoid receptor (GR) and its binding to putative glucocorticoid responsive elements in the corresponding promoter (Forster et al. 2008, Forster et al. 2005, Harke et al. 2008). In contrast, tumor cell-secreted vascular endothelial growth factor (VEGF) increases microvasculature permeability by reducing occludin expression and disrupting ZO-1-occludin organization at the cell boundary (Wang W. et al. 2001). In addition to altered TJ expression pattern, it was found that phosphorylation of TJ components is also a major trigger of junctional assembly and barrier function (Gonzalez-Mariscal et al. 2008). A clear relationship between low monolayer resistance and TJ phosphorylation was first demonstrated for ZO-1 (Stevenson et al. 1989). Since that time, numerous studies have implicated multiple protein kinases (PK) including serine/threonine (Ser/Thr) kinases (e.g. PKA, PKB, PKC, and PKG), protein tyrosine kinases (PTK) as well as corresponding protein phosphatases as potent regulators of barrier function (Cardoso et al. 2010, Gonzalez-Mariscal et al. 2008). For example, recent data indicate that PKCα-dependent Ser/Thr phosphorylation of ZO-1 decreases protein-protein interaction with occludin and claudin-1, coincident with displacement of ZO-1 from intercellular boundaries and TJ opening (Goldblum et al. 2011). Others could show, that *de novo*

Ser/Thr phosphorylation of occludin and claudin-5 is induced through RhoA activation resulting in brain endothelium hyperpermeability and TJ redistribution (Stamatovic et al. 2006)

3.2.2. Astrocytes - Inductors of BBB Integrity

Astrocytes, also known as macroglia, represent the most numerous glial cell type within the CNS (e.g. 50% of cerebral cortical volume) and they feature characteristic star-shaped morphology (Magistretti and Pellerin 1996). This morphology enables astrocytes to build up many hundreds to thousands connections to neighboring cells including endothelial cells, neurons and other glia cells, thereby acting as a communication bridge between cells of the neurovascular unit (Volterra and Meldolesi 2005). In contrast to fibrous astrocytes, localized in the white matter, protoplasmic astrocytes, the quantitatively predominating class in humans, are usually organized in domains in the gray matter close to capillaries. It was shown that one cortical astrocyte is able to link five different blood vessels and eight neuronal cell bodies, suggesting pivotal responsibilities in preserving neuronal and endothelial function (Oberheim et al. 2006).

Neuronal integrity is ensured due to supportive function of astrocytes in ion and water homeostasis, delivery of energy substrates (e.g. lactate) as well as neurotransmitter production, removal and breakdown (Abbott et al. 2006, Oberheim et al. 2006, Volterra and Meldolesi 2005). Astrocytes are now generally accepted to play decisive roles in proper brain capillary differentiation (correct association of endothelial cells and pericytes in tube like structures) and in the maintenance of barrier properties of brain capillaries (Abbott et al. 2006, Ramsauer et al. 2002). Since the cerebrovasculature is almost completely (99%) ensheathed by the end-feet of astrocytes processes, the close anatomical apposition gave rise to the suggestion that astrocyte ensheathment is critical in the development of BBB characteristics (Davson and Oldendorf 1967). However, recent research indicates that astrocytes modulate the BBB phenotype by upregulation of tight junctional proteins ZO-1 and occludin in endothelial cells by means of soluble factors (e.g. transforming growth factor-β, glial-derived neurotrophic factor and angiopoetin-1) and probably not only by physical interaction (Abbott et al. 2006, Colgan et al. 2008, Siddharthan et al. 2007).

Disturbances of the complex endothelial-astrocyte interaction appear to be involved in glia-derived neoplastic pathologies like astrocytomas (e.g. glioblastoma multiforme) and numerous pathologies with an inflammatory component including stroke, brain trauma, infectious processes (e.g. sepsis,

meningitis) as well as in chronic neurodegenerative diseases (e.g. AD, PD, and MS). In the case of astrocytomas, extremely high grade of neovascularization is accompanied by a leaky vasculature that lacks BBB phenotype, either a result of a lack of inductive factors, or owing to the release of permeability factors such as VEGF (Abbott et al. 2006, Anderson et al. 2008).

Astrocytes secrete transforming growth factor β (TGFβ), which normally downregulates brain capillary endothelial expression of tissue plasminogen activator (tPA), an enzyme known to increase BBB disruption. Under pathophysiological conditions, down regulation of TGFβ is sufficient leading to tPA-mediated BBB opening (Abbott et al. 2006, Kassner et al. 2009). The role of the cytokine tumor necrosis factor α (TNFα) in inflammation-dependent BBB dysfunction is well established but indications that paracrine actions involving endothelin-1, TNFα and interleukin-1β between human astrocytes and BMVEC seem to tremendously amplify this process (Didier et al. 2003).

3.2.3. Pericytes - Not only a Regulator of Capillary Blood Flow

Pericytes were originally discovered more than 100 years ago as perivascular cells adjacent to capillaries (Zlokovic 2008). They have morphological features of smooth muscle cells. Generally, pericytes possess a prominent cell body with several processes encircling approx. 30% of abluminal membrane surface of capillaries, thereby sharing a common basement membrane with BMVEC (Allt and Lawrenson 2001). At the ensheathing process pericytes build up focal contacts and communicate with BMVEC by means of gap junctions, AJ and TJ (von Tell et al. 2006).

Properly associated pericytes contribute to barrier integrity through mechanical stabilization, synthesis and deposition of basal lamina proteins. Positive effects of pericytes on BBB phenotype were confirmed by *in vitro* data of BMVEC co-cultured with pericytes suggesting that this cell type contributes to BBB integrity, strengthening, and vascular maturation (Nakagawa et al. 2007). In fact, recently, using a set of adult viable pericyte-deficient mouse mutants, the *in vivo* evidence was provided that pericyte deficiency increases permeability of the BBB to water and a range of low-molecular weight and high-molecular weight tracers. Furthermore, these authors showed that pericytes function at the BBB in at least two ways: by regulating BBB-specific gene expression patterns in endothelial cells, and by inducing polarization of astrocyte end-feet surrounding CNS-blood vessels (Armulik et al. 2010).

Pericytes are known to communicate with BMVEC by secretion of numerous growth factors and angiogenic compounds (e.g. TGF-β, angiopoetins 1 and 2, platelet-derived growth factor-B and sphingosine-1-phosphate) (Armulik et al. 2005). Composition of soluble factors were shown to be essential in capillary assembly, BMVEC are guided by migrating pericytes, but they were also found to have pivotal roles in stabilizing or destabilizing the sprouting and regression of existing brain vessels (von Tell et al. 2006, Zlokovic 2008). Since pericytes at the BBB exhibit strong expression of smooth muscle isoform of actin (*α*-SMA, a contractile protein) this cell type was considered to regulate capillary blood flow, however, *in vivo* function remained long controversial. Nevertheless, in 2006 it was unambiguously demonstrated that pericytes, triggered by neurotransmitters noradrenalin and glutamate, are able to regulate cerebral capillary blood flow (Peppiatt et al. 2006). Therefore, it has been speculated that pericytes contributes to the development of neuropathology in hypertension, MS, AD, and CNS tumor formation (Zlokovic 2008).

3.2.4. Neurons - Neurovascular Coupling

In the awake state, the brain uses about 16% of total energy in the body for neuronal firing and cycling of γ-amino butyric acid (GABA) and glutamate neurotransmitters. Due to a lack of energy reserves, the brain requires constant blood supply (Lok et al. 2007). Given the dynamic of neural activity and considerable metabolic demands, the microcirculation must be highly responsive to the tissue it supplies (Hawkins B. T. and Davis 2005). This phenomenon has been termed neurovascular coupling. Neuronal processes that contact intraparenchymal blood vessels originate from local interneurons or from neurons whose cell bodies are located in subcortical regions (Drake and Iadecola 2007).

Until recently, it was assumed that neurovascular coupling is mediated exclusively by changes in the tone of the smooth muscles cells encircling arterioles. This idea has been challenged by the discovery that pericytes potentially regulate cerebral blood flow at the capillary level. Furthermore, it is believed that the signaling pathways controlling pericyte constriction and dilation are similar to those for arterioles (Attwell et al. 2010, Hamilton et al. 2010). In the adult CNS, neurons do not directly contact BMVEC, instead, astrocytes mediate connection between neurons and contractile elements (smooth muscle cells in arterioles and pericytes in capillaries) (Iadecola 2004). Hence, both neuronal and glial inputs would be expected to modulate microcirculation (Kim et al. 2006) but there is increasing evidence suggesting a more prominent role for astrocytes in neurovascular coupling. This is based on

the observation that synaptic release of neurotransmitters were found to induce highly specifically $[Ca^{2+}]_i$ oscillation in astrocytes triggering astrocyte-endfeet response and concomitant microvessel diameter (Takano et al. 2006, Zonta et al. 2003). Nevertheless, both neurons and astrocytes were shown to release vasoactive neurotransmitters and neuromodulators (e.g. acetylcholine, GABA, catecholamines and neuropeptides) during synaptic activity. Other neurotransmitters, such as glutamate, are not vasoactive, but stimulate the production of powerful vasodilators in endothelial cells, neurons and astrocytes, including nitric oxide (NO) and metabolites of cyclooxygenase-2 (COX2) like prostaglandins (PG) and epoxyeicosatrienoic acids (EET) (Attwell et al. 2010, Iadecola 2004). However, the final targets of these vasoactive substances whether released from endothelial cells, astrocytes, or neurons, are the smooth muscle cells in arterioles and pericytes in capillaries (Drake and Iadecola 2007).

Under pathophysiological conditions, for example following brain ischemia, when an occluding intraluminal thrombus is cleared from a blood vessel, after a short period of hyperaemia there is a decline in blood flow (or 'no-reflow phenomenon') lasting for several hours (Ames et al. 1968). Recent evidences indicate that radicals generated during re-oxygenation inhibit formation of vasodilatory prostacyclin, EETs and NO, but also induce accumulation of vasoconstricting PGH_2, altogether resulting in pericyte constriction and long-lasting blood flow decrease (Attwell et al. 2010).

3.2.5. Microglia - Intrinsic Immune Sensors and Effectors

Microglia represent the major resident innate-immunocompetent cell type in the CNS. The precise origin of these cells is a highly debated topic. It is largely hypothesized that microglia are derived from myeloid-monocytic cells and/or their hematopoietic precursors. Nevertheless, some researchers believe that they are derived from neuroectodermal matrix cells (Lynch 2009, Polazzi and Monti 2010, Tambuyzer et al. 2009). What we currently know is that microglia comprise about 20% of the glial cell population but tissue distribution seems to be heterogeneous. Highest densities are found in the hippocampus, olfactory telencephalon, basal ganglia and substantia nigra but in general, microglia are more abundant in the gray than in the white matter (Lawson et al. 1990, Polazzi and Monti 2010). From the functional point of view, microglia represent both, immune-competent cells (they are able to kill exogenous pathogens) and glia cells with neuronal-supporting functions (the actively survey the functional status of synapses) (Polazzi and Monti 2010, Wake et al. 2009).

Microglial cells have an extremely plastic, chameleon-like phenotype, and therefore the existence of this cell type was questioned for a long time period (Graeber 2010). In the absence of pathology, microglia are in the resting state characterized by a ramified structure (small bodies and long thin processes) as well as low expression of cell surface markers and immunological molecules like cytokines and chemokines. In this state microglia are sessile but studies based on *in vivo* two-photon microscopy revealed that microglial processes are highly mobile due to continuous *de novo* formation and withdrawal. Due to this highly dynamic reorganization of protrusions it is assumed that stationary microglia are enabled to thoroughly survey their environment without disturbing fine-wired neuronal structures (Hanisch and Kettenmann 2007, Nimmerjahn et al. 2005).

Microglial cells are prepared to recognize a wide range of stress signals including structures of pathogens (e.g. the bacterial membrane component lipopolysaccharide, LPS), abnormal endogenous proteins (e.g. β-amyloid, Aβ), complement factors (e.g. C1q), cytokines/chemokines (e.g. TNFα), neurotrophic factors (e.g. nerve growth factor, NGF), plasma components (e.g. albumin), neurotransmission-related compounds (e.g. glutamate), and are able to recognize signal input via bioactive lipids (Hanisch and Kettenmann 2007, Nakamura 2002).

In response to mentioned cues, as occurring in virtually all CNS pathologies, including acute and chronic events, microglia are readily activated. Highly activated microglia undergo dramatic transformation from their resting ramified state into an amoeboid morphology. This morphology facilitates typical macrophage function, such as targeted migration throughout the parenchyma toward the site of insult (‘microgliosis’: accumulation of microglia at lesions), and the phagocytosis of microbes, cell debris, or apoptotic material (Walter and Neumann 2009). Morphological alterations are also accompanied by change into an alerted state characterized by the upregulation of a variety of surface receptors (e.g. toll-like-, mannose-, and scavenger receptors), cytokine and chemokine receptors (e.g. receptors for IL-1, IFN-γ, and TNFα) as well as induced expression of several specific surface markers (e.g. Iba1, MHC-II) (Block et al. 2007, Rock et al. 2004). Additionally, activated microglia are able to generate and/or secrete a machinery of reactive oxygen/nitrogen/chlorine species (e.g. superoxide, $O_2^{\cdot-}$; peroxinitrite, ONO_2^-; hypchlorous acid, HOCl) and secretory products including cytokines/chemokines (e.g. TNFα), proteases (e.g. matrix metalloproteinases, MMP) and proinflammatory mediators (e.g. PGE_2). Together, these factors exhibit neurotoxicity, BBB breakdown and emigration of peripheral leukocytes ultimately contributing to a self-perpetuating inflammatory cycle (***Figure 5***) (Block et al. 2007, Lefkowitz and Lefkowitz 2008, Rock et al. 2004, Zlokovic 2008).

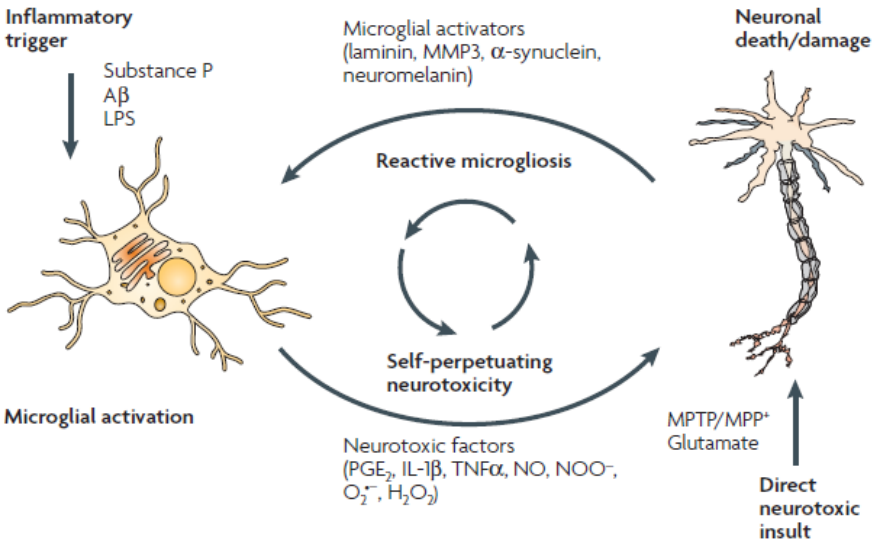

Figure 5: **Microglia drive progressive neurotoxicity.** Microglia can initiate a perpetuating cycle of neuronal damage in response to pro-inflammatory stimuli (e.g. LPS) or due to neuronal damage (e.g. $MPTP/MPP^+$) by producing neurotoxic proinflammatory factors. Aβ, amyloid-β; H_2O_2, hydrogen peroxide; IL-1β, interleukin 1β; LPS, lipopolysaccharide; MMP3, matrix metalloproteinase 3; MPP^+, 1-methyl-4-phenylpyridinium ion; MPTP, 1-methyl-4-phenyl-1,2,3,6-tetrahydropyridine; NO, nitric oxide; NOO^-, peroxynitrite; $O_2^{\bullet-}$, superoxide; PGE_2, prostaglandin E_2; TNFα, tumor necrosis factor-α (Block et al. 2007).

4. Blood-Brain Barrier Breakdown – The Vicious Cycle of Neurodegeneration

4.1. *Neuroinflammation: From Immune Privilege to Neurodegeneration*

From initial observations between the 1920s and 1950s showing that introduction of certain antigens (e.g. tumors, tissue grafts) in brain tissue do not elicit an inflammatory immune response phenotype comparable to the periphery, the concept of an 'immune privilege' of the CNS was born (Galea et al. 2007). Indeed, based on the consideration that the fragile CNS homeostasis, which is required for the proper communication of neurons, would not tolerate routine immune cell patrolling in their search for relevant antigens, certain strategies have been developed to limit the entry of peripheral immune elements as well as to limit the emergence of immune activation within the tissue itself (Amor et al. 2010, Engelhardt and Coisne 2011). Accordingly, as the CNS possesses limited regenerative capacity the inflammatory response is potentially more damaging than in the periphery (Rezai-Zadeh et al. 2009).

The immune privilege of the CNS is not wholly attributable to the presence of the BBB and is not related to the absolute absence of immunological components but rather a result of highly specialized immunities (adaptive and innate immunity) maintaining an immunosuppressive microenviroment. Therefore, the CNS is more accurately described as an immunologically specialized site rather than immunologically privileged. However, once inflammation is established a vicious cycle of innate and adaptive responses severely undermines the immune privilege of the CNS (Galea et al. 2007, Holman et al. 2011).

Neuroinflammation, *per se*, is a protective response against diverse insults, because precisely controlled neuroinflammation benefits the CNS by destroying pathogens, removing cellular debris, eliminating toxic substances, preventing spread of infections and injuries, releasing neurotrophic factors and promoting tissue repair. Regardless of the type and origin of stimuli, escaping from its tight control, the immune response can become exaggerated and destructive, and turns into chronic persistent inflammation that drives progressive neurodegeneration (Gao H. M. and Hong 2008, Wyss-Coray and Mucke 2002). The critical question is how this initial neuroinflammation is transformed into chronic and progressive neurodegeneration.

4.2. *What are the Triggers of Neuroinflammation?*

It is becoming increasingly clear that the BBB plays a crucial role in maintenance of the immune privilege of the CNS since it tightly regulates migration and infiltration of peripheral immune components into brain parenchyma. Due to the resulting immunologically insulated microenviroment the archetypal inflammatory process is initiated by endogenous immune responses causally linked to acute CNS insults (e.g. hypoxia, trauma, or environmental pathogens and toxins) or to genetic predisposition for neurodegenerative diseases (e.g. mutations in genes encoding for β-amyloid precursor- or the α-synuclein protein). As a result, noxious compounds like membrane breakdown products, abnormally processed or aggregated proteins (e.g. β-amyloid and α-synuclein), imbalanced neurotransmitters (e.g. elevated glutamate), and released/leaked cytosolic compounds elicit local neuroinflammation through a cross-talk between injured neuronal tissue and brain-resident first-line immune responders, predominantly microglia but also to some extents astrocytes (Bertram and Tanzi 2005, Gao H. M. and Hong 2008).

However, in addition to endogenous triggers, there is growing evidence that exogenous immune responses, which correspond to severe systemic inflammation in the periphery, might impact on the healthy and diseased CNS (Banks and Erickson 2010, Perry 2010, Rezai-Zadeh et al. 2009). For example, systemic application of the potent inflammogen of gram-negative bacteria LPS causes typical sepsis behavior characterized by fever, anorexia, weight loss, and reduction of activity in rodents but also progressive loss of dopaminergic neurons in the substantia nigra compacta (Ferrari and Tarelli 2011, Qin L. et al. 2007). Since the peripheral LPS passage across the BBB is low, it might induce brain inflammation indirectly (Banks and Robinson 2010).

Recently, it was reported that BMVEC express toll-like receptors (TLR) 2, 3, 4 and 6, which are essential in the recognition of pathogen-associated molecular patterns (PAMPs, highly conserved structural motifs of pathogens) like bacterial LPS, lipoproteins, lipopeptides, zymosan from fungi, and various viral DNAs and RNAs (Nagyoszi et al. 2010). Accordingly, luminal TLR4-activation on BMVEC by LPS is suggested to deliver the proinflammatory signal across the BBB directly to brain-resident immune cells, possibly through abluminal release of cytokines and lipid mediators (Cardoso et al. 2010, Perry et al. 2007). Indeed, recently it was demonstrated that TNFR1/R2$^{-/-}$ mice failed to show brain neuroinflammation in response to systemic LPS, supporting the aspect that TNFα is critical for the transfer of inflammation from the periphery to the CNS (Qin L. et al. 2007).

4.3. *Neuroinflammation – The Threshold Determines the Outcome*

Apart from the type and origin of initial inflammatory stimuli, induction of neuronal tissue injury or direct activation of innate immune response results in the same inflammatory cascades (e.g. release of inflammatory and neurotoxic factors, see *chapter 3.2.5.*), thus further exacerbating neuronal damage. For example, the neurotoxin 1-methyl-4-phenyl-1,2,3,6-tetrahydropyridine (MPTP, a by-product of synthetic heroin) is able to initiate dopaminergic neuronal death and microgliosis in the substantia nigra pars compacta causing parkinsonism in primates including humans (Langston and Ballard 1983). Since neither MPTP nor its toxic metabolite MPP^+ can directly activate microglia, inflammatory response directed to neuronal lesions is assumed to be a secondary process, initiated by danger-associated molecular patterns (DAMPs, e.g. modified proteins, heat shock proteins, chromatin, and uric acid) from damaged or stressed tissue (Amor et al. 2010, Gao H. M. et al. 2003). In contrast to MPTP, LPS initiates neurotoxicity entirely through selective activation of TLR4 in microglia and subsequent release of inflammatory mediators like NO and $O_2^{\cdot -}$ (Gao H. M. et al. 2002, Gibbons and Dragunow 2006, Qin L. et al. 2005).

Although it is far from being clear which factors might drive 'beneficial' neuroinflammation into a vicious cycle of disease progression, there is substantial evidence indicating that multiple factors including magnitude and period of insult, vulnerability of individuals, and concurrent events might decide over the outcome. Indeed, if the inflammatory response is timely and precisely regulated, (e.g. during non-severe variants of stroke, hypoxia, and trauma) and if the insult is stopped or removed, the beneficial effects of the inflammation will overcome detrimental effects. As a result, the CNS will recover from injury. In contrast, if initial insult(s) cross a certain threshold (e.g. severe acute injuries), if the insult(s) are persistent and associated with long-standing immune response activation (e.g. during neurodegenerative disorders including MS, AD, PD, HD ALS, and tauopathies) or if the regulating system of the immune response fails (e.g. anti-inflammatory cytokines 4 and 10, TGF-β, and inhibitory proteins like soluble TNFα receptor) chronic inflammation becomes established (Frank-Cannon et al. 2009, Gao H. M. and Hong 2008).

4.4. *BBB-Dysfunction – Cause, Contributor or Consequence of Neurodegeneration?*

Recent evidence indicates that, generally, the inflammatory component of neurological disorders and diseases like MS, AD, PD, meningitis, encephalitis, stroke, head trauma, AIDS-related dementia, schizophrenia, and cerebral palsy appears to play important roles in the development and/or progression of disease. Specifically, disturbances of BBB integrity/functionality due to inflammation have been implicated to be directly involved in the pathology of several neurological diseases (de Boer and Gaillard 2006, Stolp and Dziegielewska 2009). However, since accurate disease etiology and an integrative picture of disease pathogenesis is largely missing, it remains highly controversy up to now if BBB alterations/dysfunction cause the diseases, participate in its pathogenesis, or simply be a consequence of neurodegeneration (Carvey et al. 2009, Haass 2010). Nevertheless, there is emerging evidence from a variety of animal models that BBB (dys)function represents the cause, a progressor and the consequence of neural tissue degeneration.

4.4.1. BBB - Offender of Neuroinflammation

One hypothesis suggests that inflammation during brain development and aging ('first hit hypothesis') might play an important role in a number of neurological disorders most likely due to short- or long-term alterations in the structure and function of the BBB, leading immediately to neurodevelopmental disorders (e.g. cerebral palsy) or sensitizing the brain to future damage ('second hit hypothesis'; e.g. PD or AD) (Stolp and Dziegielewska 2009, Whitton 2007). For example, prolonged inflammatory response in new born rats, induced by LPS, resulted in significantly increased BBB permeability to ^{14}C-sucrose and ^{14}C-inulin in adults compared to untreated controls (Stolp et al. 2005). These findings correlate with the observation of leaky microvessels during AD, PD, MS, ALS, stroke and TBI, as a result of highly elevated VEGF levels and microangiogenesis during neurogenesis (Carvey et al. 2009, Nag et al. 2011, Seabrook et al. 2010, Zlokovic 2008). In fact, it was demonstrated that intranigral injection of VEGF causes neuroinflammation and loss of dopaminergic neurons suggesting BBB dysfunction as an early event of neuroinflammation (Rite et al. 2007).

Another example for the deleterious effects of BBB dysfunction (but not compromise) in the establishment of neuroinflammation is the pathology of MS. It is widely accepted that CNS-invasion of myelin-reactive $CD4^+$ T-cells that likely recognize a structurally similar viral antigen ('molecular mimicry') is the key pathoetiological event in MS. It has been long presumed that myelin-antigens are

insulated in the immune-privileged CNS-environment from the peripheral immune-system. However, since the finding of auto-aggressive T-cells in the peripheral blood of healthy individuals it is suggested that the pathology might be a consequence of maladaptive CNS entry of these cells (Compston and Sawcer 2002, Rezai-Zadeh et al. 2009).

4.4.2. BBB - Deterioration of Neuroinflammation

I. Leukocyte Recruitment during Inflammation. It is widely accepted that exacerbated leukocyte traffic into the CNS represents a critical stage in disease progression in a diverse range of disorders including chronic neurodegeneration, stroke, brain trauma, vasculitis, and infection (Greenwood et al. 2011). Under non-pathological conditions the number of peripheral leukocytes in brain parenchyma is low since migration and infiltration are tightly regulated at the level of the BBB (Rezai-Zadeh et al. 2009). For example, it has been estimated that immune surveillance of the brain under non-inflammatory conditions is approx. 100-fold lower compared to other tissues like spleen or heart (Greenwood et al. 2011). However, under inflammatory conditions, e.g. meningitis, leukocyte count in the CSF dramatically increases from below 5 cells mm^{-3} up to more than 1000 cells mm^{-3} (Seehusen et al. 2003).

Sites of Infiltration. Basically, it is possible to define three distinct routes of leukocyte entry into the nervous tissue. The first pathway, and perhaps the most extensively studied, is from blood into parenchymal perivascular space across the BBB (Ransohoff et al. 2003). The term BBB in the context of leukocyte infiltration can be confusing. Physiologically, the term refers to the vascular segment of the capillaries that regulate diffusion of solutes but inflammatory response primarily occurs at the level of post-capillary venules. Although post-capillary venules display morphological differences compared to capillaries (larger diameter, 50 vs. 6 µm; presence of a perivascular space; etc.), they share a variety of identical features like low permeability, formation of TJ or presence of pericytes and glia limitants. Therefore, this vessel type has been termed ‘neuroimmunological BBB’ (Owens et al. 2008). In the second pathway, leukocytes extravasate across the fenestrated endothelium to choroid-plexus stroma and further across the choroid-plexus epithelium into the CSF. A third route of leukocyte entry into the brain is represented by emigration from post-capillary venules at the pial surface of the brain into the subarachnoid space and the Virchow-Robin perivascular space (Man et al. 2007).

Diapedesis of Leukocytes. Regardless of endothelium location, leukocyte migration follows the multistep paradigm of leukocyte-endothelial interactions (***Figure 6***) at brain barriers (Greenwood et al. 2011, Man et al. 2007). Accordingly, the first step involves overcoming the shear stress of blood flow through transient cell-cell interactions mediated by L-selectins on leukocytes and E- and P-selectins on activated endothelial cells. These transient associations (tethering) result in leukocytes rolling along the vessel in flow direction giving leukocytes the opportunity to scan endothelial surfaces for luminal chemokines immobilized by proteoglycans or other moieties. Chemokine receptor activation initiates rapid conformational changes of the integrins LFA-1 and VLA-4, inducing the transition from a low to high affinity state and firm interaction with endothelial counter-receptors (e.g. ICAMs and VCAMs). Once leukocytes have arrested on endothelial surface they polarize and start to crawl through tightly regulated integrin/CAM-mediated adhesive events, finding the optimal site for transmigration. The last stage in leukocyte recruitment is diapedesis, which is the targeted penetration of vascular wall into the perivascular space (Greenwood et al. 2011, Man et al. 2007). Although leukocyte diapedesis has long been assigned to take place in paracellular manner requiring a transient disruption of inter-endothelial junctions, there is growing evidence supporting the concept of transcellular migration, most likely through filopodia-like membrane protrusions (Feng et al. 1998, von Wedel-Parlow et al. 2011, Wolburg et al. 2005).

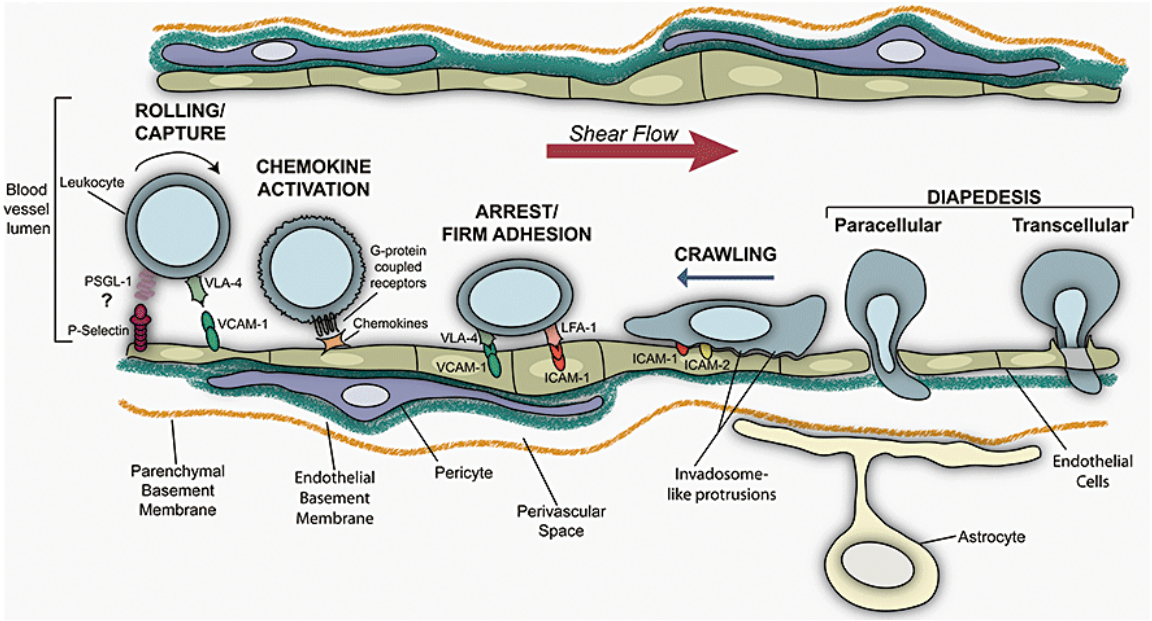

Figure 6: **Schematic representation of the major phases of leukocyte capturing by BMVEC and migration through the BBB.** ICAM, intercellular adhesion molecule; NO, nitric oxide; PECAM, platelet endothelial cell adhesion molecule; PSGL-1, P-selectin glycoprotein ligand 1; VCAM, vascular cell adhesion molecule; VLA4, very late antigen 4 (Greenwood et al. 2011).

Regulation of Infiltration. In general, leukocyte recruitment by endothelial cells is tightly regulated by expression and activity of surface molecules (e.g. selectins, integrins), which, in turn, depends on activation state of both, endothelium and leukocyte. Potent activators are pro-inflammatory cytokines (e.g. TNFα; interferon γ, INFγ; or IL1β) and other mediators, independent of cytokine signaling, like LPS (Greenwood et al. 2011, Larochelle et al. 2011, Zhou et al. 2009). For example, chronic overexpression of IL1β within the CNS using a transgenic mouse model resulted in infiltration of neutrophils, macrophages and T-cells (Shaftel et al. 2007). Moreover, intracerebroventricular injection of LPS caused TLR4/CD14- and partially MyD88-dependent neutrophil emigration into brain parenchyma while low doses of systemic LPS (0.5-2 mg/kg) induced ample neutrophil adherence in the cerebral vasculature but hardly no infiltration of surrounding tissue (Zhou et al. 2009, Zhou et al. 2006).

Secondly, approx. 50 different chemokines are considered as crucial migration regulators of cells of both, the innate and the adaptive immune system. Although about 20 different chemokine receptors are expressed on virtually every brain cell, all brain tissue chemokines are expressed by glia cells and infiltrating leukocytes (Cardona et al. 2008). However, 4 different chemokine subfamilies (CC, CXC, CX_3C and C subfamily) are essential in the recruitment of different leukocyte populations (Ubogu et al. 2006). For example, CXCL12 receptors have been reported to regulate the access of monocytes and lymphocytes to CNS parenchyma (Bleul et al. 1996). Within the CNS, the abluminal expression pattern of CXCL12 functions to retain CXCR4 and CXCR7 expressing leukocytes within the perivascular space. In the animal model of experimental autoimmune encephalomyelitis (EAE) and in human MS, CXCL12 translocates to the vessel lumen, a process that is accompanied by the release of perivascular leukocytes into parenchyma and by further recruitment of systemic leukocytes. However, infiltration of the brain parenchyma is associated with demyelination and enlarged lesion areas (Holman et al. 2011, McCandless et al. 2006). Moreover, expression and release of CXC chemokines with glutamic acid-leucine-arginine (ELR)-domain by encephalitogenic $CD4^+$ Th17-cells are essential in neutrophil-mediated development of EAE since $CXCR2^{-/-}$ mice showed a 96% reduction of neutrophil infiltration into brain parenchyma after chronic IL1β overexpression (Carlson et al. 2008, Shaftel et al. 2007).

Pharmacological Intervention of Leukocyte Infiltration. Due to above mentioned aspects mediating CNS inflammation, adhesion molecules and chemokine receptors represent attractive targets in the amelioration of neurological disorders with an inflammatory component. Strategies targeting α-4 integrins by humanized monoclonal antibody Natalizumab have been successfully used to treat MS (Ropper 2006). Other strategies, which aim to antagonize CC- and CXC- subfamilies of chemokine

receptors, are currently in phase I-III clinical trials for treating a variety of infectious-, metabolic-, neurodegenerative- and neoplastic pathologies. Interestingly, the compound SCH527123 (developed by Schering-Plough Ltd., USA), a potent antagonist for CXCR1, is currently in a Phase II clinical trial for the treatment of COPD due to two beneficial properties: On the one hand, it was shown to inhibit neutrophil chemotaxis and on the other, the compound could interfere with the release of myeloperoxidase (MPO) by leukocytes of the innate immune system (Charo and Ransohoff 2006, Gonsiorek et al. 2007, Matsushima et al. 2011).

II. BBB Dysfunction. One kind of BBB dysfunction is compromised barrier function. In disease pathology, barrier dysfunction can range from mild and transient tight junction opening to chronic barrier breakdown (Abbott et al. 2010). Carvey and colleagues (Carvey et al. 2009) suggest that BBB alterations in response to neurotoxins and during MS are not system-wide, but rather localized to small areas. However, disruption of the normal boundaries between the peripheral blood and the parenchymal compartments, as a result of physical injury, inflammatory processes and/or due to adaptations to degenerative processes (aberrant angiogenesis) are dismal. All the mentioned events peak in focal hypoxic conditions as well as in uncontrolled influx of neurotoxic xenobiotics, plasma proteins and proteases, complement factors, ions, metals, neurotransmitters, cytokines, erythrocytes and leukocytes, that are normally excluded from the brain. On the whole, barrier breakdown has detrimental outcomes: it induces/amplifies neuronal cell death and hyperactivation of the local innate immune system, it reinforces leukocyte recruitment, and it increases ROS production/lipid peroxidation. Most importantly, all these processes ultimately enhance neuroinflammation and neurodegeneration in a self-sustaining manner (Carvey et al. 2009, Larochelle et al. 2011, Zlokovic 2008).

Another kind of BBB dysfunction includes impaired detoxification capacity and anti-inflammatory capability via compromised function of efflux systems (Carvey et al. 2009). For example, it has been shown that the function of the BBB-localized detoxifying enzyme, P-glycoprotein (P-gp, ABCB1), decreases in specific brain regions with aging. However, P-gp polymorphisms have been identified as a risk factor for PD whereas P-gp deficiency at the BBB has been shown to increase Aβ-deposition in an mouse model for AD. These pathologies suggest a causal relationship between Aβ/neurotoxin clearance through BBB-located ABC-transporters and the pathogenesis of neurodegenerative diseases (Cirrito et al. 2005, Westerlund et al. 2009).

4.4.3. BBB - Victim of Neuroinflammation

To provide an effective immune response (e.g. antimicrobial activities, recruitment of additional immune cells, initiation of the adaptive immunity, and tissue repair) the initial 'danger' signal (e.g. pathogens, tissue damage) must be amplified (Glass et al. 2010).

Well-characterized subsets of key players in this scenario, either in the CNS or in the periphery, are proinflammatory cytokines (e.g. TNFα, INFγ and IL1β) (Allan and Rothwell 2001), reactive oxygen/nitrogen/chlorine species (e.g. $O_2^{\cdot-}$, ONO_2^-, and HOCl) (Barnham et al. 2004, Yap et al. 2007), and a variety of cell- and plasma-derived proinflammatory mediators including proteases (e.g. MMPs and thrombin) (Rohatgi et al. 2004, Rosenberg 2009), and vasoactive compounds (e.g. NO, histamine, and bradykinin) (Fernandez-Novoa and Cacabelos 2001, Knott and Bossy-Wetzel 2009). Additionally, it is becoming increasingly apparent that a plethora of lipid mediators originating from enzymatic or oxidative degradation/modification of glycerophospholipids (e.g. platelet activating factor (PAF), lysophospholipids (lysoPL), lysophosphatidic acid (LPA), eicosanoids, and γ-hydroxy-alkenals), sphingolipids (e.g. ceramides) and cholesterol (e.g. oxysterols) are obviously involved in the pathogenesis of neurodegeneration (Bernhart et al. 2010, Farooqui et al. 2010, Fruhwirth et al. 2007, Wymann and Schneiter 2008).

There is emerging evidence accumulating that the BMVE itself represent a central target for the action of pro-inflammatory mediators derived from luminal, abluminal or endogenous sources (Deli et al. 2005, Stanimirovic and Satoh 2000). Cellular sources of pro-inflammatory mediators include activated microglia, astrocytes, peripheral leukocytes (mainly neutrophils and monocytes/macrophages, to some extent lymphocytes and natural killer cells) but also BMVEC themselves (Larochelle et al. 2011). However, paracrine or autocrine acting mediators are able to influence barrier function of BMVEC either directly or indirectly.

For example, pro-inflammatory cytokines and ROS directly affect vascular function and integrity due to specific activation of the corresponding receptor or due to oxidative damage of cellular molecules. However, these processes result in the induction of intracellular signaling cascades like MAPK-pathways. Mentioned signaling events are typically accompanied with cytoskeletal reorganization as well as with altered protein expression, phosphorylation, and distribution of AJ- and TJ-associated proteins (Gonzalez-Mariscal et al. 2008, Kallmann et al. 2002, Sprague and Khalil 2009). Moreover, cytokine-promoted opening of the BBB has been linked to protein degradation of TJ and the basal

lamina. Searching for the underlying mechanisms, consecutive studies could demonstrate that MMPs play an important role in this kind of BBB disruption (Forster 2008, Rosenberg 2009).

An increase in oxidative stress can also lead to oxidative damage of cellular components including proteins and lipids. For instance, exogenously added 4-hydroxy-2-nonenal (4-HNE), the major product of arachidonic acid (AA) peroxidation, adversely affects BBB integrity (Mertsch et al. 2001). Most importantly during neuroinflammation, cytokines and ROS induce enzymes involved in degradation of (ether)phospholipids such as phospholipases A_2 (PLA_2) leading to liberation of polyunsaturated fatty acids (predominantly AA) and to formation of the remnant lysoPL (Jensen et al. 2009, Ong et al. 2010). Subsequent processing of degradation products mainly via cyclooxygenase 2 (COX2), 5-lipoxygenase (5-LOX), lysophosphatidyl choline acetyltransferase (LPCAT), and autotaxin (ATX) result in the formation of PG, leukotriens, PAF and LPA (Stanimirovic and Satoh 2000). However, all these lipid mediators have been implicated to induce changes of the BBB permeability predominantly via engagement of G-protein coupled receptors (GPCR) and activation of downstream signaling events (Fang et al. 2011, Fukumoto et al. 2010, Nitz et al. 2003, Wang M. L. et al. 2006). Nevertheless, we are just at the beginning to understand the diversity of pro-inflammatory lipid mediators and how they mediate the process of BBB dysfunction.

5. Myeloperoxidase (MPO) - Friend and Foe

5.1. *Phagocytes - Mechanisms of Host-Defense and Tissue-Destruction*

The 'first line defense' against infectious agents or 'nonself' substances that penetrate the body's physical barriers is constituted by the innate immune system, especially by phagocytes (Smith J. A. 1994). The term phagocyte originates from the ability to ingest microbes (e.g. bacteria, fungi, protozoa, and viruses). Thereby, opsonized (via immunoglobulins and/or complement) or non-opsonized invaders are engulfed into a structure called phagosome and subsequently killed by a bombardment with oxidants and contents of intracellular granules (Lee et al. 2003). In addition to host defense, phagocytes have also a pivotal role in the resolution of inflammation, thus protecting tissue from harmful exposure to inflammatory and immunogenic contents of dying cells (Kantari et al. 2008, Maderna and Godson 2003).

In humans, based on the total number of circulating leukocytes (approx. 10^7 cells/ml), the quantitatively most important phagocyte populations are represented by neutrophil granulocytes (50-70%) and monocytes (approx. 6%). Nevertheless, circulating leukocyte populations display marked species differences. For example, the circulating leukocyte profile for rodents is considered to be much less (approx. 70%) neutrophilic as it is for humans, although total numbers of leukocytes are nearly equal (Haley 2003).

Neutrophils and monocytes/macrophages share several characteristics like the arsenal of antimicrobial mechanisms (e.g. oxidants, some granule proteins, and iron-withholding enterobactins), the expression of cell surface receptors as well as the secretion of cytokines and chemokines. But generally, the antimicrobial capacity of neutrophils is much higher since monocytes/macrophages lack several antimicrobial granule proteins (e.g. elastase, cathepsin G and lactoferrin) and the metabolic burst is less extreme (Dale et al. 2008, Silva 2010).

Under non-pathological conditions macrophages are the main scavenger phagocytes, efficiently removing erythrocytes, dead cells and cell debris. Therefore, neutrophils are rare in the tissues and body cavities; they are present as quiescent cells in blood and bone marrow. By contrast, during infection or tissue destruction, when the scavenging capacity of macrophages is overwhelmed, immediate response of neutrophils ('first infiltration wave') represents a powerful backup (Mosser and Zhang 2008, Rydell-Tormanen et al. 2006).

Until a few years ago, neutrophils were thought to employ essentially two major strategies to encounter invaders. The first strategy is represented by phagocytosis (*see above*). The second line of attack embraces the extracellular release of antimicrobial agents. If a phagocyte fails to engulf its target (e.g. if the target is too large) or if the cell becomes over-activated ('primed') due to the presence of inflammatory stimuli (e.g. TNFα, LPS, IL8, and adhesion), the non-specific noxious machinery of neutrophils is externalized. This process, termed degranulation, has been implicated as a major causative factor of tissue damage (Cowburn et al. 2008, Klebanoff 2005, Lacy 2006).

Recently, a third strategy was uncovered by Brinkmann and colleagues. They demonstrated that as early as 10 min after stimulation with phorbol myristate acetate (PMA), LPS or IL8 neutrophils displayed prominent extracellular web-like structures composed of decondensed chromatin decorated with cytoplasmic and granule proteins including MPO, NADPH oxidase, elastase, MMP9, and cathepsin G (***Figure 7***). These neutrophil extracellular traps (NETs) are suggested to be highly effective in pathogen killing most probably due to a combination of microbe immobilization and providing high local concentrations of antimicrobial components (Brinkmann et al. 2004, Papayannopoulos and Zychlinsky 2009). However, recent data indicate that the interaction of neutrophils with LPS- or TNFα activated platelets or endothelial cells induce NET formation which concomitantly triggers the damage to endothelium during sepsis and small vessel vasculitis (Clark et al. 2007, Gupta et al. 2010).

In summary, the abundance of neutrophils and the unspecific biocidal potency of oxidants/azurophilic granules make the activated neutrophil a dangerous cell that must be tightly controlled (Silva 2010)

5.2. *Oxidative stress - Multiple Sources for a Variety of Species*

The brain is known to possess the highest oxygen turnover of any organ in the body. Although it contains high levels of both, polyunsaturated lipids and redox-active metal (e.g. free iron), the classical antioxidant capacity is considered to be rather low. This makes the brain particularly vulnerable for oxidative insults. In fact, there is an emerging body of evidence showing that oxidative stress at least contributes to the pathogenesis of neurodegenerative diseases (Halliwell 2001, Sayre et al. 2008).

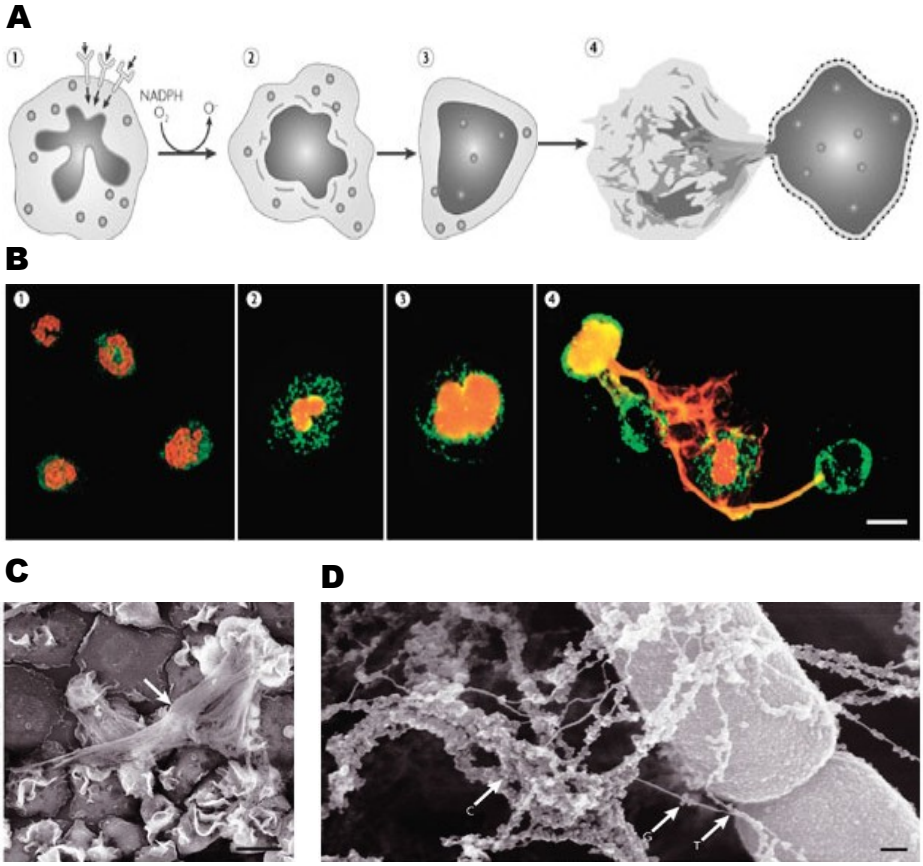

Figure 7: **Formation of Neutrophil Extracellular Traps (NETs).** (**A**) Schematic representation showing the steps involved in NET formation. (**B**) Fluorescent micrographs showing the steps of these events (green, neutrophil elastase; red, histone-DNA complex). Activation of neutrophils leads to the formation of ROS (1). The nuclear membranes disintegrate and the integrity of the granules is gradually lost (2). Nuclear material fills most of the cell, mixing with the contents of the granules (3). During the final stage, the cells round up, contract and finally release NETs (4). (**C**) Scanning electron micrograph (SEM) showing stimulated neutrophils forming NETs (as indicated by the arrow). (D) SEM showing a detailed view of NETs trapping Shigella flexneri. The 'threads' (T), globular domains (granule proteins, G) and cables (chromatin, C) are indicated (Brinkmann and Zychlinsky 2007).

5.2.1. H_2O_2 - Essential Precursor for the MPO System

It had been suggested that all metabolically active cells in the CNS generate ROS in low quantities since about 2% of oxygen consumed by mitochondria is converted to $O_2^{\cdot -}$ (Votyakova and Reynolds 2001). However, during neurodegeneration disproportionate production of ROS is primarily caused by

mitochondrial complex I (NADH dehydrogenase) and complex III (ubiquinone Q-cytochrome b) (Adam-Vizi 2005). With regards to endothelial cells, $O_2^{\cdot -}$ additionally arises as products of enzymatic systems like vascular NAD(P)H oxidase (vNOX) and, under special circumstances, NOS or as byproducts of AA (PGH synthase and lipoxygenases) and purine base (xanthine oxidase) metabolism (Kukreja et al. 1986, Madamanchi et al. 2005).

Under normal conditions, $O_2^{\cdot -}$ generation is considerably low and non-toxic for cells. ROS at moderate concentrations function as signaling molecules, involved in regulatory processes e.g. regulation of the cerebral vascular tone (Faraci 2006). By contrast, highly elevated ROS formation of non-phagocytotic cells was found to contribute in several pathologic settings (e.g. BBB dysfunction during stroke). However, measurable $O_2^{\cdot -}$ production by BMVEC is by far lower compared to $O_2^{\cdot -}$ production by activated phagocytes (Kahles et al. 2007, Li J. M. and Shah 2003). In phagocytes, formation of $O_2^{\cdot -}$ is predominantly catalyzed by the NAD(P)H oxidase complex [Eq. 1] during the oxidative burst, an event likely yielding in millimolar quantities, high enough to ensure efficient invader killing. Moreover, it was shown that in response to an Aβ challenge $O_2^{\cdot -}$ levels highly depend on the type of phagocyte (neutrophils >> monocytes > microglia) (Bianca et al. 1999).

$$2O_2 + NADPH \rightarrow 2O_2^{\cdot -} + NADP^+ + H^+ \qquad \text{[Eq. 1]}$$

The phagocytic NADPH oxidase (PHOX) consists of two integral membrane proteins, $p22^{phox}$ and $p91^{phox}$ and four cytosolic components: $p47^{phox}$, $p67^{phox}$, $p40^{phox}$, and the small GTPase Rac (Wilkinson and Landreth 2006). Phagocytosable particles (e.g. bacteria, yeast), chemotactic factors (e.g. formylated tripeptide, fMLP) as well as bioactive compounds (e.g. phorbol ester, PMA; AA; and diacyl glycerols) were shown to induce the respiratory burst. This process is initiated by protein kinases like PKC, p21-activated kinase-1 (PAK1), MAPK, Akt, or phosphatidylinositol-3 kinase (PI3K). However, these kinases mediate phosphorylation of $p47^{phox}$ and/or $p67^{phox}$, which results in the subsequent translocation of cytosolic components to the plasma membrane (Robinson 2009).

As demonstrated by patients suffering from chronic granulomatous disease (CGD, a disorder characterized by repeated, severe, bacterial and fungal infections), defects in $O_2^{\cdot -}$ production due to mutations in the PHOX subunits tremendously impact on the functionality of the innate immune system (Curnutte et al. 1974, Segal et al. 2000).

Within the normal cellular environment (aqueous, physiological pH) $O_2^{\cdot-}$ reacts rather sluggish with biologically important molecules. This leads to the suggestion that $O_2^{\cdot-}$ by itself is non-toxic to pathogens. In contrast, chemical reactivity of $O_2^{\cdot-}$ is considerably increased at acidic pH or within a non-polar environment through formation of the hydroperoxyl radical ($HO_2^{\cdot}$), as being present within the phagosome and hydrophobic regions of biomembranes. However, $O_2^{\cdot-}$ is readily dismutated, either spontaneously or catalyzed by the phagocytic enzyme superoxide dismutase (SOD), into O_2 and H_2O_2 [Eq. 2] (Klebanoff 2005).

$$2O_2^{\cdot-} + 2H^+ \rightarrow 2H_2O_2 \qquad \text{[Eq. 2]}$$

5.2.2. The MPO-H_2O_2-Halide System - Source of Highly Destructive Oxidants

Since exogenously generated $O_2^{\cdot-}$ does not kill bacteria directly and H_2O_2 is only bactericidal at high concentrations (mM range) there is biological demand for a much more potent antimicrobial system. Among the microbiocidal systems in phagocytes the MPO-H_2O_2-halide system seems to be one of the most powerful, as MPO-derived oxidants are reported to be 100-fold more toxic than H_2O_2 (Hampton et al. 1998, Handa et al. 2010, McKenna and Davies 1988).

The heme-containing enzyme MPO (EC 1.11.1.7) is highly expressed in neutrophils (2-5% of total cellular protein), less in monocytes. Unlike tissue macrophages in the periphery, which are not positive for MPO, microglia rarely express this protein. Final processed MPO, stored in azuorophilic granules, is a highly cationic and glycosylated protein with a molecular mass of 146 kDa. It is a tetramer comprised of a heavy chain (58.5 kDa) dimer and light chain (14.5 kDa) dimer joined by single disulfide bridge (Lefkowitz and Lefkowitz 2008, Malle et al. 2007).

In combination with H_2O_2, MPO is able to oxidize halides (X^-, Cl^-, Br^-, and I^-) and pseudohalides (e.g. thiocyanate, SCN^-) to their corresponding hypo(pseudo)halous acid (HOX) [Eq. 3]. Additionally, nitrite (NO_2^-) and a range of phenols (e.g. tyrosine) can also become oxidized thereby forming radical species like nitrogen dioxide ($NO_2\bullet^-$), or phenoxyl radicals (***Figure 8***). Generally, the oxidation process is initiated by the reaction of the Fe(III), at the catalytic heme, with H_2O_2. Consequently, a highly reactive oxoiron(IV) intermediate containing a porphyrin π-cation radical [Fe(IV=O) $Por\bullet^+$] is formed

(compound I). Once produced, compound I mediates either halogenation or peroxidation by one- or two electron oxidation reactions (Dolphin et al. 1971, Malle et al. 2007).

$$H_2O_2 + X^- + H^+ \rightarrow HOX + H_2O \ (X^- = Cl^- , Br^-, I^- \text{ or } SCN^-) \qquad \text{[Eq. 3]}$$

Under physiological conditions (pseudo)halogen oxidation is the principal reaction of the MPO-H_2O_2 system. In biological fluids like plasma, there is a more than 1000 fold molar excess of Cl^- (100-140 mM Cl^-) compared to other (pseudo)halogens (20-100 µM Br^-, 20-120 µM SCN^-, < 1 µM I^-). Even though Cl^- is the predominant substrate for the MPO-H_2O_2 system, the exact nature of species formation is still a matter of debate, since Cl^- is a low affinity substrate for MPO compared to other anions (1:60:730 for Cl^-, Br^-, and SCN^-). However, it has been estimated that about 45-80% of the H_2O_2 generated by activated neutrophils is used to form 20-400 µM HOCl per hour. Remaining H_2O_2 is largely converted to HSCN, only a small quantity (< 5%) to HOBr and HOI (Hawkins C. L. 2009, Malle et al. 2006a, Yap et al. 2007).

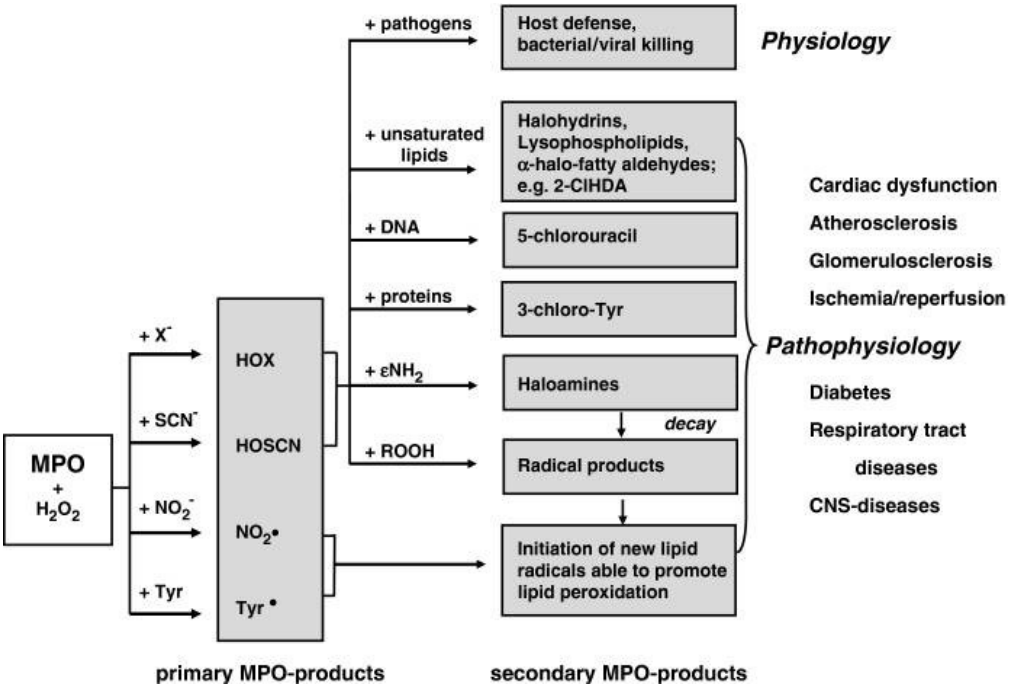

Figure 8: Primary and secondary MPO-reaction products and (patho)physiology (Malle et al. 2007)**.**

5.3. *HOCl-Attack of Biomolecules - Profound Potential to Damage Host Tissue*

The powerful antimicrobial nature of HOCl has been well documented (Hampton et al. 1998, Klebanoff 2005, Winterbourn et al. 2006). At physiologic pH, HOCl is believed to be in the equilibrium with its conjugated base hypochlorite (OCl^-) [Eq. 4]. In fact, OCl^- is the active ingredient in household bleach and the species responsible for the microbiocidal properties of chlorinated water supplies (Pullar et al. 2000). Under acidic conditions, as present in the phagolysosome, the protonated equivalent predominates. Moreover, in phagolysosomes, HOCl is also in equilibrium with chlorine gas (Cl_2) via a reaction that requires Cl^- and H^+ [Eq. 5] (Podrez et al. 2000). Several studies demonstrated that Cl_2 potentially executes oxidation/halogenation reactions normally ascribed to $HOCl/ClO^-$ (Albert et al. 2001, Hazen et al. 1996, Henderson et al. 1999).

$$HOCl \leftrightarrow H^+ + OCl^- \qquad pK_a = 7.4 \qquad \text{[Eq. 4]}$$

$$HOCl + Cl^- + H^+ \leftrightarrow Cl_2 + H_2O \qquad pK_a = 3.3 \qquad \text{[Eq. 5]}$$

All these primary oxidants generated via the $MPO/H_2O_2/Cl^-$ system are highly reactive, short-lived compounds with the ability to oxidize any susceptible group in any biological substrate (van der Veen et al. 2009). Nevertheless, rates of most reactions are markedly pH dependent as different protonation states of the oxidant ($HOCl/OCl^-$) as well as of the target molecules critically impact on reactivity (Pattison and Davies 2006).

Up to date, there is no known enzymatic scavenging mechanism for $HOCl/OCl^-/Cl_2$. The major scavengers in biological systems appear to be based on antioxidants containing thiol-groups (e.g. glutathione (GSH) and taurine) given that other antioxidants like ascorbate, phenols and hydroquinones are likely to be uncompetitive with cellular components as a result of their abundance and the high reactivity of chlorinating oxidants (Yap et al. 2007).

Since $HOCl/OCl^-$ concentrations can reach up to 5 mM at inflammatory sites there is compelling evidence that the presence of MPO is causally linked to tissue damage due to modification of biomolecules, most importantly amino acids, proteins, and lipids but also nucleobases (***Figure 8***), and carbohydrate components (Davies et al. 2008, Weiss 1989).

5.3.1. Proteins: Preferred Targets for HOCl-Modification

Proteins are likely to be the main targets of oxidation by HOCl due to their high abundance and the high reaction rate constants with this oxidant (up to 3.8 x 10^7 M^{-1} sec^{-1}). Thus, there is increasing evidence that HOCl-mediated modification of amino acids, peptides, and proteins contribute to tissue damage and dysfunctional lipoprotein metabolism (Davies 2011, Nicholls and Hazen 2009, Pattison and Davies 2006). For example, the impaired ability of HOCl-oxidized high density lipoprotein (HDL) to participate in reverse cholesterol transport was ascribed to modification of apolipoproteins (apo), mainly apoAI (Bergt et al. 1999, Marsche et al. 2002, Panzenboeck et al. 1997). Additionally, HOCl modification was shown to impair the activity of HDL-associated antiatherogenic enzymes, including phospholipid transfer protein (PLTP), lecithin cholesterol acyltransferase (LCAT), and paraoxonase (Malle et al. 2006b).

Treatment of proteins with HOCl results in modification of amino acid side chains and backbone amides as well as protein dimerization/aggregation, and fragmentation, events ultimately accompanied by enzyme inhibition and/or loss of structural function (Bergt et al. 2000, Hawkins C. L. et al. 2003). The order of reactivity at physiological pH (pH 7.4) was found to be: Methionine > cysteine >> cystine ~ histidine ~ α-amino group > tryptophan > lysine >> tyrosine ~ arginine > backbone amides > asparagine/glutamine (Pattison and Davies 2001).

Initial products of HOCl modification are mostly chlorinated, unstable residues that likely retain oxidizing capacity of HOCl. For example, exocyclic (e.g. α- and ε-amino group of lysine) and endocyclic (e.g. imidazole group of histidine) chloramines are able to induce secondary oxidation damage, only 5-50 times slower as compared to the primary oxidant HOCl itself. In the presence of low-valent redox-active metal ions (e.g. Fe^{2+} or Cu^{+}), chloramines (essentially lysine-derived) readily decompose to give rise of highly reactive, nitrogen-centered radicals. In absence of further oxidizable substrates, chloramines located at the α-amino group hydrolyze, via imine intermediate, to give aldehydes which can further generate Schiff bases with amino groups of proteins or lipids (Pattison and Davies 2005, 2006). Conversely, reaction of HOCl with aromatic side chains (e.g. tyrosine) is more than 10^5 times slower compared to the reaction with thiol containing residues but it results in the formation of rather stable chlorinated products. The preferred marker for HOCl formation *in vivo* is 3-chlorotyrosine, although the slow reaction rate constant (50 M^{-1} sec^{-1}) implies that if this product is observed, extensive damage has occurred (Curtis et al. 2011, Davies et al. 2008).

5.3.2. Chlorinated Lipids: Appearance During Neuroinflammation?

Halogenated lipids, especially halogenated fatty acids, are naturally occurring in considerable amounts in wide range of organisms including bacteria, fungi, soil biota, algae, marine invertebrates, higher plants and some animals. Flavin-halogenases and haloperoxidases are thought to be the natural source of halogenated compounds. On the other hand high concentrations of chlorinated lipids (e.g. dichlorostearic acid) were found to be connected to anthropogenic inputs as detected in the vicinity of pulp mills due to Cl_2-bleach containing effluents (Dembitsky and Srebnik 2002, van Pee et al. 2006). Nevertheless, formation of halogenated lipids in mammalian systems cannot be considered as a normal physiological process but more as damaging process during adverse conditions.

Phospholipids, fatty acids, sterols and sphingolipids comprise multiple targets that are susceptible to oxidants derived from the MPO-H_2O_2-Cl^- system. These targets include primary amine groups present in ethanolamine and serine glycerophospholipids, alkenes in aliphatic residues of esterified and non-esterified fatty acids, as well as double bonds in the gonane and sphingosine backbone of cholesterol and sphingolipids (***Figure 9***) (Ford 2010, Nusshold et al. 2010, Spickett 2007). In contrast to relatively inert phosphoryl-choline, the second order rate constants for the reaction of HOCl with phosphoryl-ethanolamine and phosphoryl-serine are similar to those of other biological amines (approx. 10^4 M^{-1} sec^{-1}). Consequently, phospholipid headgroup oxidation results in the formation of chloramines, dichlorinated amines, chlorimines, aldehydes and nitriles (***Figure 9 B*** and ***C***) (Flemmig and Arnhold 2010, Flemmig et al. 2009, Richter et al. 2008).

Some of these compounds as well as corresponding decay products (e.g. nitrogen-centered radicals) are potent inducers of secondary damage, particularly through initiation of lipid peroxidation or covalent damage of proteins/lipids (e.g. via chlorination, Schiff base formation) (Kawai et al. 2006). By contrast, reaction of HOCl with double bonds in the aliphatic hydrocarbon chain of fatty acids, in the B-ring of cholesterol, and in the sphingosine backbone of sphingomyelin were demonstrated to generate comparatively stable products including chlorohydrins, epoxides, and mono/dichlorinated compounds (***Figure 9 A***) (Carr et al. 1997b, Hazen et al. 1996, Nusshold et al. 2010, Panasenko et al. 2003). Multiple adjacent double bonds of polyunsaturated fatty acyl-chains can be entirely modified but increasingly modified residues tend to be instable thereby generating lysophospholipids (Arnhold et al. 2002). Generally, lipid chlorohydrins were shown to be toxic to dopaminergic neurons, endothelial cells, erythrocytes, and myeloid cells. This is most probably due to necrotic (e.g. ATP-depletion, cell

membrane damage), and apoptotic (e.g. increased caspase-3; poly (ADP-ribose) polymerase, PARP activity) mechanisms as well as due to other mechanisms like proteome alterations and ROS formation (Carr et al. 1997a, Dever et al. 2003, Dever et al. 2006).

However, in complex biological systems, the reaction of HOCl with lipid double bonds is kinetically unflavored (k_2: 9 M^{-1} sec^{-1}), thus it is questionable whether this chlorinated lipid species might occur in physiologically significant concentrations under *in vivo* conditions (Pattison et al. 2003, Spickett 2007). Up to now, there is only one study demonstrating that chlorohydrins are present *in vivo* (Messner et al. 2008b). In contrast to phospholipid chlorohydrins, there is emerging evidence that plasmalogen-derived oxidation products of HOCl, namely α-ClFALDs (*see chapter 6.2.*), are present in tissue under inflammatory conditions (Ford 2010).

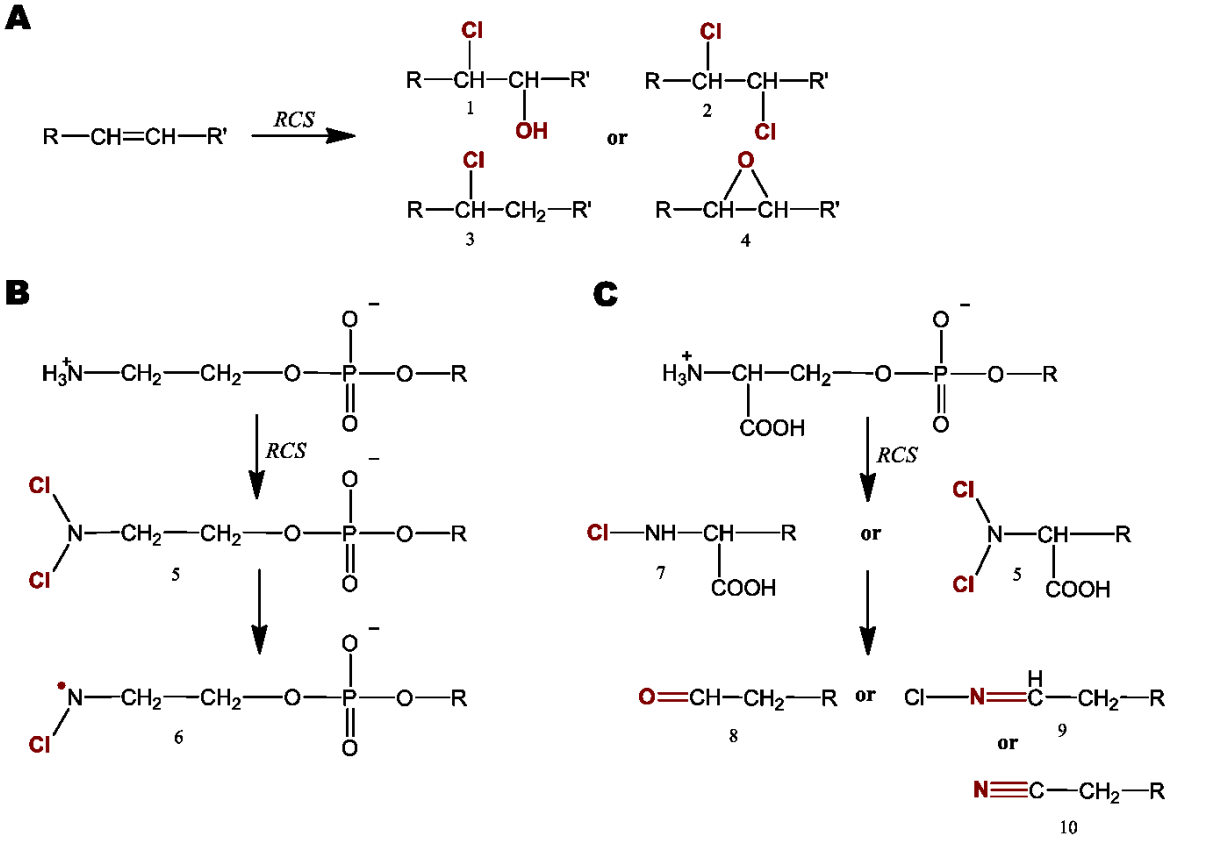

Figure 9: **Formation of various phospholipid oxidation products following reaction with MPO-derived RCS**
(**A**) Reaction with double bonds within the aliphatic chain results in the formation of chlorohydrins (1), mono- (3) or dichlorinated species (2) and epoxides (4). (**B**) The conversion of phosphoryl-ethanolamine headgroup via a dichloramine (5) leads to an N-centered radical (6). (**C**) Transient monochloramine (7) or dichloramine (5) formation of phosphoryl-serine headgroup is followed by a generation of corresponding aldehyde (8), chlorimine (9) or nitrile species (10).

6. The Crucial Role of Lipids in the CNS

The brain contains the second highest lipid content of any other organ in the body, after adipose tissue (Leskovjan et al. 2010, Sastry 1985). However, adipose tissue utilizes lipids for energy storage, while lipids have critical roles in the nervous system: Nervous structures like synaptic complexes and myelin are characterized by unique lipid composition contributing to their specialized properties (Siegel et al. 2006). Early investigations of Rossiter, Sampson and coworkers have determined the nature and approximate concentrations of many of the major lipid classes including glycerophospholipids, sphingolipids, cholesterol and cerebrosides in different areas of the brain. Thereby, they could demonstrate different lipid contents and lipid compositions of gray and white matter in healthy human brain tissue (Johnson et al. 1949, O'Brien and Sampson 1965).

Mammalian cell membranes are mainly constituted by glycerophospholipids, sphingolipids, and cholesterol. Due to specific physical properties of each constituent, changes of lipid composition induces altered membrane fluidity and altered biological function e.g. permeabilities of transport proteins and activities of membrane-bound enzymes (Sonnino and Prinetti 2010, Spector and Yorek 1985). Biological membranes are held together by hydrophobic-, coulombic-, and van der Waal forces as well as by hydrogen bonds. The number of unsaturated carbon-carbon bonds in the aliphatic groups at the *sn-1* and the *sn-2* position of the glycerophospholipid is a key factor in determining lateral diffusion velocity of membranes, thus playing important roles in events such as endo- and exocytosis, sorting of lipids, or membrane fusion (Farooqui and Horrocks 2007). It is known that in membrane compartments enriched with sphingolipids and cholesterol, fluidity is dramatically decreased resulting in the formation of nanoscale assemblies, which are referred to as lipid rafts (Korade and Kenworthy 2008, Lingwood and Simons 2010).

Emerging evidence also indicates the importance of lipid rafts in acting as signaling platforms of neurotrophic factors (e.g. neurotrophins), neuronal cell adhesion, axon guidance and synaptic transmission (Tsui-Pierchala et al. 2002). On the other hand, analysis of the molecular species of glycerophospholipids derived from cerebral cortex could show that synaptosomal plasma membranes (SPM) contain more polyunsaturated fatty acids than myelin (Farooqui and Horrocks 2007). Taken together, differences in lipid composition are most likely a reflection of different functions of cellular membranes in the nervous system: High membrane fluidity in neurons of the gray matter promote

membrane fusion, important for neuronal function, while relatively more rigid membranes of oligodendrocytes provide further support for axonal myelin integrity in the white matter (Bazan 2005).

However, there is rising evidence that lipids of the CNS have functions beyond representing structural components in neural membrane organization. They are dynamic molecules with specific distribution and catabolism as a result of highly regulated processes during biological responses (Farooqui and Horrocks 2007). In neurons, glia, and endothelial cells of the cerebrovasculature, several phospholipid pools are increasingly being recognized as reservoirs of bioactive mediators (Bazan 2003). Upon stimulation by neurotransmitters, neurotrophic factors, cytokines, membrane depolarization, ion channel activation, etc. specific phospholipases initiate the formation of various lipid messengers (Eyster 2007, Sang and Chen 2006). Multiple signaling pathways, activated by lipid intermediates, ultimately contribute to a broad spectrum of CNS responses including development, differentiation and stress response (Bazan 2005, Siegel et al. 2006).

Finally, posttranslational modification of proteins is a key mechanism in the regulation of protein localization and function. Regulated by physiological stimuli proteins are modified enzymatically by covalent attachment of various lipid species including isoprenoids (farnesyltransferase and geranylgeranyltransferases), and fatty acids like myristic acid or palmitic acid (myristyltransferase and palmitoyltransferase) as well as non-enzymatically by electrophilic lipids generated during PG synthesis (e.g. 15-deoxy-Delta^{12,14}-PGJ_2) or lipid peroxidation (e.g. 4-HNE or acrolein) (Linder 2008, Perez-Sala 2007, Selvakumar et al. 2002)

6.1. *Plasmalogens - Important Lipids for CNS Function*

Plasmalogens (pPL) constitute a class of glycerophospholipids (PL) characterized by an alkenyl chain in the *sn*-1 and an acyl-chain in the *sn*-2 position of the glycerol backbone. The alkenyl-moieties are almost exclusively constituted by C16:0, C18:0, and C18:1 hydrocarbon chains, while the *sn-2* position is predominately esterified with ω-3 or ω-6 derived polyunsaturated fatty acids. The *sn*-3 position is adorned by a headgroup, either ethanolamine or choline, attached through a phosphodiester linkage. Any PL displaying a *cis* double bond on the *sn*-1 alkyl-chain, adjacent to the ether bond ('vinyl-ether linkage'), is referred to pPL (Nagan and Zoeller 2001, Wallner and Schmitz 2011).

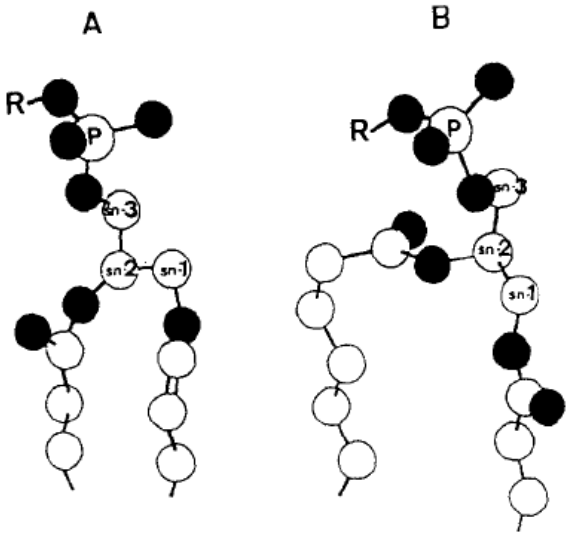

Figure 10: Structure of (**A**) choline plasmalogens and (**B**) choline glycerophospholipids (Lohner 1996)

pPL are ubiquitously found in considerable amounts as constituents of mammalian membranes in tissues as well as in plasma lipoproteins where they comprise about 20% of total PL in humans. Human heart, brain, inflammatory cells, and spermatozoa contain, with up to 50%, by far the highest amounts of plasmalogens. Ethanolamine plasmalogens (pPE) are ten times more abundant than choline plasmalogens (pPC) except in cardiac and skeletal muscles (Lessig and Fuchs 2009).

Ether phospholipids display a different molecular structure compared to their diacyl analogs (***Figure 10***): First, the perpendicular orientation of the *sn-2* acyl chain at all segments to the membrane surface results in an extended conformation and effectively longer aliphatic chain. Second, the lack of the carbonyl oxygen in position *sn*-1 affects the hydrophilicity of the headgroup and allows stronger intermolecular hydrogen-bonding between the headgroups of these lipids. Above-mentioned properties are thought to affect membrane fluidity by favoring the formation of non-lamellar structures, which is biophysically important for the regulation of membrane processes (Lohner 1996). Membrane dynamics may have significance to a plethora of cellular processes including membrane fusion (e.g. endocytosis and secretion), ion transport, intra- and extra-cellular signaling, and proper function of transmembrane proteins (Nagan and Zoeller 2001, Wallner and Schmitz 2011).

In mammals pPL synthesis depends on the peroxisomal enzymes dihydroxyacetonephosphate synthase (ADAPS) and dihydroxyacetonephosphate acyltransferase (DHAPAT). Accordingly, pPL levels are

substantially reduced in disorders based on defects in peroxisomal assembly like the Zellweger syndrome. In fact, phenotype analysis of ether-lipid deficient ($DHAPAT^{-/-}$) mice revealed a severe impairment of CNS development indicating the crucial role of plasmalogens in CNS function (Gorgas et al. 2006, Rodemer et al. 2003).

Over the last 2 decades, an increased interest has arisen with respect to antioxidative properties of plasmalogens towards a variety of stressors including singlet oxygen ($^1O_2$), $O_2^{\cdot-}$, H_2O_2, peroxy radicals, transition-metal ions, halogenating species (*see chapter 6.2.*), and UV light. This antioxidative capacity has been mainly attributed to the unique susceptibility of the vinyl-ether bond to oxidative damage due to low bond dissociation energies ('bait function') but also to the ability to bind metal ions ('chelating function'). However, the view that pPL protect against oxidative damage remain controversially since the formation of highly reactive, long chain α-hydroxy fatty aldehydes as result of vinyl-ether oxidation was demonstrated (Engelmann 2004, Loidl-Stahlhofen et al. 1995, Murphy R. C. 2001).

Brain tissue pPL form a precursor pool for plasmalogen-selective phospholipase A_2 ($pPLA_2$) hydrolysis. Receptor-mediated activation of plasmalogens by $pPLA_2$ results in the generation of potent lipid mediators (e.g. AA, lysoPL, eicosanoids, and PAF), which are known to mediate nociception, neuroinflammation, oxidative stress and neurodegeneration (Farooqui 2010, Ong et al. 2010). However, there is compelling evidence indicating that decreased plasmalogens levels in the brain can be considered as an indicator for the extent of inflammation during several neuropathological conditions, independent of the underlying mechanisms (Wallner and Schmitz 2011).

6.2. *α-Chloro Fatty Aldehydes - Plasmalogens under HOCl Attack*

In 2001, Ford and coworkers revealed that the vinyl-ether bond of plasmalogens is susceptible towards oxidation by HOCl or Cl_2. Using mass spectrometry and NMR they demonstrated that modification of 1-*O*-hexadec-1-enyl-2-octadec-9-enoyl-*sn*-glycero-3-phosphocholine (C16:0-pPC) with RCS (***Figure 11***) gives rise to the formation of an α-chloro fatty aldehyde (α-ClFALD), namely 2-chlorohexadecanal (2-ClHDA) and the remnant lysophospholipid 2-octadec-9-enoyl-*sn*-glycero-3-phosphocholine (C18:1-lyso-PC) (Albert et al. 2001, Ford 2010). Subsequent studies showed that primarily fMLP or PMA-stimulated neutrophils, and to a lesser extent monocytes, are potent sources of 2-ClHDA and 2-chlorooctadecanal (2-ClODA) generated by RCS modification of the endogenous C16- and C18-plasmalogen pools. These studies also suggested that phagocyte-derived HOCl has the potential to

impact on plasmalogen pools in the local neighborhood including those of endothelial cells, and lipoprotein particles. Moreover, heme enzyme inhibitors like 3-aminotriazole (3-ATZ) and sodium azide (NaN_3) prevented the formation of 2-ClHDA (Marsche et al. 2004, Thukkani et al. 2002, Thukkani et al. 2003b).

Recent data of Davies and coworkers pointed out that the reaction of HOCl with ethylene glycol vinyl-ether (a plasmalogen analogue) occurs approx. 180-fold faster as compared to unsaturated acyl residues identifying plasmalogens as preferential lipid targets for modification (Pattison et al. 2003, Skaff et al. 2008). Indeed, the vinyl-ether linkage was shown to be the most sensitive structure of pPC towards HOCl oxidation, while the alkene bonds within the *sn*-2 acyl residue of the lyso-PC product represent only secondary targets. Thus, with increasing HOCl concentrations α-ClFALDs/lyso-PCs are the primary products followed by lyso-PC-chlorohydrins formation. A further increase of HOCl to supraphysiological levels results in the generation of glycerophosphatidylcholine due to degradation of the *sn*-2 acyl-chain (Lessig and Fuchs 2010, Lessig et al. 2007, Messner et al. 2006).

With the discovery of α-ClFALDs it seemed to be important to determine the biological significance. The pioneering work by Ford and colleagues revealed that 2-ClHDA elicits modification of primary amines of proteins and lipids by Schiff base adduct formation and that the chlorinated fatty aldehyde is converted to a family of chlorinated lipids: In a first enzymatic step 2-chlorohexadecanoic acid (2-ClHA) or 2-chlorohexadecanol (2-ClHOH) are formed (Anbukumar et al. 2010, Wildsmith et al. 2006a, Wildsmith et al. 2006b). The chlorinated FA is either re-esterified into complex glycerophospholipids or subjected to ω-oxidation yielding 2-chloroadipic acid (2-ClAdA) (Brahmbhatt et al. 2010b, Wildsmith et al. 2006a). Several studies demonstrated that increased levels of α-ClFALDs or lipids derived therefrom are of (patho)physiological importance: 2-ClHDA acts a potent chemoattractant for neutrophils, and in concert with unsaturated species of lyso-pPL (and perhaps their chlorohydrins), which stimulate P-selectin expression of endothelial cells, these lipids participate in the recruitment of additional neutrophils (Messner et al. 2008b, Thukkani et al. 2002, Thukkani et al. 2003a). In addition to immune regulatory properties, some chlorinated lipids may elicit vascular alterations due to reduction of endothelial nitric oxide synthase (eNOS) activity (2-ClHDA) and increased production of vasoactive prostacyclin (Marsche et al. 2004, Messner et al. 2008a). However, since 2-ClHDA activates NFκB signaling in endothelial cells it appears possible that α-ClFALDs might also be involved in pro-inflammatory pathways (Ford 2010, Messner et al. 2008b).

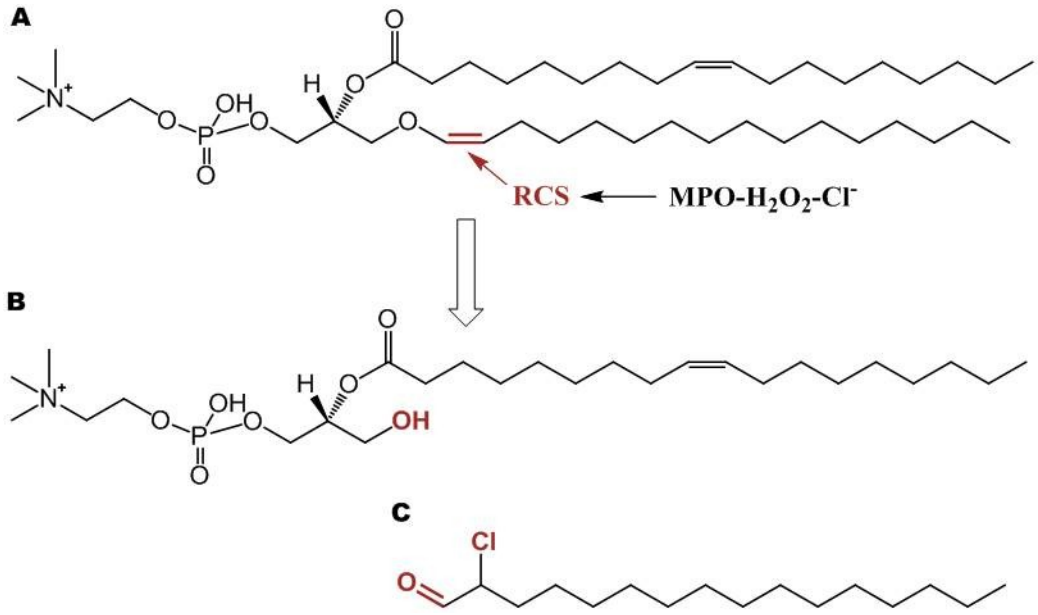

Figure 11: **Formation of α-chloro fatty aldehydes (α-ClFALDs) by activated phagocytes. (A)** Activation of the MPO-H_2O_2-Cl^- system results in the generation of reactive chlorinating species (RCS). RCS initiate the cleavage of the plasmalogen vinyl-ether linkage resulting in the formation of a (**B**) *sn*-1-lysphospholipid and an (**C**) α-ClFALD.

recent finding: Human atherosclerotic tissue displays a 1400-fold increase of α-ClFALD species compared with normal human aorta (Thukkani et al. 2003a). Myocardial tissue of rats subjected to surgical infarction showed highly elevated levels of 2-ClHDA as compared to heart tissue from rats subjected to sham surgery. Additionally, perfusion of hearts with concentrations found in infracted tissue resulted in antichronotropic and antiionotropic effects as well as in myocardial injury (Thukkani et al. 2005). More recently, also biological metabolites of α-ClFALDs including 2-ClHA and 2-ClAdA could be identified in plasma, urine, and bronchoalveolar lavage fluid of rodents challenged by either systemic LPS or by sendai-virus induced neutrophilic bronchiolitis (Anbukumar et al. 2010, Brahmbhatt et al. 2010b).

VI. MATERIALS AND METHODS

Materials

1. Animals Experiments

Male C57BL/6 mice (8-10 weeks, 20-30 g) and male Sprague-Dawely rats (250-300 g) were obtained from the Institut für Versuchstierkunde (Himberg, Austria). LPS from *Escherichia coli* (0111:B4) was from Sigma Aldrich (Vienna, Austria). Intralipid 20% was purchased from Fresenius (Austria). Pentobarbital sodium salt and heparin sodium salt were from Sigma Aldrich (Vienna, Austria). Evans Blue, sodium fluorescein, mannitol as well as bovine serum albumin (BSA) and other chemicals were also obtained from Sigma Aldrich (Vienna, Austria). Injection needles and surgery supplies were purchased from Henke Sass Wolf (Tuttlingen, Germany)

2. Cell Culture Materials

Earl's medium M199, penicillin/streptomycin, glutamine, gentamycin, dispase from Bacillus polymyxa, and trypsin were from Gibco (Vienna, Austria). Ox serum was purchased from PAA Laboratories (Linz, Austria). DMEM Ham's F12 and hydrocortisone (HC) were from Sigma Aldrich (Vienna, Austria). Plastic ware for cell culture was obtained from Costar (Vienna, Austria) or VWR (Austria). Lab-Tek® chamber slides were from Bartelt (Graz, Austria). ECIS electrode arrays (8W10E+) were from Ibidi (Germany).

3. Chemical Synthesis, Derivatization and Standards

Hexadecanoic-2,4,6,8,10,12,14,16-$^{13}C_8$ acid sodium salt, hexadecanal dimethyl acetal and heptanal were purchased from Sigma Aldrich (Vienna, Austria). Trimethylchlorosilane (TMCS), N-methyl-N-(trimethylsilyl) trifluoroacetamide (MSTFA) and acetonitrile were from Pierce (Rockford, IL, USA). Trimethylorthoformate, triethylamine, DMSO and oxalylchloride were obtained from Sigma Aldrich (Vienna, Austria). Silica gel 60 and Silica gel 60 plates were from Merck (Darmstadt, Germany).

Pentadecanoic acid, pentadecanol, dipalmitoyl-phosphatidyl choline (DPPC), pentafluorobenzyl (PFB) hydroxylamine, pentafluorobenzoyl (PFBoyl) chloride and pentafluorobenzyl bromide were purchased from Sigma Aldrich (Vienna, Austria). D-31 34:1 phosphatidylcholine (PC) or 12:0/12:0 PC as well as LIPID MAPS standards LM-1004 (17:0-14:1 PC), LM-1102 (17:0-20:4 phosphatidylethanolamine), LM-1303 (21:0-22:6 phosphatidylserine), and LM-1504 (17:0-14:1 phosphatidylinositol) were from Avanti® Polar Lipids (Alabaster, AL, USA). Organic solvents and other chemicals were obtained from Sigma, Roth (Vienna, Austria), and Merck (Darmstadt, Germany).

4. *In Vitro* Experiments

Sodium hypochlorite (NaOCl), hydrogen peroxide (H_2O_2) and 3-(4,5-dimethyl-2-thiazolyl)-2,5-diphenyltetrazolium bromide (MTT) were purchased from Sigma Aldrich (Vienna, Austria). 1-*O*-1'-(Z)-octadecenyl-2-hydroxy-*sn*-glycero-3-phosphocholine (C_{18}-plasmenyl lyso-PC) was from Avanti® Polar Lipids (Alabaster, AL, USA). 5-(and-6)-carboxy-2',7'-dichlorodihydrofluorescein diacetate (carboxy-H_2DCFDA), 5,5′,6,6′-tetrachloro-1,1′,3,3′-tetraethylbenzamidazolocarbocyanine iodide (JC-1) and human recombinant TNFα were from Invitrogen (Vienna, Austria). MPO was from Planta Naturstoffe (Vienna, Austria) and cellulose acetate from Sartorius AG (Goettingen, Germany). The Bradford protein assay was from Bio-Rad (Vienna). Apigenin, curcumin, genistein, naringenin, phloretin, phloridzin and resveratrol were obtained from Sigma Aldrich (Vienna, Austria). N-formylmethionyl-leucyl-phenylalanine (fMLP), PD098059 and staurosporine were from Calbiochem (La Jolla, CA, USA). Palmitate, methionine, taurine, N-2-mercaptopropionyl glycine (MPG), N-acetyl-L-cysteine (NAC), colchicine and myriocin were purchased from Sigma Aldrich (Vienna, Austria). All other chemicals and solvents were from Sigma Aldrich and Roth (Vienna, Austria).

5. Protein analysis

ELISA for mouse MPO (HK210 kit) was from Hycult Biotechnology (Uden, The Netherlands). Phenylmethylsulfonyl fluoride (PMSF), aprotinin, leupeptin, pepstatin and other protease inhibitors were purchased from Sigma Aldrich (Vienna, Austria). Polyvinylidene difluoride (PVDF) transfer membrane (Biotrace™ PVDF) was from Pall Corporation (Vienna, Austria). Detergents and other chemicals were from Sigma Aldrich (Vienna, Austria). ECL and ECL SuperSignal Western Blotting Substrate were obtained from Pierce (Rockford, IL). ECL Plus™ Western Blotting Detection Reagents

were from GE Healthcare (Vienna, Austria) and CURIX Ultra UV-G X-ray films were from Agfa (Mortsel, Belgium). DyLight 650 Microscale Antibody Labeling Kit was purchased from Thermo Fisher Scientific (Rockford, IL, USA) and 4', 6'-diamidino-2-phenylindole dihydrochloride (DAPI) was from Sigma Aldrich (Vienna, Austria). Ultra V Blocking solution and AEC Substrate System was from Lab Vision Corp. (Fermont, CA, USA). Mayer's hemalum and Kaiser's glycerol gelatin was purchased from Merck (Vienna, Austria). Antibody diluent for immunohistochemistry was from Dako (Carpinteria, CA, USA), and Moviol from Calbiochem-Novabiochem (La Jolla, USA). Antibodies used in this study are listed in ***Table 1*****.**

Table 1: Primary antibodies

Target	Type	Source	Supplier
human MPO	polyclonal	rabbit	Dako (Vienna, AUT)
von Willebrand factor	polyclonal	rabbit	Dako (Vienna, AUT)
mouse neutrophils (FITC labeled)	monoclonal	rat	Abcam (Cambridge, UK)
nitrotyrosine	polyclonal	rabbit	Millipore (Vienna, AUT)
human ZO-1	polyclonal	rabbit	Zymed (Vienna, AUT)
human VE-Cadherin	monoclonal	mouse	Santa Cruz Biotech. (CA, USA)
rat p42/44 MAPK ERK1/2	monoclonal	rabbit	Cell Signaling (Beverly, MA, USA)
human phospho-p42/44 MAPK ERK1/2 (Thr202/Tyr204)	monoclonal	rabbit	Cell Signaling (Beverly, MA, USA)
human phospho-p38MAPK (Thr183/Tyr185)	polyclonal	rabbit	Cell Signaling (Beverly, MA, USA)
human p38MAPK	monoclonal	mouse	Cell Signaling (Beverly, MA, USA)
human phospho-SAPK/JNK1/2 (Thr180/Tyr182)	polyclonal	rabbit	Cell Signaling (Beverly, MA, USA)
human SAPK/JNK1/2	polyclonal	rabbit	Cell Signaling (Beverly, MA, USA)
human caspase-3	polyclonal	rabbit	Santa Cruz Biotech. (CA, USA)

Table 2: Secondary antibodies

Target	Labeling/Conjugation	Source	Supplier
rabbit IgG	Cy3	goat	Jackson Dianova (Hamburg, GER)
rabbit IgG	Cy5	goat	Jackson Dianova (Hamburg, GER)
mouse IgG	Cy2	goat	Jackson Dianova (Hamburg, GER)
rat IgG	Cy2	goat	Jackson Dianova (Hamburg, GER)
rabbit IgG	HRP	goat	Pierce (Rockford, IL, USA)
mouse IgG	HRP	goat	Santa Cruz Biotech. (CA, USA)

6. RNA Analysis

Paris Kit was purchased from Ambion (Brunn a. Gebirge, Austria). Dithiothreitol, First Strand Buffer and SuperScript II Reverse Transcriptase were from Invitrogen (Vienna, Austria). Random hexamer primers and dNTPs were obtained from Amersham Biosciences (Vienna, Austria). QuantiFast SYBR Green PCR kit was from Qiagen (Vienna, Austria). Primer assays are listed in ***Table 3.***

Table 3: Primer sequences

Target gene	Primer pos.	Sequence	Amplicon size (bp)
MPO, NM_010824.2	forward	5`-GCCAGCAGCCATGAAGAAGT-3`	304
	reverse	5`-CCGGATCTCATCCACCACAA-3`	
TNFα, NM_013693	-	QT00104006, Qiagen	112
COX2, NM_011198	-	QT00165347, Qiagen	95
NOS2, NM_010927	-	QT00100275, Qiagen	118
TBP1, NM_013684	-	QT00198443, Qiagen	114

7. Buffers

Chemicals for buffers were purchased from Sigma Aldrich (Vienna, Austria), Roth (Vienna, Austria) and Merck (Darmstadt, Germany)

Table 4: Buffers

Buffer	Components	pH
Cell culture		
PBS	140 mM NaCl, 2.7 mM KCl, 8.1 mM Na_2HPO_4, 1.5 mM KH_2PO_4	7.4
HBSS	140 mM NaCl, 5.4 mM KCl, 0.3 mM Na_2HPO_4, 0.4 mM KH_2PO_4, 1.7 mM $CaCl_2$, 2.3 mM $MgCl_2$, 4.2 mM $NaHCO_3$, 5.6 mM glucose	6.0 or 7.4
Lysis Buffer	50 mM Tris-HCl, 1% (v/v) NP-40, 150 mM NaCl, 1 mM Na_3VO_4, 1 mM NaF, 1 mM EDTA	7.4
SDS-PAGE		
Sample Buffer	150 mM Tris-HCl, 4% (w/v) SDS, 20% (v/v) glycerol, 5% (v/v) 2-mercaptoethanol	6.8
Gel Buffers	1.5 M Tris-HCl,	8.8
	500 mM Tris-HCl	6.8
Running Buffer	250 mM Tris-HCl, 2 M glycine, 35 mM SDS	
Immunoblotting		
Blotting Buffer	150 mM Tris-HCl, 400 mM glycine, 10% (v/v) MeOH	
TBS-T	25 mM Tris-HCl, 150 mM NaCl, 0.05% (v/v) Tween 20	7.5
Stripping Buffer	60 mM Tris-HCl, 2% (w/v) SDS, 100 mM 2-mercaptoethanol	6.8

Methods

1. PREPARATION OF 2-ClHDA, 2-ClHpA AND REAGENT NaOCl

1.1. *Synthesis of 2-ClHDA*

Synthetic 2-ClHDA was prepared and purified from hexadecanal dimethyl acetal (HDA-dma) as the starting compound as previously described (Marsche et al. 2004). Briefly, HDA-dma (Sigma) in acetonitrile (1.25%, w/v) was added to a suspension of $MnCl_2$ (2.5%, w/v) and MnO_2 (2.5%, w/v). Then TMCS (10%, v/v) was added and the reaction mixture was heated to 40°C. After 16 h, 0.5 M NaOH (75%, v/v) was added for alkalization, 2-ClHDA dma was extracted with hexane, and purified using a Silica 60 column and hexane/diethyl ether (90:10, v/v) as eluent. For each experiment 2-ClHDA was freshly prepared (deprotected) by refluxing the dimethyl acetal derivative in trifluoroacetic acid/CH_2Cl_2 (1:1, v/v) at 80°C for 1h. Organic phase was brought to dryness and stock solutions were prepared in DMSO, EtOH abs. or hexane. Purity was confirmed by TLC, EI-GC-MS as well as by NICI-GC-MS of the corresponding pentafluorobenzyl (PFB) oxime derivative (*see below*).

1.2. *Synthesis of 2-Chloroheptanal (2-ClHpA)*

2-ClHpA (the model compound for 2-ClHDA) was synthesized in co-operation with O. Kappe and T. Glasnov (KFU Graz) as previously described (Stevens et al. 1954). Briefly, to a solution of 1 eq. heptanal in CH_2Cl_2, stirring in an ice-bath, 1 eq. of thionyl chloride in CH_2Cl_2 was slowly added, thereby maintaining the temperature between 15-40°C. After additional 30 min, the reaction mixture was heated to reflux temperature for the same time period. Subsequently, 2-ClHpA was distilled at reduced pressure and condensed in a cold trap.

1.3. *Determination of NaOCl-Concentration*

Due to instability of NaOCl solutions (Fabian and Walker 1982) the concentration of reagent NaOCl was determined for each experiments using the molar absorption coefficient for NaOCl of 350 cm^{-1} at 292 nm at pH 12 (Morris 1966). Stock solutions of NaOCl were prepared in Milli-Q water.

2. IN VITRO BBB MODEL

2.1. *Brain Microvascular Endothelial Cells (BMVEC)*

2.1.1. Isolation and Establishment of Primary Cultures

BMVEC were isolated from porcine brains obtained from the local slaughterhouse by a combination of mechanical disintegration, enzymatic digestion and centrifugation steps according to Goti and coworkers (Goti et al. 2002). Following removal of meninges and the secretory areas, the brain cortex (gray and white matters) was minced using a sterile cutter with staggered rolling blades. Minced tissue was suspended in 'preparation medium' (M199 containing 1% P/S (v/v), 1% gentamycin (v/v) and 0.35% glutamine (v/v)) and incubated with solid dispase (0.1%, w/v) for 1 to 2 h at 37°C in water bath with gentle stirring. Dextran solution (16%, w/v) was added to get a final 10% (w/v) dextran suspension followed by centrifugation at 6800 *g* for 10 min at 4°C. The resulting pellet was resuspended in 'medium A' (M199 containing 10% ox-serum, 1% P/S, 1% gentamycin and 0.35% glutamine v/v). Larger vessels were separated by a filtration step through 180 µm nylon mesh. Microvessels were digested with 0.03% (w/v) collagenase/dispase for 5 min at 37°C in a water bath with gentle stirring. Following collection of released BMVEC cell aggregates by low spin centrifugation at 900 rpm or 140 *g* for 10 min at RT they were further purified by density gradient centrifugation. Therefore, the yield of one brain was re-suspended in 5 ml plating medium, 'medium A' and centrifuged on a discontinuous Percoll gradient (20 ml 1.03 g/ml bottom-layered with 15 ml 1.07 g/ml) at 1300 *g* for 10 min at RT in a swinging bucket rotor without brake. BMVEC clusters, which were gathered at the interface of the two phases, were washed in 'medium A', and plated onto six to eight 75 cm^2 culture flasks coated with 60 µg/ml collagen in phosphate buffered saline (PBS), pH 7.4, aspirating collagen solution after 5 min. After 1 day in culture cells were washed twice with PBS and cultivated in medium B (M199 containing 10% ox-serum, 1% P/S, and 0.35% glutamine; v/v).

2.1.2. Cultivation of Cells

After two to three days, when confluence was almost reached, BMVEC were sub-cultured by trypsinization and seeding onto disposal collagen-coated cell culture ware: 6-, 12-, 24-, and 96-well plates (60 µg/ml collagen in PBS), onto Permanox chamber slides (120 µg/ml collagen in PBS) or onto

8W10E+ ECIS arrays (200 µg/ml collagen in 150 mM NaCl) at densities between 20000 cells/cm^2 (multiwell plates and chamber slides) and 40000 cells/cm^2 (ECIS arrays).

2.1.3. Cell Experiments

Before starting cell culture experiments BMVEC were overnight pre-incubated with serum-free 'medium B'. In contrast, for immunofluorescence microscopy - and ECIS experiments 'medium B' was replaced by 'induction medium' (DMEM Ham's F12 medium containing 1% P/S, 0.35% glutamine and 500 nM HC to induce tight junctions).

During cell experiments BMVEC were incubated in serum-free medium B, induction medium or HBSS (pH 6 or pH 7.4) in the absence or presence of 2-ClHDA, NaOCl, H_2O_2, MPO, structural analogues of 2-ClHDA (palmitate, HDA and 2-ClHDA dma), polyphenols, SPTLC- or MAPKK-inhibitors (myriocin and PD098059), thiol compounds (MPG, NAC, methionine), and apoptosis inducers (staurosporin and colchicin) at the indicated concentrations for the indicated time periods. Freshly deprotected 2-ClHDA and HDA, palmitiate, polyphenols, PD098059, myriocin, and staurosporine were prepared as stock solutions in DMSO.

For each cell experiment using 2-ClHDA/HDA/2-ClHDA dma/palmitate as a stimulus final concentration of vehicle DMSO in culture medium was 0.4% (v/v). Reagent NaOCl, H_2O_2, MPO, thiol compounds and colchicine were prepared as 250x stock solutions in water. For experiments examining the impact of neutrophil activation on BMVEC barrier function, 2.5 x 10^6 neutrophils were primed with 10 ng/ml TNFα for 15 min at RT followed by co-incubation with BMVEC for 15 min and stimulation with 10 µM fMLP (stock added in EtOH, final concentration of vehicle was 0.2%).

2.1.4. Counting of BMVEC

To determine the number of BMVEC in multiwell plates, cells of trypsinized confluent monolayers were counted using CASY cell counter (Schärfe System GmbH) according to the manufacturer's recommendations.

2.2. *Model for In Vitro BBB Function: Electrical Cell-Substrate Impedance Sensing (ECIS)*

To determine the effects of immune cells, oxidants and other compounds on barrier integrity of BMVEC impedance was monitored using the ECIS Z system (***Figure 12***) (Applied Biophysics, Troy, NY). Briefly, cells were plated on 250 µm collagen-coated gold electrodes of 8W10E+ arrays (Applied Biophysics) and cultured to confluence while measurement was taken every minute at 4 kHz alone or in combination with 64 kHz monitoring barrier function or membrane capacitance. After overnight induction of tight junctions by means of HC (induction medium, *see chapter 2.1.3.*) average baseline impedance readings varied between 2000 and 5000 Ω at 4 kHz and between 600 and 800 Ω at 64 kHz. Only after achieving stable basal impedance readings > 2000 Ω endothelial cells were exposed to experimental conditions.

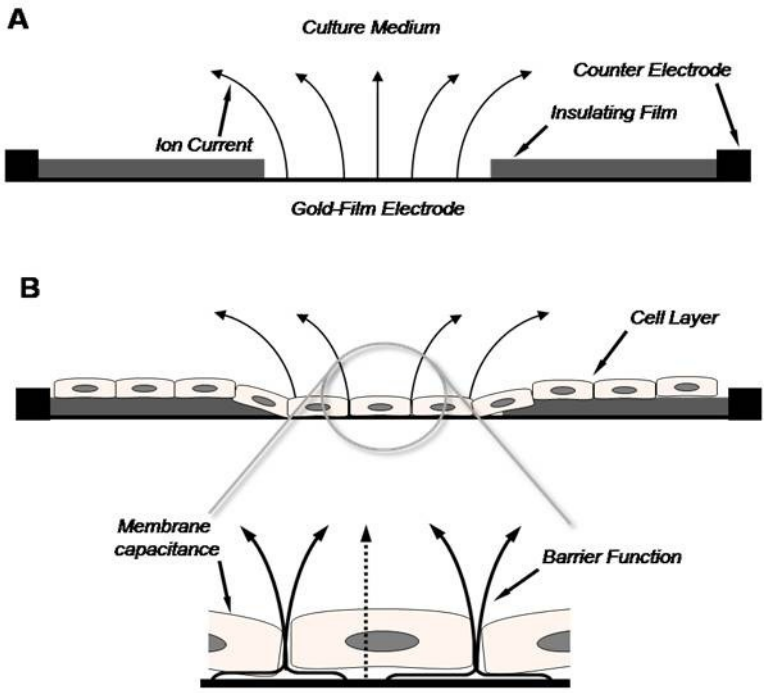

Figure 12: **Principle of ECIS**

(**A**) Using the free ions in the culture media, the instrument generates an AC current flow between a small active gold-film electrode and a counter electrode located in specialized tissue culture arrays. (**B**) When cells attach and spread upon the active electrode, the current flow is restricted to spaces under and between the cells, as the cell membrane acts as an insulator. Restriction of the AC current results in measurable impedance changes, that can be monitored in real-time (Mitra et al. 1991, Ramirez et al. 2010).

To avoid pronounced impedance changes due to altered culturing conditions (e.g. temperature of medium, O_2/CO_2 saturation in medium) aliquots of culture medium, taken out from array wells, were transferred to sterile, pre-warmed Eppendorf-tubes. Immediately after addition of investigated compounds, oxidants or cells, medium was re-added to BMVEC.

2.3. *Analysis of Barrier Architecture: Immunofluorescence of BMVEC*

BMVEC were cultured on Permanox chamber slides to confluence. The cells were treated with vehicle or 2-ClHDA at the indicated concentrations for 3 h.

2.3.1. Double-Labeling of ZO-1 and VE-cadherin

After treatment slides were rinsed twice with PBS, dried for 1 to 2 h at RT, and stored at -20°C until required. Cells were fixed in acetone for 5 min at RT, and rehydrated in PBS for 5 min. After blocking of nonspecific adsorption with UV ultra block, BMVEC were sequentially incubated for 60 min at RT with the primary antibody and with the corresponding fluorescent-labeled secondary antibody. Primary antibodies were mouse anti-human VE-cadherin IgG and rabbit anti-human ZO-1 IgG diluted 1:200 and 1:50 with antibody diluent. Cy-2 labeled goat anti-mouse IgG as well as Cy-5 labeled goat anti-rabbit IgG (diluted 1:300 in antibody diluent) were used as secondary antibodies. In-between antibody incubations, and before mounting with Moviol, samples were rinsed three times in PBS for 5 min at RT. Slides were analyzed on a confocal laser scanning microscope (Leica SP2, Leica Lasertechnik GmbH, Heidelberg, Germany) using 488 nm for excitation of Cy-2 and 647 nm for Cy-5. Emission was detected at 500 to 535 nm for Cy-2 and 665 nm to 750 nm for Cy-5.

2.3.2. Double-Labeling of F-Actin Cytoskeleton and Nuclei

For double immunofluorescence, 2-ClHDA- or vehicle-treated cells were immediately rinsed twice with PBS, fixed in 4% formaldehyde (in PBS) for 10 min at RT, and permeabilized in ice-cold acetone for 3 min. Subsequently, after re-hydration in PBS, cells were pre-incubated with 1% (w/v) BSA in PBS before F-actin cytoskeleton was stained with 165 nM rhodamine phalloidin solution in 1% (w/v) BSA in PBS for 20 min at RT according to the manufacturer's recommendations (Molecular Probes,

Invitrogen). Slides were rinsed 3 three times before a counterstaining of nuclei was performed with DAPI (1:1000 in PBS) for 10 min at RT. Samples were rinsed three times in PBS for 5 min at RT and mounted with Moviol. Immunofluorescence was analyzed on a confocal laser scanning microscope (Leica SP2, Leica Lasertechnik GmbH, Heidelberg, Germany) using 405 nm for excitation of DAPI and 543 nm for TRITC (rhodamine). Emission was detected at 430 to 450 nm for DAPI and 555 nm to 620 nm for TRITC.

3. PREPARATION OF HUMAN POLYMORPHONUCLEAR LEUKOCYTES

Human polymorphonuclear leukocytes (PMNL) were kindly provided by the Institute of Experimental and Clinical Pharmacology. Briefly, blood samples were taken from healthy volunteers, in accordance to a protocol by the Ethics Committee of the Medical University of Graz. PMNL (containing approx. 98% neutrophils and 2% eosinophils) were prepared as previously described using dextran sedimentation of erythrocytes followed by centrifugation on Histopaque gradients (Schratl et al. 2006). All separation steps were performed at RT. The resulting purity and viability of neutrophils was typically greater than 95%.

4. ANIMAL MODELS

Animal experiments were performed in accordance with animal care ethics approval and guidelines, as per animal care certificate No. BMWF-66.010/0035-II/10.b.2008, No. BMWF-66.010/0104-II/10b/2009 and No. BMWF-66.010/0055-II/3b/2011 of the Austrian Federal Ministry of Science and Research (Vienna, Austria). All animals were kept on a 12 h light/dark cycle with free access to food and water.

4.1. *Model for In Vivo Neuroinflammation*

Neuroinflammation was induced in C57BL/6 mice by i.p. injection of a single dose of LPS (150 µg or 250 µg/30 g). After indicated time periods mice were killed by cervical dislocation, brains were removed, snap frozen in liquid N_2, and stored at -70°C or immediately further processed for analysis.

4.1.1. qPCR (performed by S. Waltl)

To generate cDNA templates, total brain RNA was isolated using Paris Kit and 5 µg RNA was reverse transcribed according to the manufacturer's instructions using 200 U SuperScript II Reverse Transcriptase and random hexamer primers. Primers for MPO were designed using NCBI primer blast (***Table 3***). qPCR reactions were performed with an Applied Biosystems 7900HT Fast Real Time PCR System, using the QuantiFast SYBR Green PCR kit and primer assays for tumor necrosis factor α (TNFα), inducible nitric oxide synthase (iNOS), cyclooxygenase-2 (COX2), and TATA-box binding protein 1 (TBP1) (*Table 3*). Samples were run in triplicates for each experiment with TBP1 as an internal control. For analysis of the expression profiles the public domain program Relative Expression Software Tool – REST 384 Vers. 2 (http://www.gene-quantification.com/download.html) was used (Pfaffl et al. 2002).

4.1.2. Measurement of MPO Mass in Murine Brain Homogenates

MPO protein mass was measured using a specific sandwich ELISA according to the manufacturer's recommendations (HK210 kit) and normalized on total protein content as determined by the Bradford assay.

4.1.3. Immunohistochemistry and Triple Immunofluorescence in Murine Brain Cryosections

Serial sagittal cryosections (5 µM) were collected on glass slides, air dried for 2 h at RT, fixed in acetone for 5 min at RT and stored at -40°C until required. For triple immunofluorescence rabbit anti-von Willebrand factor was Dylight 650-labeled according to the manufacturer's recommendations (DyLight 650 Microscale Antibody Labeling Kit). Prior to immunostaining, sections were thawed and air dried for 30 min at RT followed by fixation in acetone for 5 min at RT. After re-hydration in PBS, sections were blocked with UV ultra block for 10 min.

For immunohistochemical studies sections were incubated with rabbit anti-human MPO (1:500) and horseradish peroxidase (HRP)-labeled goat anti-rabbit IgG (1:200) each for 30 min. After AEC development and termination by washing with distilled water according to the manufacturer's recommendations (Lab Vision AEC Substrate System) the sections were counterstained with Mayer's

hemalum and mounted with Kaiser's glycerol gelatin. Analysis of sections was performed with a Zeiss Axiophot microscope equipped with a Zeiss Axiocam HRC.

For triple immunofluorescence antibodies against primary epitopes (rabbit anti-human MPO, 1:500 or rabbit anti-nitrotyrosine, 1:75; and rat anti-mouse neutrophils, 1:50) were sequentially incubated for 30 min at RT with corresponding Cy-2 or Cy-3 labeled secondary antibodies (Cy-3 labeled goat anti-rabbit IgG, Cy-2 labeled goat anti-rat IgG; each 1:300; Cy-2 labeling was used to enhance FITC-signal) followed by a blocking step with rabbit non-immune IgG (1:25) and incubation (30 min) with Dylight-650 labeled von Willebrand factor (1:75).
Immunofluorescence stained sections were mounted with Moviol and analyzed on a confocal laser scanning microscope (Leica SP2, Leica Lasertechnik GmbH, Heidelberg, Germany) using 488 nm for excitation of Cy-2, 543 nm for Cy-3 and 647 nm for Dylight 650. Detected emission wavelengths were 500 to 535 nm for Cy-2, 555 nm to 620 nm for Cy-3, and 665 nm to 750 nm for Dylight-650.

All incubations were performed in a moist chamber at RT in dark (for immunofluorescence) and PBS was used for three consecutive washing steps (each 5 min) between the incubation steps and before mounting. All antibodies were diluted with antibody diluents.

4.2. *Model for In Vivo BBB Function: In Situ Brain Perfusion*

Rats were perfused via the common carotid arteries and the magnitude of permeability changes was assessed using sodium fluorescein (SF) as a low- and Evans Blue albumin (EB) as a high molecular weight marker as previously described (Hawkins B. T. and Egleton 2006).

Briefly, Sprague-Dawely rats were anesthetized with 50 mg/kg pentobarbital while body temperature was maintained at 37°C using a heating panel. If necessary, animals got an additional dose of 25 mg/kg is during the course of the surgery. After endotracheal intubation the right common carotid artery was exposed and cannulated (cannulas were heparinized), whereas the right external carotid artery and the left common carotid artery were ligated (***Figure 13***). After sectioning of jugular veins animals were perfused for 5 min with oxygenated Ringer solution (supplemented with 18 g/l BSA) at a flow rate of 3 ml/min/hemisphere using a peristaltic pump. Subsequently, perfusion was switched for 90 min to Ringer containing 0.4% DMSO (vehicle) or 25 µM 2-ClHDA. For the assessment of BBB function perfusion with Ringer supplemented with SF (1 g/l) and EB (1 g/l, mixed the night before to allow

maximal binding of the dye to albumin) for 5 min and the washout with Ringer without dyes for 7 min were followed.

Animals were decapitated, the brains were immediately removed, and cerebral hemispheres were dissected. Brain hemispheres were mechanically homogenized in 3 ml 7.5% (w/v) trichloroacetic acid, and the resulting suspension was neutralized with 5M NaOH and measured by fluorimetry (excitation 484 nm, emission 540 nm) on a Victor 1420 multilabel counter for SF determination.

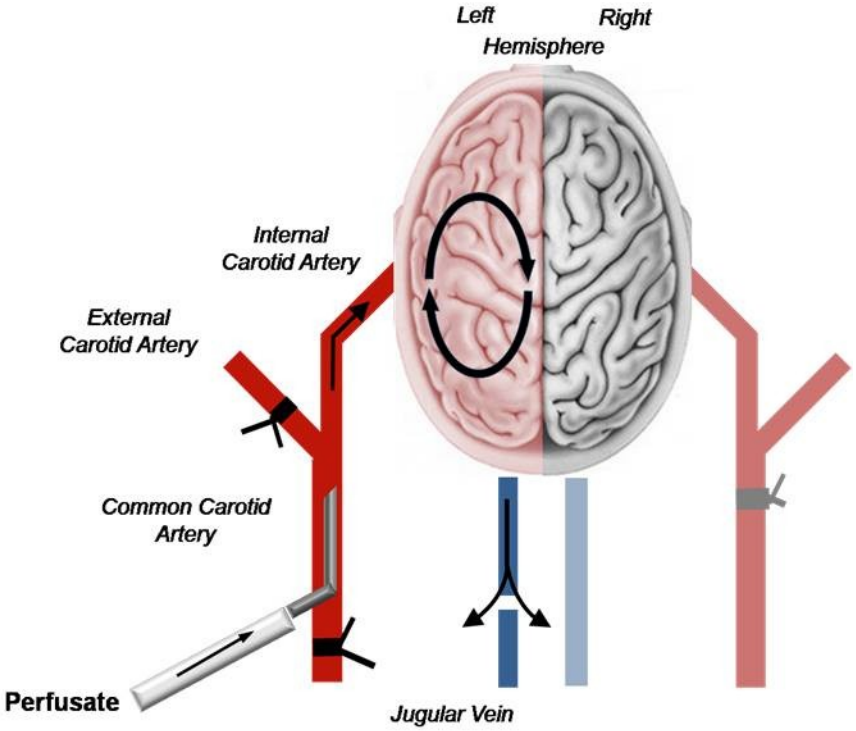

Figure 13: Schematic representation of the *in situ* rat brain perfusion technique

5. MODIFICATION EXPERIMENTS

5.1. *Sn-2-Lyso-Plasmalogen with NaOCl*

Liposomes from lysoPLs were prepared by dispersing 100 nmol 1-*O*-1'-(Z)-octadecenyl-2-hydroxy-*sn*-glycero-3-phosphocholine (C_{18}-plasmenyl lyso-PC) in 1 ml H_2O using sonication (4 x 10 sec on ice). Modification was performed at pH 7 by addition of 250 nmol NaOCl for 1 h at RT. For analysis of plasmalogen-derived octadecanol 25 nmol C_{18}-plasmenyl lyso-PC were hydrolyzed by sonication in 0.1M HCl followed by an incubation for 1 h at RT. Subsequently, lipids were extracted according to the Folch procedure (Folch et al. 1957), converted to the corresponding PFB-oxime derivative, dissolved in 100 µl hexane, and analyzed by NICI-GC-MS.

5.2. *Murine Brain Lipid Extracts with NaOCl*

Animals were killed by cervical dislocation, brains were removed, snap frozen in liquid N_2, and homogenized in a mortar. The powdered material was transferred to pre-weighed Pyrex tubes and extracted according to the Folch procedure. Liposomes from brain lipids were prepared by dispersing 50 mg brain lipids in 1 ml H_2O using sonication (4 x 10 sec on ice). Modification with NaOCl (1 - 500 µg/100 µg lipid) was performed at pH 7 over night at RT. Based on a percentage brain lipid (lipid fraction contributes approx. 10 % of total wet brain tissue) composition of 65% total phospholipids, 11% total sphingolipids and 20% cholesterol (O'Brien and Sampson 1965), these weight ratios correspond to molar NaOCl:lipid ratios of approx. 0.1:1 (1 µg NaOCl/100 µg lipid) to 50:1 (500 µg NaOCl/100 µg lipid). Subsequently, lipids were extracted, dissolved in 1 ml $CHCl_3$/MeOH (1:1, v/v), and analyzed by Fourier-transform ion cyclotron resonance mass spectrometry (FT-ICR-MS) in co-operation with H. Köfeler (MUG). Moreover, lipid fraction were converted to PFB-oxime derivatives and α-chloro fatty aldehydes (2-ClHDA, 2-ClODA and 2-ClODEA) were quantified by NICI-GC-MS using 2-Cl[$^{13}C_8$]HDA as internal standard. Total plasmalogen aldehydes (HDA, ODA, ODEA) were quantified after acidic hydrolysis in 0.5 M HCl (overnight at 37°C), preparation of PFB-oxime derivatives, and subsequent NICI-GC-MS analysis using 2-Cl[$^{13}C_8$]HDA as internal standard.

5.3. *Cerebrovascular Endothelial Cells*

5.3.1. NaOCl

BMVEC were plated in 6-well trays and allowed to grow for 2-3 days to confluence (9×10^5 cells) before serum-deprived medium was replaced by HBSS and cells were treated with increasing concentrations of reagent NaOCl (added as a 250 x stock) for 30 min at 37 °C in HBSS in the presence of 100 ng 2-Cl[$^{13}C_8$]HDA (added as 250 x stock in MeOH) as internal standard. Subsequently, lipids from HBSS layers were extracted twice in hexane/methanol (5:1; v/v, 2 ml) while lipids from cells were extracted using two consecutive extractions (30 min each) with 1 ml of hexane/isopropanol (3:2; v/v) on a rotary shaker (1000 rpm). Following extraction combined lipids fractions were converted to PFB-oxime derivatives and α-chloro fatty aldehydes (2-ClHDA, 2-ClODA and 2-ClODEA) were quantified by NICI-GC-MS using 2-Cl[$^{13}C_8$]HDA as internal standard. Total plasmalogen aldehydes (HDA, ODA, ODEA) were quantified after acidic hydrolysis in 0.5 M HCl (overnight at 37°C), preparation of PFB-oxime derivatives, and subsequent NICI-GC-MS analysis using 2-Cl[$^{13}C_8$]HDA as internal standard.

5.3.2. MPO–H_2O_2–Chloride System

After BMVEC were brought to confluence in 6-well trays 1.8 x 10^6 cells (cells of two wells) were trypsinized, washed twice with 1 ml and resuspended in 200 µl PBS (50 mM, pH 5) supplemented with 140 mM NaCl. Cells were incubated in the presence of MPO (70 nM final concentration) and 2.5 µg 2-Cl[$^{13}C_8$]HDA at 37 °C with shaking. Reaction was started by the addition of H_2O_2 (200 µM final concentration; eight additions of 25 µM H_2O_2 at 4-min intervals (Bergt et al. 2000)) and stopped by removing cationic MPO using cellulose acetate. Subsequently, BMVEC modification was allowed to proceed at 37°C for a further 30 min. After modification lipids were extracted twice in hexane/methanol (5:1; v/v, 2 ml), PFB oximes were prepared and α-chloro fatty aldehydes were quantified by NICI-GC-MS using 2-Cl [$^{13}C_8$] HDA as internal standard.

5.4. *Phloretin*

5.4.1. NaOCl

For examining the susceptibility to HOCl-dependent chlorination 55 nmol of phloretin (added as 250 x stock in EtOH) were modified with 110 nmol reagent NaOCl (added as a 250 x stock) in 1 ml PBS for 1 h at RT. Subsequently, reaction mixture was extracted twice with 2 ml of EtOAc followed by conversion to trimethylsilyl (TMS)-ether derivatives and EI-GC-MS analysis.

5.4.2. 2-ClHpA

To investigate covalent trapping of 2-ClHpA by phloretin preliminary experiments were performed in medium B at 35 °C for 5 days leading to similar results as in the experiment at 80 °C described below. Briefly, 250 mg of phloretin (0.91 mmol, 1 eq.), 332 µl of 2-chloroheptanal (2.28 mmol, 339 mg, 2.5 eq.) and 115 mg of $NaHCO_3$ (1.37 mmol, 1.5 eq.) were added to 10 ml of H_2O:DMSO (2:1, v/v). The suspension was then stirred for 2 h at 80 °C until no more starting material could be detected (HPLC, 285 nm). After cooling to ambient conditions the reaction mixture was extracted twice with 25 ml EtOAc and washed with saturated NaCl. The organic solvent was removed under reduced pressure; the residue was transferred to a silica-samplet and dried for 2 h at 50 °C in a drying oven. Subsequently, the silica-samplet was subjected to automated flash chromatography with petroleum ether/ethyl acetate (0 to 45% gradient) as eluent to provide 187 mg (53%) of the pure product as a brownish solid. The resulting compound was analyzed in co-operation with R. Saf (TU Graz). Therefore, EI (70 eV) mass spectra were recorded on a Waters GCT Premier equipped with direct insertion (DI).

6. IN VITRO ASSAYS

6.1. *MTT-Test*

To investigate the effects of 2-ClHDA, structural analogues of 2-ClHDA, and reagent NaOCl on BMVEC viability in the absence or presence of polyphenols, myriocin, and thiol compounds an assay based on the compound 3-(4,5-Dimethylthiazol-2-yl)-2,5-diphenyltetrazolium bromide (MTT, ***Figure 14***) was used (Kratzer et al. 2007). BMVEC were grown in 12-, 24- or 96-well plates to confluence before the cells were treated with 2-ClHDA or reagent NaOCl in serum-deprived medium at the indicated concentrations and for the indicated time periods. In the case of co-treatment cells were pre-incubated with polyphenols, myriocin and thiol compounds at indicated concentration for 30 min before 2-ClHDA or NaOCl was added. After treatment, medium containing tested compounds was replaced by 'MTT medium' (1.2 mM, dissolved in serum-free medium, 100 µl per well) added to cells and incubated for 1 to 2 h at 37°C under standard conditions. Cells were washed with PBS, and cell lysis was performed with 100 µl lysis solution (isopropanol:1 M HCl, 25:1 (v/v)) on a rotary shaker (1000 rpm, 15 min). Absorbance was measured at 570 nm on a Victor 1420 multilabel counter and corrected for background absorption (650 nm).

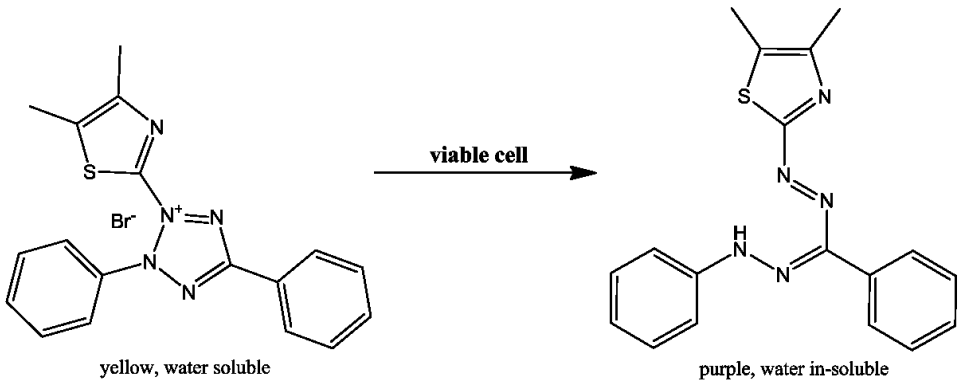

Figure 14: **Principle of the MTT-test**
Reduction of the water-soluble tetrazolium salt MTT metabolically active cells (viable and early apoptotic) leads to precipitation of colored formazans. MTT reduction is mostly attributable to oxidoreductases localized at mitochondria, in cytoplasm and in regions of plasma membranes (Bernas and Dobrucki 2002).

6.2. *JC-1 Assay*

To examine the mitochondrial membrane potential (Δψm) of BMVEC - after treatment with 2-ClHDA or NaOCl - an assay based on the compound JC-1 ***(Figure 15)*** was performed (Nusshold et al. 2010). Briefly, BMVEC were grown to confluence in black 96-well plates before 2-ClHDA or reagent NaOCl were added in serum-deprived medium at the indicated concentrations and for the indicated time periods. Cells were then incubated with JC-1 (10 µM, added to serum-free medium as 2 mM stock in DMSO, 100 µl per well) at 37°C in the dark for 90 min followed by two washing steps with PBS. Fifty microliters of PBS were then added to each well and the fluorescence intensities were read at 484/540 nm (ex/em) for detection of the green substrate and 544/590 nm (ex/em) for detection of the red substrate on a Victor 1420 multilabel counter. The results were analyzed in terms of the ratio of red to green fluorescence intensities. Therefore, results are not linked to the number of viable cells.

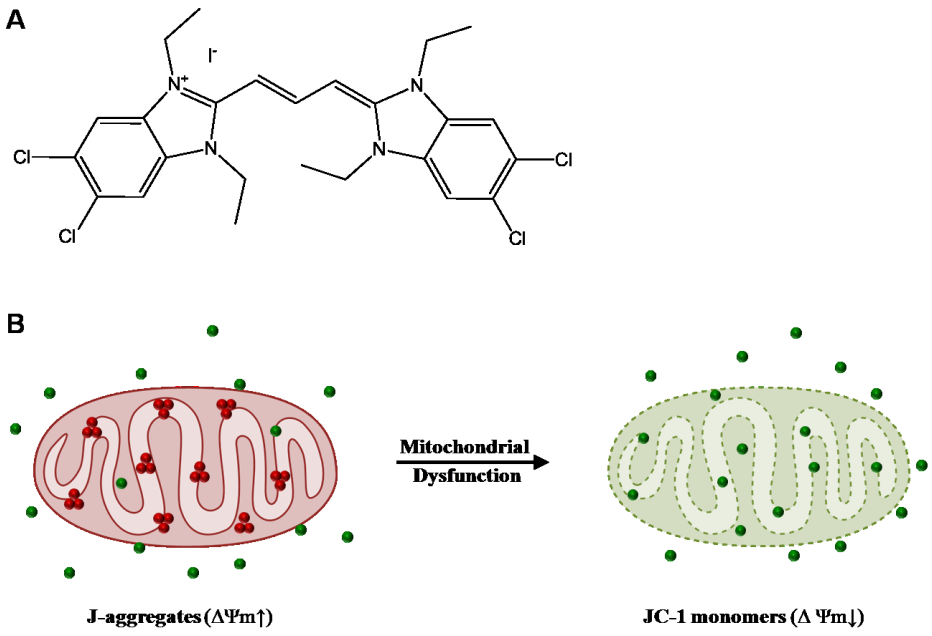

***Figure 15*: Principle of the JC-1 assay**

(**A**) Structure of the JC-1 monomer. (**B**) JC-1 is a cationic carbocyanine dye that exhibit green fluorescence. JC-1 accumulates in healthy mitochondria, where it forms J-aggregates that exhibit red fluorescence. Changes in the mitochondrial membrane potential (ΔΨm) as occurring during apoptosis results in decreased mitochondrial JC-1 concentrations, which can be followed by an increase of green fluorescence (Bedner et al. 1999).

6.3. *Measurement of ROS*

ROS formation was explored by using an assay based on the redox-sensitive fluorescent dye carboxy-H_2DCFDA (***Figure 16***). BMVEC were grown to confluence in black 6-well plates before cells were incubated with H_2DCFDA dissolved in PBS (10 µM, added as 300x stock in DMSO) for 1 h at 37°C in the dark. Subsequently, H_2DCFDA in PBS was replaced by serum-deprived medium containing indicated concentrations of 2-ClHDA, followed by incubation of cells for the indicated time periods at 37°C in dark. Incubations were stopped by washing the cells two times with ice-cold PBS and, then, the plates were kept on ice for 10 min. Cell lysis was performed with 300 µl lysis solution (3% Triton X-100 in PBS) on a rotary shaker (1350 rpm) at 4°C in the dark for 60 min. Afterwards, 50 µl EtOH abs. was added to each well and shaking was continued for another 15 min to ensure complete solubilization of deacetylated and oxidized DCF. The cell lysates were transferred to Eppendorf tubes and centrifuged to remove cellular debris (13,000 rpm, 4°C, 10 min). One hundred microliters of the supernatant were transferred to black 96-well microtiter plates and fluorescence intensity was measured at 484/540 nm (excitation/emission) on a Victor 1420 multilabel counter (Wallac). An aliquot of the supernatant was used for estimation of protein concentration using the Bradford assay.

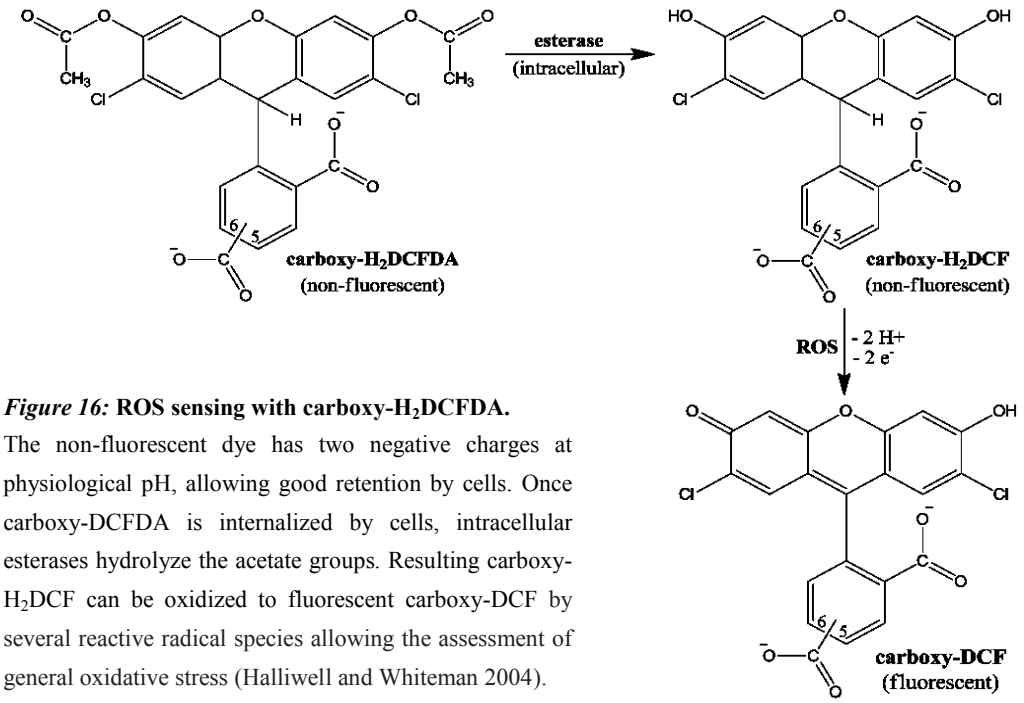

Figure 16: **ROS sensing with carboxy-H_2DCFDA.**
The non-fluorescent dye has two negative charges at physiological pH, allowing good retention by cells. Once carboxy-DCFDA is internalized by cells, intracellular esterases hydrolyze the acetate groups. Resulting carboxy-H_2DCF can be oxidized to fluorescent carboxy-DCF by several reactive radical species allowing the assessment of general oxidative stress (Halliwell and Whiteman 2004).

7. DETERMINATION OF 2-ClHDA STABILITY AND METABOLISM

7.1. *Stability in the Presence of a Mixed Primary Mouse Brain Cell Suspension*

Mouse brains were collected from animals killed by cervical dislocation. For each sample, 400 mg brain tissue was minced and supplemented to a final volume of 2 ml with HBSS (with 1 g/l glucose) containing 0.25 U dispase. After incubation for 90 min at 37°C with stirring enzymatic digestion was stopped by washing (120 *g*, 10 min, RT) the brain cell suspension for 3 times with 2 ml HBSS (supplemented with 1 g/ml glucose) containing 1 mM EDTA. Subsequently, 2 ml brain cell suspension was supplemented with 2-ClHDA (17 µg; 30 µM final concentration) and further incubated at 37°C under gentle stirring. At indicated time points 125 µl aliquots were removed, snap frozen in liquid N_2, and stored at -70°C until further processing. Lipids were extracted in the presence of 0.75 µg 2-Cl[$^{13}C_8$]HDA according to the Folch procedure, converted to corresponding PFB-derivatives and quantified by NICI-GC-MS using 2-Cl[$^{13}C_8$]HDA as internal standard (see below). A one-phase exponential decay model ($A*e^{-kt}$) was used to fit experimental data using Prism 5.0 (GraphPad Software).

7.2. *Stability in Human Plasma*

Human plasma from healthy, normolipidemic subjects was obtained from the Department of Blood Group Serology and Transfusion Medicine (Medical University Graz). Briefly, 10 ml plasma were spiked with 50 µM 2-ClHDA (added as 250 x stock in DMSO) and incubated at 37°C under gentle stirring. At the indicated times 500 µl aliquots were removed, snap frozen in liquid N_2 and stored at -70°C until further processing. Following lipid extraction (Folch et al. 1957) PFB-oximes were prepared and relative 2-ClHDA contents were analyzed of by NICI-GC-MS (see below). A one-phase exponential decay model ($A*e^{-kt}$) was used to fit experimental data using Prism 5.0 (GraphPad Software).

7.3. *Stability in Murine Vasculature*

C57BL/6 mice received a single intravenous injection of either 350 µg 2-ClHDA/30 g body weight in 100 µl Intralipid 20%/PBS/sesame oil, 47:40:13 (v/v) or 100 µl vehicle. At the indicated time periods 100 µl EDTA-blood (5 mM EDTA) was obtained by retro-orbital puncturing. After addition of one 1 µg 2-Cl[$^{13}C_8$]HDA samples were snap frozen in liquid N_2 and stored at -70°C until further processing. Lipids were extracted according to the Folch procedure. Subsequently, PFB-oximes were prepared and 2-ClHDA was quantitatively analyzed by NICI-GC-MS using 2-Cl[$^{13}C_8$]HDA as internal standard (see below). A one-phase exponential decay model ($A*e^{-kt}$) was used to fit experimental data using Prism 5.0 (GraphPad Software).

7.4. *Stability in BMVEC Culture*

BMVEC were plated in 6-well trays and allowed to grow to confluence (9×10^5 cells). Cells were incubated with 4.1 µg 2-ClHDA (250 x stock in DMSO; 10 µM final concentration). At indicated time periods lipids from the culture medium were extracted twice in hexane/methanol (5:1; v/v, 2 ml) in the presence 100 ng 2-Cl[$^{13}C_8$]HDA. After conversion to corresponding PFB-oxime derivatives 2-ClHDA was quantitated by NICI-GC-MS analysis using 2-Cl[$^{13}C_8$]HDA as internal standard (see below). A one-phase exponential decay model ($A*e^{-kt}$) was used to fit experimental data using Prism 5.0 (GraphPad Software).

7.5. *Metabolism of 2-ClHDA by BMVEC*

BMVEC, plated in 6-well trays, were grown to confluence (9×10^5 cells). Cells were incubated with 4.1 µg 2-ClHDA (250 x stock in DMSO; 10 µM final concentration) for the indicated time periods. Subsequently, lipids from culture medium were extracted twice with hexane/methanol (5:1; v/v, 2 ml) in the presence of 2-Cl[$^{13}C_8$]HDA, pentadecanoic acid and pentadecanol (each 100 ng). Cellular lipids were extracted in the presence of above mentioned internal standards (each 100 ng) using two consecutive extractions (30 min each) with 1 ml of hexane/isopropanol (3:2; v/v) on a rotary shaker (1000 rpm). Following preparation of PFB-oxime and PFB-ester derivatives 2-ClHDA, 2-ClHA and 2-ClHOH were quantitated by NICI-GC-MS analysis using 2-Cl[$^{13}C_8$]HDA, pentadecanoic acid or pentadecanol as internal standards.

7.6. *Quantification of 2-ClHA Re-Esterification into the Polar Lipid Fraction*

BMVEC plated in petri dishes (10 cm) were grown to confluence (5.5 x 10^6 cells). Cells were incubated with 22.3 µg 2-ClHDA (250 x stock in DMSO; 10 µM final concentration) for the indicated time periods. Subsequently, cellular lipids were extracted in the presence of the internal standard pentadecanoic acid (1.5 µg) using two consecutive extractions (30 min each) with 5 ml of hexane/isopropanol (3:2, v/v) on a rotary shaker (1000 rpm). Lipids were reconstituted in 1 ml $CHCl_3$/MeOH (1:1, v/v), and 500 µl were converted to the corresponding PFB-esters, and analyzed by NICI-GC-MS as described below (free 2-ClHA). For isolation of polar lipid fraction remaining 500 µl of cellular lipids were separated on silica gel 60 plates using hexane/diethyl ether/acidic acid (70:30:1, v/v/v) as the mobile phase. Fractions co-migrating with DPPC standard were scraped off, and extracted from the TLC sorbent using $CHCl_3$/MeOH (2:1, v/v). For generation of free fatty acids, polar lipids were dispersed in 500 µl 0.5 M NaOH by sonication and vortexing, and incubated for 1 h in a boiling water bath. Subsequently, samples were cooled to RT, neutralized by addition of 500 µl 0.5 M HCl, and acidified with acetic acid. Released free fatty acids were extracted according to the Folch procedure, converted to the corresponding PFB-ester derivative, and quantitated by NICI-GC-MS (esterified 2-ClHA).

8. ANALYTICAL TECHNIQUES

8.1. *Fourier Transform-Ion Cyclotron Resonance-Mass Spectrometry (FT-ICR-MS)*

Analysis was performed by H. Köfeler (Core Facility Mass Spectrometry, MUGi Graz) on an Accela U-HPLC coupled to a LTQ-FT Ultra hybrid mass spectrometer (Thermo Scientific, Vienna, Austria). Samples were diluted (1:100) in chloroform/methanol (1:1, v/v). Either D-31 34:1 phosphatidylcholine (PC) or 12:0/12:0 PC as well as LIPID MAPS standards (Avanti® Polar Lipids) LM-1004 (17:0-14:1 PC), LM-1102 (17:0-20:4 phosphatidylethanolamine), LM-1303 (21:0-22:6 phosphatidylserine), and LM-1504 (17:0-14:1 phosphatidylinositol) were used as internal standards. Lipid samples were separated on a Thermo Hypersil GOLD C18 column (100 x 1 mm, 1.9 µm particle size). Solvent A was water with 1% ammonium acetate and 0.1% formic acid. Solvent B was acetonitrile/2-propanol (5:2; v/v) with 1% ammonium acetate and 0.1% formic acid. The gradient ran from 35% to 70% B in 4 min, then to 100% B in another 16 min with a hold for additional 10 min. The flow rate was 250 µl/min. Data acquisition was done by FT-ICR-MS full scan in preview mode, a resolution of 200k, and < 2 ppm mass accuracy with external calibration. The spray voltage was set to 5000 V, capillary voltage to 35 V, and the tube lens was at 120 V. Capillary temperature was at 250°C. From the FT-ICR-MS preview scan the 4 most abundant m/z values were picked in data dependent acquisition mode, fragmented in the linear ion trap analyzer and ejected at nominal mass resolution. Normalized collision energy was set to 35%, the repeat count was 2, and the exclusion duration at 60 sec.

8.2. *Synthesis of Stable-Isotope Labeled 2-ClHDA*

2-Chloro-[2,4,6,8,10,12,14,16-$^{13}C_8$]-hexadecanal (2-Cl[$^{13}C_8$]HDA) and 2-ClHDA were synthesized and purified as previously described (Albert et al. 2001) with some modifications (***Figure 17***). Briefly, 1 eq. hexadecanoic-2,4,6,8,10,12,14,16-$^{13}C_8$ acid was reduced to hexadecanol-[2,4,6,8,10,12,14,16-$^{13}C_8$] by using 4 eq. $LiAlH_4$ (refluxed at 50°C overnight in dry diethyl ether; the reaction was quenched by addition of ethyl acetate and Milli-Q water). Hexadecanal-[2,4,6,8,10,12,14,16-$^{13}C_8$] was synthesized by partial oxidation of 1 eq. hexadecanol-[2,4,6,8,10,12,14,16-$^{13}C_8$] in CH_2Cl_2 at -70°C for 1 h under a stream of N_2 utilizing oxalyl chloride-activated dimethyl sulfoxide (3 eq. oxalyl chloride and 6 eq. DMSO) as a catalyst. The reaction mixture was quenched by addition of 12 eq. triethylamine, stirred for additional 10 min, and allowed to warm at RT. After washing the reaction mixture with Milli-Q water

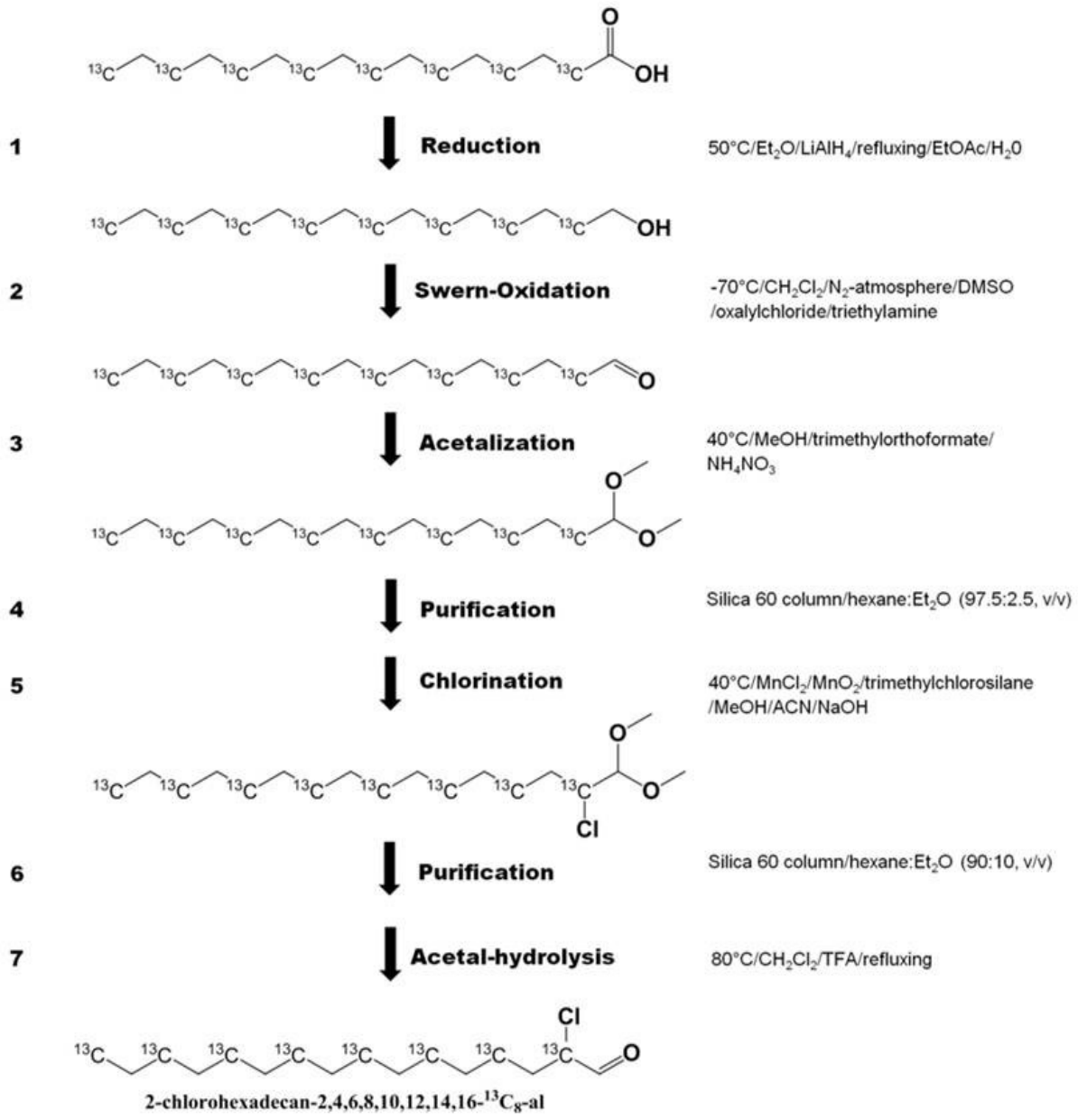

Figure 17: Summary of 2-Cl[$^{13}C_8$]HDA synthesis

the organic phase was brought to dryness and converted to the dimethyl acetal (dma) derivative by addition of methanol:trimethyl orthoformate (90:10, v/v) and NH_4NO_3 and incubation for 48 h at 40°C. Subsequently, hexadecanal-[2,4,6,8,10,12,14,16-$^{13}C_8$] dimethyl acetal (HDA-[$^{13}C_8$] dma) was purified using a Silica 60 column and hexane/diethyl ether (97.5:2.5, v/v) as eluent. For synthesis of 2-Cl[$^{13}C_8$]HDA dma, HDA-[$^{13}C_8$] dma in acetonitrile (1.25%, w/v) was added to a suspension of $MnCl_2$ (2.5%, w/v) and MnO_2 (2.5%, w/v). Then trimethylchlorosilane (10%, v/v) was added and the reaction mixture was heated to 40°C. After 16 h, 0.5 M NaOH (75%, v/v) was added for alkalization, 2-Cl[$^{13}C_8$]HDA dma was extracted with hexane, and purified using a Silica 60 column and hexane/diethyl ether (90:10, v/v) as eluent. For each experiment 2-Cl[$^{13}C_8$]HDA was freshly prepared by refluxing the dimethyl acetal derivative in trifluoroacetic acid/CH_2Cl_2 (1:1 , v/v) at 80°C for 1h. Purity was confirmed by TLC, as well as by EI-GC-MS and NICI-GC-MS of the corresponding PFB-oxime derivative (*see below*).

8.3. *Pre-Separation of Brain Lipid Extracts by Thin Layer Chromatography*

For 2-ClHDA quantification in brain tissue of mice suffering from neuroinflammation lipid extracts from one brain (2.5 µg 2-Cl[$^{13}C_8$]HDA added as I.S.), were reconstituted in 500 µl $CHCl_3$ and fractionated on silica gel 60 plates using hexane/diethyl ether/acidic acid (90:10:1, v/v/v) as the mobile phase. Fractions co-migrating with an authentic 2-ClHDA standard were scraped off, extracted from the TLC sorbent, converted to the corresponding PFB-oximes, and analyzed by GC-MS as described below.

8.4. *Derivatization*

8.4.1. Chlorinated- and Non-Chlorinated Fatty Aldehydes

2-ClHDA as well as lipid extracts from brain tissue or cell culture (containing 2-Cl[$^{13}C_8$]HDA as I.S.) were dissolved in 100 µl ethanol and 100 µl of a solution of PFB-hydroxylamine in ethanol (6 mg/ml, w/v). After 1 h at 25°C, 1 ml of distilled water was added, and the PFB oxime derivative was extracted with hexane/diethyl ether (4:1, v/v) and dried under N_2. The samples were redissolved in 100 µl hexane, transferred to autosampler vials, and stored at -20°C until NICI-GC-MS analysis.

8.4.2. Chlorinated Fatty Acids

Lipid extracts from cell culture (containing pentadecanoic acid as I.S.) were converted to corresponding PFB-ester derivative in 100 µl 0.35% (v/v) PFB-Br in acetonitrile and 20 µl N,N-diisopropylethylamine. After 30 min at RT derivatization reagents were vacuum evaporated with an Eppendorf concentrator 5301. The samples were redissolved in 100 µl hexane, transferred to autosampler vials, and stored at -20°C until GC/MS analysis.

8.4.3. Chlorinated Fatty Alcohols

Lipid extracts from cell culture (containing pentadecanol as I.S.) were converted to corresponding PFB-ester derivative in 100 µl 0.4% (v/v) PFBoyl-Cl in acetonitrile. After 1 h at 80°C PFBoyl-Cl solution was vacuum evaporated with an Eppendorf concentrator 5301 at 45°C. The samples were redissolved in 100 µl hexane, transferred to autosampler vials, and stored at -20°C until GC/MS analysis.

8.4.1. Phloretin

Extracted phloretin was converted to its corresponding TMS-ether derivative in 100 µl MSTFA-solution (MSTFA/pyridine 2:1, v/v; 1% TMCS, v/v). After 1 h at RT the sample was transferred to autosampler vials, and stored at -20°C until GC/MS analysis.

8.5. *Electron Impact-Gas Chromatography-Mass Spectrometry (EI-GC-MS)*

A Thermo Scientific Trace GC coupled to a DSQII mass spectrometer was used. The GC was fitted with a SGE BPX5 capillary column (15 m, 0.25 mm inner diameter, 0.25 µm methyl silicone film coating). The injector was operated in the splitless mode at 180°C. Helium was used as carrier gas at a flow rate of 1 ml/min. Initial column temperature was 80°C for 2 min, followed by an increase of 30°C/min to 170°C, an isothermal hold of 2 min, a second increase at 30°C/min to 230 °C, an isothermal hold for 3 min and increased by 20°C/min to 300°C with a hold for 3 min. The transfer line was kept at 310°C and the ion source was 200°C. Electron impact spectra were recorded with electron energy of 70 eV, and an emission current of 100 µA. Samples were monitored either in full scan mode or in selected ion monitoring mode (SIM).

8.6. *Negative Ion Chemical Ionization-Gas Chromatography-Mass Spectrometry (NICI-GC-MS)*

Samples were separated on a Thermo Scientific Trace GC Ultra (helium was used as carrier gas, 2 ml/min) with a SGE BPX5 capillary column (15 m, 0.25 mm inner diameter, 0.25 µm methyl silicone film coating) and analyzed using a DSQII mass spectrometer (Thermo Scientific). Injector temperature was set to 230°C and ion source temperature was 200°C. The oven temperature was maintained at 100°C for 5 min, increased during the first ramping step at a rate of 20°C/min to 175°C, and held at 175°C for 1 min. In the second ramping step the temperature was raised at a rate of 15°C/min to 280°C and held at 280°C for additional 2 min. All spectra were monitored in NICI (methane was used as reagent gas), either in full scan mode or using SIM mode. In SIM target compounds were identified at molecule specific mass-to-charge ratios (***Table 5***), characteristic isotope distribution of chlorine (Cl^{35}/Cl^{37}, 3:1) and retention times (not listed due to minute variations caused by column cutting). Quantitation was performed by peak area comparison with internal standards (*Table 5*).

Table 5: Identification and quantification to target compounds in SIM

Target compound	m/z	Internal standard (I.S.)	m/z	I.S. (ng)
Fatty aldehydes				
2-ClHDA	288/290, 414	2-Cl[$^{13}C_8$]HDA	288/290, 422	100 - 2500
HDA	254, 415			100 - 500
2-ClODA	316/318, 442			100 - 500
ODA	282, 443			100 - 500
2-ClODEA	314/316, 440			100 - 500
ODEA	280, 441			100 - 500
Fatty acids				
2-ClHA	289/291, 254	pentadecanoic acid	241	100-1500
Fatty alcohols				
2-ClHOH	470/472, 435	pentadecanol	422	100

8.7. *Sodium Dodecylsulfate Polyacrylamide Gel Electrophoresis (SDS-PAGE) and Immunoblotting of Caspase-3 and MAPK-Proteins*

BMVEC were plated in 6-well trays and allowed to grow to confluence (9×10^5 cells). Cells were incubated in the absence or presence of 2-ClHDA, reagent NaOCl, colchicine or staurosporine at the indicated concentrations and for the indicated time periods. For protein isolation, the cells were washed twice with ice-cold PBS and then scraped in 50-100 µl lysis buffer containing 1 mM PMSF and 1 µg/ml each aprotinin, leupeptin, and pepstatin. After removing cellular debris by centrifugation (13,000 rpm, 4 °C, 10 min) the protein content was determined using the Bradford assay. Protein extracts were diluted in sample buffer, heated to 95 °C for 5 min before proteins were separated by SDS–PAGE (10 or 12% PA-gels, 150 V). Subsequently, proteins were electrophoretically transferred onto PVDF membranes (150 mA, 45 min). Nonspecific adsorption was blocked by incubation with 5% (w/v) nonfat milk powder in Tris-buffered saline Tween 20 (TBS-T). Following primary antibodies were applied by overnight incubation at 4°C: Rabbit anti-caspase-3 (diluted 1: 400 in 5% (w/v) nonfat milk (in TBS-T)) or phosphospecific antibodies against mouse ERK1/2- (p-ERK1/2), rabbit p38- (p-p38), and rabbit JNK1/2 (p-JNK1/2) (diluted 1:500 in 3% (w/v) BSA (in TBS-T)). Immunoreactive bands were visualized using HRP-conjugated goat anti-rabbit IgG and goat anti-mouse IgG (1:5000 and 1:2500 in 5% (w/v) nonfat milk powder in TBS-T, 2 h, RT) and subsequent ECL SuperSignal (caspase-3) or ECL Plus (p-MAPK) development. For normalization, membranes were stripped with Stripping buffer at 50°C for 30 min with gentle shaking and reprobed with primary antibodies against the following pan-proteins (overnight, diluted 1:1000 in 5% (w/v) non fat milk in TBS-T): rabbit ERK1/2, mouse p38 and rabbit JNK1/2. Detection of immunoreactive bands was performed as mentioned above with HRP-conjugated goat anti-rabbit or goat anti-mouse secondary antibodies using the ECL system.

8. STATISTICAL ANALYSES

Data are presented as means ± SD or SEM. To test differences in groups statistical significance was determined by one- or two way ANOVA with Dunnett or Bonferroni correction, by Student's unpaired *t* test (two-tailed) or (for qPCR data) by REST 38, version 2 (Pfaffl et al. 2002). All values of $p \leq 0.05$ were considered significant. $^*p < 0.05$, $^{**}p < 0.01$, $^{***}p < 0.001$.

VI. RESULTS

*CHAPTER 1 NEUROINFLAMMATION - THE ROLE OF CHLORINATIVE STRESS IN PLASMALOGEN DEFICIENCY**

* published data:

Üllen, A; Fauler, G; Köfeler, H; Waltl, S; Nusshold, C; Bernhart, E; Reicher, H; Leis, HJ; Wintersperger, A; Malle, E; Sattler, W. **Mouse brain plasmalogens are targets for hypochlorous acid-mediated modification *in vitro* and *in vivo*.** Free Radic Biol Med. 2010; 49(11):1655-1665

Background:

The mammalian brain is particularly sensitive towards oxidative damage, a result of the high oxygen demand and the high content of unsaturated lipids in the CNS (Halliwell 2006). Potential sources of reactive species in the brain are mitochondria, amyloid-β peptides, redox-active iron, the NADPH-oxidase complex, and MPO (Halliwell 2006, Klebanoff 2005, Yap et al. 2007). Since elevated levels of reactive species induce cellular damage of neurons (Yap et al. 2006), endothelial cells (Fisher 2008) and astrocytes (Choi J. J. et al. 2007a) oxidative/chlorinative stress is implicated in neurodegeneration. Potential cellular and extracellular targets of reactive species are proteins, lipids, carbohydrates and nucleic acid (Bandyopadhyay et al. 1999, Rees et al. 2008). Loss of glycerophospholipids, predominantly plasmalogens, was reported for several neuropathological conditions including ischemia (Viani et al. 1995), AD (Ginsberg et al. 1995, Han X. et al. 2001), Down syndrome (Murphy E. J. et al. 2000), GD (Moraitou et al. 2008) or EAE (Singh I. et al. 2004). Although increasing evidence points toward MPO as a disease-amplifying enzyme in neurodegeneration (Yap et al. 2007) the role of chlorinative stress in plasmalogen loss remains controversial due to downregulation of key enzymes involved plasmalogen synthesis (Cimini et al. 2003, Singh I. et al. 2004) and activation of a plasmalogen-specific phospholipase under inflammatory conditions (Farooqui 2010).

Aims:

Above-mentioned evidence implicates that MPO is present in brain tissue of MS and AD patients and that local activation of MPO might contribute to neuropathology apparently via plasmalogen modification.

i. Therefore, the first aim of this study was to characterize the loss of plasmalogens and concomitant product formation in response to reagent HOCl in a complex matrix of mouse brain lipid extracts by ESI FT-ICR-MS and GC-MS analysis *in vitro*.

ii. The second aim, an *in vivo* approach, was designed to obtain evidence for MPO-mediated modification of brain plasmalogens in the CNS. During these studies a mouse model of neuroinflammation should be established by the means of a single LPS bolus. To ensure successful induction of inflammation brain inflammatory markers had to be checked. Once established, this mouse model should provide evidence about the impact of neuroinflammtion on brain plasmalogen composition and formation of 2-ClHDA via the MPO-H_2O_2-chloride system.

1. Mouse Brain Plasmalogens are Preferential Lipid Targets for HOCl Modification: *In vitro* evidence

1.1. *Phospholipid Composition of Mouse Brain Lipids*

ESI-MS technique for phospholipid- and other polar lipid analysis has been applied for the research of intracellular lipid trafficking (Schneiter et al. 1999) and lipid-mediated signaling (Novgorodov et al. 2007, Smith J. C. et al. 2008). Many other approaches targeted phospholipidomic analyses, however, they do not offer sufficiently precise identification of molecular species in each class, and consequently, detailed knowledge about the mouse glycerophospholipidome has been very limited (Taguchi and Ishikawa 2010, Yang K. et al. 2007a). One reason for this observation might be the rather low resolution and mass accuracy of mass spectrometers used in these reports.

Therefore, in a first series of experiments the quantitative composition of the total mouse brain phospholipidome was analyzed with very high resolution (200 k) at < 2 ppm mass accuracy by hybrid linear ion trap-Fourier transform-ion mass spectrometry in co-operation with H. Köfeler (MUG).

The major contribution is provided by phosphatidylcholine (PC; 37%), followed by phosphatidyl-ethanolamine (PE; 25%), plasmenyl PE (pPE; 23%), phosphatidylserine (PS; 12%), phosphatidyl-inositol (PI; 3%), and plasmenyl PC (pPC; 0.2%) (***Figure 18***). Next, the molecular species composition of these phospholipids was analyzed (***Figure 19 A-F***; the detailed composition including m/z values is displayed in the Supplementary Data, ***Table I and II***).

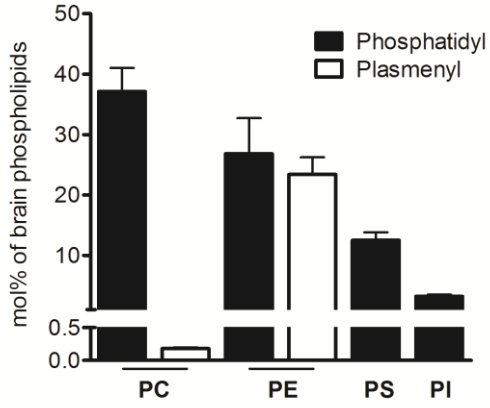

Figure 18: **Composition of the total murine brain glycerophospholipid fraction**

C57BL/6 mice were killed by cervical dislocation, brains were removed, homogenized in liquid N_2, lipids were extracted (twice) using a modified Folch extraction, dried under N_2, redissolved in $CHCl_3$/MeOH (1:1, v/v), and analyzed in the presence of internal standards by a hybrid linear ion trap FT-ICR-MS in positive or negative ESI mode. Data shown represent mean values ± SD from three different mouse brains.

The predominant species within the PC family are 32:0, 34:1, and 36:1 accounting for approx. 70% of total PC (***A***). In the pPC group 34:0 is the most abundant species (54%; ***B***). Within the PE family 38:4 and 40:6 predominate (61%; ***C***) while in the pPE cluster 36:1, 36:2, and 40:6 (43%; ***D***) are the most abundant members. PI contains 63% of 38:4 (***E***) and the major subspecies in PS is 40:6 (63%; ***F***).

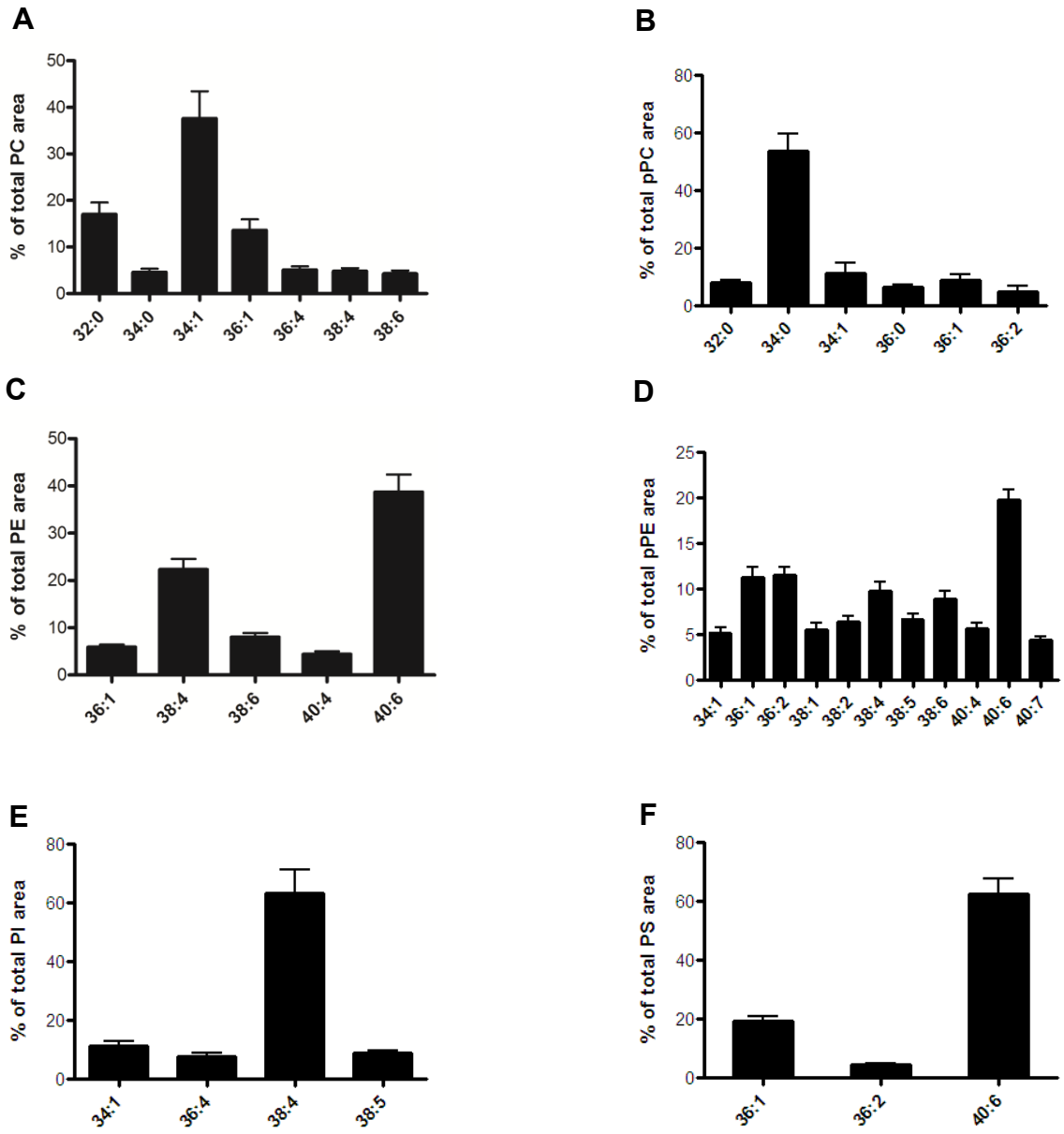

Figure 19: **Molecular subspecies composition of the total murine brain glycerophospholipids fraction**

C57BL/6 mice were killed by cervical dislocation, brains were removed, homogenized in liquid N_2, lipids were extracted (twice) using a modified Folch extraction, dried under N_2, redissolved in $CHCl_3$/MeOH (1:1, v/v). Subspecies of (**A**) PC, (**B**) pPC, (**C**) PE, (**D**) pPE, (**E**) PI, and (**F**) PS of murine brain lipid extracts were analyzed in the presence of internal standards by hybrid linear ion trap FT-ICR-MS in positive or negative ESI mode. Only molecular species contributing > 4% of total area are shown. Data shown represent mean values ± SD from three different mouse brains.

1.2. *Mouse Brain Plasmalogens are the Preferred Lipid Targets for HOCl-Modification*

Lipids comprise an enormous number of chemically distinct molecules which are at this time generally classified into 8 groups: glycerolipids, glycerophospholipids, sphingolipids, sterol lipids, fatty acyls, prenol lipids, saccharolipids, and polyketides (Fahy et al. 2009, Fahy et al. 2005). Random permutations of fatty acids with various backbones and backbone positions as well as combination of different headgroups would hypothetically produce an enormous number of species (Adibhatla et al. 2006). However, up to now LIPID MAPS Consortium has integrated more than 10000 lipid species (Fahy et al. 2009) in their database (http://www.lipidmaps.org). Although plasmalogens are known to be susceptible to oxidation (Albert et al. 2001, Farooqui and Horrocks 2001a) it remained unclear how these compounds behave in the presence of thousands of other brain lipid species.

To elucidate this aspect mouse brain lipid extracts were incubated with reagent NaOCl at increasing mass ratios. FTICR-MS analyses revealed almost quantitative consumption of unsaturated pPE species at oxidant:lipid mass ratios ranging from 1:100 to 10:100 (***Figure 20 A***). In contrast, PE species were more resistant to HOCl treatment (***B***) with quantitative modification occurring at oxidant:lipid mass ratios ranging from 50:100 to 500:100 although observed modification rate of both classes, pPE and PE, increased with the number of hydrocarbon chain double bonds. The corresponding remnant lyso-compounds (formed upon HOCl attack of the vinyl-ether bond and subsequent abstraction of 2-chloroaldehydes from the *sn-1* position (Thukkani et al. 2003a)) are detectable at oxidant:lipid ratios between 1:100 and 50:100 in a transient manner (***C***). Lysophospholipids containing an unsaturated *sn-2* acyl residue (20:4 and 18:1; m/z = 501.3 and 479.3, respectively) are less stable at higher oxidant:lipid ratios as compared to their corresponding saturated counterparts (16:0 and 18:0; m/z = 453.3 and 481.3). Comparable observations were made for pPC and PC subspecies: pPC species are modified at low oxidant:lipid ratios (***D***), while almost complete modification of PC species is observed only at higher HOCl concentrations (50:100 and 500:100; ***E***). PC species appeared to be the most stable phospholipid class analyzed in this approach. Even at a 5-fold reagent HOCl excess over lipids approx. 20% of the 32:0 and 34:0 species were still detectable. Additionally, susceptibility in respect to modification correlated with increasing grade of unsaturation while acyl-chain length did not influence. With regards to lyso-PC formation the accumulation of the unsaturated 20:1 species is transient (m/z = 549.4), whereas accumulation of the corresponding saturated lyso-PC compounds (16:0 and 18:0; m/z = 495.3 and 523.4) occurs in a HOCl-dependent manner (***F***).

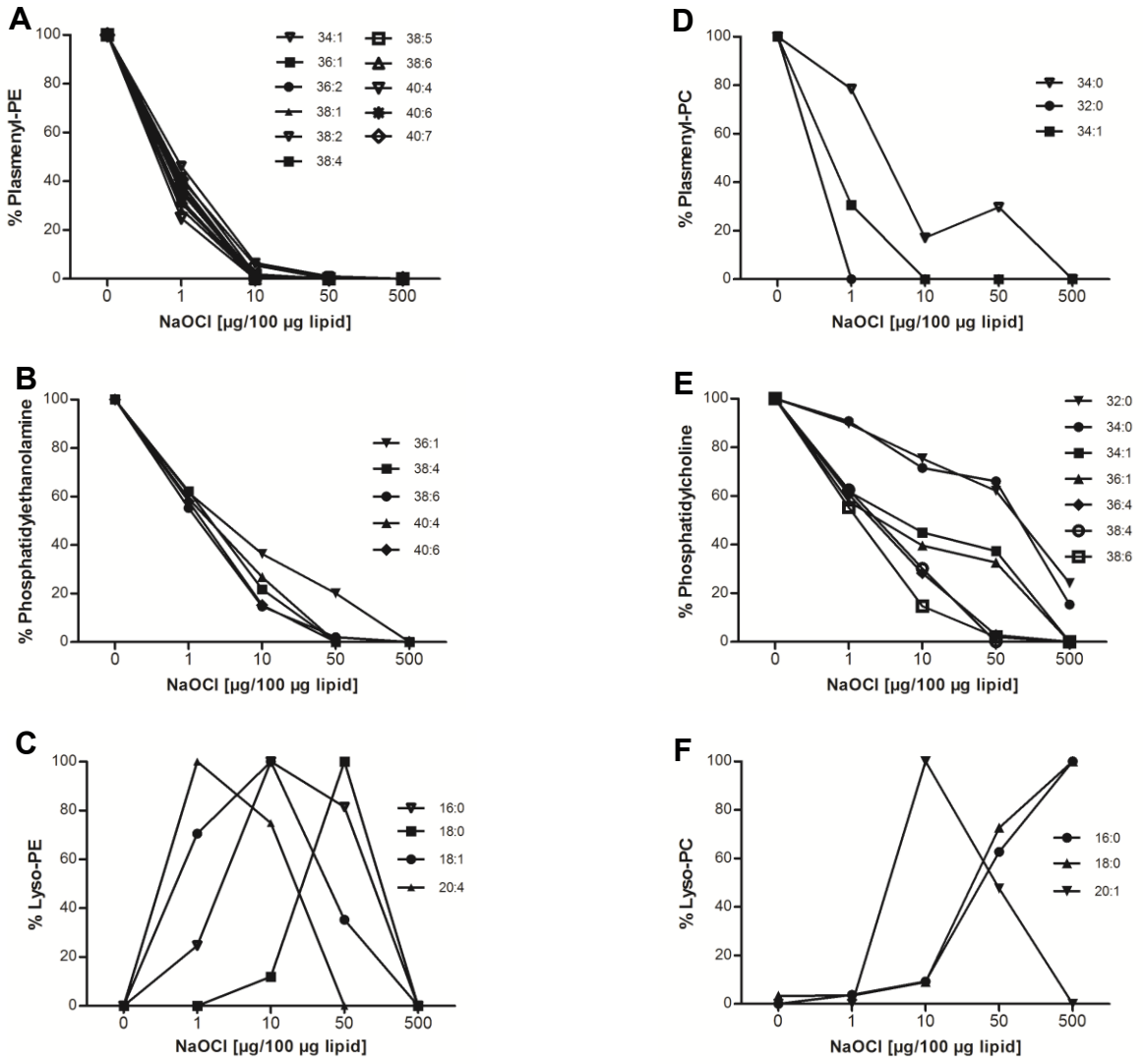

Figure 20: **Brain 1-*O*-alkenyl-2-acyl glycerophospholipids are more sensitive towards HOCl modification than diacyl glycerophospholipids**

Brain lipid extracts were prepared as described in *Figure. 19* and modified at the indicated NaOCl concentrations at RT for 16 h. Analysis was performed by FT-ICR-MS in the positive ESI mode. (**A-C**) Effects of increasing NaOCl:lipid ratios on the composition of pPE, PE, and lyso-PE. (**D-E**) Effects of increasing NaOCl:lipid ratios on the composition of pPC, PC, and lysoPC. Oxidant:lipid ratio is given in terms of w/w. Results are mean values of duplicate determinations.

2. The Vinyl-Ether Linkage of Plasmalogens is Susceptible to HOCl: Release of alpha-Chloro Fatty Aldehydes

2.1. *Plasmalogens Bear a Masked Aldehyde: Vinyl-Ether Linkage between the sn-1 Aliphatic Chain and the Glycerol Backbone*

In contrast to alkyl- and acyl counterparts the *sn-1* alkenyl linkage of plasmalogens has been reported to be prone to acid-catalyzed hydrolysis leading to release of a long-chain fatty aldehyde and a *sn*-1 lyso-phospholipid (Murphy E. J. et al. 1993). This instability can be easily exploited for plasmalogen quantification by measurement of aldehydes originating from plasmalogens. Therefore, several procedures - based on gas chromatography coupled to flame ionization detection or mass spectrometry - have been established to quantify different derivatized long chain fatty aldehydes (Felde and Spiteller 1995, Ingrand et al. 2000, Weisser and Spiteller 1996, Weisser et al. 1997). Moreover, Albert and coworkers could show that the alkenyl-linkage represents a target for reactive chlorinating species leading to oxidative damage of plasmalogens and concomitant release of an α-chloro fatty aldehyde (α-ClFALD (Albert et al. 2001).

Octadecanal (ODA) and 2-chlorooctadecanal (2-ClODA) were released from 25 nmol or 100 nmol C18-plasmenyl Lyso-PC by either hydrochloride (***Figure 21 A***) or NaOCl (***Figure 22 A***) modification. ***Figure 21*** and ***22*** shows representative total ion chromatograms (***B***) and mass spectra (***C***) of pentafluorobenzyl-oxime derivatives of ODA and 2-ClODA eluting at 15.26 and 15.91. Under our analytical conditions the molecular ions (M^-) at m/z 463 (PFB-oxime of ODA) and 497 (PFB-oxime of 2-ClODA) were detected in low abundance (insets). PFB derivatives of ODA and 2-ClODA resulted in the formation of the same distinct fragment ions (***Figure 21 D*** and ***Figure 22 D***, m/z: 178, 181, 196, 282/316, 442/443) although intensity ratios between these fragment ions were completely different suggesting that the presence of a chlorine-residue resulted in altered compound ionization behavior. Moreover, fragment ions observed at 316/318 (2-ClODA) of approx. 3:1 is indicative for the presence of two chlorine isotopes ($^{35}Cl/^{37}Cl$) in the analyte (Thukkani et al. 2003b).

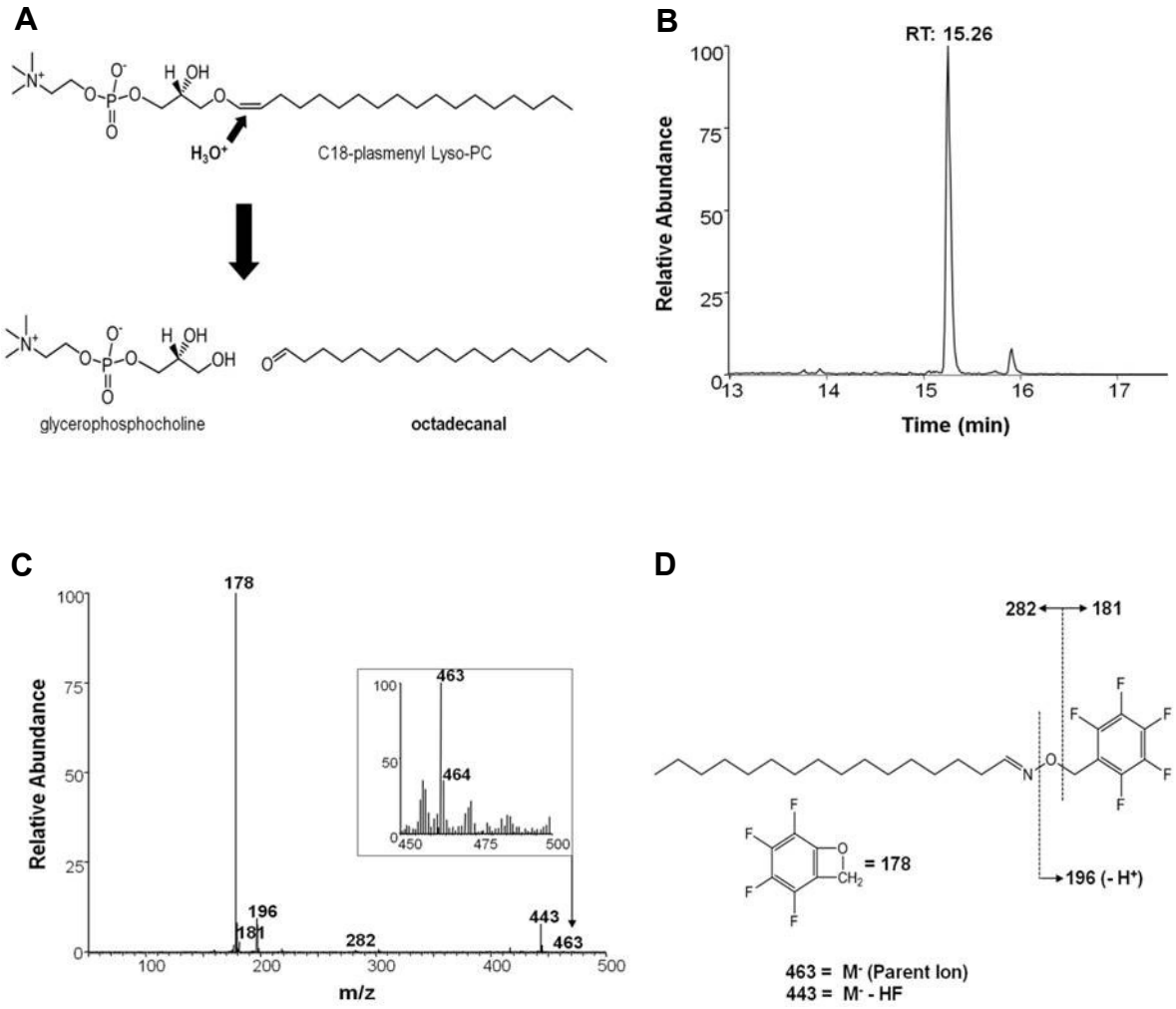

Figure 21: **NICI-GC-MS analysis of plasmalogen-derived octadecanal (ODA)**

(**A**) Reaction pathway leading to the formation of ODA and the remnant glycerophosphocholine. For analysis of fatty aldehyde formation 25 nmol C_{18}-plasmenyl lyso-PC were hydrolyzed in 0.1M HCl at RT for 1 h. (**B**) Total ion current trace and the corresponding (**C**) full scan NICI spectra of ODA PFB-oxime derivative (0.25 nmoles injected) eluting at 15.26 min. Isotope distribution of the molecular ions is indicated by an inset. (**D**) Proposed fragmentation pattern and mass assignment.

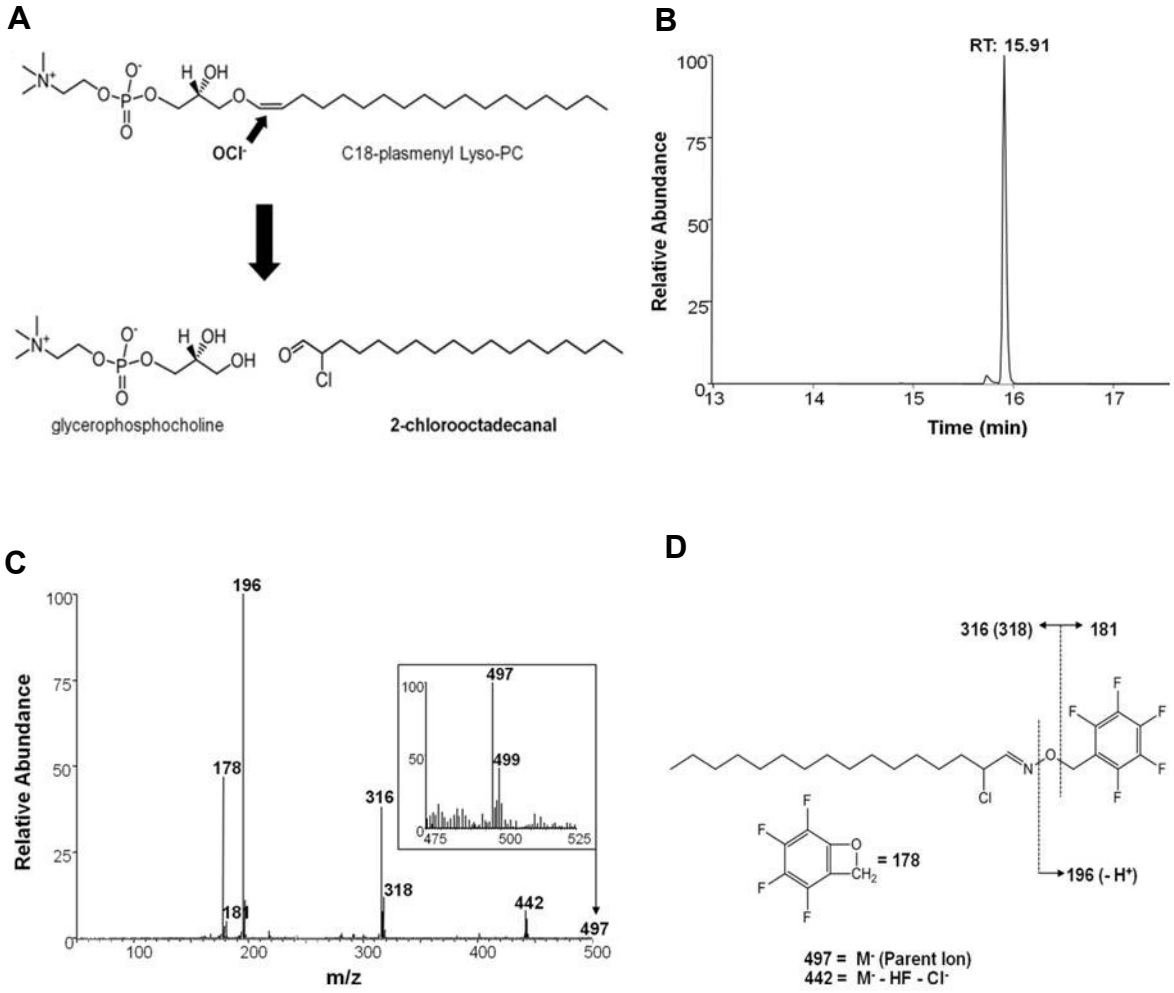

Figure 22: **NICI-GC-MS analysis of plasmalogen-derived of 2-chlorooctadecanal (2-ClODA)**

(**A**) Reaction pathway leading to the formation of 2-ClODA and the remnant glycerophosphocholine. For analysis of α-chloro fatty aldehyde formation 100 nmol C_{18}-plasmenyl lyso-PC were modified by addition of a 2.5-fold molar excess of NaOCl and incubation at RT for 1 h. (**B**) Total ion current trace and the corresponding (**C**) full scan NICI spectra of 2-ClODA PFB-oxime derivative (1 nmol injected) eluting at 15.91 min. Isotope distribution of the molecular ions is indicated by an inset. (**D**) Proposed fragmentation pattern and mass assignment.

2.2. *Synthesis of 2-ClHDA and 2-Cl[$^{13}C_8$]HDA*

Due to a virtually infinite α-ClFALD (native and stable isotope-labeled) demand for the majority of experiments performed in this thesis and due to a lack of commercial availability 2-ClHDA and 2-Cl[$^{13}C_8$]HDA were chemically synthesized as outlined in Material and Methods (***Figure 17***).

Yield and purity of each synthesis or purification step of was monitored by EI-GC-MS analysis. Analysis of the last synthesis products revealed the presence of 2 different compounds eluting at 8.96 min and 9.69 min for non-labeled products as well as 8.94 min and 9.67 min for isotope-labeled ones (***Figure 23 A*** and ***B***, TIC chromatograms). These products were identified as 2-ClHDA dma or 2-Cl[$^{13}C_8$]HDA dma (retention time: 9.69 min or 9.67 min) and palmitoyl methyl ester or $^{13}C_8$-palmitoyl methyl ester (retention time: 8.96 min or 8.94 min), side-products of chlorine addition reaction. Due to these side-products, varying between 10-40% in each preparation, α-ClFALD dma content, was extrapolated from sample mass. Fragmentation patterns of these α-chlorinated palmitaldehyde dimethylacetals (***C*** and ***D***, mass spectra) were similar as previously described (Albert et al. 2009). Base peak of 2-ClHDA dma and 2-Cl[$^{13}C_8$]HDA dma were observed at m/z 75. Molecular ions (M^+) and additional fragments of 2-ClHDA dma were detected in low abundance (insets) at m/z 319, m/z 289, m/z 253 and m/z 221 as well as m/z 327, m/z 297, m/z 261 and m/z 229 for 2-Cl[$^{13}C_8$]HDA dma. The intensity ratios of the fragment ions observed at 288/290 (2-ClHDA) and 296/298 (2-Cl[$^{13}C_8$]HDA) of approx. 3:1 is indicative for the presence of two chlorine isotopes ($^{35}Cl/^{37}Cl$) in the analyte.

For NICI-GC-MS analysis dma-group was decapped and 2-ClHDA or 2-Cl[$^{13}C_8$]HDA was converted into the PFB derivative. ***Figure 24*** shows chromatograms and mass spectra of the PFB-oxime derivatives of 2-ClHDA (***A*** and ***B***) and 2-Cl[$^{13}C_8$]HDA (***C*** and ***D***) eluting at 14.97 min. Molecular ions (M^-) at m/z 469 (PFB-oxime of 2-ClHDA) and 477 (PFB-oxime of 2-Cl[$^{13}C_8$]HDA), were detected in low abundance (insets). The intensity ratios of the fragment ions observed at 288/290 (2-ClHDA) and 296/298 (2-Cl[$^{13}C_8$]HDA) of approx. 3:1 is indicative for the presence of two chlorine isotopes ($^{35}Cl/^{37}Cl$) in the analyte. The additional fragment ions observed at m/z 414 (or 422 for 2-Cl[$^{13}C_8$]HDA), 196, 181, and 178 are characteristic for the 2-ClHDA PFB-oxime derivatives (Thukkani et al. 2002).

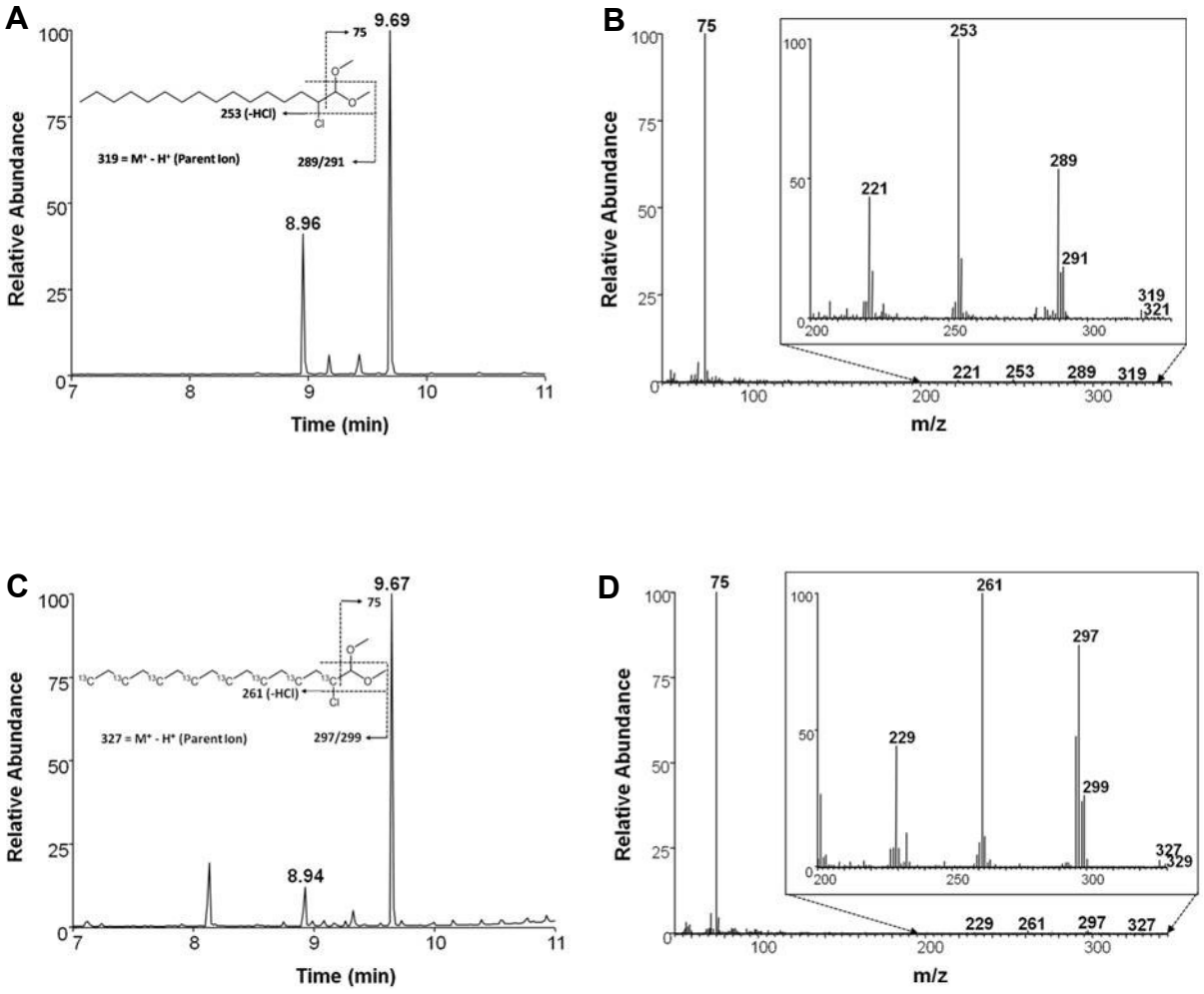

Figure 23: **EI-GC-MS analysis of synthetic 2-ClHDA dma and 2-Cl[$^{13}C_8$]HDA dma**

Total ion current traces of (**A**) 2-ClHDA dma (**B**) or 2-Cl[$^{13}C_8$]HDA dma (each 1 µg injected) after Silica 60 column purification. Compounds eluting at 9.69 and 9.67 min were identified as (**C**) 2-ClHDA dma and (**D**) 2-Cl[$^{13}C_8$]HDA dma by specific fragmentation patterns obtained from full scan EI spectra. Proposed fragmentation patterns and mass assignments are indicated in the insets. Peaks eluting at 8.96 and 8.94 min (**A** and **C**) correspond to unlabeled or labeled palmitoyl methyl esters, which represent side products of α-chlorination.

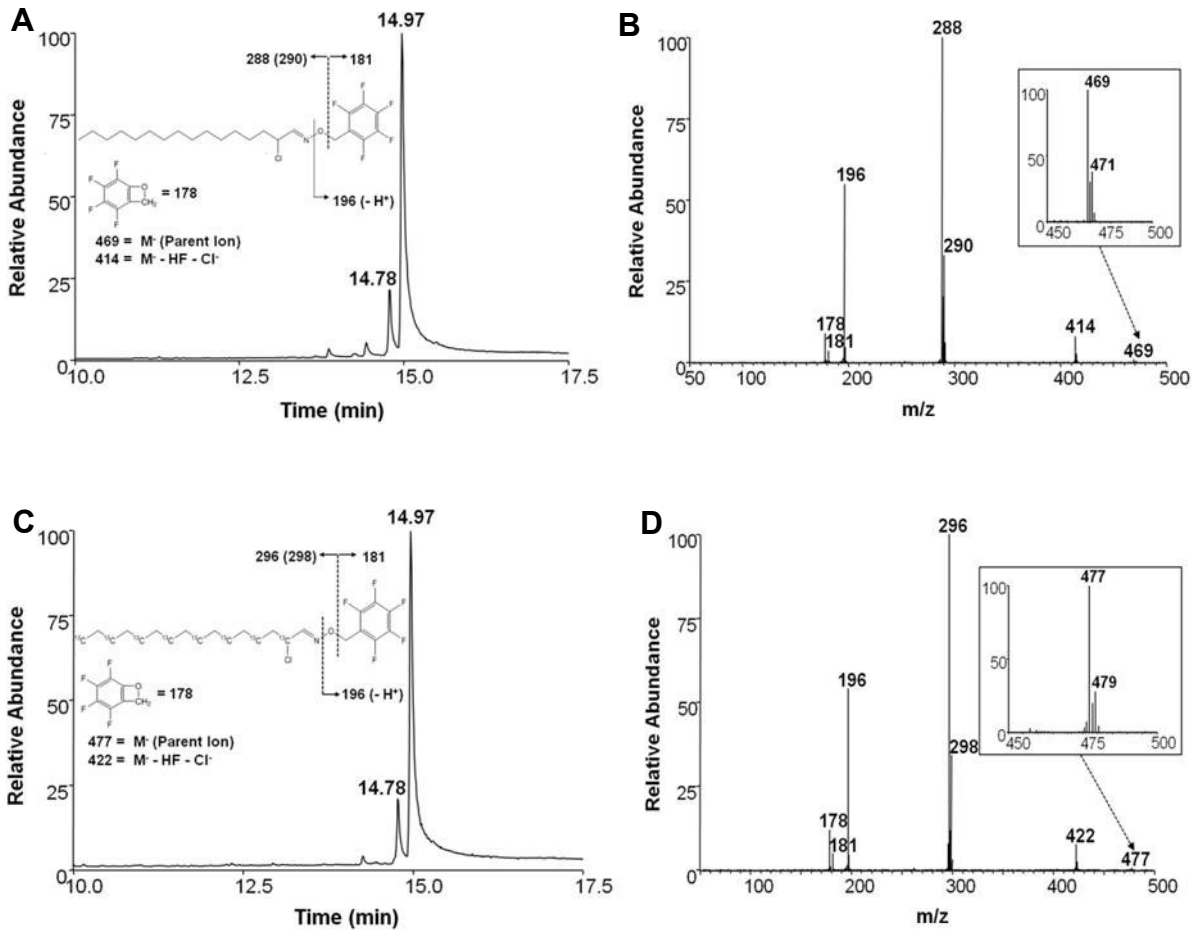

Figure 24: **NICI-GC-MS analysis of synthetic 2-ClHDA and 2-Cl[$^{13}C_8$]HDA**

For NICI-GC-MS analysis dma-group was decapped and 2-ClHDA/2-Cl[$^{13}C_8$]HDA was converted into the PFB derivative. (**A** and **C**) Total ion current traces of 0.5 nmoles (injected) of 2-ClHDA- and 2-Cl[$^{13}C_8$]HDA PFB-oxime derivative. (**B** and **D**) Corresponding full scan NICI spectra. Proposed fragmentation pattern and isotope distribution of the molecular ion are shown in the insets. Peaks eluting at 14.78 and 14.94 min correspond to the *syn*- and *anti*-isomers of 2-ClHDA-/2-Cl[$^{13}C_8$]HDA PFB-oxime derivatives. Mass assignment of the molecular ions is indicated in the inset.

2.3. *HOCl-Modification of Mouse Brain Plasmalogens Provoke the Formation of alpha-Chloro Fatty Aldehydes and Remnant Lysophospholipids*

Plasmalogens comprise multiple targets for electrophilic attack of HOCl. There are numerous studies showing that HOCl induces N-halogenation of the ethanolamine headgroup yielding chloramines (Carr et al. 1998, Pattison et al. 2003) and that HOCl attack to double bonds in mono- and polyunsaturated fatty acyl chains causes chlorohydrin formation (Winterbourn et al. 1992), lipid peroxidation (Panasenko et al. 1994) and hydrolytic cleavage of the modified acyl chain (Arnhold et al. 2002). However, HOCl-treatment of plasmalogens present in cellular membranes or lipoproteins gives rise to the formation of lysophospholipids and α-ClFALDs by affecting the vinyl-ether linkage (Thukkani et al. 2002, Thukkani et al. 2003b).

To investigate whether this route (***Figure 25 A***) is also relevant to the CNS, brain lipids were modified with reagent HOCl. The decrease of selected plasmalogen species (the alkenyl residue at the *sn*-1 was identified by MS/MS experiments; *sn*-1 = 16:0, 18:0, and 18:1) was followed by FT-ICR-MS. In parallel, formation of 2-chloroaldehydes was quantified by NICI-GC-MS using 2-Cl[$^{13}C_8$]HDA as internal standard (outlined in Materials and Methods). In line with data shown in *Figure 20*, pPE species containing 16:0, 18:0, and 18:1 at the *sn*-1 position were quantitatively modified at a oxidant:lipid ratio of 5:100 (***B***). In addition to 2-ClHDA we could detect other α-ClFALDs generated by HOCl attack of plasmalogen subspecies (Messner et al. 2006). Depending on the alkenyl residue present in the *sn*-1 position (18:0 or 18:1) either 2-ClODA, or 2-ClODEA was formed. In contrast to formation of saturated α-ClFALDs, which reached a plateau at oxidant:lipid ratios of 5:100, yields of monounsaturated 2-ClODEA declined at higher ratios (***C***). Moreover, the oxidant:lipid ratio at which the corresponding pPE species are quantitatively consumed (5:100) closely corresponds to the HOCl concentration at which maximal α-ClFALDs yields were obtained (4.1, 3.3, and 1 µmol/g brain tissue for 2-ClHDA, 2-ClODEA, and 2-ClODA, respectively) (***B*** and ***C***).

The next experiments were designed to compare the total fatty aldehyde content with the amount of chloroaldehydes formed after treatment of mouse brain lipids with NaOCl. To analyze the total aldehyde content of mouse brain lipid extracts, plasmalogens were subjected to acidic hydrolysis (0.1 M HCl, RT, overnight), and the released aldehydes were converted to the PFB-oxime derivatives and then quantified by NICI-GC-MS (***Figure 25 D***). In a parallel set of experiments, lipids were modified with reagent HOCl and α-ClFALDs were quantified. These analyses revealed that 1-*O*-hexadecanal

(16:0) and 1-*O*-octadecenal (18:1) plasmalogens were nearly quantitatively consumed by reagent HOCl, while only inbetween 15 and 20% of the corresponding 1-*O*-octadecanal (18:0) plasmalogen was modified by HOCl (***D***).

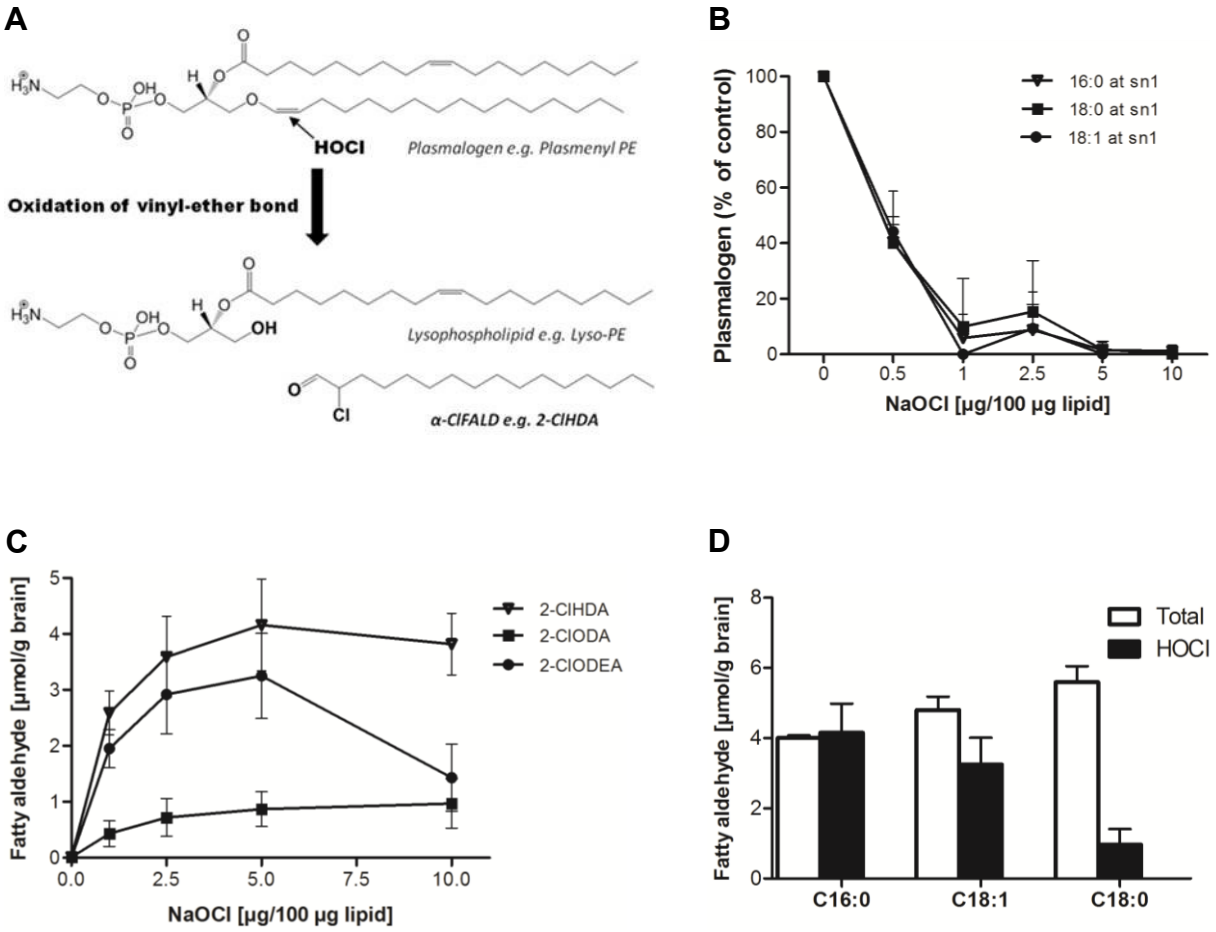

Figure 25*: HOCl-modification of brain lipid extracts results in a decrease of selected pPE species and concomitant formation of the corresponding 2-chloro fatty aldehydes *in vitro

(**A**) Reaction pathway leading to the formation of 2-ClHDA and the corresponding lysophospholipid. (**B**) MS/MS analysis of selected pPE subspecies containing 16:0, 18:0 and 18:1 at *sn*-1 position modified in the presence of the indicated oxidant:lipid ratios (w/w). (**C**) NICI-GC-MS analysis of the corresponding 2-chloro fatty aldehydes in NaOCl-modified mouse brain lipid extracts. 2-Cl[$^{13}C_8$]HDA was used as internal standard. (**D**) NICI-GC-MS analysis of total fatty aldehyde after an overnight hydrolysis step at room temperature using 0.1 M HCl (termed 'Total') and 2-chloro fatty aldehyde concentrations after NaOCl modification of mouse brain lipid extracts. Data shown represent mean values ± SD from triplicate determinations.

3. Neuroinflammation is Accompanied by Altered Brain Plasmalogen Levels and α-Chloro Fatty Aldehyde Formation

3.1. *Systemic LPS Induces Inflammation in Brain Tissue*

Animal models became an essential and inevitable tool for the exploration of molecular and cellular mechanisms of chronic and acute neurodegeneration in human disorders like AD, PD, MS, stroke and TBI (Beal 2001, Bornemann and Staufenbiel 2000, Cernak et al. 2004, Graham et al. 2004, Sriram and Steiner 2005), however, only a few are really predictive to the human response (Amor et al. 2010).

Choosing the most suitable model one has to consider benefits, limitations, expenses and possible drawbacks like high-invasiveness of surgical interventions (Sicard and Fisher 2009) or potential hazards of neurotoxins (Przedborski et al. 2001). Since several lines of evidence suggest that single peripheral LPS exposure in adult mice results in neuroinflammation that persists for a long time period after peripheral events have abated (Godbout et al. 2005, Qin L. et al. 2007, Semmler et al. 2008) this study aimed testing this simple, inexpensive and straightforward *in vivo* model to explore chlorinative stress during neuroinflammation.

Therefore, the time course of LPS-induced inflammation in brain tissue was followed by qPCR analysis for MPO and inflammatory markers TNFα, COX2 and iNOS (Experiments were performed by Sabine Waltl). Analyses of LPS-treated mice revealed significantly induced transcriptional activation in brain tissue of all four markers (***Figure 26 A***). At the earliest time point (6 h) the highest induction was observed for iNOS (60-fold), followed by TNFα (9-fold), MPO (4-fold), and COX2 (3-fold). Thereafter iNOS, TNFα and COX2 levels started to decline while MPO appeared to be induced in a second phase after 24 h. At the latest time point analyzed (72 h) COX2 levels returned to baseline values while MPO, TNFα and iNOS (not significantly) mRNA still remained elevated. To get an indication about MPO protein levels, brain protein extracts were analyzed by ELISA. In line with qPCR data (*Figure 26 A*), systemic endotoxin application increased cerebral MPO protein concentrations 6, 24, and 48 h post application but only concentration at 24 h could be considered significant (***B***).

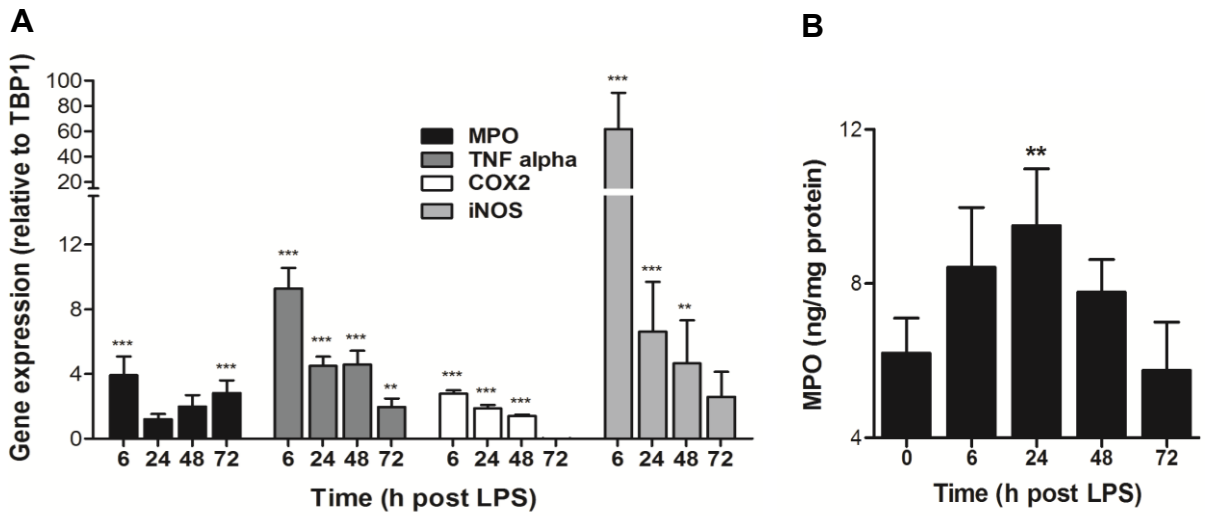

Figure 26: **Systemic LPS induces upregulation of brain inflammatory markers *in vivo***

Eight weeks old male C57BL/6 mice received systemic LPS (150 µg/30 g; i.p.) at time zero. At the indicated time periods animals were killed by cervical dislocation, brains were removed and total brain RNA was isolated and reverse transcribed. cDNA was amplified using the primer pairs/assays described in *Table 3*. For ELISA measurements murine brain homogenates were used. (**A**) Relative gene expression of target genes is presented in relation to TBP1. Gene expression ratios were calculated by REST© as described in Materials and Methods. (**B**) Time-dependent accumulation of MPO protein in brain of LPS-treated mice as determined by ELISA. Results shown represent mean values ± SD of four animals per time point (*** $p<0.001$; ** $p<0.01$).

3.2. *Brain Plasmalogen Homeostasis is Impaired upon Inflammation*

Due to a lack of available information about lipidomic alterations in brain tissue during sustained neuroinflammation induced by peripheral sepsis the following approach was designed to evaluate the outcome of neuroinflammatory conditions on plasmalogen levels *in vivo*.

In this approach brain plasmalogen composition of mice receiving a single systemic endotoxin injection was analyzed by FT-ICR-MS. Overall plasmalogen loss at 48 and 96 h post LPS exposure accounted for approx. 10 and 18% (***Figure 27 A***) exclusively through contribution by pPE species (***Figure 27 B***, 48 h: -11%, 96 h: -18%) because LPS treatment did not result in a general loss of pPC subclass (***Figure 27 C***). Analysis of the pPE composition revealed significantly decreased levels of the 34:1, 36:1, 38:1, 38:4, 38:6, 40:4, 40:5, and 40:6 species, which were evident at all time points (***Figure 28 A***). In contrast, for pPC species a slight but statistically significant decrease was observed for the 32:0, 34:1,

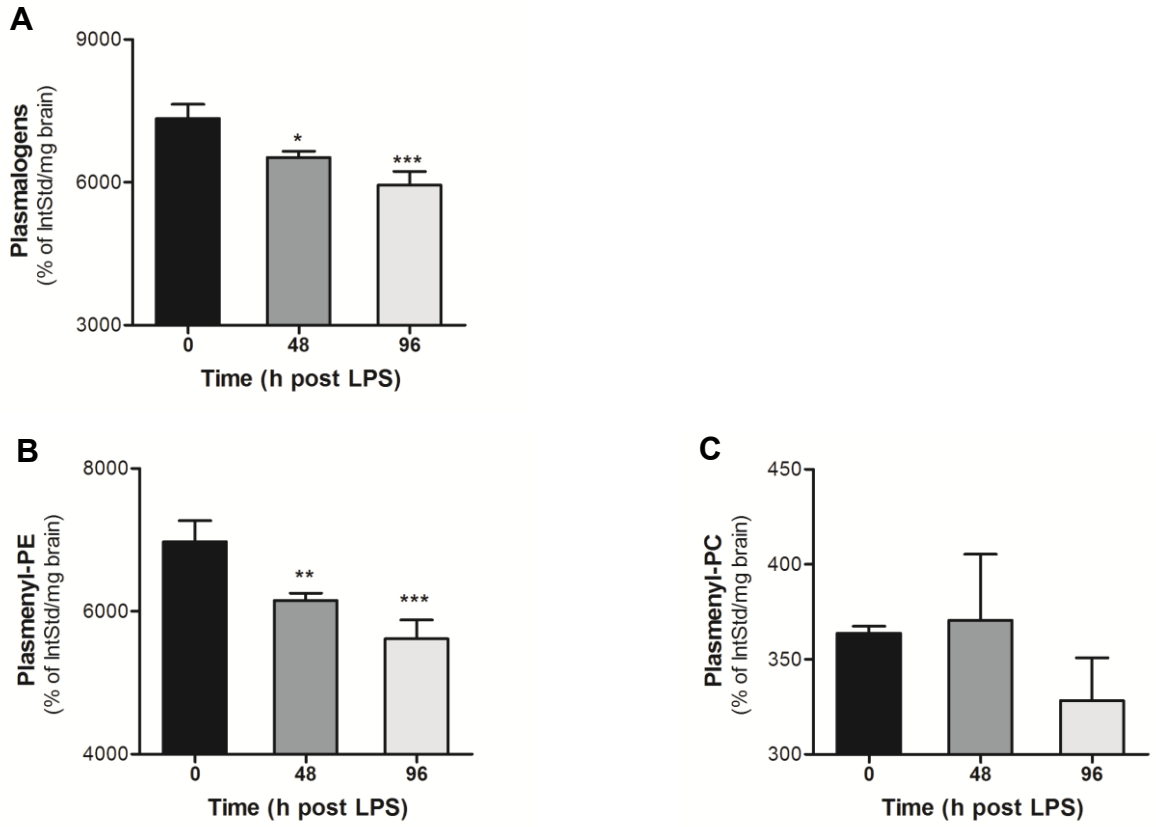

Figure 27: **Systemic LPS decreases plasmalogen levels *in vivo***

Eight weeks old male C57BL/6 mice received systemic LPS (150 µg/30 g; i.p.) at time zero. At the indicated time periods animals were killed by cervical dislocation, brains were removed, lipids extracted and analyzed by FT-ICR-MS using d_{31}-34:1 PC as internal standard. Data are given in terms of (**A**) total plasmalogens (sum of pPE and pPC), (**B**) pPC and (**C**) pPE. Results shown represent mean values ± SD of three animals per time point (*p<0.05; ** p<0.01; *** p<0.001).

36:1, and 36:2 species. However, levels of most abundant 34:0 species remained constant over analyzed time period (***Figure 28 B***).

To gain knowledge about the role of the *sn*-1 alkenyl-chain in the progressive loss of plasmalogens during neuroinflammation plasmalogens were sorted by *sn*-1 chain length and the degree of saturation identified by MS/MS experiments (*sn*-1 = 16:0, 18:0, 18:1). Whereas plasmalogens with saturated alkenyl-chains decreased by approx. 10-15% and 20-25% during the first two to four days, loss of plasmalogens with C18:1 alkenyl-chains was not that pronounced (***Figure 29 A***, 48h: -5%, 96 h: -10%).

Evaluation of a potential link between numbers of double bonds within hydrocarbon chains and frequency of loss (***B***) could show that highly unsaturated plasmalogens containing four to six double bonds declined by up to 25% at investigated time points. Conversely, levels of plasmalogen with one

double bond remained constant during the first 48 h but significantly decreased within the following 2 days of inflammation.

3.3. *Oxidative Modification of Brain Tissue Plasmalogens*

Since systemic LPS application is coupled to an increase of brain MPO mRNA and protein levels (*Figure 26*) and is paralleled by loss of plasmalogen species (*Figure 27-29*), oxidative modification via intermediate formation of HOCl is likely to occur.

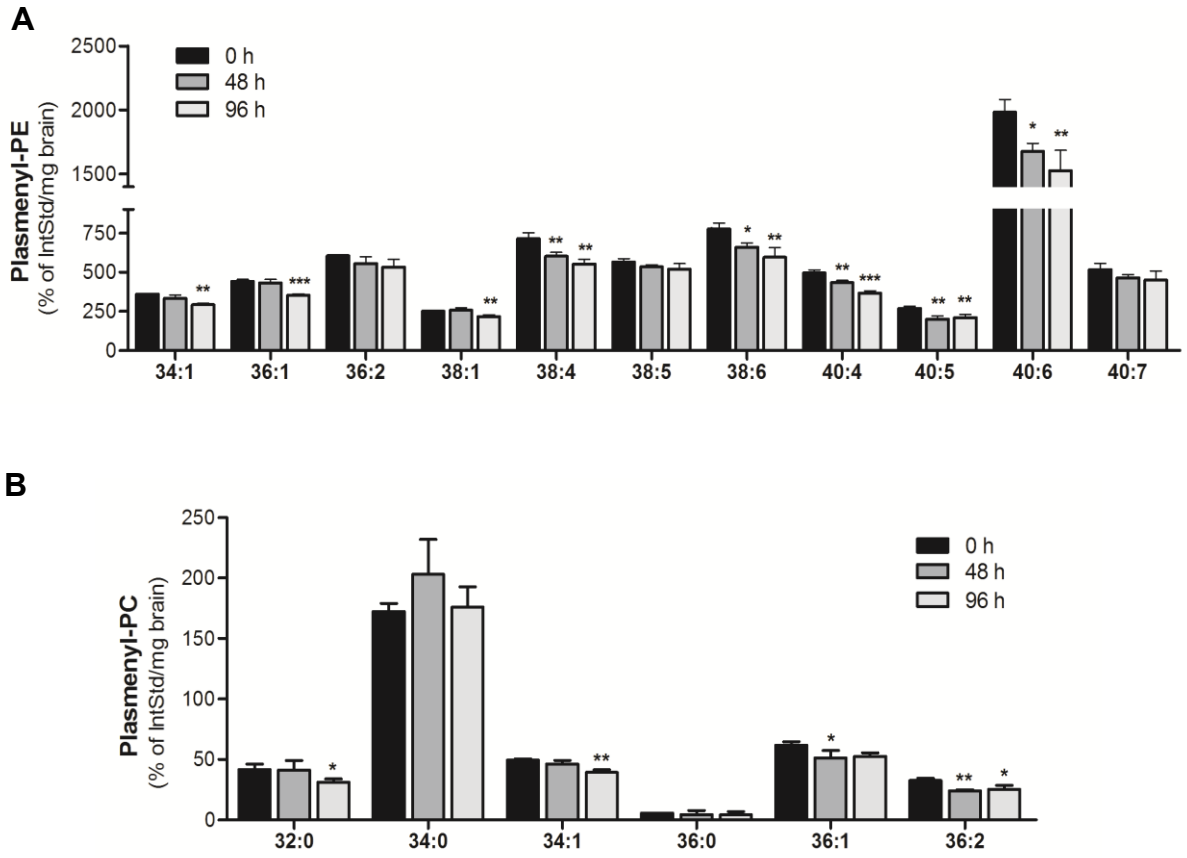

Figure 28: **Impact of systemic LPS on plasmalogen subspecies levels**

Eight weeks old male C57BL/6 mice received systemic LPS (150 µg/30 g; i.p.) at time zero. At the indicated time periods animals were killed by cervical dislocation, brains were removed, lipids extracted and analyzed by FT-ICR-MS using d_{31}-34:1 PC as internal standard. Data are given in terms of (**A**) pPE subspecies and (**B**) pPC subspecies. Results shown represent mean values ± SD of three animals per time point (*p<0.05; ** p<0.01; *** p<0.001).

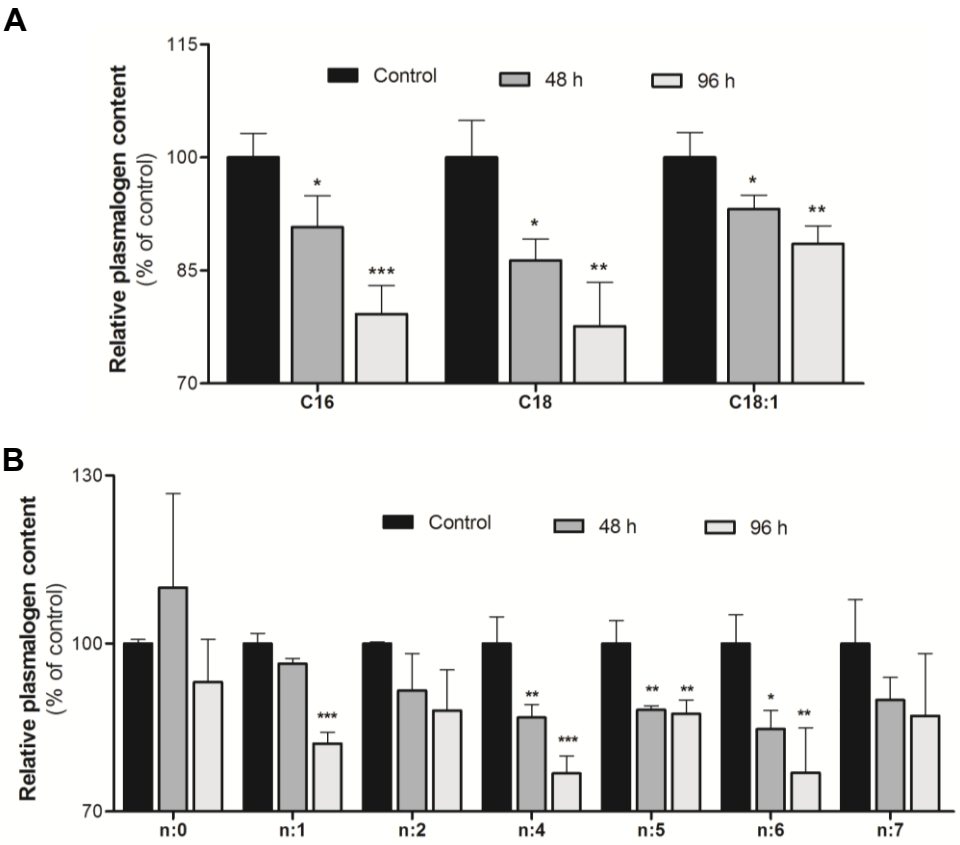

Figure 29: **Specificity of plasmalogen loss**

Eight weeks old male C57BL/6 mice received systemic LPS (150 µg/30 g; i.p.) at time zero. At the indicated time periods animals were killed by cervical dislocation, brains were removed, lipids extracted and analyzed by FT-ICR-MS using d_{31}-34:1 PC as internal standard. Data are given in terms of pPL subspecies sorted by either (**A**) the alkenyl-chain at the *sn*-1 position (based on MS/MS experiments) or (**B**) by cumulative unsaturation of aliphatic chains at *sn*-1 and *sn*-2 positions in the glycerol backbone. Results shown represent mean values ± SD of three animals per time point (*p<0.05; ** p<0.01; *** p<0.001).

To provide evidence of chlorinative stress in the CNS, the accumulation of MPO-derived 2-ClHDA was quantified in brain lipid extracts of LPS-treated animals by NICI-GC-MS. Along this line it is important to note that during *in vivo* experiments it was impossible to identify 2-ClHDA when PFB-oxime derivatives were prepared directly from total brain lipid extracts. However, a pre-separation of brain lipid extracts by TLC as described in Materials and Methods (to obtain an enriched 2-chloro fatty aldehyde fraction) and subsequent NICI-GC-MS analysis of PFB-oxime derivatives clearly revealed the presence of significantly elevated 2-ClHDA levels in brain lipids of endotoxin-treated mice (***Figure 30***). ***Figure 30 A*** shows selected ion-monitoring (SIM) traces of PFB-oxime derivatives of 2-ClHDA (analyzed from brain lipid extracts prepared 6 h post LPS; diagnostic ions at m/z = 288 and 290) and 2-

Cl[$^{13}C_8$]HDA (m/z = 296 and 298) used as internal standard. Ion intensity ratios are close to 3:1 as expected for a chlorinated analyte (***B***). Quantitative data for time dependent 2-ClHDA generation in brains of LPS-treated mice are shown in ***C***. Within 6 hours post LPS-treatment 2-ClHDA concentration increased almost 50-fold to approx. 2 µg/g wet brain tissue and gradually declined to 0.4 µg/g wet brain tissue during following 3 days. Based on the assumption of approx. 80% of wet brain tissue is water the estimated molar 2-ClHDA content present in brain during the first three days of neuroinflammation was between 2 and 10 µM.

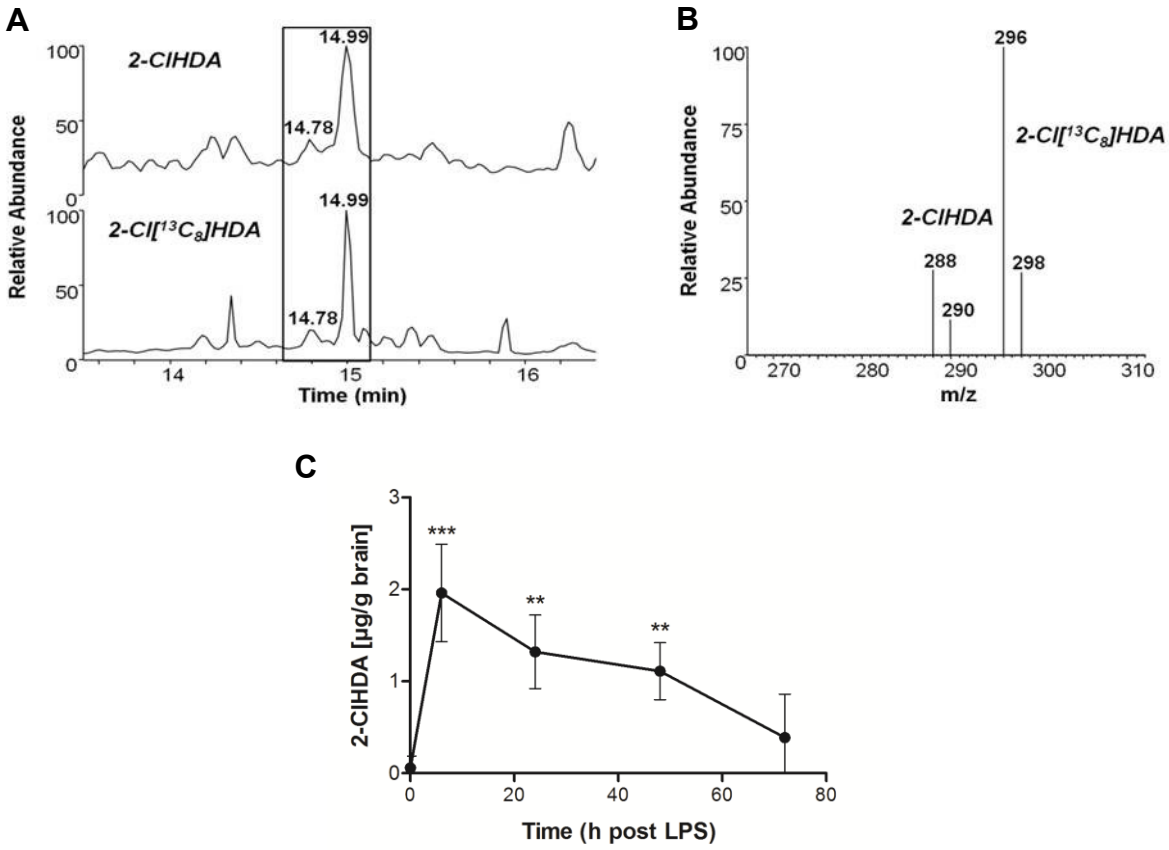

Figure 30: **Systemic LPS induces cerebral 2-ClHDA formation *in vivo***

C57BL/6 mice received a single systemic LPS injection (150 µg/30 g; i.p.) at time zero. At the indicated time periods, animals were killed by cervical dislocation, brains were removed, lipids were extracted, pre-separated by TLC, extracted from the plates, and converted to the corresponding PFB-oxime derivatives. 2-ClHDA concentrations were quantified by selected ion monitoring NICI-GC-MS analysis using 2-Cl[$^{13}C_8$]HDA as internal standard. (**A**) SIM trace of a representative brain lipid sample (upper panel; 6 h post LPS injection; m/z = 288) and the internal standard (lower panel; m/z = 296). Boxed area indicates position of 2-ClHDA and 2-Cl[$^{13}C_8$]HDA. (**B**) Fragment ion intensity ratios of 2-ClHDA (m/z = 288, 290) and the internal standard (m/z = 296, 298) of the peak highlighted in (A). (**C**) Time-dependent formation of 2-ClHDA in brains of mice receiving a single systemic LPS dose. Results shown represent mean values ± SD from four different animals per time point (**p<0.01; ***p<0.001 compared to time zero).

3.4. *Stability of α-Chloro Fatty Aldehydes in Brain Tissue*

Several studies have shown that α-ClFALDs, produced under pro-inflammatory conditions, can bind to cellular components (Wildsmith et al. 2006b) and become metabolized *in vitro* and *in vivo* (Anbukumar et al. 2010, Brahmbhatt et al. 2010b, Wildsmith et al. 2006a).

To get an indication about the life-time of 2-ClHDA in brain tissue, 2-ClHDA (17 µg) was incubated in the presence of a crude primary brain cell suspension and the 2-ClHDA content was time-dependently analyzed. Non-linear regression analysis of the data shown in ***Figure 31*** was fitted using a one-phase exponential decay function. This curve fit revealed a τ/2 of approx. 40 min for 2-ClHDA in the presence of mixed primary brain cell population.

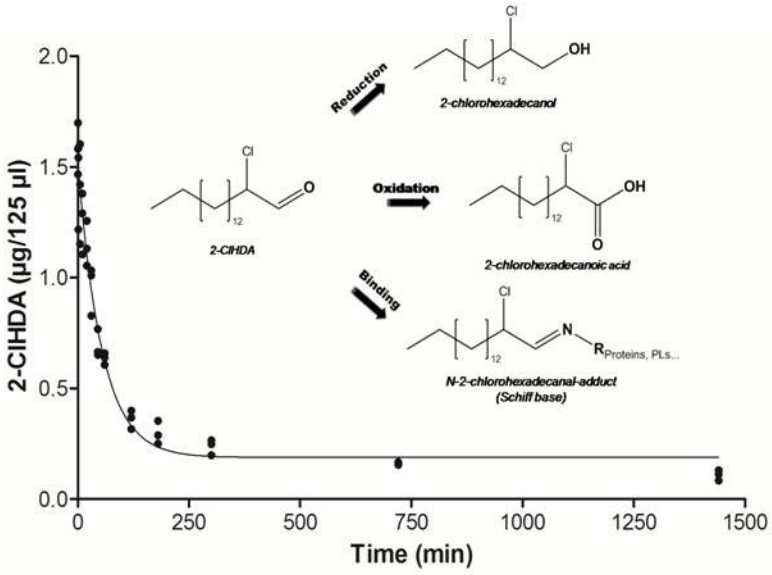

Figure 31: **Stability of 2-ClHDA in mixed primary mouse brain cell suspension**
Mixed brain cell suspensions prepared from three individual mouse brains in HBSS (supplemented with glucose) were spiked with 2-ClHDA (stock added in DMSO; 30 µM final concentration). At the indicated time periods quantitative analysis of 2-ClHDA was performed by NICI-GC-MS using 2-Cl[$^{13}C_8$]HDA as internal standard. Experimental data were fitted by non-linear regression analysis ($R^2 = 0.96$) as described in Material and Methods. The inset displays proposed decay pathways for 2-ClHDA.

*CHAPTER 2 ALPHA-CHLORO FATTY ALDEHYDES INDUCE BLOOD-BRAIN BARRIER DYSFUNCTION **

* submitted manuscript:

Üllen, A; Fauler, H; Nusshold, C; Bernhart, E; Reicher, H; Holzer, P; Leis, HJ; Malle, E; Sattler, W. **Phloretin ameliorates 2-chlorohexadecanal-mediated brain microvascular endothelial cell dysfunction *in vitro***

* manuscript in preparation:

Üllen, A; Fauler, H; Waltl, S; Nusshold, C; Bernhart, E; Reicher, H; Painsipp, E; Holzer, P; Wintersperger, A; Malle, E; Sattler, W. **Myeloperoxidase derived 2-ClHDA mediate BBB breakdown *in vitro* and *in vivo***

Rationale:

Loss of BBB integrity can be considered as a key characteristic of neurodegeneration since this event can be observed in numerous CNS-pathologies including infectious or inflammatory encephalopathy. BBB dysfunction and/or barrier compromise facilitates entry of immune cells that would assist the neurodegenerative process creating a milieu where neuroinflammation is maintained in a self-sustaining process (Abbott et al. 2006, Carvey et al. 2009, Zlokovic 2008).

It is well known that inflammatory mediators in the blood destabilize TJ leading to barrier dysfunction as part of sepsis (Li Q. et al. 2009). Experimental evidence indicates that oxidized phospholipids like 1-palmitoyl-2-(5-oxovaleroyl)-*sn*-glycero-3-phosphocholine (POVPC) and 1-palmitoyl-2-glutaroyl-*sn*-glycero-3-phosphocholine (PGPC) (Chen-Quay et al. 2009), and the lipid peroxidation product 4-HNE affect cell permeability by modulating tight junction proteins (Usatyuk et al. 2006). However, little is known about the role of ether phospholipid-derived modification products in the scenario of BBB breakdown.

The first part of this thesis revealed the formation of substantial amounts of 2-ClHDA upon neuroinflammation, a plasmalogen-derived modification product almost undetectable in the brain under physiological conditions. 2-ClHDA present in biological tissues was shown to act as neutrophil chemoattractant as well as to elicit myocardial damage, COX2 expression and eNOS inhibition (reviewed in (Ford 2010)) indicating that 2-ClHDA has the potential to induce pronounced deteriorations of CNS function. Nevertheless, there are no data available exploring the properties of 2-ClHDA with particular regards to CNS-pathologies.

Aims:

The first part of this thesis focused on the investigation of MPO-derived chlorinative damage of brain plasmalogens, thus potentially exacerbating cognitive impairment. In the second part I will focus on the product level of this oxidation process. During this part I hypothesized that formation of α-chloro fatty aldehydes (α-ClFALDs) during encephalopathy might not only represent a 'consequence' but also a 'cause' for neuropathological changes

i. Therefore, the first aim of the second part was to examine *in vivo* alterations at the BBB in mice receiving a single i.p. endotoxin injection. To get deeper insight into mechanisms governing α-ClFALD formation at the cerebrovasculature immunohistochemical studies on brain cryosections of LPS-treated mice should be combined with mechanistic studies in an *in vitro* model of the BBB.

ii. The second aim within this part was to elucidate the impact of α-ClFALDs on *in vitro* and *in vivo* BBB function, to characterize the underlying lipotoxic signaling pathways and to identify potential detoxification routes in cerebrovasculature endothelial cells.

1. Neuroinflammation – What happens at the BBB?

1.1. *Accumulation of MPO at the Cerebrovasculature*

In the first part of this thesis it was already shown, that peripheral LPS exposure in adult mice induces MPO expression in the brain on mRNA and protein levels. To get an indication about MPO localization in inflamed brain tissue an immunohistochemical study was performed.

Therefore, LPS- and control-treated animals were sacrificed after 6 h – the time point where highest cerebral MPO expression and most pronounced 2-ClHDA formation were observed – and brain cryosections were analyzed for MPO. Representative micrographs are shown in ***Figure 32***. In contrast to control animals (***A***) systemic inflammation resulted in enhanced recruitment of MPO-positive leukocytes to the cerebrovasculature, an observation that was most prominent at large subarachnoid vessels (***C,*** large arrows; negative control using non-immune antibodies is shown in ***B***). Furthermore, LPS-treatment resulted in sporadic emigration of MPO-positive leukocytes to brain parenchyma (***D,*** large arrows), however, the extent of infiltration was minor compared to the overall number of adherent cells. Interestingly, in addition to cell-associated MPO substantial amounts of secreted MPO could be detected (***C***, small arrows).

To gain knowledge about the population of adherent leukocytes during sepsis and to study MPO localization at cerebral vessels in more detail brain cryosections of mice sacrificed after 6 h post LPS-treatment were examined for endothelial cells (von Willebrand factor, vWF), neutrophils, and MPO. Representative micrographs are shown in ***Figure 33.*** Immunofluorescence microscopy could clearly identify MPO-positive leukocytes adhering to the cerebrovasculature (***D*** and ***I***) and infiltrating the brain parenchyma (***I*** and ***K***) as neutrophils. Interestingly, these studies also revealed the release of MPO by adherent neutrophils towards the endothelium most likely indicating neutrophil extracellular trap (NET) formation (large arrows) at the BBB (***C***). Furthermore, MPO externalization by activated leukocytes also resulted in considerable deposition of MPO at the luminal (small arrows) and, presumably by transcytotic mechanisms, also at the abluminal side (large arrows) of the cerebrovasculature. Some cerebral vessels displayed MPO deposition although luminal neutrophils or other MPO-positive leukocytes were not present (***K*** and ***L***), an observation, which might be indicative for MPO distribution via the blood-stream.

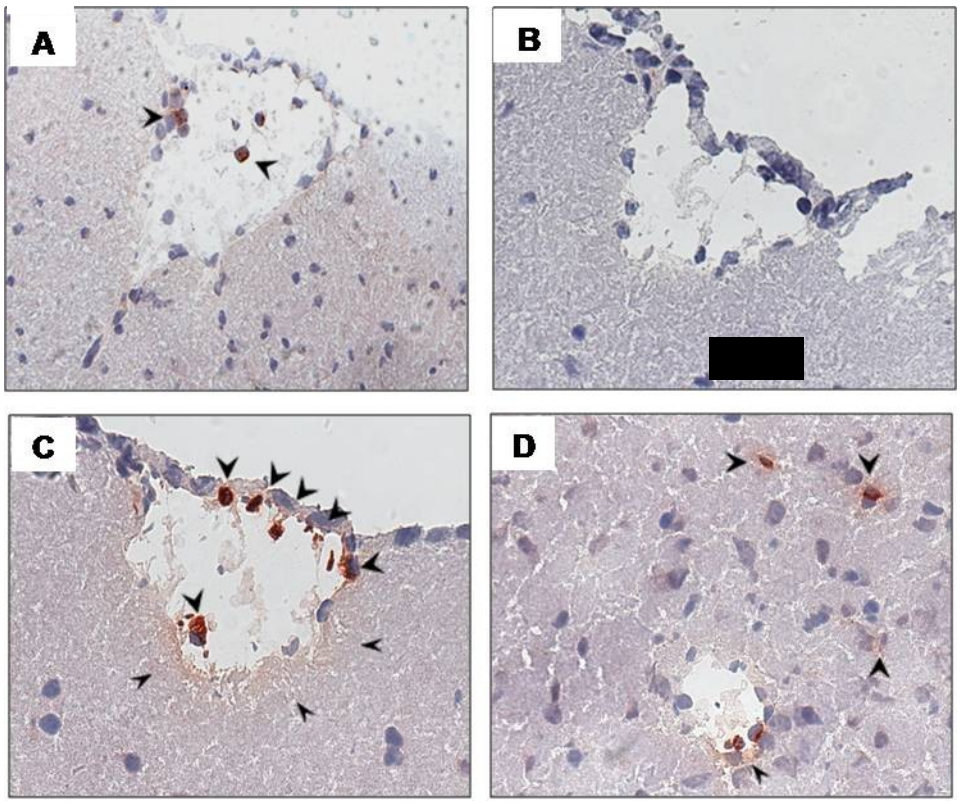

Figure 32: **Immunohistochemical detection of MPO in mouse brain tissue during sepsis**
C57BL/6 mice received (**A**) PBS or (**B-D)** a single systemic LPS injection (250 µg/30 g; i.p.). After 6 h, animals were killed by cervical dislocation, brains were removed and snap frozen in liquid nitrogen. (**A**, **C** and **D**) Immunolabeling of MPO was performed on serial sagittal cryosections (5 µm) of brain tissue using rabbit anti-human MPO IgG (1:500) and HRP labeled goat-anti rabbit IgG (1:300) as primary and secondary antibodies. MPO (red) was visualized using the AEC system. (**B**) Negative control using rabbit polyclonal non-immune IgG as primary antibodies. Sections were counterstained with Mayer's hemalum. Large arrows indicate cell-associated MPO, small arrows indicate secreted MPO (**A, C** and **D**).

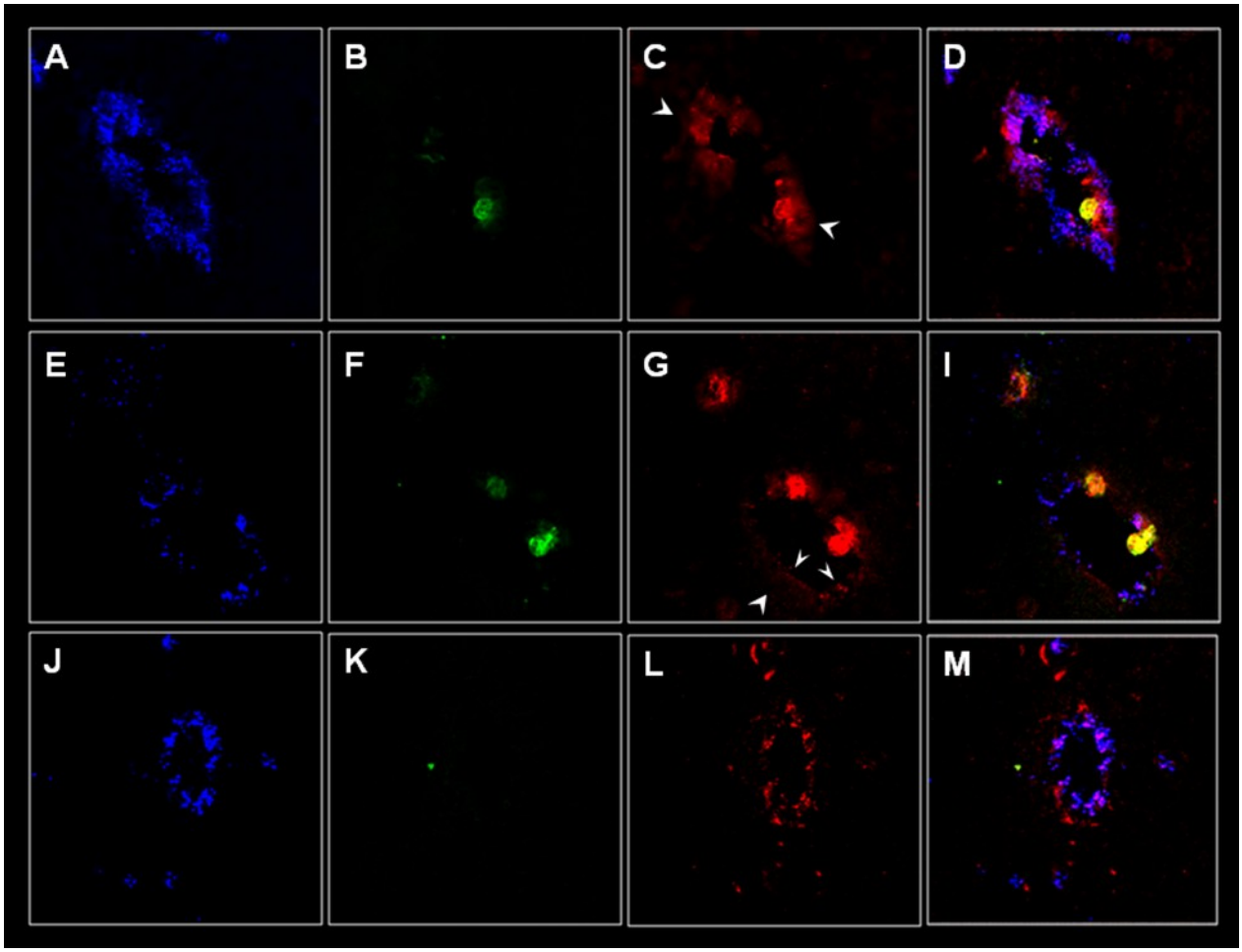

Figure 33: **Systemic inflammation induces neutrophil activation and MPO deposition at the BBB**

C57BL/6 mice received a single systemic LPS injection (250 µg/30 g; i.p.). After 6 h, animals were killed by cervical dislocation, brains were removed and snap frozen in liquid nitrogen. Immunofluorescence labeling of (**A**, **E** and **J**) cerebral endothelium, (**B**, **F** and **K**) neutrophils and (**C**,**G** and **L**) MPO was performed on serial sagittal cryosections (5 µm) of brain tissue using Dylight 650-labeled rabbit anti-human vWF (1:75), FITC-labeled rat anti-mouse neutrophil IgG (1:50) and rabbit anti-human MPO IgG (1:500) as primary antibodies. Triple immunofluorescence of Dylight 650-labeled anti-human vWF IgG, Cy3-labeled anti-rabbit IgG and Cy2-labeled anti-rat IgG was performed by confocal laser scanning microscopy using a Leica SP2. Overlays of red, blue and green channels are shown in **D**, **I** and **M**. Large arrows indicate (**C**) putative formation of neutrophil extracellular traps (NETs) or (**G**) MPO at abluminal side of the endothelium. Small arrows indicate luminal MPO deposition.

1.2. *Cerebral Vessels are Attacked by Reactive Intermediates*

It was repeatedly shown that MPO is able to initiate the formation of several reactive oxygen/nitrogen species including nitrogen dioxide (NO_2·), nitryl chloride (NO_2Cl), singlet oxygen ($^1O_2$), hydroxyl radical (·OH) and ozone (O_3) through a MPO-catalyzed peroxidation process or indirectly via transient formation of reactive HOCl (Klebanoff 2005, Yap et al. 2007). Recently, it was demonstrated that in response to zymosan-induced sepsis $MPO^{-/-}$ mice display significant lower nitration of protein-associated tyrosine residues (NO_2Tyr) compared to wild-type controls suggesting a pivotal role of MPO in RNS formation (Baldus et al. 2001). To test whether this route is also relevant for our experimental conditions, brain cryosections of mice exposed to peripheral LPS (6 h) were analyzed by triple immunofluorescence (BMVE, neutrophils and NO_2Tyr-epitopes). As shown in ***Figure 34,*** LPS treatment resulted in ample NO_2Tyr formation, which co-localized with cerebral vessels (**D** and **I**). Accordingly, these data indicate LPS treatment induces extensive generation of RNS like ONO_2^- or NO_2· and most likely other reactive intermediates at the BBB.

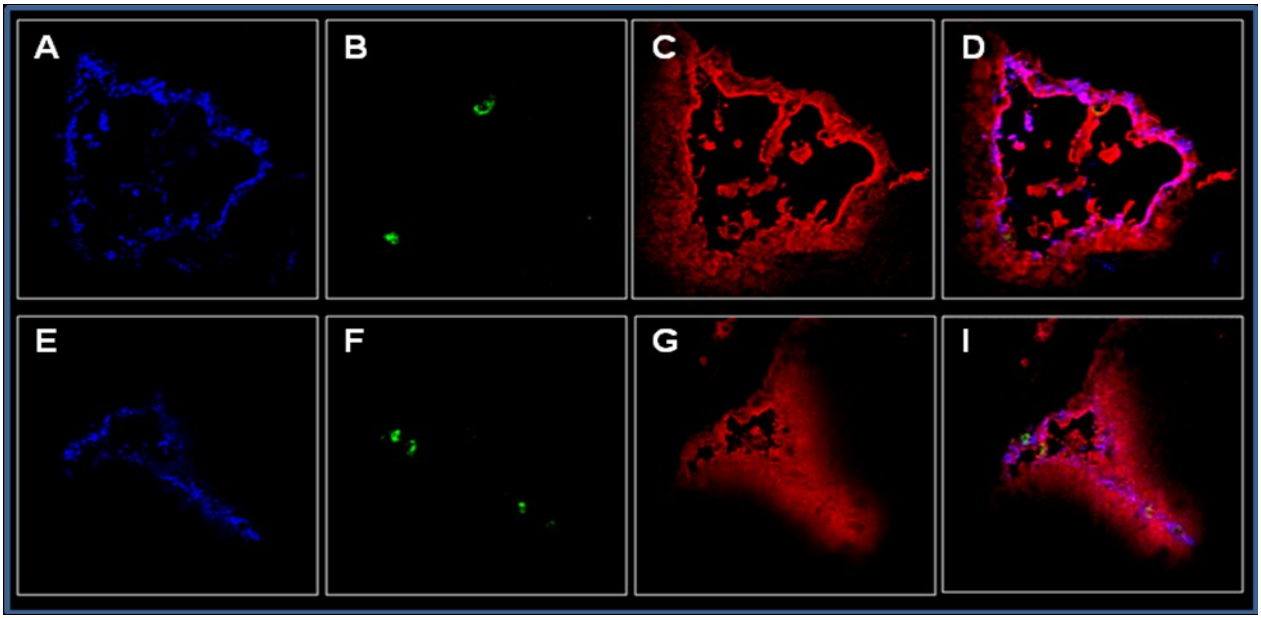

Figure 34: **Reactive nitrogen species induce tyrosine nitration (NO_2Tyr) of cerebrovascular proteins**
C57BL/6 mice received a single systemic LPS injection (250 µg/30 g; i.p.). After 6 h, animals were killed by cervical dislocation, brains were removed and snap frozen in liquid nitrogen. Immunofluorescence labeling of (**A** and **E**) cerebral endothelium, (**B** and **F**) neutrophils and (**C**, and **G**) NO_2Tyr epitopes was performed on serial sagittal cryosections (5 µm) of brain tissue using Dylight 650-labeled rabbit anti-human vWF (1:75), FITC-labeled rat anti-mouse neutrophil IgG (1:50) and rabbit anti-human NO_2Tyr IgG (1:50) as primary antibodies. Dylight 650-labeled anti-human vWF IgG, Cy3-labeled anti-rabbit IgG and Cy2-labeled anti-rat IgG

were detected by confocal laser scanning microscopy (Leica SP2). Co-localization of nitrotyrosine epitopes and cerebral vessels are shown in **D** and **I**.

1.3. *Activation of Neutrophils Impacts on Barrier Function of BMVEC*

Due to the discovery that LPS-induced peripheral inflammation is accompanied by substantial activation of circulating neutrophils at the lumen of cerebral vessels the next set of *in vitro* experiments was designed to examine the impact of this process on BBB integrity. Therefore, BMVEC - the major constituents of the BBB - were exposed to conditions simulating physiological and pathophysiological environment while *in vitro* barrier function was monitored in real-time using the ECIS system. To simulate the 'healthy state' non-pre-stimulated neutrophils were added to give a density in the range of neutrophil counts found in whole blood (~ 5×10^6 cells/ml, (Inglis et al. 2004)). In contrast, in the setting of peripheral inflammation neutrophils were primed with TNFα - a cytokine that was markedly elevated in response to LPS treatment (*Figure 26*) - and stimulated with fMLP, a potent inducer of NADPH oxidase activity (Lehmann et al. 2009). As shown in ***Figure 35 A*** and ***B***, fMLP stimulation was without effects on endothelial barrier function in the absence of neutrophils. Addition of neutrophils was associated with slight decrease of barrier function but it returned to baseline during 3 h of incubation. However, fMLP-dependent activation of the ROS generating machinery in TNFα primed neutrophils severely impaired barrier function within 3 h by approx. 40%.

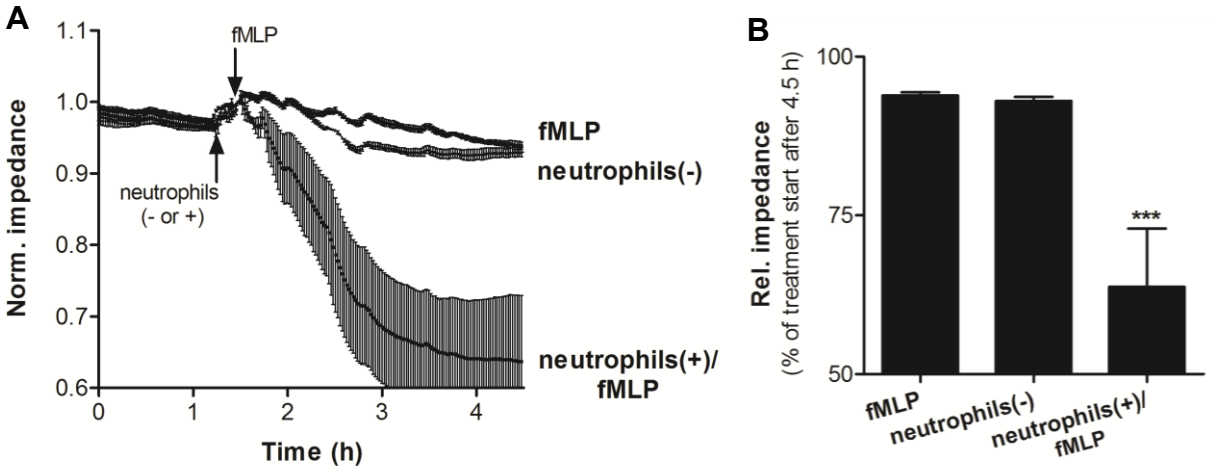

Figure 35: **BMVEC barrier function is severely compromised by activated neutrophils**

BMVEC were plated on gold microelectrodes and cultured to confluence. Barrier function of HC-induced endothelial monolayers (7.5×10^4 cells) was continuously monitored by impedance sensing at 4 kHz. (**A**) After stabilization, cells were challenged (arrow) with 2.5×10^6 TNFα-treated neutrophils (neutrophils(+)), the same number of non-pre-treated cells (neutrophils(-)) or equal volume of medium. After 15 min, fMLP (10 µM) or vehicle (0.2% EtOH) was added (arrow). (**B**)

Relative barrier function at the indicated time period. Impedances were normalized to treatment start and represents mean values ± SD of four independent experiments (*** p<0.001, one-way ANOVA).

1.4. *Neutrophil-dependent Barrier Dysfunction: Impact of the MPO-H_2O_2-Cl^- System?*

In vitro studies indicated that ROS formation by neutrophils undergoing the respiratory burst was associated with collateral damage to barrier integrity of BMVEC. However, *in vivo* studies of mice exposed to peripheral LPS suggested that this could be initiated by the presence of externalized MPO.

To examine the impact of accumulating MPO at cerebral vessels BMVEC were exposed under weak acidic conditions to either 500 µM H_2O_2 alone or in combination with nanomolar concentrations of MPO while barrier function was monitored by ECIS (***Figure 36 A***). These experiments revealed that the MPO-H_2O_2-Cl^- system significantly increased barrier dysfunction, most probably due to HOCl generation (***B***). In line, exogenously added methionine (Met, a potent HOCl scavenger) significantly attenuated barrier-compromising effects of MPO-mediated H_2O_2 conversion.

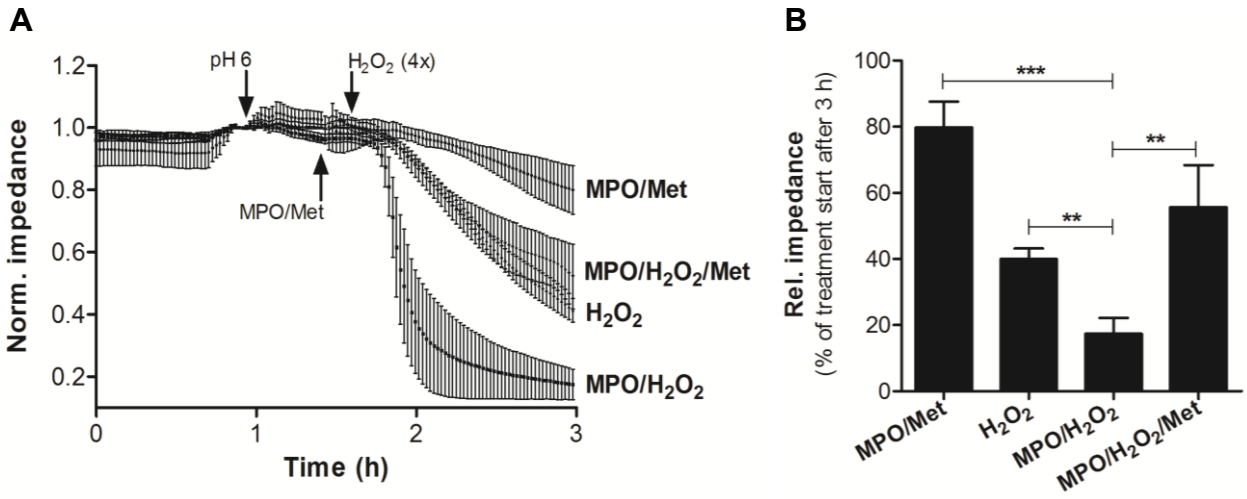

Figure 36: **MPO fuels barrier dysfunction through generation of HOCl**

BMVEC were plated on gold microelectrodes and cultured to confluence. Barrier function of HC-induced endothelial monolayers was continuously monitored by impedance sensing at 4 kHz. (**A**) After stabilization, induction medium was changed (arrow) to slightly acidic conditions (HBSS, pH 6). As indicated, after 30 min of pre-conditioning BMVEC were incubated (arrow) with 120 nM MPO in the absence or presence of 5 mM methionine (Met) prior cells were challenged (arrow) with 4x 125 µM H_2O_2 every 3 min. (**B**) Relative barrier function at the indicated time period post treatment. Impedance was normalized to treatment start and represents mean values ± SD of four independent experiments (**p<0.01, *** p<0.001, one-way ANOVA).

1.5. *BMVEC Contain an Endogenous Pool of Plasmalogens*

Plasmalogens are known to be indispensable lipid components of plasma membranes of many cell types (Lessig and Fuchs 2009).

To assess plasmalogen content of the major BBB constituents, BMVEC were subjected to acidic hydrolysis as outlined in Material and Methods. Released aldehydes (***Figure 37 A***) were converted to the PFB-oxime derivatives and quantified by NICI-GC-MS. These experiments revealed that 1-*O*-16:0 and 1-*O*-18:0 represent the majority of plasmalogen subspecies (>90%), each type accounting for approx. 16 nmol/10^6 cells, while only about 7% (approx. 2 nmol/10^6) contained a 1-*O*-octadecenal (18:1) chain at *sn*-1 position (***B***).

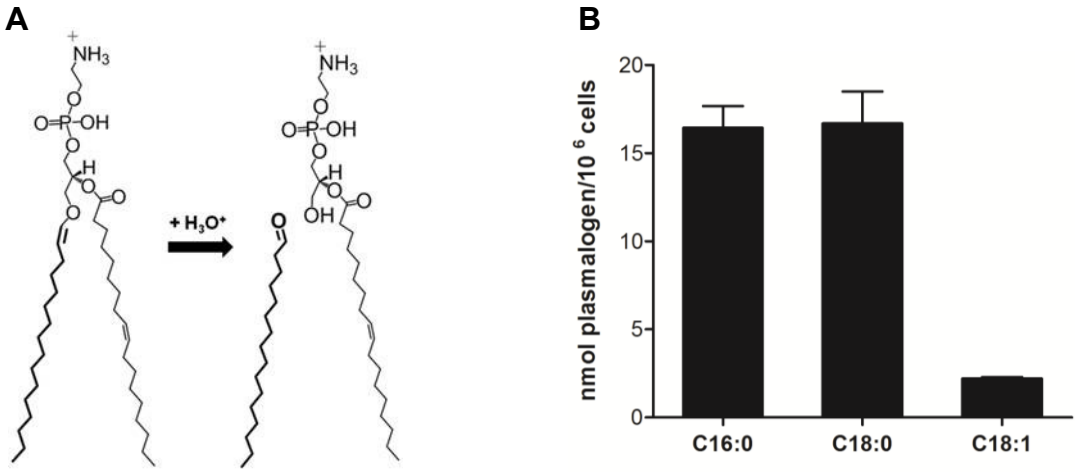

Figure 37: **Identification and quantification of endogenous BMVEC plasmalogens**
(**A**) Schematic presentation of the principle of plasmalogen quantification. (**B**) 9×10^5 BMVEC were hydrolyzed overnight in 0.5 M HCl at 37°C in the presence of 100 ng 2-Cl[$^{13}C_8$]HDA. Following extraction, PFB oximes were prepared, and total fatty aldehyde contents (HDA, ODA and ODEA) were quantitated by NICI-GC-MS analysis. Fatty aldehyde concentrations were converted to plasmalogen concentrations by the assumption of a product:educt ratio of 1:1. Results shown represent mean values ± SD from 4 independent experiments.

1.6. *Endogenous Plasmalogen Pool is Targeted by HOCl*

Since several lines of evidence suggest that RCS released from activated leukocytes target endothelial cell plasmalogens (Messner et al. 2006, Thukkani et al. 2002) the next set of experiments was aimed to test whether this aspect is also relevant to the BBB.

First, BMVEC were modified with increasing concentrations (50 to 500 µM, 30 min) of reagent HOCl. Following lipid extraction and conversion to corresponding PFB-oxime derivatives α-ClFALDs were analyzed by NICI-GC-MS. As shown in ***Figure 38 A*** reagent HOCl induced the modification of the alkenyl residue present in the *sn*-1 position (16:0, 18:0 or 18:1) resulting in the formation of 2-ClHDA (m/z 288/290), 2-ClODA (m/z 316/318) or 2-ClODEA (m/z 314/316). At a concentration range of 50 to 300 µM NaOCl 1-*O*-hexadecanal (16:0) and 1-*O*-octadecanal (18:0) plasmalogens were modified in a concentration-dependent manner yielding in 0.3 to 3.0 µg 2-ClHDA/10^6 cells and 0.1 to 3.2 µg 2-ClODA/10^6 cells. At reagent HOCl concentrations >300 µM no significant further increase in α-ClFALD formation was observed. In contrast, 0.2 µg 2-ClODEA/10^6 cells was initially detected by modification with 200 µM NaOCl and this lipid concentration remained unchanged even at higher oxidant concentrations.

To obtain data in a more physiological context *in vitro* modification of BMVEC was repeated with the difference that reagent HOCl was replaced by the MPO-H_2O_2-Cl^- system as outlined in Materials and Methods. NICI-GC-MS data revealed approx. 0.6 to 0.7 µg/10^6 cells of either 2-ClHDA or 2-ClODA and approx. 0.2 µg 2-ClODEA/10^6 cells (***Figure 38 B***). Data evaluation of chloroaldehyde amounts formed after BMVEC modification (either with NaOCl or MPO-H_2O_2-Cl^- system) compared with the total fatty aldehydes is shown in ***C***. These analysis revealed modification rates of approx. 50% for 1-*O*-hexadecanal (16:0), about 30% for 1-*O*-octadecanal (18:0) and about 25% for 1-*O*-octadecenal (18:1) plasmalogens. In contrast, the MPO-H_2O_2-Cl^- system was less effective accounting for approx. 10% (16:0- and 18:0-species) to 25% (18:1-species) of plasmalogen modification.

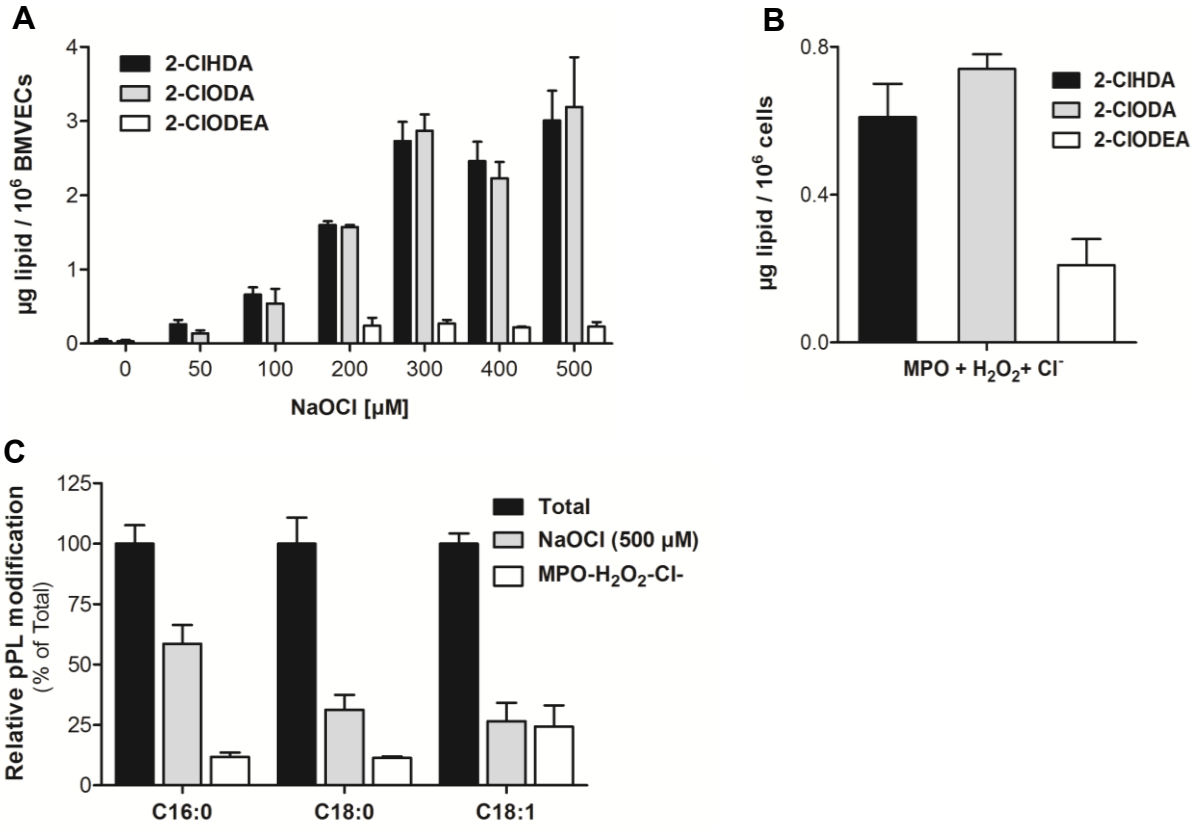

Figure 38: **Hypochlorite modification of endogenous BMVEC plasmalogens**

(**A**) 9 × 10^5 BMVEC were treated with the indicated concentrations of NaOCl for 30 min at 37 °C in HBSS in the presence of 100 ng 2-Cl[$^{13}C_8$]HDA. (**B**) Trypsinized BMVEC (1.8 x 10^6) were resuspended in PBS (50 mM, pH 5, supplemented with 140 mM NaCl, 70 nM MPO and 2.5 µg 2-Cl[$^{13}C_8$]HDA) and incubated at 37 °C with shaking. Modification was started by the addition of H_2O_2 (200 µM final concentration; eight additions of 25 µM H_2O_2 at 4-min intervals. (**C**) Maximal 2-ClHDA amounts were compared to total aldehyde content, which was determined by overnight incubation of BMVEC in 0.5 M HCl. (**A-C**) Following extraction of reaction products, PFB oximes were prepared, and chlorinated and non-chlorinated fatty aldehydes were quantitated by NICI-GC-MS by peak area comparison. Results shown represent mean values ± SD from 3 (**A**) or 4 (**B**) independent experiments.

1.7. *Vascular Stability of α-Chloro Fatty Aldehydes*

Under basal conditions cerebral blood flow ranges from 50 to 75 ml/100 g of brain tissue per minute and differs between the white and gray brain matter (Harukuni and Bhardwaj 2006). Marsche and co-workers showed that 2-ClHDA is associated with high-density lipoproteins (Marsche et al. 2004). Due to these chlorolipid-lipoprotein interactions it is likely that α-ClFALDs formed at brain capillaries might be released into the microcirculation.

To gain knowledge about the lifetime of α-ClFALDs at the cerebrovasculature in the absence of potentially metabolizing cells (Anbukumar et al. 2010, Brahmbhatt et al. 2010b, Wildsmith et al. 2006a) 2-ClHDA was incubated in human plasma at a concentration of 50 µM and 2-ClHDA content was time-dependently analyzed. Non-linear regression analysis of the data shown in ***Figure 39 A*** was fitted using a one-phase exponential decay function. This curve fit revealed a τ/2 of approx. 32 h for 2-ClHDA in blood plasma. A second approach aimed to investigate the *in vivo* lifetime of α-ClFALDs circulating in the vasculature. Therefore, as outlined in Materials and Methods, a single bolus of 350 µg 2-ClHDA/30 g body weight (approx. 70 µM based on the assumption of approx. 60% water content in mice with 30 g body weight) was intravenously injected and 2-ClHDA amounts were time-dependently quantified in blood. Non-linear regression analysis using a one-phase exponential decay function revealed a τ/2 of approx. 40 sec for 2-ClHDA in circulating blood (***B***).

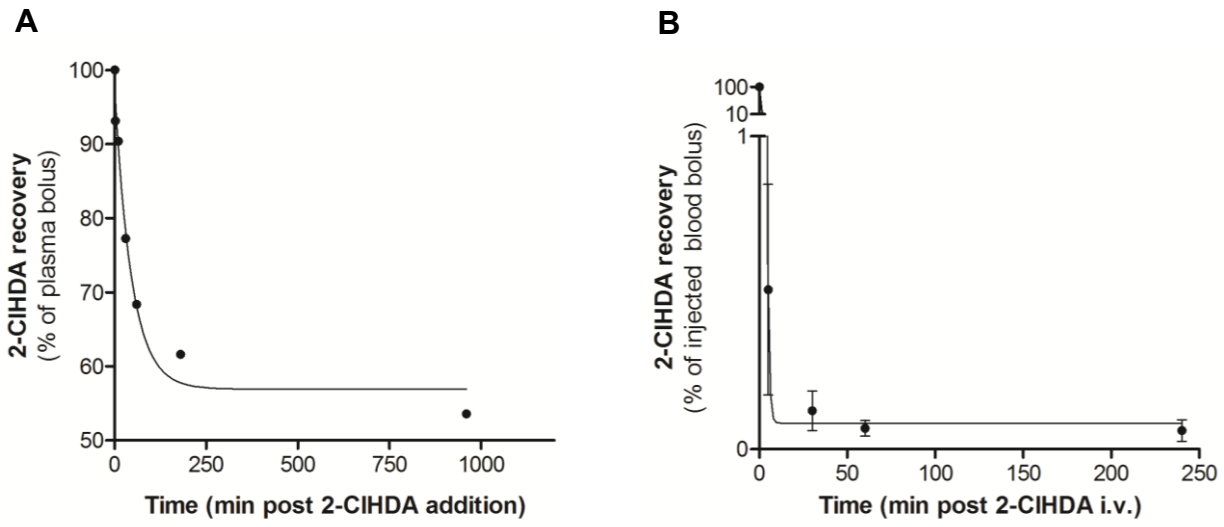

Figure 39: **2-ClHDA stability *in vitro* and *in vivo***

(**A**) Human plasma, obtained from healthy, normolipidemic subjects was spiked with 2-ClHDA (stock added in DMSO; 50 µM final concentration). At the indicated times PFB oximes of extracted lipids were prepared and 2-ClHDA was quantitatively analyzed by NICI-GC-MS. Results are values of a single determination. Experimental data were fitted by non-linear regression analysis according to $C_t = C_o \times e^{-0.0215*t}$ ($R^2 = 0.98$). (**B**) C57BL/6 mice received a single intravenous injection of 100 µl 2-ClHDA, (350 µg/30 g in Intralipid 20%/PBS/sesame oil, 47:40:13 (v/v)). At the indicated times 100 µl blood, which was obtained by retro-orbital puncturing, were quantitatively analyzed for 2-ClHDA by NICI-GC-MS using 1 µg 2-Cl[$^{13}C_8$]HDA as internal standard. Results represent mean values ± SD of triplicate determinations. Experimental data were fitted by non-linear regression analysis according to $C_t = C_o \times e^{-1.091*t}$ ($R^2 = 0.99$).

2. Metabolism of α-Chloro Fatty Aldehydes at the Cerebrovasculature

Since the life-time of 2-ClHDA in plasma and in the circulation significantly differed, it was likely that α-ClFALDs released from HOCl-modified brain capillaries are subject to re-uptake and metabolism by the endothelium (Wildsmith et al. 2006a).

2.1. *2-ClHDA is Taken Up by BMVEC*

In the first set of experiments stability of 2-ClHDA was investigated in the presence of BMVEC. For that purpose 2-ClHDA (15 nmoles/well) was added to culture medium and 2-ClHDA content was measured time-dependently as outlined in Materials and Methods. Non-linear regression analysis using a one-phase exponential decay function revealed a τ/2 of approx. 2 h for 2-ClHDA in culture medium in the presence of BMVEC (***Figure 40 A***). This half-time could indicate uptake of 2-ClHDA by BMVEC. NICI-GC-MS analysis of cellular lipid extracts demonstrated a time-dependent increase of 2-ClHDA amounts achieving maximal quantities of approx. 1 nmol within 2 h of incubation. Longer incubations times resulted in decreased levels of 2-ClHDA indicating potential metabolism (***B***).

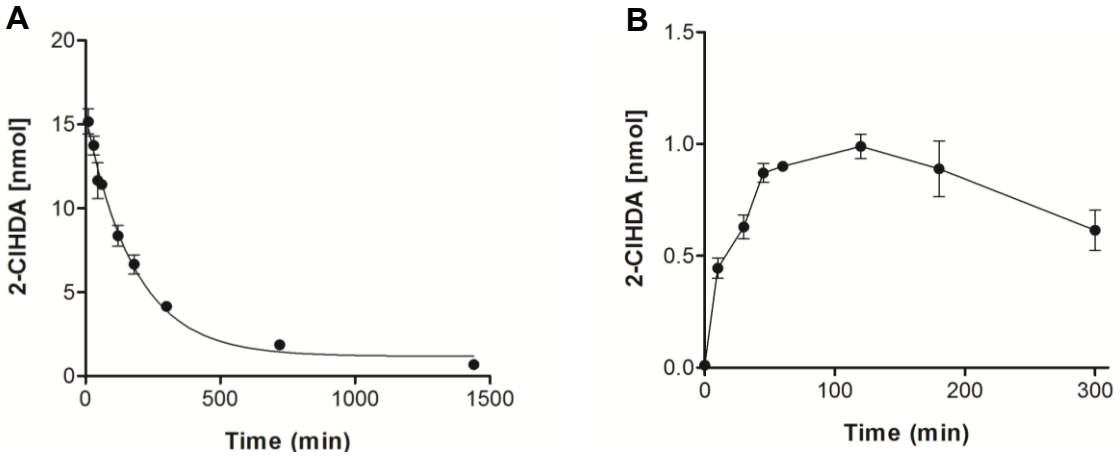

Figure 40: **Uptake kinetics of exogenous 2-ClHDA by BMVEC**
Cells (9×10^5) were incubated with 15 nmol 2-ClHDA (stock added in DMSO; final concentration 10 µM). At the indicated time periods, cellular lipids and lipids of the culture medium were extracted in the presence of 100 ng 2-Cl[$^{13}C_8$]HDA. After conversion to corresponding PFB-oxime derivatives 2-ClHDA content of (**A**) the culture medium and (**B**) BMVEC were quantitated by NICI-GC-MS analysis. Results represent mean values ± SD of three independent experiments. Experimental data of 2-ClHDA decay in culture medium (**A**) were fitted by non-linear regression analysis according to $C_t = C_o \times e^{-0.0056*t}$ ($R^2 = 0.98$).

2.2. *Functional Aldehyde Group becomes Oxidized and Reduced*

Quantification of 2-ClHDA-derived metabolites appeared to be pivotal for this project. Therefore, the first task to accomplish was to establish appropriate NICI-GC-MS methods for fatty alcohol and fatty acid analysis.

Figure 41 shows NICI-GC-MS chromatograms and mass spectra of the PFB-ester derivatives of 2-ClHA (***A*** and ***B***) and of the corresponding internal standard pentadecanoic acid (***C*** and ***D***) eluting at 14.95 min and 13.55 min. Under analytic conditions used in this study molecular ions (M^-) at m/z 470 (PFB-ester of 2-ClHA) and 422 (PFB-ester of pentadecanoic acid) were not detectable. Base peaks were observed at m/z 289 (2-ClHA) as well as m/z 241 (pentadecanoic acid) and intensity ratio of the fragment ions 289/291 of approx. 3:1 is indicative for the presence of two chlorine isotopes ($^{35}Cl/^{37}Cl$) in the analyte. Additional fragment ions were only observed for 2-ClHA PFB-ester derivative at m/z 196 and m/z 254.

NICI-GC-MS chromatograms and mass spectra of PFB-ester derivatives of 2-ClHOH and corresponding internal standard pentadecanol are shown in ***Figure 42***. PFB-ester derivatives of fatty alcohols showed different retention times compared to their PFB-derivatized carboxyl counterparts (14.88 min and 13.61 min, ***A*** and ***C***). In contrast to fatty acids, M^- at m/z 470 (PFB-ester of 2-ClHOH) and 422 (PFB-ester of C15-FOH) were highly abundant (***B*** and ***D***). Moreover, the intensity ratio of the fragment ions 470/472 of approx. 3:1 is indicative for the presence of two chlorine isotopes ($^{35}Cl/^{37}Cl$). In case of 2-ClHOH additional fragment ions could be allocated at m/z 178 and m/z 435.

Due to more pronounced fragmentation of α-chloro lipids compared to non-chlorinated internal standards ion counts of different fragments were summed up for data evaluation.

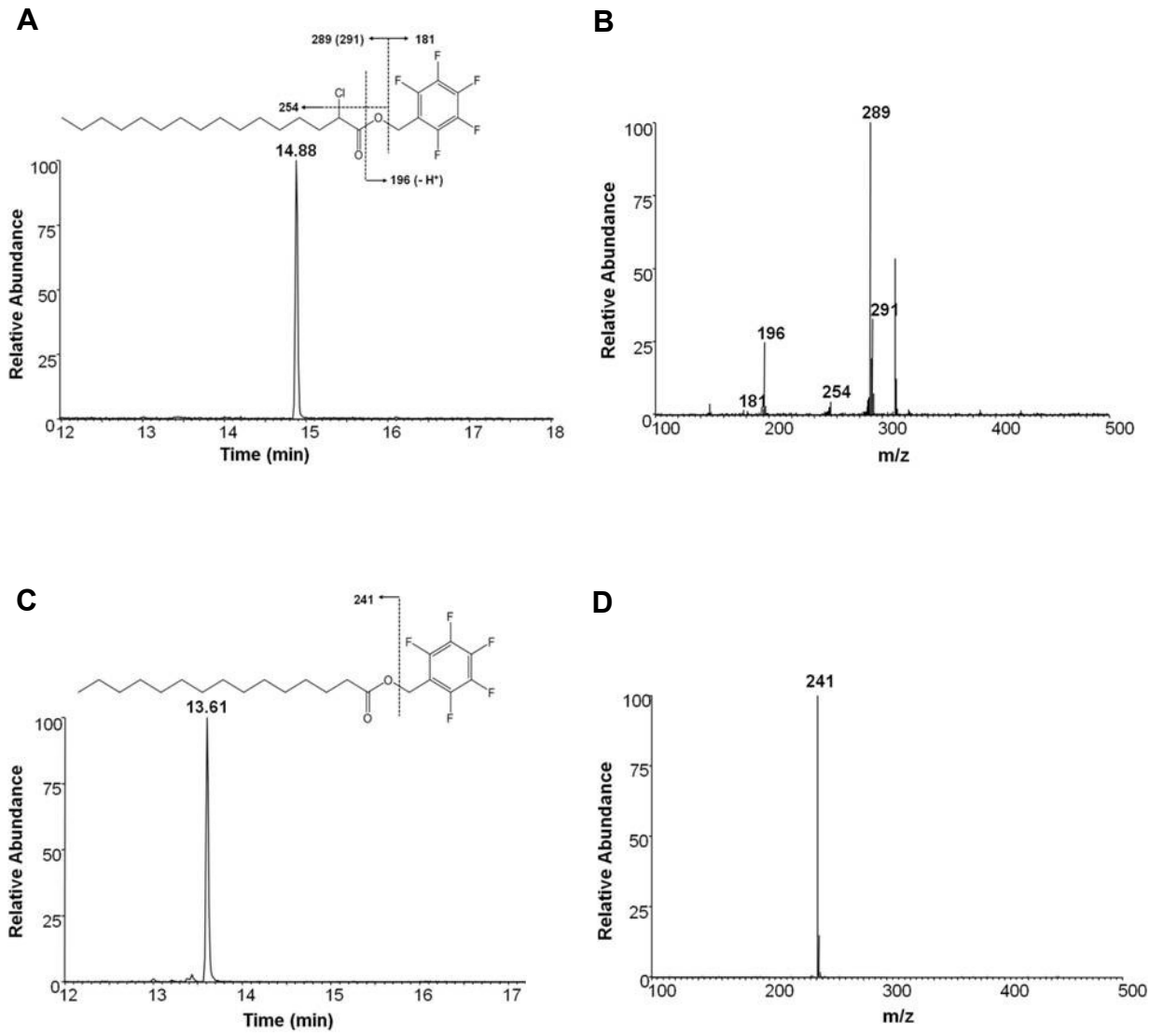

Figure 41: **NICI-GC-MS analysis of 2-ClHA and pentadecanoic acid**

For NICI-GC-MS analysis 2-ClHA and pentadecanoic acid were converted into PFB ester derivatives. (**A**) Single ion current trace (m/z 289) of 0.5 nmol 2-ClHA injected and (**C**) total ion current trace of pentadecanoic acid (3 nmoles). Corresponding full scan NICI spectra of peaks eluting at 14.88 min (2-ClHA, **B**) and 13.61 min (pentadecanoic acid, **D**). Proposed fragmentation patterns and mass assignments are shown in the insets.

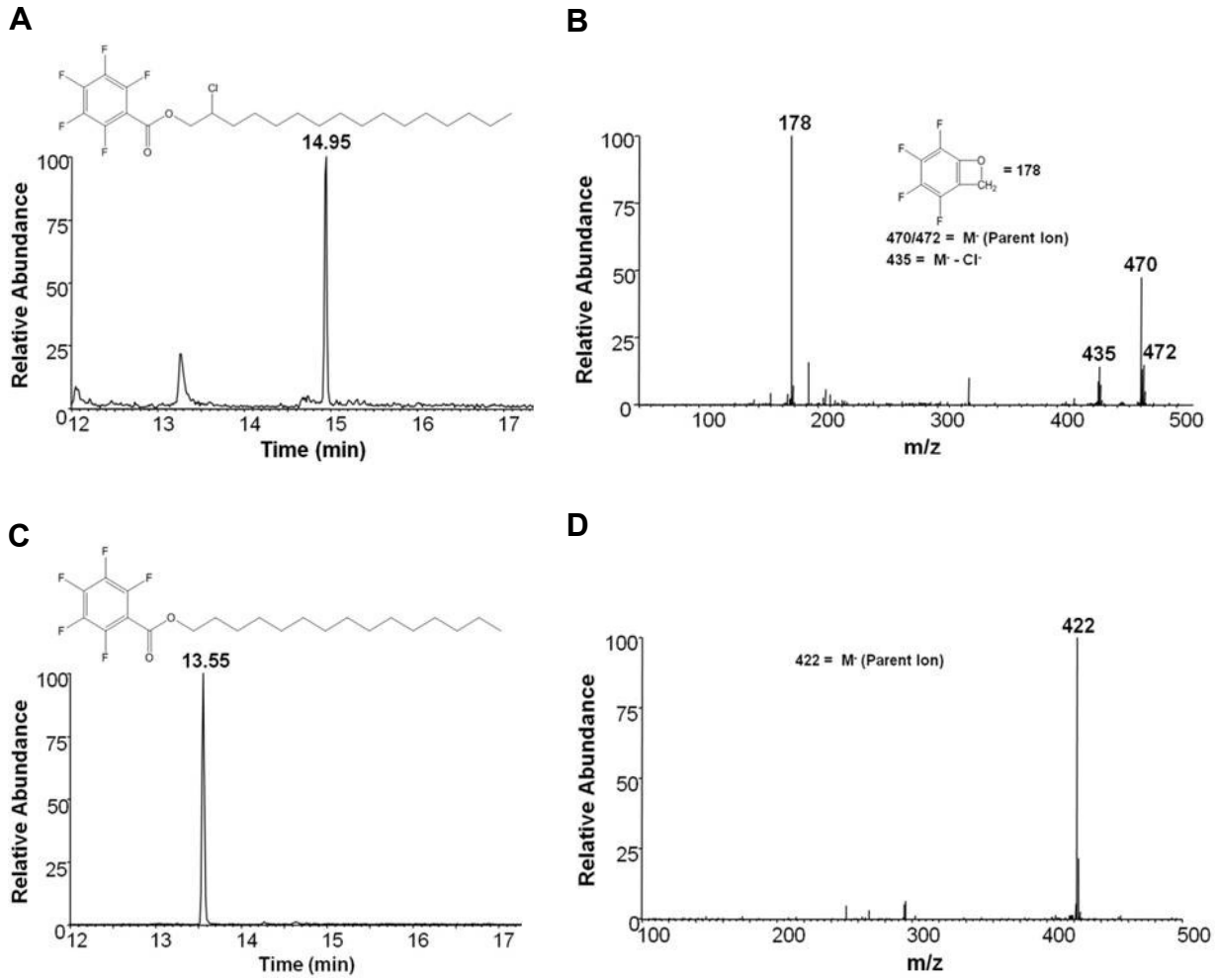

Figure 42: **NICI-GC-MS analysis of 2-ClHOH and pentadecanol**

For NICI-GC-MS analysis 2-ClHOH and pentadecanol were converted into PFB ester derivatives. (**A**) Single ion current trace (m/z 470) of 2-ClHA, 1 nmol injected, and (**C**) total ion current trace of pentadecanol (3 nmoles). Corresponding full scan NICI spectra of peaks eluting at 14.95 min (2-ClHOH, **B**) and 13.55 min (pentadecanol, **D**). Proposed fragmentation patterns and mass assignments are shown in the insets.

To corroborate the hypothesis of α-ClFALD metabolism at the cerebrovasculature 2-ClHDA (15 nmoles/well) was added to culture medium. Subsequently, 2-ClHA- and 2-ClHOH contents were time-dependently quantified in both, cell monolayers and corresponding supernatants, as outlined in Material and Methods.

NICI-GC-MS analysis of PFB-derivatives demonstrates that BMVEC oxidize and reduce 2-ClHDA to its respective chlorinated fatty acid and chlorinated fatty alcohol (***Figure 43 A*** and ***B***). Within the first two hours of incubation 2-ClHOH and 2-ClHA accumulated in the cell monolayer in concentrations of approx. 1.9 and 0.4 nmol, respectively. While 2-ClHOH concentrations were slightly decreasing at longer time periods 2-ClHA levels remained constant (**A**). Moreover, both chlorinated lipids were detectable in the culture medium (approx. 10% of cell-associated 2-ClHOH and 35% of cell-associated 2-ClHA at highest intracellular concentrations), indicating cellular release of lipid metabolites and/or synthesis via extracellular redox events (**B**).

A time course of precursor- (2-ClHDA added at t=0) product relationship (sum of 2-ClHDA, 2-ClHOH, and 2-ClHA in cells and medium, termed 2-ClHX) is shown in ***Figure 43 C***. It is evident that at early time points (up to 60 min) loss of 2-ClHDA and accumulation of 2-ClHX were equal, nevertheless recovery of 2-ClHDA and its metabolites after 5 h accounts for only 25% of total added 2-ClHDA implicating other possible routes involved in chloroaldehyde loss e.g. binding to proteins or lipids, as well as catabolism of 2-ClHA by omega-oxidation and subsequent beta-oxidation (Brahmbhatt et al. 2010b, Wildsmith et al. 2006a, Wildsmith et al. 2006b).

2.3. *Chlorinated Lipids become Esterified into Complex Lipids*

One of the pathways contributing to loss of 2-ClHDA is its oxidation to 2-ClHA and subsequent re-incorporation into the inert storage pool of complex lipids (Wildsmith et al. 2006a). In order to clarify the ability of BMVEC to form chlorinated complex lipids, cells were incubated in the presence of 2-ClHDA (80 nmol/well); after 6, 12, and 24 h cellular lipids were extracted, pre-separated by TLC, hydrolyzed, and after derivatization analyzed by NICI-GC-MS. These experiments revealed that approx. 30% of the total cellular 2-ClHA content is recovered from the polar lipid fraction within the time period investigated (***Figure 43 D***).

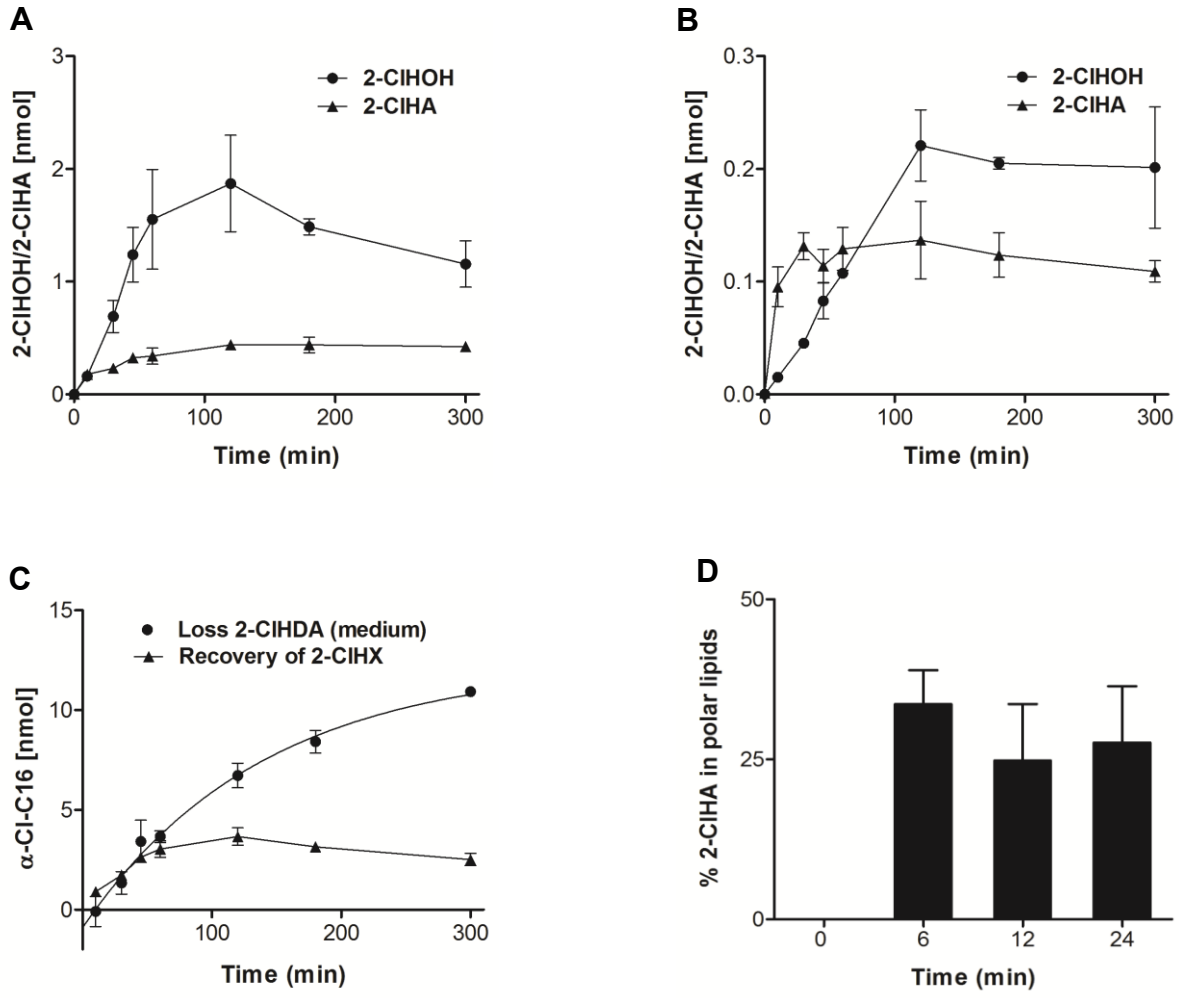

Figure 43: **Metabolism of exogenous 2-ClHDA by BMVEC**

Cells (9×10^5) were incubated with 15 nmol 2-ClHDA (stock added in DMSO; final concentration 10 µM). At the indicated time periods, cellular lipids and lipids of the culture medium were extracted in the presence of 100 ng pentadecanol and 100 ng pentadecanoic acid as internal standards. After conversion to corresponding PFB-ester derivatives 2-chlorohexadecanoic acid (2-ClHA) and 2-chlorohexadecanol (2-ClHOH) concentrations were quantitated in (**A**) cell monolayers or (**B**) culture medium by NICI-GC-MS analysis. (**C**) Loss of 2-ClHDA vs. recovery of 2-ClHX (the sum of 2-ClHDA, 2-ClHOH, and 2-ClHA in cells and medium). (**D**) Cells (5.5×10^6) were incubated with 80 nmol 2-ClHDA (stock added in DMSO; final concentration 10 µM). At the indicated time periods, cellular lipids were extracted. After pre-separation of lipid classes by TLC and subsequent extraction from TLC plates, free fatty acids were generated by alkaline hydrolysis. After conversion to corresponding PFB-ester derivatives 2-ClHA concentrations were quantitated by NICI-GC-MS analysis with pentadecanoic acid as internal standard. Results represent mean values ± SD of triplicate determinations.

3. Alpha-Chloro Fatty Aldehydes Impact on BBB-Function

All data obtained in this study indicate that under neuroinflammatory conditions pathophysiological relevant concentrations of α-ClFALDs are formed at the cerebrovasculature via HOCl-mediated attack of endogenous or exogenous plasmalogen pools. During the following chapter the molecular pathways of 2-ClHDA-induced BBB dysfunction were explored.

3.1. *2-ClHDA is a Powerful Inducer of In Vitro Barrier Dysfunction*

The first major task in this context was to investigate *in vitro* barrier function of BMVEC - the major constituents of the BBB - in the presence of HOCl and HOCl-derived chloroaldehydes.

For that reason BMVEC were challenged with increasing concentrations of NaOCl and 2-ClHDA while *in vitro* barrier function was monitored in real-time using the ECIS system.

These experiments demonstrated that 2-ClHDA induces pronounced barrier dysfunction in a concentration-dependent manner (***Figure 44 A***) where 5 μM appeared to be a threshold concentration: Higher concentrations (25 μM) induced almost complete loss of barrier function while lower concentrations (less than 5μM) were without effect (data not shown). Statistical significance of barrier disruption at all investigated concentrations was initially observed within 30 min and peaked inbetween 2 and 5 hours of incubation (***B***).

In contrast, reagent HOCl induced BBB dysfunction only in the high micro molar range: 100 μM provoked a slight decrease in barrier function during long incubation periods, whereas higher concentrations induced rapid and almost complete loss of barrier integrity ***(C*** and ***D***).

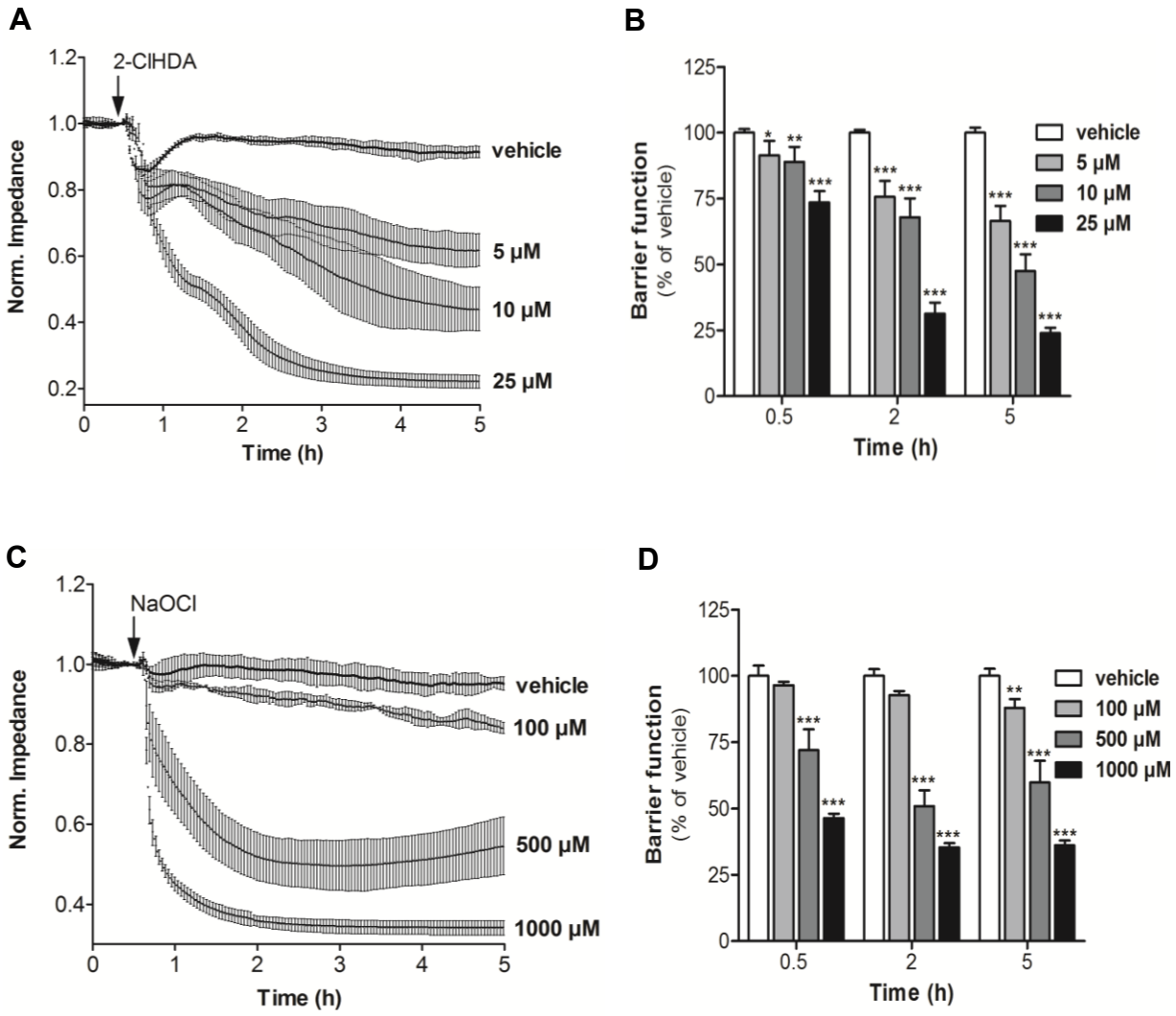

Figure 44: **BMVEC barrier function is severely compromised by 2-ClHDA or NaOCl**

BMVEC were plated on gold microelectrodes and cultured to confluence. Barrier function of HC-induced endothelial monolayers was continuously monitored by impedance sensing at 4 kHz. After stabilization, cells were challenged (arrow) with either 2-ClHDA (**A**) or NaOCl (**C**) at various concentrations. Relative barrier function of 2-ClHDA (**B**) and NaOCl (**D**) at the indicated times post treatment. Impedance was normalized to treatment start and represents mean values ± SD of four independent experiments (*p<0.05; ** p<0.01; *** p<0.001, two-way ANOVA).

3.2. *Barrier Dysfunction is Accompanied by Reorganization of the Actin-Cytoskeleton*

Several studies have shown that BBB breakdown is accompanied with morphological changes and rearrangement of the F-actin cytoskeleton (Shiu et al. 2007, Usatyuk and Natarajan 2004).

Therefore, morphological changes of the BMVEC monolayer as result of 2-ClHDA treatment are likely to occur. To examine this aspect BMVEC were challenged with increasing concentrations of 2-ClHDA for 3 h and an immunofluorescence study of actin-cytoskeleton (red) and nuclei (blue) was performed (***Figure 45***). In contrast to vehicle (**A**) 2-ClHDA concentrations, which were already shown to be associated with severe barrier dysfunction induced noticeable intercellular gap formation (***B,*** arrows). These alterations became more evident with increasing concentrations (***C,*** arrows) although high concentrations (> 50 µM) resulted in entire loss of endothelial cells (data not shown), presumably due impaired cell viability caused by apoptosis and/or necrosis.

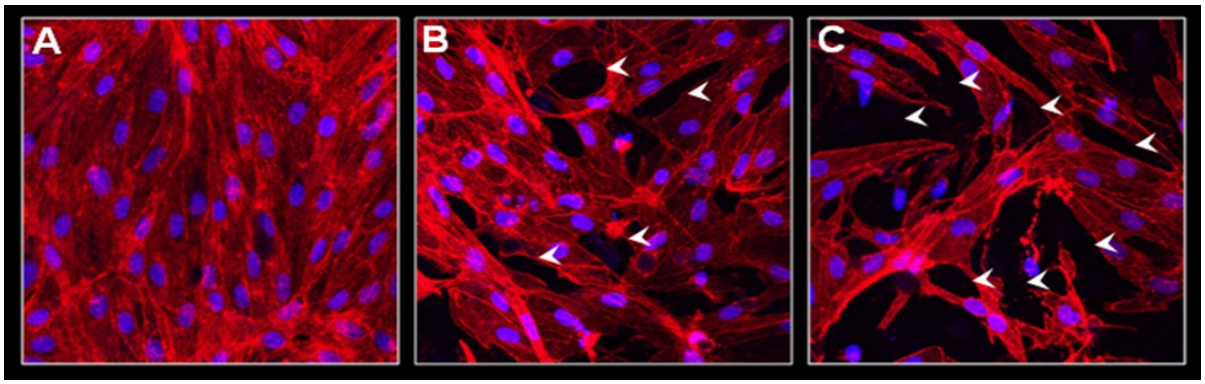

Figure 45: **Effects of 2-ClHDA on the actin cytoskeleton of BMVEC**
For immunofluorescence studies BMVEC were cultured on coverslips to confluence. After incubation for 3 h with (**A**) vehicle, (**B**) 10 µM or (**C**) 25 µM of 2-ClHDA F-actin-cytoskeleton (red) and nuclei (blue) were stained using rhodamine-labeled phalloidin and DAPI. Confocal laser scan microscopy, as outlined in Material and Methods, was used for visualization. Intercellular gap are marked by arrows.

3.3. *In Vivo Rat Model: BBB-Function is Affected by 2-ClHDA*

The next set of experiments aimed to corroborate *in vitro* results under *in vivo* conditions. Due to high instability of α-ClFALDs *in vivo in situ* brain perfusion technique appeared to be the most convenient method for BBB delivery by circumventing peripheral circulation (Takasato et al. 1984).

In preliminary experiments the surgical procedures and perfusion conditions to evaluate BBB (dys)function were established with Ringer- or hyperosmolar mannitol solutions, using Evans Blue albumin (EB) and sodium fluorescein (SF) as permeability markers (data not shown). ***Figure 46 A*** and ***B*** show that significant BBB dysfunction was observed in this *in vivo* rat model. In contrast to vehicle control (***a*** and ***c***) the perfusion of 25 µM 2-ClHDA for 90 min via the carotid artery significantly increased EB leakage into the brain, induced edema formation (***b*** and ***d***), and resulted in cerebral accumulation of the low molecular weight BBB permeability marker SF (***B***).

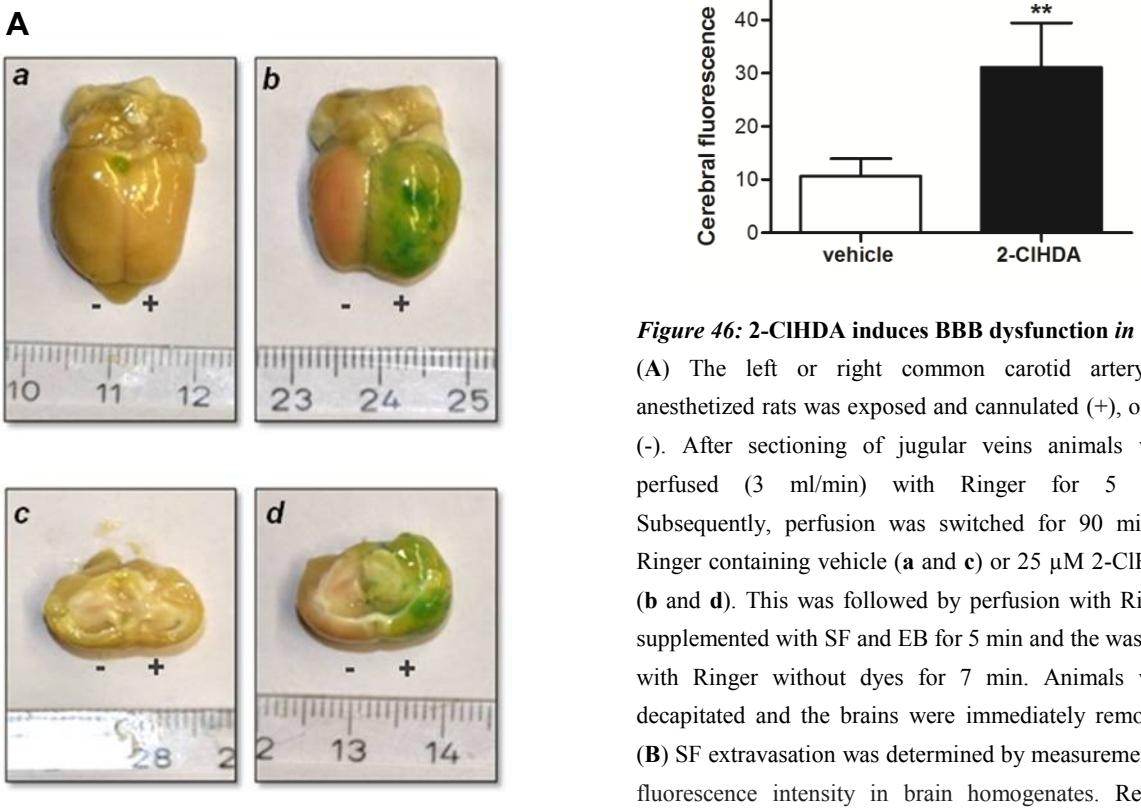

Figure 46: **2-ClHDA induces BBB dysfunction *in vivo*** (**A**) The left or right common carotid artery of anesthetized rats was exposed and cannulated (+), or not (-). After sectioning of jugular veins animals were perfused (3 ml/min) with Ringer for 5 min. Subsequently, perfusion was switched for 90 min to Ringer containing vehicle (**a** and **c**) or 25 µM 2-ClHDA (**b** and **d**). This was followed by perfusion with Ringer supplemented with SF and EB for 5 min and the washout with Ringer without dyes for 7 min. Animals were decapitated and the brains were immediately removed. (**B**) SF extravasation was determined by measurement of fluorescence intensity in brain homogenates. Results shown represent mean values ± SD from four different animals (** $p<0.01$, Students t-test)

4. BBB-Dysfunction is Based on Cellular Alterations

Given the observation that α-ClFALDs are potent inducers of BBB dysfunction subsequent experiments were designed to correlate these observations to alterations in BMVEC constituting this barrier.

4.1. *Cell Viability is Crucial for the Loss of Barrier Integrity*

The first approach aimed to evaluate cytotoxic properties of 2-ClHDA and reagent NaOCl in BMVEC. Therefore, BMVEC were incubated in the absence or presence of different concentrations of 2-ClHDA and NaOCl up to 24 h and cell viability was assessed using the MTT test.

These data demonstrated that exposure of BMVEC to 2-ClHDA (***Figure 47 A***) and reagent HOCl (***B***) impaired cell viability in a time- and concentration-dependent manner. Interestingly, 2-ClHDA mediated cytotoxicity to BMVEC - with LC_{50} values of approx. 50 µM (1 h), 25 µM (3 h), and 15 µM (5 h) - at much lower concentrations as compared to reagent HOCl. Of note, LC_{50}s of highly cytotoxic NaOCl were between 10-20 fold higher as compared to 2-ClHDA.

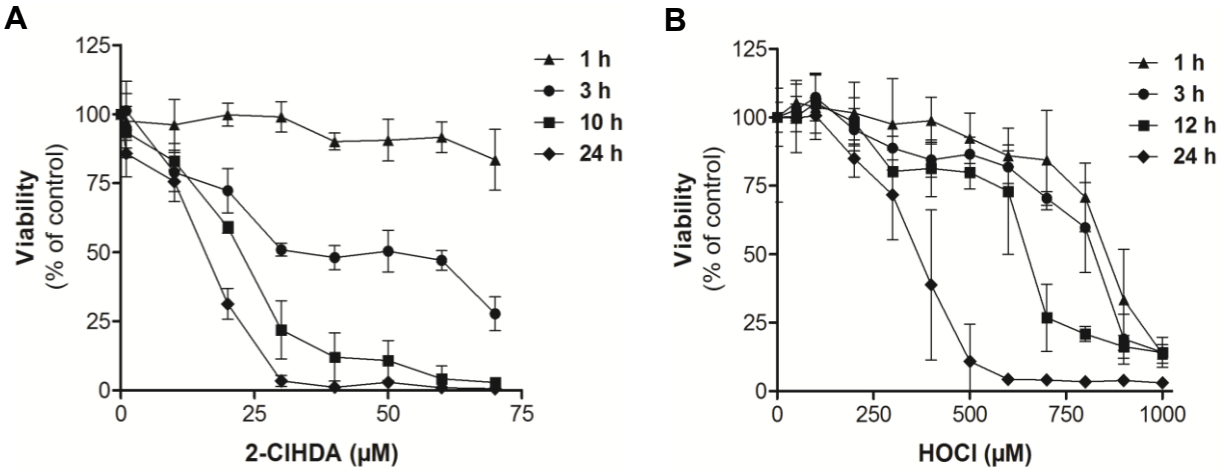

Figure 47: **2-ClHDA impairs BMVEC viability**

Cells (1.6×10^5) were incubated in the absence or presence of (**A**) 2-ClHDA or (**B**) reagent HOCl at indicated concentrations for the indicated time periods. Cell viability was analyzed using the MTT test. Results are expressed as % of controls and represent mean values ± SD of triplicate (**A**) or quadruplicate (**B**) determinations.

4.2. *Cytotoxic Properties have Structural Specificity*

2-ClHDA consists of three major chemical entities, i) a C16 aliphatic hydrocarbon chain, ii) an aldehyde residue, and iii) a chlorine residue at C2.

To get an indication about the structural requirements that mediate cytotoxicity, in addition to 2-ClHDA three structurally related C16 analogues, namely hexadecanal (HDA), palmitic acid, and 2-ClHDA-dma were analyzed for their cytotoxic potential (***Figure 48 A***). Cytotoxicity decreased in the order 2-ClHDA > HDA > palmitic acid > 2-ClHDA-dma (***B***). In these experiments 2-ClHDA reduced cell viability by 60% (25 µM) and 90% (50 µM), while the non-chlorinated analogue, HDA, impaired cell viability by approx. 40% (25 µM) and 50% (50 µM). Palmitic acid, a fatty acid with potent lipotoxic properties, induced a 20% reduction of viability at the highest concentration used (50 µM). The chemically inert 2-ClHDA dma was without effect on cell viability. Hence, the presence of chlorine significantly augments the cytotoxic properties of HDA indicating that 2-ClHDA is a mediator with high lipotoxic potential.

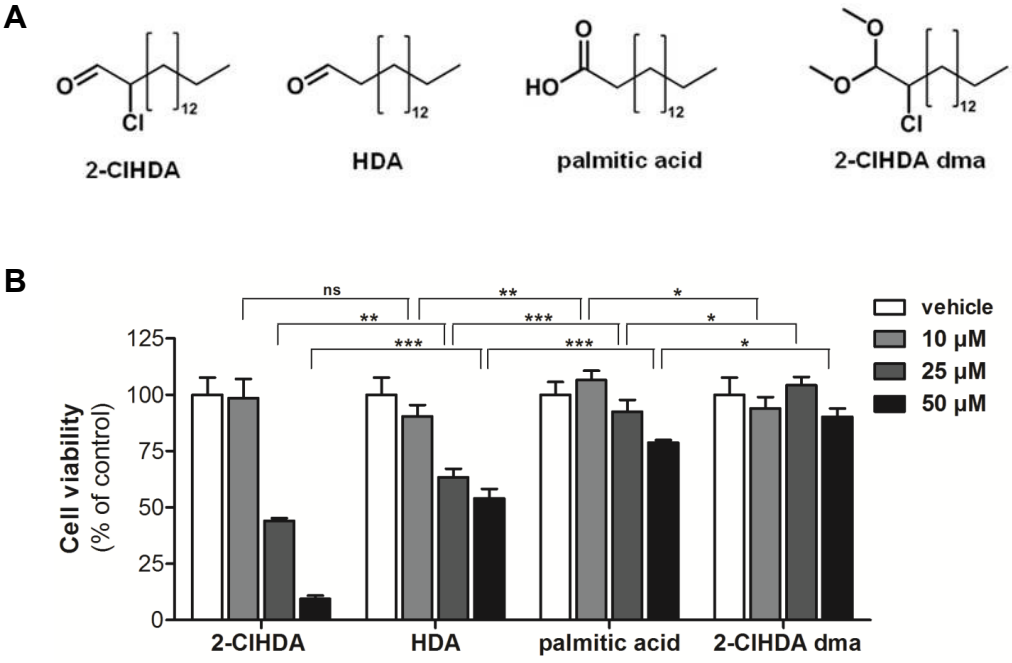

Figure 48: **Headgroup-dependent reduction of cell viability of BMVEC**

(**A**) Structures of four different C16 compounds used in viability assays. (**B**) Cells (3.5×10^5) were challenged overnight with 2-ClHDA or structural analogs (shown in A) at indicated concentrations. Following treatment, BMVEC viability was analyzed by the MTT test. Results are expressed as % of controls and represent mean values ± SD of triplicate determinations (ns = not significant, *p<0.05; ** p<0.01; *** p<0.001; two-way ANOVA).

4.3. *2-ClHDA induces Caspase-3 dependent Apoptosis*

The present findings demonstrate that long chain α-ClFALDs have the potential to mediate cytotoxic properties.

To investigate the ability of 2-ClHDA to induce apoptosis in BMVEC, particularly concentrations where rather low impairment of cell viability occurs, the cells were incubated in the absence and presence of 2-ClHDA (1 to 25 µM) for 5 h. As shown in ***Figure 49 A*** concentrations of ≥ 5 µM induced caspase-3 activation. While 2-ClHDA at 5-10 µM resulted in partial proteolytic cleavage of procaspase 3, 25 µM resulted in almost quantitative conversion into active caspase-3. In contrast, HOCl (***B***), even when used at 1000 µM, did not induce procaspase-3 processing.

4.4. *Mitochondrial Function is Impaired by 2-ClHDA*

To determine if impaired cell viability and/or apoptosis (caused by 2-ClHDA/HOCl treatment) is accompanied by mitochondrial dysfunction, JC-1 cytotoxicity assays that rely on measurements of the mitochondrial membrane potential (Δψm) were performed.

Therefore, cells were incubated in the absence or presence of 2-ClHDA and HOCl, respectively, at different concentrations for various time periods. After incubation with JC-1, Δψm was determined fluorometrically. Results were analyzed in terms of the ratio of red to green fluorescence intensities, thus results are not linked to the number of viable cells. JC-1 assays indicated that 2-ClHDA treatment was accompanied by a rapid decrease of the red/green ratio, indicating a collapse of Δψm in a time- and concentration-dependent manner (***Figure 50 A***) with IC_{50} values of approx. 25 µM (1 h), 12.5 µM (3 h), and 5 µM (5 h). Treatment of BMVEC with HOCl also resulted in a decrease of Δψm, however, IC_{50} values were apparently 20 to 40-fold higher (500 µM at 3 h and 100 µM at 5 h) compared to those of 2-ClHDA (***B***).

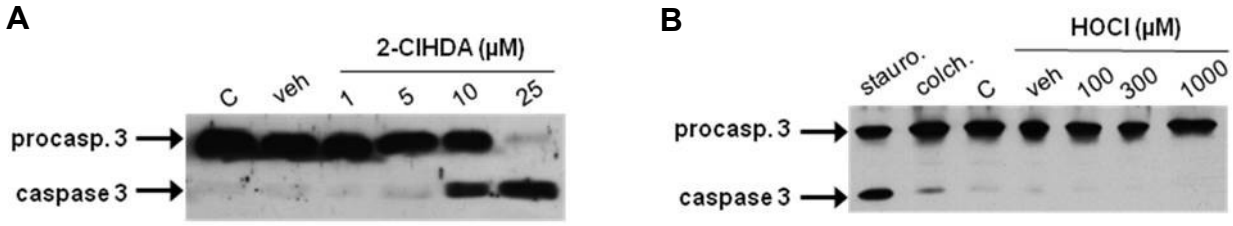

Figure 49: **Induction of the apoptotic machinery in response to 2-ClHDA**

BMVEC were incubated for 5 h with (**A**) 2-ClHDA or (**B**) NaOCl. Staurosporine ('stauro.') and colchicine ('colch.') were used as known inducers of apoptosis. After treatment, cells were lyzed; aliquots of protein lysates were subjected to SDS-PAGE and transferred to PVDF. Immunoreactive bands were detected with rabbit polyclonal anti-caspase 3 (primary antibody) and peroxidase-conjugated secondary antibodies using the ECL-system. Procaspase 3 was detected at 32 kDa and caspase 3 at 17 kDa.

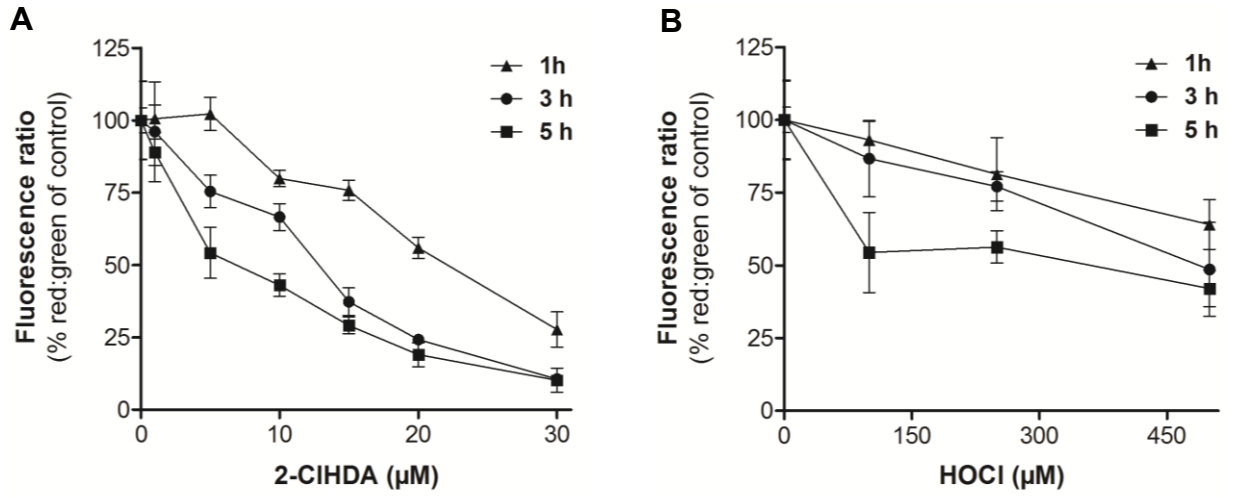

Figure 50: **Mitochondrial membrane potential (Δψm) of 2-ClHDA- and NaOCl-treated BMVEC**

BMVEC were incubated in the absence or presence of 2-ClHDA (**A**) or NaOCl (**B)** at the indicated concentrations for the indicated time periods. Following treatment, Δψm was analyzed using the JC-1 assay, as outlined in Material and Methods. Data were calculated by division of red fluorescence by green fluorescence. Results are expressed as % of red to green fluorescence ratio compared to controls, and represent mean values ± SD of three independent experiments.

4.5. *2-ClHDA Treatment Leads to Increased Formation of Intracellular ROS in BMVEC*

It is known that electrophilic lipids, such as 4-HNE, and the cyclopentenones 15-deoxy-$\Delta^{12,14}$-prostaglandin J_2 and 15-J_2-isoprostane induce formation of ROS in endothelial cells most probably by direct interaction with mitochondria and/or alterations of the intercellular redox balance (Landar et al. 2006). Accordingly, 2-ClHDA mediated mitochondrial dysfunction could result in ROS formation.

To measure the generation of intracellular ROS an assay based on the redox sensitive dye carboxy-H_2DCFDA was used for 2-ClHDA-treated BMVEC. The outcome of these experiments demonstrated that 2-ClHDA induced ROS production only at concentrations in the range of 15 to 50 µM (***Figure 51 A***), conditions that were shown to decrease cell viability and impair mitochondrial function in BMVEC.

Next, a potential protective role of thiol compounds such as N-acetyl cysteine (NAC) or N-mercaptopropionyl glycine (MPG) against oxidative stress was tested. Thus, BMVEC were pretreated with NAC or MPG before they were challenged with different concentrations of 2-ClHDA. Cell viability was measured by the MTT test (***B***). The results of these experiments demonstrated that neither NAC nor MPG were able to restore cell viability.

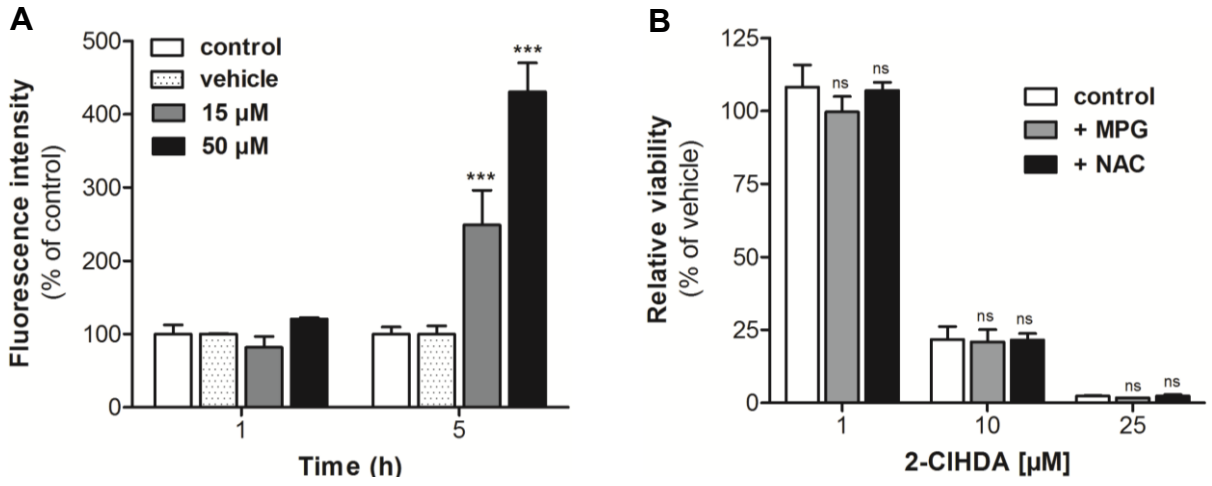

Figure 51: **2-ClHDA induces intracellular ROS formation in BMVEC**

(**A**) ROS formation was determined using the redox-sensitive tracer carboxy-H_2DCFDA. Cells were pre-incubated with non-fluorescent carboxy-H_2DCFDA followed by treatment with 2-ClHDA at the indicated concentrations for the indicated time periods. (**B**) After pretreatment with 1 mM of either NAC or MPG for 1 h BMVEC were overnight challenged with 2-ClHDA at indicated concentration. Cell viability was determined by the MTT test. Results are expressed as % of control, and represent mean values ± SD of three independent experiments performed in triplicate (*** $p<0.001$, ns = not significant; two-way ANOVA).

4.6. *MAPK Signaling is Activated upon 2-ClHDA Treatment*

Extensive research has documented crucial roles of ERK1/2- and stress-activated protein kinase (JNK1/2 and p38)-signaling events in the regulation of barrier integrity during environmental stress including reactive carbonyls (Gonzalez-Mariscal et al. 2008, Usatyuk and Natarajan 2004).

Consequently, to gain insight in 2-ClHDA-induced cellular signaling events BMVEC were incubated in the absence or presence of 2-ClHDA or NaOCl and MAPK activation was investigated (***Figure 52***). Western blot analysis revealed that 2-ClHDA treatment induced all 3 main groups of MAPKs in a similar manner to reagent NaOCl but apparently in concentrations 30 to 40 times less compared to the oxidant (***A***-***C***). While JNK1/2 (***B***) were activated at 2-ClHDA concentrations of ≥ 10 µM, ERK1/2 and p38 were activated at lower concentrations (5 µM, *A* and *C*). These conditions have no adverse effects on cell viability. To get an indication about the time course of MAPK activation, BMVEC were treated with 25 µM 2-ClHDA and protein phosphorylation was followed in a time-dependent manner. Western blot analysis suggested a lipotoxic activation pattern of stress-activated protein kinases with a first maximum between 10 and 45 min, followed by a substantially more pronounced activation between 60 and 180 min (***D*** and ***E***). In contrast to rather slow activation of stress-activated protein kinases ERK1/2 was induced within one minute post 2-ClHDA addition and remained activated up to 3 h (***F***).

4.7. *Impact of 2-ClHDA on Junctional Architecture*

A body of evidence demonstrates that BBB dysfunction is commonly accompanied by alterations of the molecular composition, function and dynamics of the junction proteins (Coisne and Engelhardt 2011).

To reveal a possible involvement of junction architecture alterations in 2-ClHDA-mediated barrier dysfunction ZO-1 and VE-cadherin morphology was examined by immunofluorescence microscopy (***Figure 53***). Therefore, BMVEC were challenged either with vehicle (***A-C***) or with 2-ClHDA (***D-F***). After a treatment with 15 µM for 3 h two major alterations were observable: On the one hand junctions turned into frizzy-like structures (small arrows, ***E***) indicating impaired junctional interactions. On the other hand these changes in the barrier architecture were associated with pronounced redistribution of ZO-1 from the cell surface into the nucleus (large arrows, ***D***).

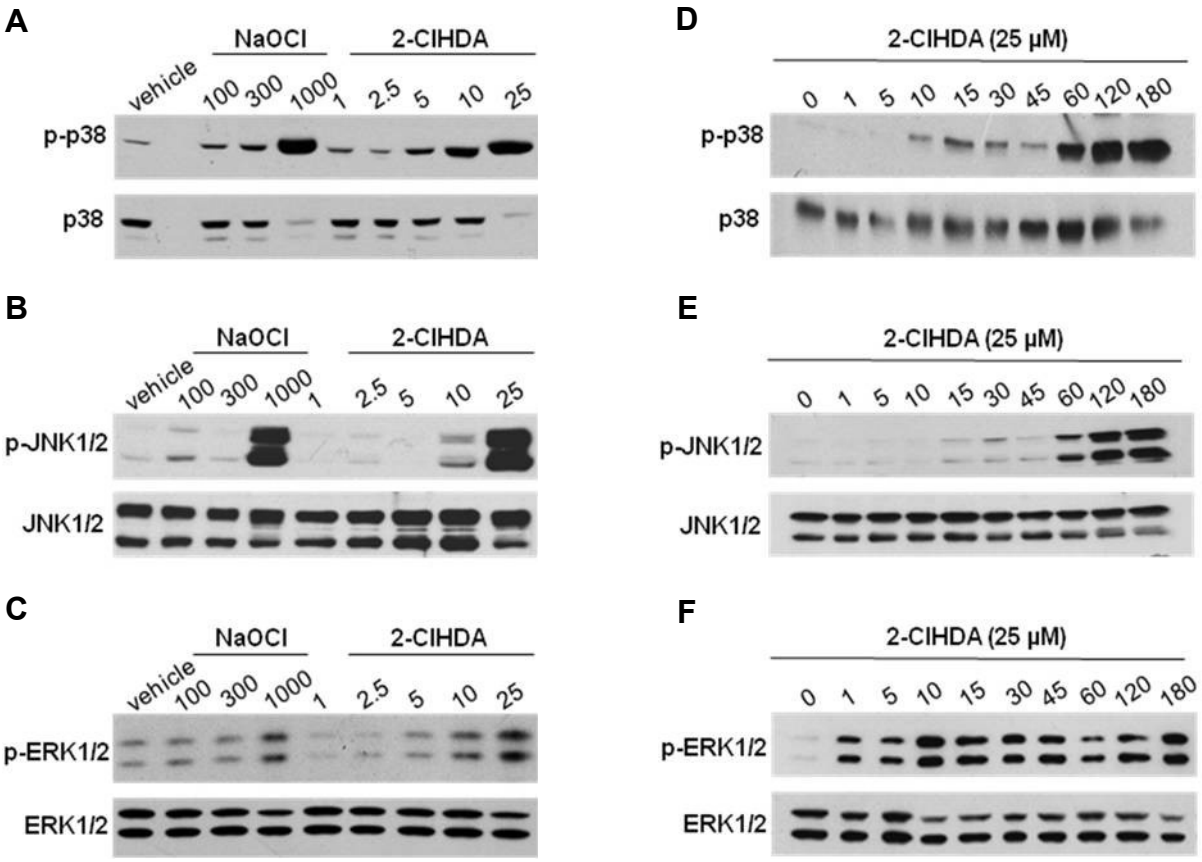

Figure 52: **Activation of MAP kinase pathways by 2-ClHDA**

(**A-C**) Concentration-dependent phosphorylation of MAPK. BMVEC were incubated for 3 h with 2-ClHDA or NaOCl at indicated concentrations (µM). (**D-F**) Time course of 2-ClHDA-induced MAPK phosphorylation. BMVEC were challenged with 25 µM 2-ClHDA for the indicated time periods (min). After treatment, cells were lyzed, aliquots of protein lysates were subjected to SDS-PAGE and transferred to PVDF. Pan- or phospho-specific polyclonal antibodies against p38 (**A, D**), JNK1/2 (**B, E**) or ERK1/2 (**C, F**) were used as primary antibodies. Immunoreactive bands were visualized with peroxidase-conjugated secondary antibodies using the ECL-system.

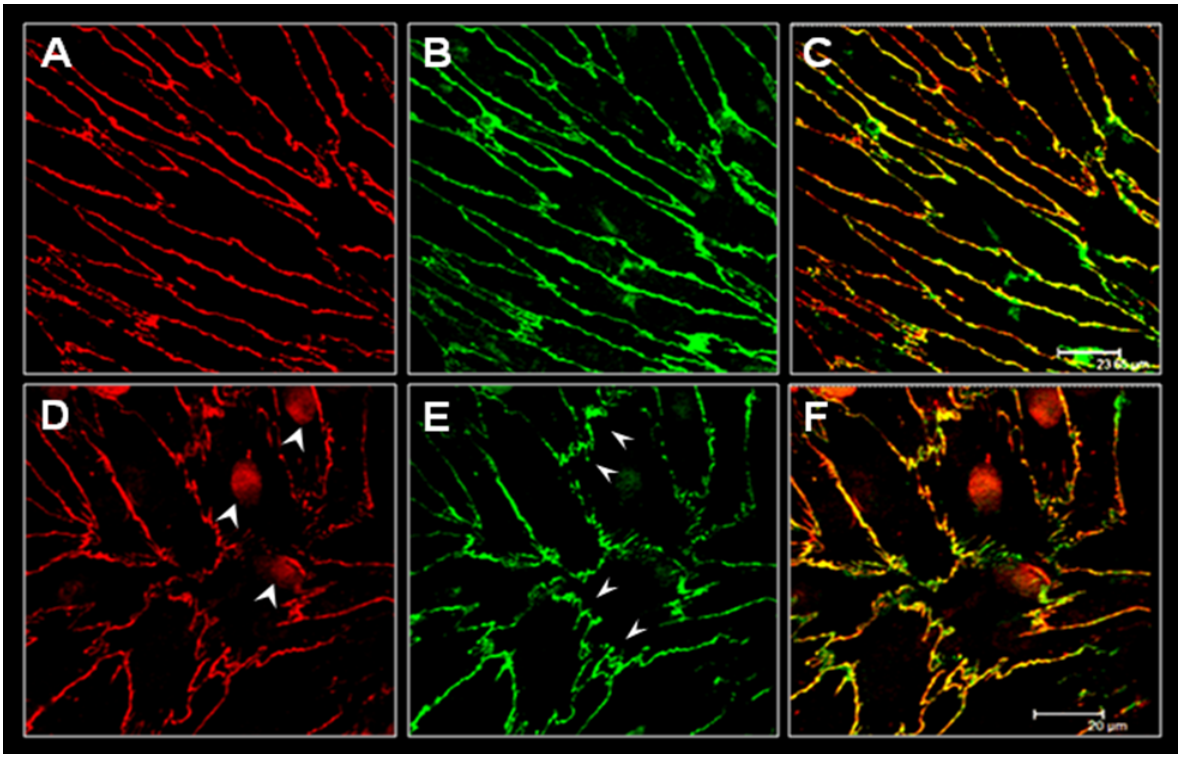

Figure 53: **2-ClHDA mediated alterations of the junctional architecture**

For immunofluorescence studies BMVEC were cultured on coverslips to confluence. After incubation for 3 h with vehicle (**A-C**) or with 15 µM 2-ClHDA (**D-F**) immunofluorescence labeling of ZO-1 (**A** and **D**, red) and VE-cadherin (**B** and **E**, green) was performed using polyclonal rabbit anti-human ZO-1 IgG (1:50) and mouse monoclonal anti-human VE-cadherin IgG (1:200) as primary antibodies. As outlined in Material and Methods, immunofluorescence detection of Cy5-labeled anti-rabbit IgG and Cy2-labeled anti-mouse IgG was performed by confocal laser scan microscopy. Sites of frizzy-like structures (small arrows) and nuclear ZO-1 redistribution (large arrows) in response to 2-ClHDA treatment are marked.

CHAPTER 3 PHARMACOLOGICAL INTERVENTION STRATEGIES TO INTERFERE WITH MPO-MEDIATED BARRIER DYSFUNCTION

* submitted manuscript:

Üllen, A; Fauler, H; Nusshold, C; Bernhart, E; Reicher, H; Holzer, P; Leis, HJ; Malle, E; Sattler, W. **Phloretin ameliorates 2-chlorohexadecanal - mediated brain microvascular endothelial cell dysfunction *in vitro***

Rationale:

BBB breakdown as result of endothelial dysfunction can be considered as a key characteristic of the pathogenesis of inflammatory brain diseases (Grammas et al. 2011). Increasing evidence suggests that neutrophil-endothelial interactions, particularly the generation of ROS and proinflammatory lipids, are critical events in microvessel damage and hyperpermeability (DiStasi and Ley 2009, He 2010). Thus, increasing interest is directed to the discovery and development of natural products or small molecule-based inhibitors to attenuate adverse effects mediated by inflammatory oxidative enzymes like NADPH oxidase or MPO (Choi D. K. et al. 2010) .

Aims:

Since the second part of this thesis revealed that peripheral inflammation induces neutrophil recruitment and activation at the cerebrovasculature it was hypothesized that MPO-derived chlorinative damage of cerebrovascular endothelial cells - directly via HOCl or indirectly via 2-ClHDA generation - potentially aggravates BBB dysfunction and neurodegeneration. By identification of several new promising targets it appeared indispensible to discover and explore pharmacological intervention strategies that interfere with inflammation-dependent BBB dysfunction.

i. Thus, the first aim of the third part of this thesis was directed to the investigation of inhibitors that reverse 2-ClHDA-mediated activation of signaling cascades involved in barrier dysfunction and of apoptotic cell death of BMVEC.

ii. The second aim was to elucidate the role of neuroprotective flavonoids and non-flavonoid polyphenols during chlorinative and α-chloro carbonyl stress in the CNS, and to particularly characterize their ability to ameliorate barrier dysfunction of BMVEC.

1. Inhibition of *De Novo* Sphingolipid Synthesis

Within this study 2-ClHDA was already shown to be redirected into the inert storage pool of complex lipids via formation and activation of the chlorinated fatty acid, thus it is likely that 2-chloropalmitoyl-CoA also enters *de novo* sphingolipids biosynthesis through formation of 4-chloro-3-keto-sphinganine catalyzed by serine-palmitoyltransferase (SPTLC) (***Figure 54 A***). Since palmitate-induced apoptosis was reported to correlate with *de novo* synthesis of ceramides one can speculate about formation and involvement of these highly potent apoptosis inducers in 2-ClHDA-mediated BMVEC dysfunction (Hannun 1996, Paumen et al. 1997).

To test whether the ceramide pathway contributes to 2-ClHDA-induced apoptosis the effects of myriocin (a potent inhibitor of SPTLC) on cell viability were investigated. Findings obtained using the MTT-test data revealed that the inhibition of ceramide synthesis partially restored cell viability by approx. 10 to 25% (***B***).

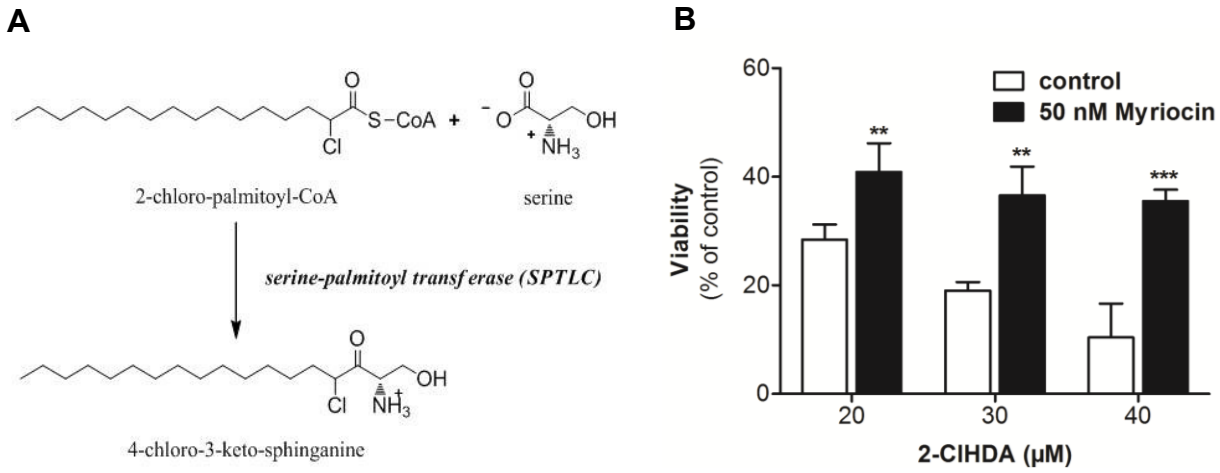

Figure 54: **SPTLC inhibition partially attenuates 2-ClHDA-mediated impact on cell viability**
(**A**) Proposed mechanism of 2-ClHA entry into *de novo* biosynthesis of ceramides via SPTLC catalysis. **(B)** Impact of SPTLC inhibition on 2-ClHDA mediated cytotoxicity. Following pretreatment for 30 min with 50 nM myriocin BMVEC were challenged for 5 h with 2-ClHDA at indicated concentrations. Following treatment cell viability was analyzed by the MTT test. Results are expressed as % of controls and represent mean values ± SD of quadruplicate determinations (** $p<0.01$; *** $p<0.001$, two-way ANOVA).

2. Inhibition of MAPK Signaling

Based on the observation that the rapid process of 2-ClHDA-mediated barrier dysfunction is accompanied by rapid activation of ERK1/2 subgroup the next trial to intervene pursued the inhibition of this signaling cascade.

Therefore, as outlined in Material and Methods, BMVEC were challenged with 5 µM 2-ClHDA while ERK1/2 signaling pathway was selectively blocked by co-treatment of BMVEC with the MAPKK-inhibitor PD098059. Impedance at 4000 Hz was monitored in real-time to measure barrier function (***Figure 55***). ECIS data revealed rapid barrier dysfunction in response to 2-ClHDA. In contrast, a co-treatment of cells with PD098059 resulted in a transient increase in barrier function (***A*** and ***B***). Barrier integrity remained significantly elevated during an incubation period of approx. 60-70 min while at longer incubation periods impedance values dropped to levels observed with 2-ClHDA. These data are consistent with the time course of MAPK activation (stress response after 60 min post 2-ClHDA addition, *Figure 52*) identifying the ERK1/2 signaling pathway as a potential, and early contributor to 2-ClHDA-induced barrier dysfunction.

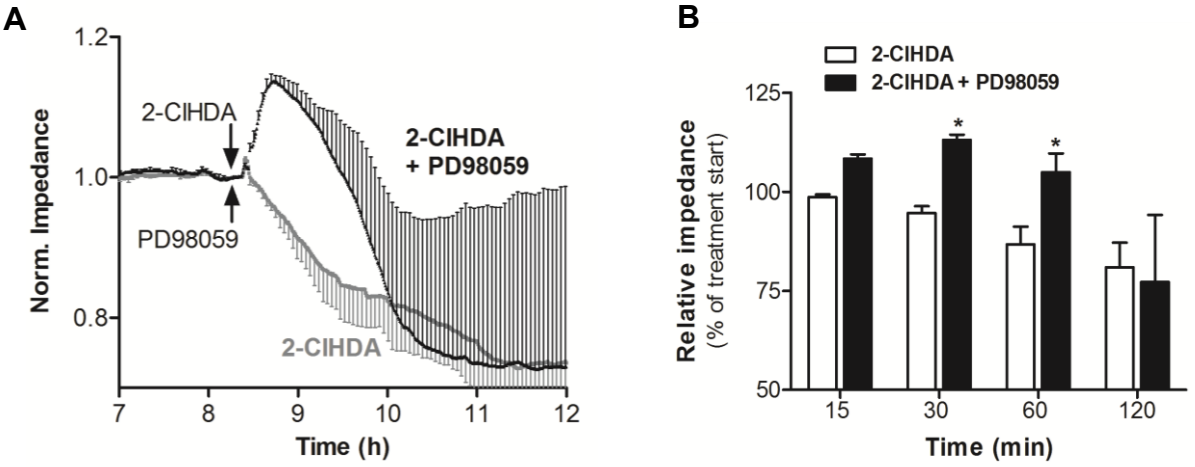

Figure 55: **Inhibition of ERK1/2 signaling causes transient rescue of barrier dysfunction**

(**A**) BMVEC were plated on gold microelectrodes and cultured to confluence. Barrier function of HC-induced endothelial monolayers were continuously monitored by impedance sensing at 4 kHz. After stabilization, cells were challenged (arrow) with 5 µM 2-ClHDA in absence or presence of 100 µM PD98059. (**B**) Relative barrier function at the indicated time points post treatment with 2-ClHDA in the absence or presence of PD98059. Impedance was normalized to treatment start and represent mean values ± SD of three independent experiments (* $p<0.05$; two-way ANOVA).

3. Dietary Benefits of Polyphenols to BMVEC Dysfunction?

Increasing evidence suggests that flavonoid and non-flavonoid polyphenols - ubiquitously present in fruits, vegetables and spices - have beneficial effects in a variety neurodegenerative disorders including BBB dysfunction (Darvesh et al. 2010, Theoharides 2009, Zhang F. et al. 2010a, Zhang S. et al. 2010b). Therefore, subsequent *in vitro* experiments were performed to investigate the potential of these compound classes to rescue MPO-mediated (particularly induced by α-ClFALDs and HOCl) BBB dysfunction.

3.1. *Screening for Viability-Promoting Polyphenols*

Effects of representative compounds of 6 different polyphenol classes - apigenin (a flavone), curcumin (a diarylheptanoid), genistein (an isoflavone), naringenin (a flavanone), phloretin (a dihydrochalcone), and resveratrol (a stilbenoid) (***Figure 56***) - were investigated on BMVEC viability.

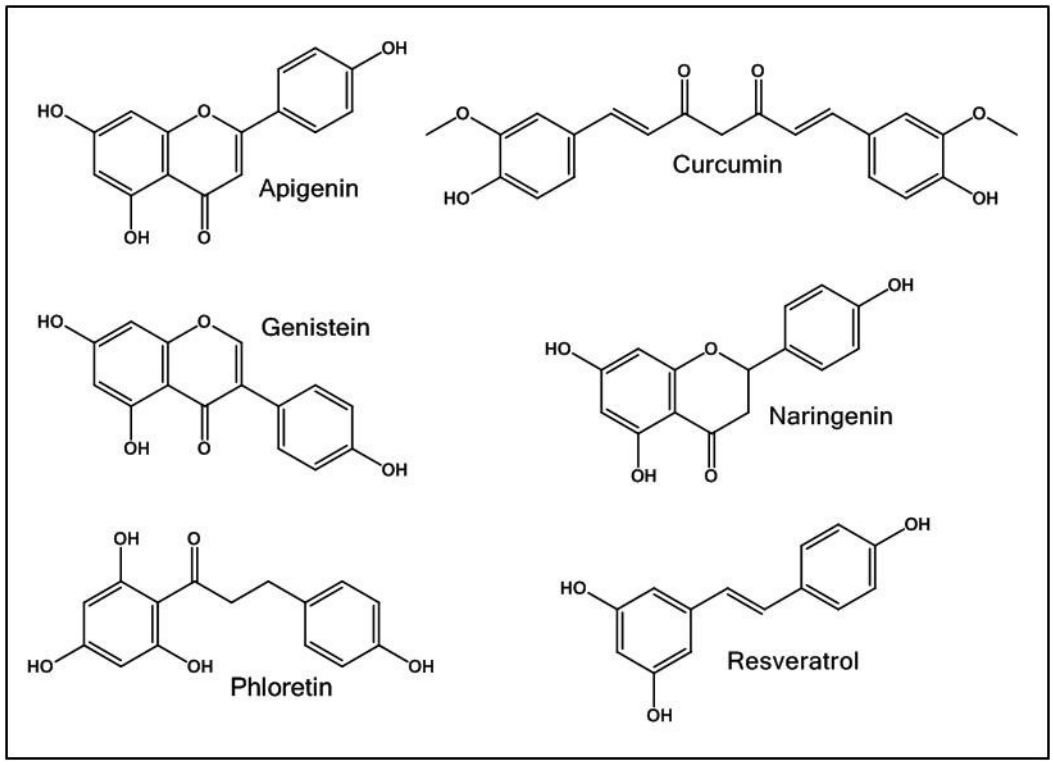

***Figure 56*:** Structures of polyphenols used during the present study

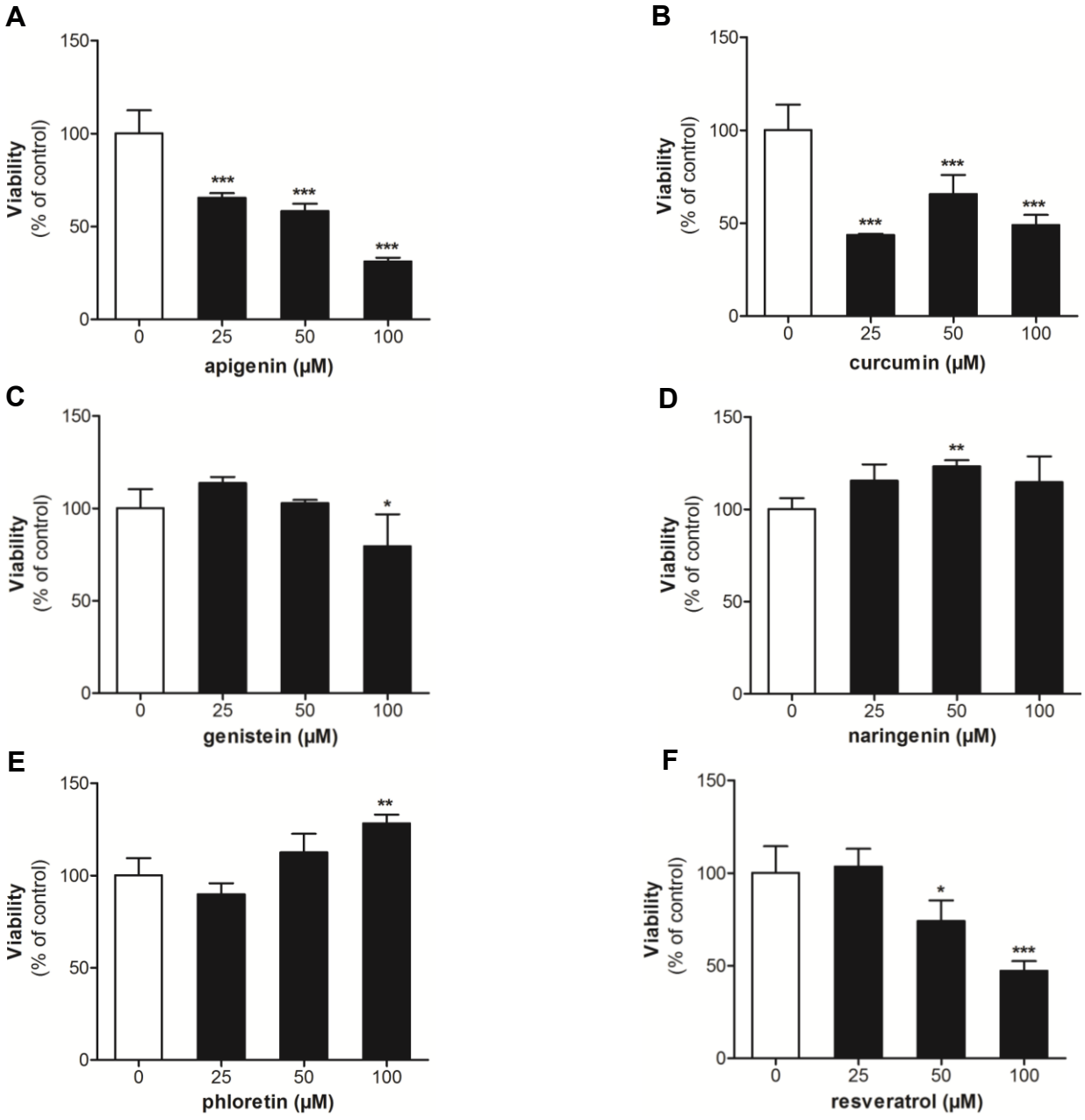

Figure 57: **Effects of different polyphenols on BMVEC viability**

BMVEC were incubated in the presence of (**A**) apigenin, (**B**) curcumin, (**C**) genistein, (**D**), naringenin, (**E**) phloretin, and (**F**) resveratrol at the indicated concentrations (over night). Cell viability was assessed by the MTT test. Results are expressed as % viability of vehicle-treated (DMSO; 0.4%, v/v) cells and represent mean values ± SD of quadruplicate determinations (* $p<0.05$, ** $p<0.01$; *** $p<0.001$; one-way ANOVA).

Effects of flavonoid and non-flavonoid polyphenols on BMVEC viability are shown in ***Figure 57***. Three out of six, apigenin (**A**), curcumin (**B**), and resveratrol (**F**) decreased BMVEC viability. The remaining compounds, i.e. genistein (**C**), naringenin (**D**), and phloretin (**E**) had either no (except genistein at 100 µM) or a beneficial effect on cell viability.

To get an idea about the potential to ameliorate 2-ClHDA-induced cytotoxicity the latter three compounds were investigated in more detail. Under the conditions applied (25 µM 2-ClHDA, 16 h) genistein (up to 100 µM) had no significant effect on BMVEC survival. Naringenin slightly and significantly enhanced cell viability, while phloretin provided significant and quantitatively the most pronounced protection against 2-ClHDA-induced cell death (***Figure 58 A***). Most importantly, phloretin provides protection against 2-ClHDA-induced BMVEC death also at lower concentrations (25 and 50 µM; **B**).

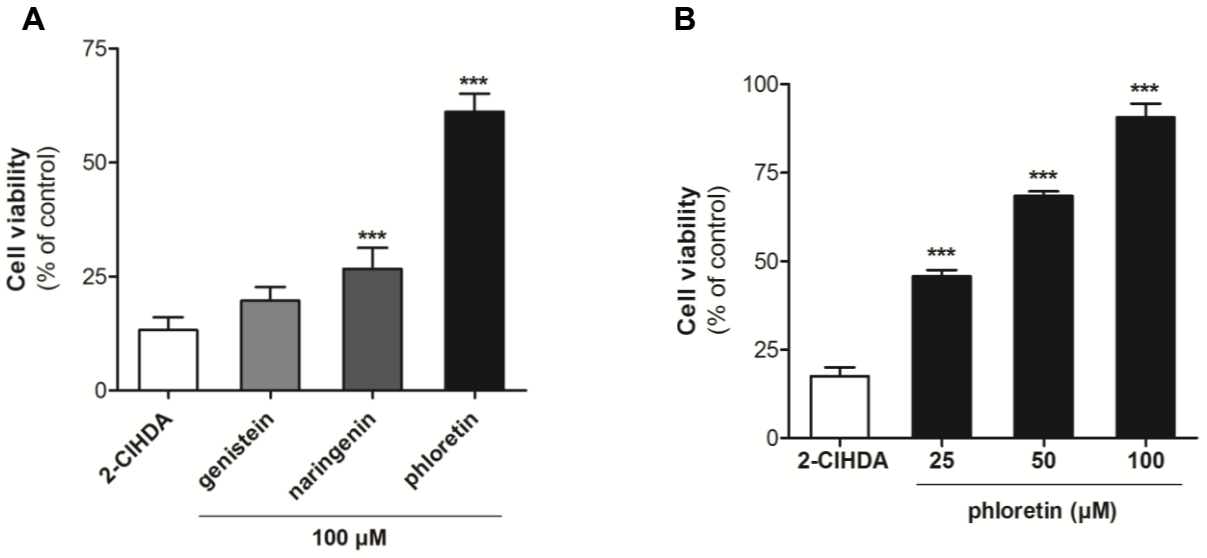

Figure 58: **Impact of selected polyphenols on 2-ClHDA-induced cell death in BMVEC**

(**A**) After pretreatment with genistein, naringenin, or phloretin for 30 min cells were incubated with 25 µM 2-ClHDA for 16 h. (**B**) After pretreatment for 30 min cells with phloretin at indicated concentrations cells were exposed to 25 µM 2-ClHDA for 5 h. Cell viability was determined with the MTT assay. Results are expressed as % of controls and represent mean values ± SD of quadruplicate determinations (** $p<0.01$; *** $p<0.001$; one-way ANOVA).

3.2. *Phloridzin: Structural Homolog of Phloretin*

Phloretin is naturally occurring in apples as glucoside conjugate e.g. phloretin-2'-*O*-glucoside, also named phloridzin. After dietary ingestion the glucose moiety of phloridzin is rapidly hydrolyzed by the enzyme lactase phloridzin hydrolase (***Figure 59 A***). The corresponding aglycone phloretin rapidly enters the circulation by selective uptake by the intestine (Boyer and Liu 2004, Crespy et al. 2001b, Ehrenkranz et al. 2005, Kahle et al. 2005).

To get insights into the structural requirements for cell protection against 2-ClHDA the efficacy of phloretin was compared with its dietary precursor. In contrast to non-glycosylated phloretin, its glycosylated analogue was without effect or even decreased cell viability at higher concentrations (**B**). These findings suggest that the hydroxyl group at C2 of phloretin is likely involved in BMVEC protection.

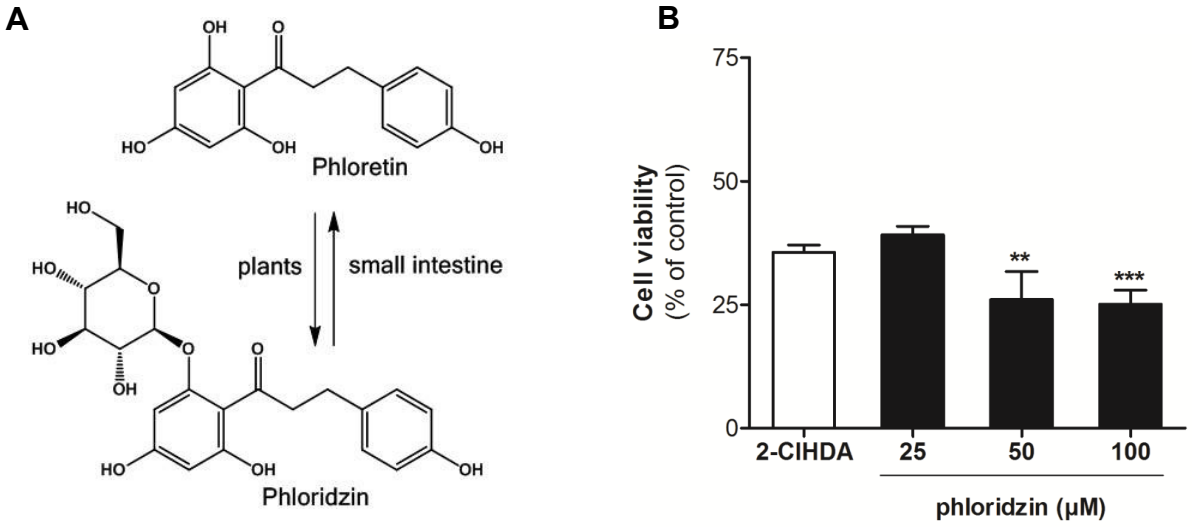

Figure 59: **Glycosylation of the hydroxyl group at C2 abrogates protection**

(**A**) Phloridzin, the natural glycoside of phloretin in plants, is hydrolyzed to corresponding aglycone after ingestion. (**B**) After pretreatment of cells for 30 min with phloridzin at indicated concentrations cells were exposed to 25 µM 2-ClHDA for 5 h. Cell viability was determined with the MTT assay. Results are expressed as % of controls and represent mean values ± SD of quadruplicate determinations (** $p<0.01$; *** $p<0.001$; one-way ANOVA).

3.3. *Phloretin Restores Barrier Integrity of 2-ClHDA-treated BMVEC*

Next, the effects of phloretin on 2-ClHDA-mediated barrier dysfunction were investigated. In these experiments BMVEC were pre-treated with phloretin prior to a challenge with 2-ClHDA. Impedances measuring barrier function (4 kHz) and integrity of the cell monolayer (64 kHz) were continuously monitored using the ECIS system.

ECIS experiments revealed that barrier dysfunction was rapidly induced in response to 2-ClHDA (***Figure 60 A***; the 30 h time point is shown in ***B***). Disruption of the cell monolayer lagged by approx. 2 to 2.5 h behind (***C***; 30 h time point is shown in Fig. ***D***). 2-ClHDA-induced barrier dysfunction was significantly attenuated by phloretin (barrier integrity remained constant during 15 h at approx. 50% of the starting impedance, ***A***) whereas integrity of the cell monolayer was almost completely conserved during the time periods investigated (***C***). These data clearly indicate dual effects - signaling events and cytotoxicity - of 2-ClHDA on barrier function and the capability of phloretin to maintain the integrity of the cell monolayer but not to restore barrier function completely.

3.4. *Phloretin Ameliorates HOCl-Induced Cytotoxicity*

Flavonoids are best known for their antioxidant activity because their redox potential is comparable to that of ascorbate or α-tocopherol (Galleano et al. 2010). Polyphenols are able to prevent HOCl-dependent damage to the vasculature most likely by acting as HOCl- scavengers (Boersma et al. 2001, Firuzi et al. 2004).

Due to altered properties of chlorinated flavonoids (Binsack et al. 2001) and the lack of information about HOCl-scavenging properties of chalcones the next set of experiments aimed at investigating antioxidant properties and potential viability benefits towards HOCl-challenged BMVEC. Cell viability data revealed that even 25 µM phloretin were sufficient to reverse adverse effects of 5- to 10-fold molar excess of NaOCl (***Figure 61***). Even at NaOCl concentrations of 500 µM the presence of phloretin (50 µM) resulted in a significant rescue of BMVEC viability.

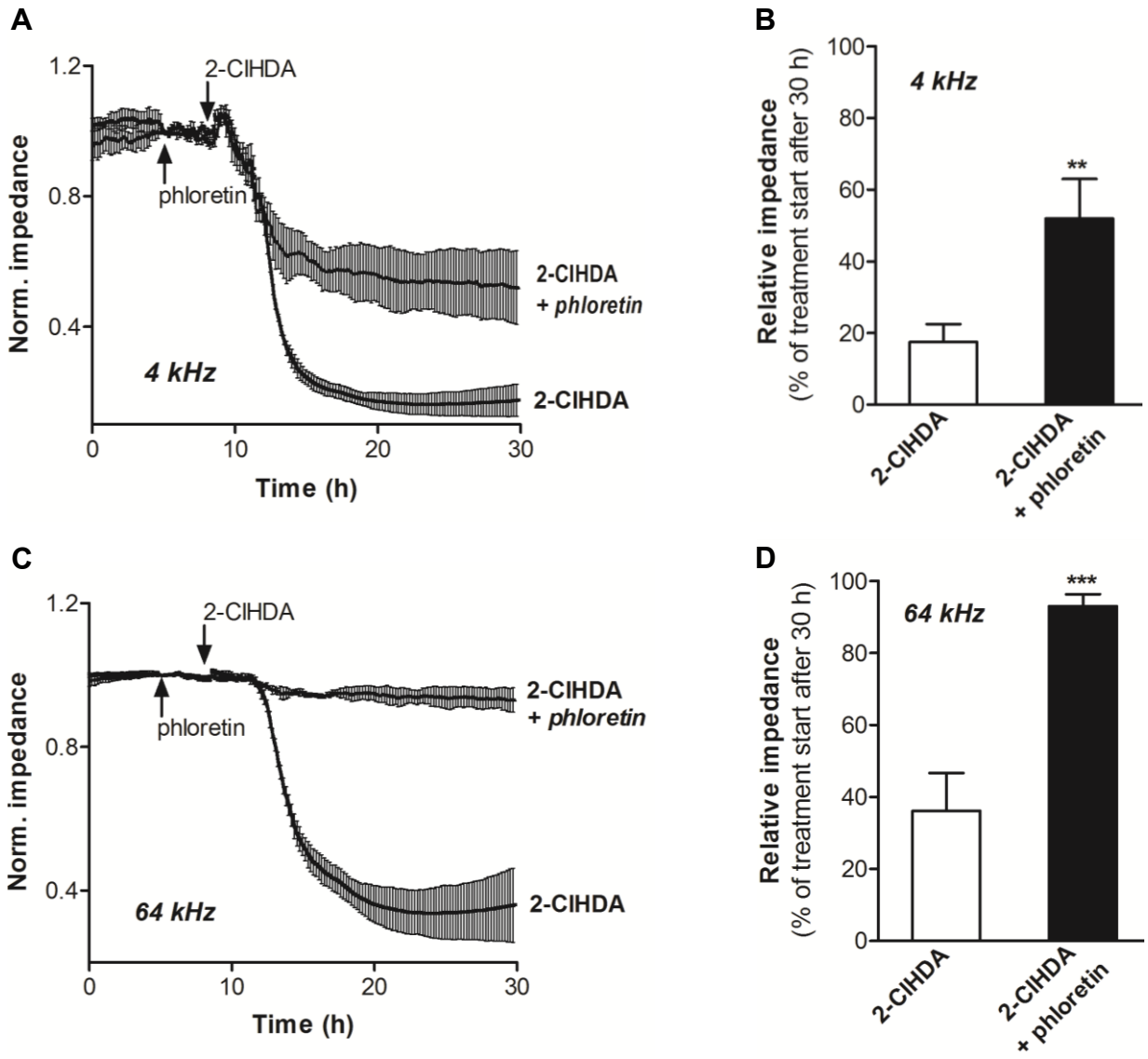

Figure 60: **Phloretin rescues barrier function of 2-ClHDA-treated BMVEC**

Cells were plated on gold microelectrodes and cultured to confluence. Impedance of HC-induced monolayers (7.5×10^4 cells) was continuously monitored at (**A**) 4 kHz and (**C**) 64 kHz. The 30 h time point is shown in (**B**) and (**D**). After stabilization, cells were pretreated with 100 µM phloretin or vehicle for 3 h and then challenged with 25 µM 2-ClHDA. Impedances were normalized to treatment start (addition of phloretin) and represent mean values ± SD of four independent experiments. (** $p<0.01$; *** $p<0.001$; Students t-test)

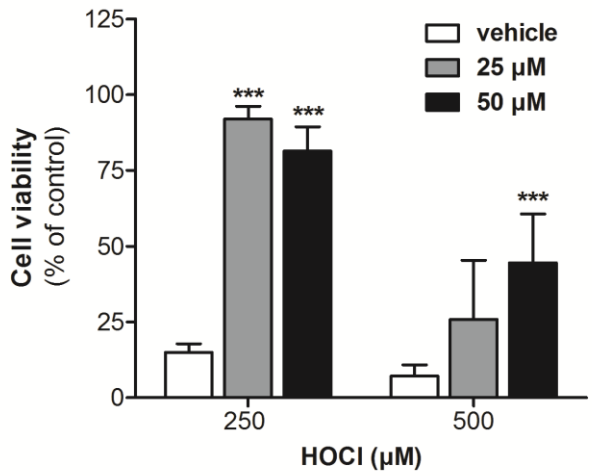

Figure 61: **Phloretin attenuates HOCl-mediated cytotoxicity to BMVEC**

BMVEC were pretreated with phloretin at indicated concentrations in HBSS for 30 min followed by an overnight challenge with NaOCl at indicated concentrations (in HBSS). Cell viability was determined by the MTT test. Results are expressed as % viability of vehicle-treated (containing DMSO at the highest concentration used; 0.4%, v/v) controls and represent mean values ± SD of quadruplicate determinations (*** $p<0.001$; two-way ANOVA).

3.5. *Phloretin Reduces Cellular 2-ClHDA Content*

Phloretin is known to act as an unspecific inhibitor of fatty acid uptake (Luiken et al. 1997, Mitchell R. W. et al. 2009). To get deeper insight into the mechanisms of viability-promoting effects of phloretin the impact of this compound on cellular import of 2-ClHDA was investigated.

During these experiments BMVEC were pretreated with phloretin and then challenged with 2-ClHDA. Subsequently, cellular 2-ClHDA levels and corresponding levels in culture medium were quantified by NICI-GC-MS analysis over a given time period. Phloretin pretreatment decreased the amount of cell-associated 2-ClHDA by approx. 70 % at all time points investigated (***Figure 62 A***); these data suggest an inhibition of 2-ClHDA uptake by phloretin. Surprisingly, NICI-GC-MS data further revealed that 2-ClHDA levels in the cellular supernatant, supplemented with phloretin, were significantly lower compared to controls; again, this effect was time-dependent (***B***).

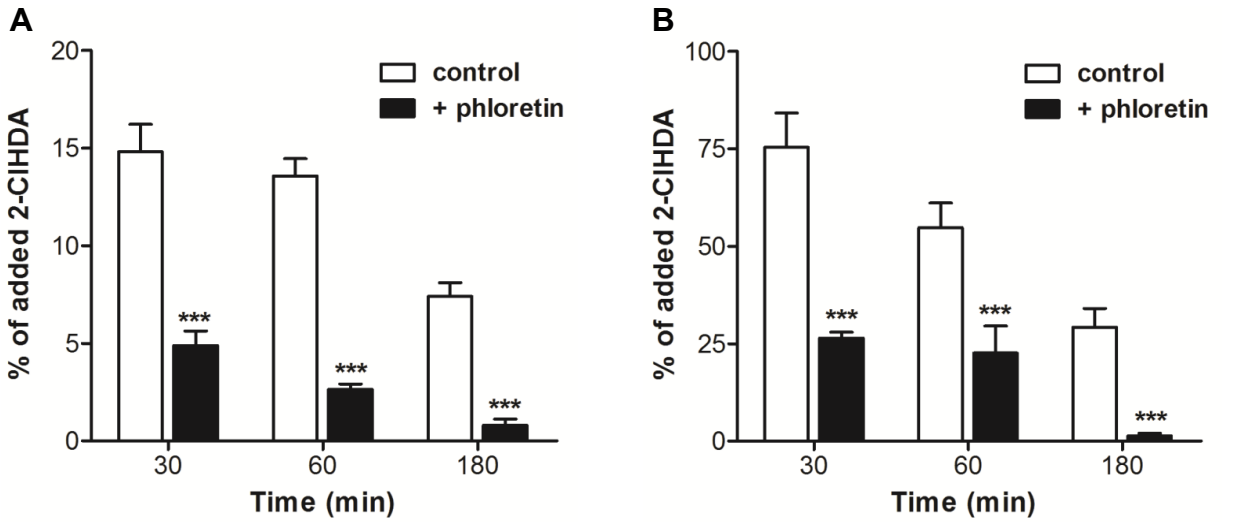

Figure 62: **Phloretin reduces extra- and intracellular 2-ClHDA levels in BMVEC cultures**
Following pretreatment with phloretin (100 µM, 1 h), cells (9×10^5) were incubated with 25 µM 2-ClHDA. At the indicated time points, cellular lipids and lipids of the cellular supernatant were extracted. After conversion to corresponding PFB-oxime derivatives 2-ClHDA concentrations in (**A**) cellular, and (**B**) culture medium lipid extracts were quantitated by NICI-GC-MS analysis. Results are expressed as % of added 2-ClHDA and represent mean values ± SD of triplicate determinations. (*** $p<0.001$; two-way ANOVA)

3.6. *α-ClFALDs are Covalently Trapped by Phloretin*

Whether reduced levels of 2-ClHDA could be attributed to covalent adduct formation of 2-ClHDA and phloretin a cooperative approach was initiated with O. Kappe (KFU Graz), T. N. Glasnov (KFU Graz) and R. Saf (TU Graz). Therefore, the model compound for 2-ClHDA, 2-chloroheptanal (2-ClHpA) was chemically synthesized and incubated with phloretin in serum-free medium. After extraction free 2-ClHpA was removed and the remaining reaction mixture was analyzed by electron impact-high resolution mass spectrometry (EI-HRMS).

Under analytic conditions used in this study the molecular ions (M^+) of the investigated compound was identified at m/z 386/387 (***Figure 63***). The isotope distribution of the analyte indicated a loss of chlorine during covalent adduct formation. Moreover, additional fragment ions detected at m/z 84, m/z 107, m/z 120, m/z 210, m/z 238, m/z 265, and m/z 386 provided a more detailed structural information about the newly formed compound (insets). These experiments likely indicated a bimolecular nucleophilic substitution (S_N2) reaction between the carbon 2 of 2-ClHpA and a hydroxyl group of the phloroglucinol ring, a trapping mechanism where HCl is abstracted.

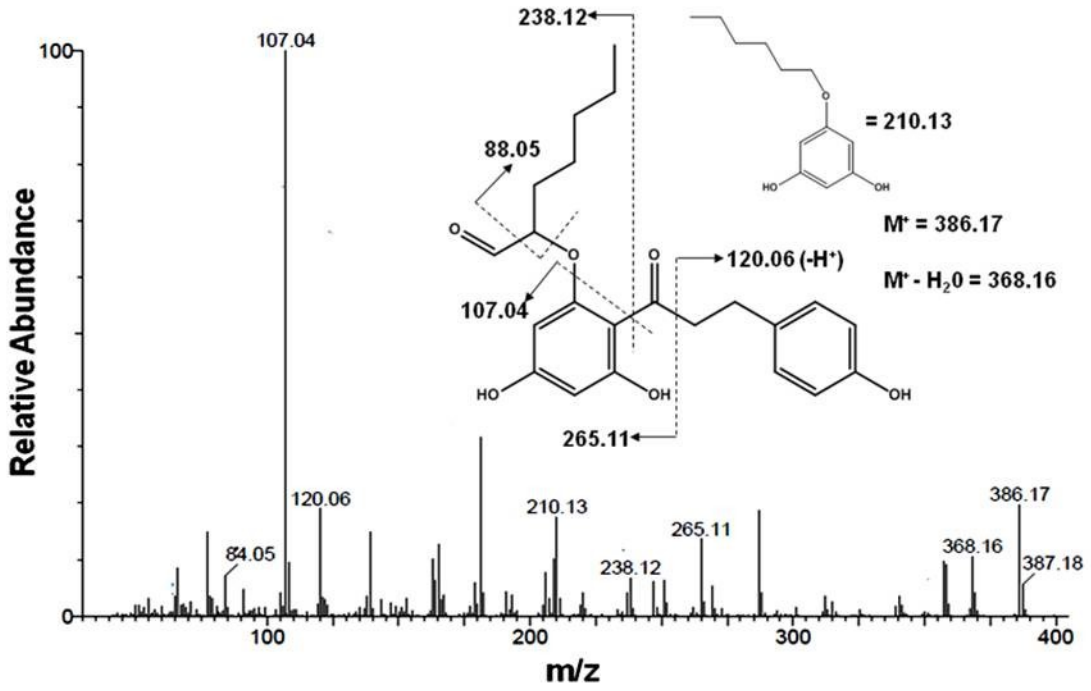

Figure 63: **EI-HRMS spectrum of covalent 2-ClHpA trapping by phloretin**

To analyze a candidate adduct formation phloretin was incubated with a 2.5-fold molar excess of 2-ClHpA in medium B. After extraction, unbound 2-ClHpA was removed by automated flash chromatography and the sample was analyzed by EI-HRMS through direct insertion. Proposed fragmentation pattern and mass assignment is shown in the inset.

3.7. *Phloretin is a Scavenger for HOCl*

Due to beneficial effects of phloretin on BMVEC viability the next series of experiments aimed at investigating the HOCl scavenging properties of phloretin. During these experiments phloretin was modified with a 2-fold molar excess of reagent HOCl followed by modification analysis of the corresponding TMS-derivative by EI-GC-MS. Results are shown in ***Figure 64***.

In addition to unreacted phloretin (m/z 562) eluting at 10.68 min we could identify two additional peaks at 10.92 min and 11.03 min with m/z 596 and m/z 630 (***A*** and ***C***). The intensity ratios of the molecular ions and fragment ions of approx. 3:1 (peak at 10.92 min) and approx. 9:6:1 (peak at 11.03 min) were indicative for the presence of two chlorine isotopes ($^{35}Cl/^{37}Cl$) corresponding to mono- and dichlorinated derivatives of phloretin (***B***). Moreover, the observed fragmentation pattern provided information that carbon 2 and 5 of phloroglucinol group are targets for HOCl-dependent phloretin chlorination (**C**).

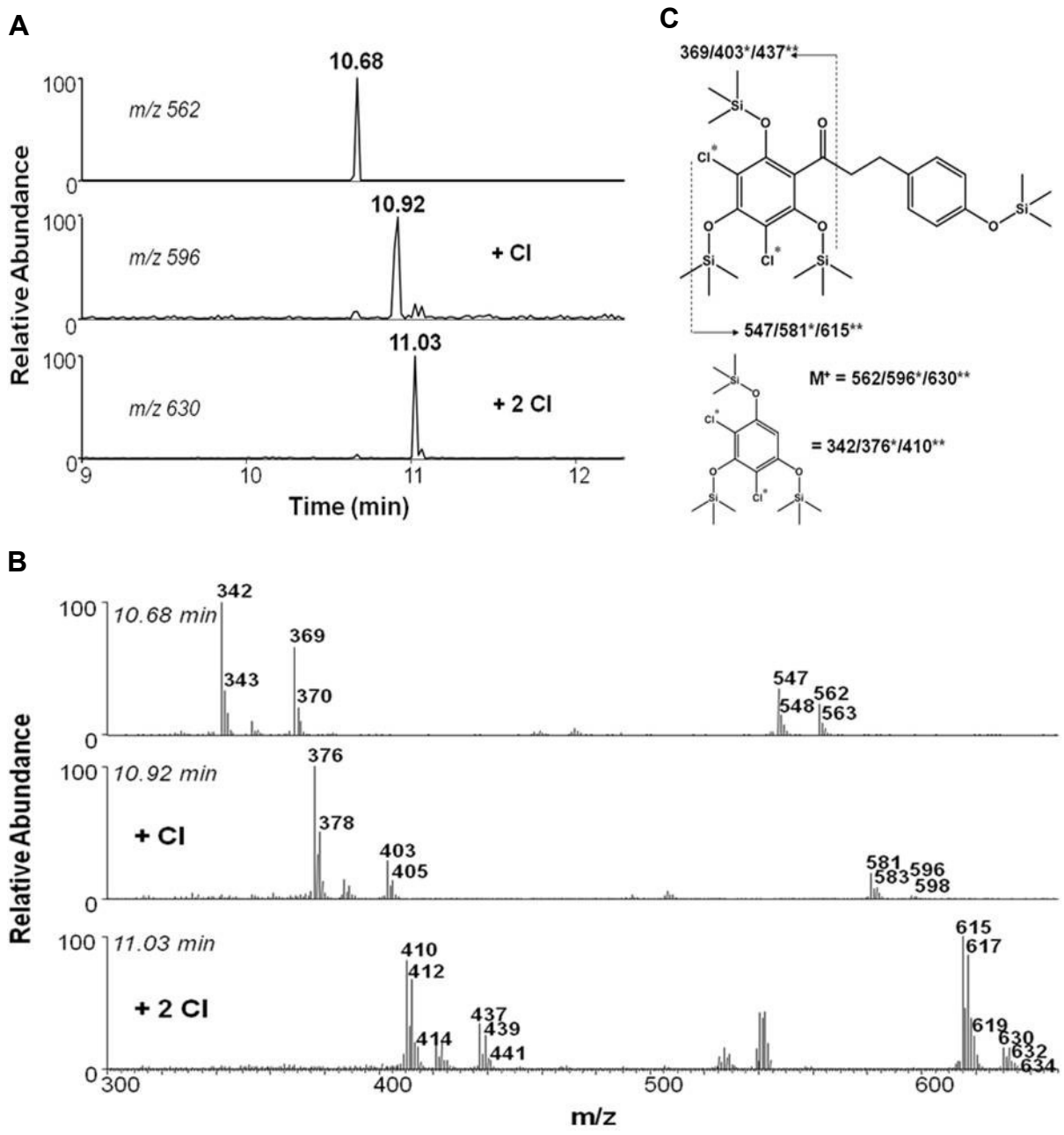

Figure 64: **EI-GC-MS analysis of HOCl-modified phloretin**

Phloretin was modified in PBS with 2-fold excess of reagent HOCl for 1 h. After extraction, phloretin was converted to the corresponding TMS-derivative and analyzed (1 nmol injected) by EI-GC-MS. (**A**) Single ion traces of native phloretin (upper panel), monochlorinated phloretin (middle panel) and dichlorinated phloretin (lower panel). (**B**) EI mass spectra of compounds eluting at 10.68 min (native phloretin, upper panel), 10.92 min (monochlorinated phloretin, middle panel) and at 11.03 min (dichchlorinated phloretin, lower panel). (**C**) Proposed fragmentation pattern and mass assignment of native, mono- and dichlorinated phloretin (stars indicate the presence of chorine residues at carbons 2 or 4).

VII. DISCUSSION

1. General Aspects and Rationale of this Project

It is estimated that neurological disorders including neuropsychiatric disorders and disorders/injuries with neurological sequelae will contribute to 13% of European and 6% of global burden of disease until 2015. Thus, humans suffering from neurological disorders spend more years worldwide living with a disability (total disability-adjusted life years, DALYs) compared to other diseases like HIV, malignant neoplasms, ischemic heart disease, or even respiratory diseases. About 4% of total DALYs are attributable to the most frequently occurring neurodegenerative diseases (AD, PD and MS) in the European population (Aarli et al. 2006). The most prevalent of these disorders, AD and other dementias, affected an estimated 35.6 million people world-wide in 2010 and the number of patiens will double every 20 years (Ballard et al. 2011, Ferri et al. 2005, Prince and Jackson 2009). AD is getting characteristics of an epidemic that increases its pace with increasing life-expectancy of the population (***Figure 65***). In 2005, the costs for demented patients were in the range of €130 billions in the European Union. Since the increase in AD evidently affects also low and middle income countries we are facing a global socio-economic dilemma. Therefore, effective research strategies optimizing pharmacological and psychological treatments are urgently needed (Forman et al. 2004, WHO 2002).

Although the pharmaceutical industry is aggressively marketing currently approved drugs for the treatment of neurodegenerative disorders, these medications are mostly limited to a transient symptomatic benefit, without slowing or stopping disease progression. A major problem in developing new and efficient therapeutics relates to our incomplete understanding of disease etiology and pathogenesis as well as an inadequate understanding of the complexity of neurodegenerative disorders. Given this complexity, a major obstacle in the investigation of new therapeutic targets is most likely the finding of potential effectors in pathogenic pathways as well as the discovery of corresponding inhibitors by target-driven screening approaches (Lang 2010, Lansbury 2004).

While acute neurodegeneration can largely be allocated to distinct events like hypoxia, trauma, infection, or intoxication, the early onset of chronic neurodegenerative diseases is less clear but might include specific combinations of genetic predispositions (e.g. mutations in genes amyloid-precursor protein, APP; apolipoprotein E, APOE, α-synuclein, SNCA; or superoxide dismutase, SOD), enviro-

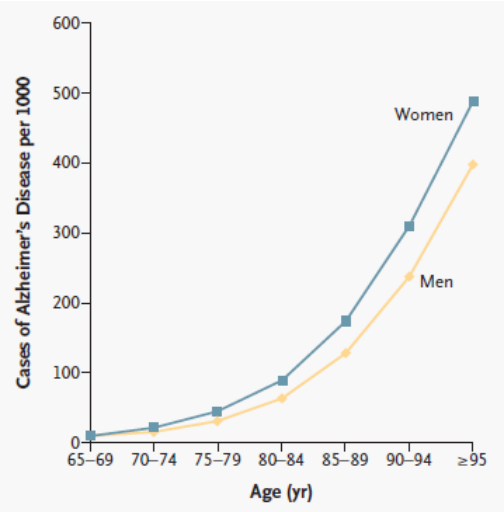

Figure 65: Prevalence of Alzheimer's Disease as a function of Age in Men and Women (Nussbaum and Ellis 2003).

mental stressors (e.g. metals/metalloids, air pollution, or pesticides) and age-related factors (e.g. impaired clearance of Aβ via cerebrovascular ATP-binding cassette transporter C1, ABCC1) (Bertram and Tanzi 2005, Douglas and Dillin 2010, Krohn et al. 2011, Migliore and Coppede 2009).

Despite the heterogeneity of early events in the preclinical period there is an increasing body of evidence showing that activation of innate inflammatory processes as well as inflammation-derived downstream effectors, BBB dysfunction and oxidative/chlorinative/nitrosative stress constantly emerge as central players in advanced neurodegeneration (Herrmann and Obeid 2011). Since neuroinflammation is an accepted inducer for disease amplification and aggravation of the clinical phenotype in patients, BBB dysfunction and oxidative/chlorinative/nitrosative stress represent universal targets to provide more effective treatments to slow down or stop the progression of inflammation-related CNS disorders (Grammas et al. 2011, Iadecola 2010, Mosley et al. 2006, Qian et al. 2010).

Mounting evidence points towards the possibility that aberrant MPO expression and RCS formation might represent pivotal effectors initiating/amplifying the vicious circle of neurodegeneration. Accordingly, MPO activation must be considered as an important pharmaceutical target to ameliorate the pathogenesis of neurodegeneration (Maki et al. 2009, Malle et al. 2007, Yap et al. 2007).

Another obvious challenge in clinical neuroscience is the specific identification of markers that accurately track the progression of the underlying disease and that serve as surrogate endpoints replacing traditional clinical endpoints (Lansbury 2004, Stanzione and Tropepi 2011). Although changes in the lipid profile of nervous tissues were reported for several neuropathological conditions including ischemia (Viani et al. 1995), AD (Ginsberg et al. 1995, Han X. et al. 2001), Down syndrome (Murphy E. J. et al. 2000), and GD (Moraitou et al. 2008) the triggers for these disorders remain still unclear. Moreover, there is accumulating evidence that lipid levels, particularly those of plasmalogens and cholesterol, correlate with the decline in cognitive function of patients suffering from dementia. Although statins (HMG-CoA reductase inhibitors) provided originally promising results and were thought to reduce the risk of developing AD, prospective studies and clinical trials resulted in inconsistent data (Di Paolo and Kim 2011, Presecki et al. 2011). However, the potential of plasmalogen metabolism as novel therapeutical targets as well as disease progression- and therapy response markers is currently under investigation (Farooqui et al. 2006, Wood et al. 2010). This lack of data might reflect an inadequate understanding of the complex network of glycerophospholipids and glycerophospholipid-derived lipid mediators involved in neurodegenerative processes (Frisardi et al. 2011).

Generally, for providing new effective therapeutical developments it seems to be crucial to get a more profound understanding of the complex mechanistic nature of neurodegenerative diseases. Along this line, this thesis project was driven by the hypothesis that activation of the innate immune system (an event clearly linked to neurodegeneration (Bajramovic 2011)) could give rise to altered brain plasmalogen turnover, thereby providing new biomarkers and potential effectors in the vicious cycle of neurodegeneration.

2. Plasmalogen Loss: A Profound Biomarker for Neuroinflammation?

Quantitative analysis of the phospholipidome using very high resolution mass spectrometry revealed high quantities of ether-phospholipids in brain tissue. Plasmalogens were shown to contribute between 50 and 80% of total PE in gray and white matter, respectively (Han X. et al. 2001). This is consistent with findings of the present study where PE and pPE were present in almost equimolar amounts while the pPC content in mouse brain was minute and below 0.5 mol%. With regard to subspecies composition pPE are mostly unsaturated with saturated species contributing ≈ 2%. This observation is in agreement with previous findings (Han X. et al. 2001, Taguchi and Ishikawa , Yang K. et al. 2007a) and is most likely a reflection of pPE function: species with a low degree of unsaturation are present in

white matter myelin providing support for axonal membrane integrity (Han X. L. and Gross 1990). The highly unsaturated species are mainly found in synaptic vesicles (over 60 mol%) of gray matter where they may promote membrane fusion. Due to axonal dysfunction as well as altered synaptic structure and function plasmalogen deficiency might impact on signal transmission and may link neurodegeneration to dysfunction of the cholinergic system (Furey 2011, Leskovjan et al. 2010).

Specific alterations in plasmalogen levels have been detected in the earliest stage of clinically recognizable AD but appear to be generally related to neurodegeneration (Glaser and Gross 1995, Han X. 2005). However, plasmalogen homeostasis during systemically induced neuroinflammation remains still elusive. To investigate this aspect an *in vivo* mouse model for neuroinflammation using a single systemic LPS injection was used. This treatment regimen causes progressive loss of neurons in the substantia nigra in male mice (Liu et al. 2008). Under normal conditions peripheral LPS passage across the BBB is low (Banks and Robinson 2010). However, LPS treatment induces TNFα-receptor-dependent signal transduction to the brain where TNFα synthesis is further amplified (Qin L. et al. 2007). This event creates a milieu of persistent and self-propelling neuroinflammation, a scenario where bioactive lipids (e.g. lysoPLs or PGs formed via COX2) take a central regulatory role (Farooqui et al. 2007).

By the means of our mouse model we could unambiguously demonstrate that the inflammatory response to LPS induced a progressive loss of about 20% of cerebral plasmalogens within the analyzed time period. Compared to human data generated by Han and coworkers, showing an association between plasmalogen deficiency and the severity of AD (-10 mol% at very mild dementia and -30 mol% at severe dementia), our data lead to the hypothesis of a transient impact on CNS function after LPS treatment (Han X. et al. 2001). This hypothesis is in line with recently published data by Painsipp and coworkers providing evidence of prolonged depression-like behavior in mice caused by a systemic LPS challenge. This aspect is further supported by the findings that dementia, aging and mood disorders are associated with dysfunction of the cholinergic system (Furey 2011, Painsipp et al. 2011).

In general, our data support the assumption that plasmalogen loss could represent a biomarker that accurately tracks neuroinflammation. Furthermore, due to their short half-life and indications of level retrieval after disease treatment, plasmalogens (0.5 h for PC and 3 h for PE) might also act as a response marker of desired therapeutic effect (Moraitou et al. 2008, Wallner and Schmitz 2011).

3. The Role of Chlorinative Stress in Plasmalogen Deficiency

Higher tissue plasmalogen levels in long-lived compared to short-lived rodents have been suggested to confer a lower susceptibility to oxidative stress and to contribute to an extended lifespan (Mitchell T. W. et al. 2007). Indeed, the presence of the vinyl-ether linkage and the high degree of unsaturation make plasmalogens extremely susceptible to oxidative damage. Therefore, oxidative stress as observed in aging and virtually all diseases with an inflammatory component might be a key event in eliciting plasmalogen deficits, however, the extent of oxidative degradation have remained controversial (Barnham et al. 2004, Lessig and Fuchs 2009, Wallner and Schmitz 2011).

Under physiological conditions MPO-generated oxidants play an important role in killing invading pathogens, thereby contributing to host defense (Klebanoff 2005). However, chronic activation of MPO results in elevated levels of RCS, thus favoring chloramine and α-ClFALD formation, modifications potentially leading to tissue and/or organ injury in the periphery (Grone et al. 2002, Hazell et al. 1996, Thukkani et al. 2005, Thukkani et al. 2003a). Nevertheless, the impact of chlorinative stress on the cerebral plasmalogen pool remained to be elucidated.

A first set of *in vitro* experiments aimed at characterizing HOCl-modification of plasmalogens in the complex matrix of brain lipids. The rate constants for HOCl-dependent plasmalogen modification are approx. 10-fold higher as compared to their non-vinyl ether containing counterparts (Skaff et al. 2008). In line, our *in vitro* data revealed higher sensitivity of brain plasmalogens towards HOCl when compared to diacyl glycerophospholipids. This is most likely a reflection of the *cis* vinyl-ether bond as a preferred HOCl-target and is further in line with previous observations that vinyl-ether cleavage by HOCl is kinetically favored compared to chlorohydrin formation (Lankalapalli et al. 2009, Messner et al. 2006). Moreover, the polar headgroup of pPE is also subject to HOCl or HOBr attack leading to the formation of halamines, which are able to induce oxidation of a plasmalogen model compound albeit chloramines have a much slower oxidation kinetics than the corresponding bromamines (Skaff et al. 2008). In addition protein-derived chloramines are able to initiate secondary plasmalogen modification: The most potent are histidine chloramine analogues (with reaction kinetics only 5-30-fold slower than HOCl) while *N*-acetyl-lysine and taurine chloramines are less effective (approx. 10^5-fold slower than HOCl (Pattison and Davies 2005, Skaff et al. 2008)).

During the present study the decrease of plasmalogen species was accompanied by accumulation of lysoPLs and the corresponding 2-chloroaldehydes derived from the *sn*-1 vinyl-ether group in the

glycerol backbone of pPL. The observed transient accumulation of lysoPLs in response to HOCl-treatment is most likely a result of secondary modification reactions occurring at the remnant lysophospholipid, where chloramine formation at the ethanolamine head group (Richter et al. 2008), chlorohydrin formation in the alkene side chains (Spickett 2007), or *sn*-2 acyl abstraction (Lessig et al. 2007, Panasenko et al. 2003) may be involved.

A second part of this study aimed to corroborate *in vitro* data by the *in vivo* mouse model of neuroinflammation using a single systemic LPS injection. We have observed a biphasic increase of MPO on mRNA level and a transient increase of MPO on protein level. This might be a result of a superimposition of transcriptional regulation and import of mature MPO into the brain, which is comparable to findings reported for a murine stroke model: There, MPO-positive neutrophils were detected at days 1 and 3 while MPO-positive macrophages/microglia were detected at later stages up to three weeks post stroke induction (Breckwoldt et al. 2008). This raises the question about the origin of cerebral MPO: Multiple resident cell types as astrocytes (Choi D. K. et al. 2005), microglia (Reynolds et al. 1999), and neurons (Green et al. 2004) were reported to contain and/or express MPO. Alternatively, MPO could be imported by invading neutrophils or monocytes (Breckwoldt et al. 2008, Ji et al. 2007). Independent of the source of cerebral MPO it was shown that $MPO^{-/-}$ mice are more resistant to MPTP-induced neurotoxicity than their wild-type littermates, a fact reflected by decreased loss of neurons in the substantia nigra of $MPO^{-/-}$ animals (Choi D. K. et al. 2005). On the other hand, astrocyte-specific overexpression of human MPO in a mouse model for AD resulted in cognitive decline, and in the accumulation of the lipid peroxidation product 4-HNE along with the formation of phospholipid- and plasmalogen-derived hydro(pero)xides (Maki et al. 2009).

Since we have detected substantial amounts of 2-ClHDA (2 µg/g wet brain containing approx. 80% water resulting in a concentration of approx. 10 µM) only in endotoxin-injected mice we could substantiate the theory of chlorinative stress during acute neuroinflammation. These 2-ClHDA concentrations are in a comparable range reported for a rat model of myocardial infarction (approx. 1 µM (Thukkani et al. 2005)) and for human atherosclerotic lesion material (approx. 10 µM (Thukkani et al. 2003a)). Other α-ClFALDs (2-ClODA and 2-ClODEA) were not investigated but their formation is likely since loss of plasmalogen species containing C18- or C18:1 alkenyl residues were also observed after LPS treatment. Taken together, these findings provide substantial evidence that MPO-dependent plasmalogen modification is a neuroinflammatory event.

Our *in vitro* and *in vivo* data permit a rough estimation of MPO-mediated events contributing to overall plasmalogen loss: The cerebral concentration of 1-*O*-hexadecenyl plasmalogens is about 4 µmol/g tissue. The plasmalogen loss 96 h post LPS exposure was approx. 20% corresponding to an overall loss of approx. 800 nmol/g tissue of 1-*O*-hexadecenyl-containing plasmalogen species. Maximal concentration of 2-ClHDA was 2 µg/g brain equivalent to 7.3 nmol 2-ClHDA/g tissue. Thus, MPO-dependent 2-ClHDA formation accounts for roughly 1% of total cerebral plasmalogen loss *in vivo*. However, this might be an underestimation: *in vitro* incubation of 2-ClHDA in the presence of a mixed primary brain cell suspension revealed a t/2 of approx. 40 min for 2-ClHDA. This could result from further metabolism of 2-ClHDA by fatty aldehyde dehydrogenase (FALDH) (Anbukumar et al. 2010). FALDH (classified as ALDH3A2; SwissProt P51648) is expressed in brain and when mutated or absent causes severe neurological symptoms (Rizzo and Carney 2005). Alternatively, oxidation of 2-ClHDA to 2-ClHA and subsequent incorporation into the polar lipid fraction could re-direct 2-ClHDA via 2-ClHA into an inert and stable storage pool (Wildsmith et al. 2006a). Finally, Schiff base formation between α-ClFALDs and ethanolamine-containing glycerophospholipids and/or the α-amino group of protein lysine residues (Stadelmann-Ingrand et al. 2004, Wildsmith et al. 2006b) could account for the observed time-dependent decrease in cerebral 2-ClHDA concentrations.

Our data further indicate that MPO-dependent modification reactions contribute to but might not represent the only cause for brain plasmalogen deficiency under neuroinflammatory conditions. This is supported by the fact that glycerol-3-phosphate-*O*-acyltransferase, a key enzyme in plasmalogen biosynthesis is significantly downregulated by TNFα (which was significantly upregulated during the present study) under *in vitro* and *in vivo* conditions (Cimini et al. 2003, Singh I. et al. 2004). Activation of a plasmalogen-specific phospholipase could be another factor contributing to plasmalogen loss under inflammatory conditions. We could observe an initial (48 h) loss of plasmalogen species containing 4 to 6 double bonds followed by the loss monounsaturated species (96 h). This finding supports the concept of profound phospholipase A_2 activation in brain during LPS-induced neuroinflammation. Plasmalogens, containing arachidonic acid (C20:4) or docosahexaenoic acid (C22:6) in the *sn*-2 position, are among the first targets for second-messenger generation during the initial phase of the signal-transduction process. This may be followed by the activation of other phospholipases (e.g. $iPLA_2$) which have higher specificity for monosaturated fatty acids in the *sn*-2 position (Farooqui and Horrocks 2001b, Horrocks et al. 2006)

4. LPS-induced Neuroinflammation: The BBB under Chlorinative Attack?

Above-mentioned evidence implicates that MPO-mediated chlorinative stress contributes to CNS dysfunction in adult mice after a single exposure to LPS. However, the sources of cerebral MPO remained unclear. Zhou and colleagues reported that systemic administration of a low dose (0.5 mg/kg body weight) of LPS causes neutrophil-endothelial interactions in the cerebral microvasculature between 4 to 24 h post treatment but no neutrophil infiltration into the CNS parenchyma. The authors suggested that this observation was most probably caused by too little chemoattractant production due to limited activation of brain resident microglia. In contrast, higher doses (2 or 10 mg/kg i.p.) resulted in BBB breakdown, induced chemokine production thereby presumably guiding neutrophil emigration across post-capillary venules (Zhou et al. 2009). This is in agreement with our data from wild-type mice. We could identify profound recruitment of MPO-positive neutrophils to the cerebrovasculature but only a sporadic tendency of brain parenchyma infiltration after 6 h post induction of high dose endotoxemia (8 mg/kg i.p.). The observed absence of monocyte recruitment is a characteristic feature of the present *in vivo* model, and sets it apart from other murine models using intracerebral LPS injection or TBI (Bohatschek et al. 2001, Montero-Menei et al. 1996, Zhang Z. et al. 2006).

Recruitment of blood-derived MPO-positive granulocytes induced by peripheral endotoxin (1 mg i.p.) was shown to be ICAM-1 expression-dependent and to be accompanied by sustained leakage of human serum albumin suggesting a direct relationship between leukocyte recruitment and BBB disruption (Bohatschek et al. 2001). In fact, transient middle cerebral artery occlusion (MCAO) in P-selectin$^{-/-}$ mice resulted in the same infarct volume compared to wild-type mice but PMNL recruitment and BBB injury were significantly ameliorated (Jin et al. 2010).

Activated PMNLs are a major source of ROS during inflammation, thus playing an important role in BBB disruption (Pun et al. 2009). Using an *in vitro* BBB model we could demonstrate that activation of TNFα-primed neutrophils with fMLP in the presence of BMVEC results in a severe loss of barrier function. Thus, it is reasonable to assume that LPS-activated neutrophils adherent to the cerebral vessels might cause local damage to the BBB. However, activation of ROS production via fMLP activation had several limitations as we were unable to ameliorate ROS formation by the potent HOCl-scavengers taurine and methionine (Jerlich et al. 2000) (our preliminary data). This finding is reminiscent to other studies showing that ROS formation via activation of NOX2 (in our experimental

setup fMLP) is essential but insufficient to induce NET formation and HOCl release (Remijsen et al. 2011).

Generally, PMNLs were regarded to exert vascular injury only after adherence to the endothelial barrier. This concept has been put aside since increased intraluminal degranulation of leukocytes was observed resulting in a release of MPO that is accessible to the endothelium (Lau and Baldus 2006, Malle et al. 2000). Our *in vivo* studies support the latter assumption as substantial accumulation of externalized MPO at the cerebrovasculature in response to LPS treatment was found. This event has important implications: On the one hand, it is becoming increasingly evident that MPO externalization via NETosis is a critical event mediating PMNL recruitment via electrostatic interactions between the positive charge of MPO and the negatively charged glycocalix of PMNLs as well as due to stimulation of CD11b/CD18 integrins (Klinke et al. 2011, Lau et al. 2005). Interestingly, our observation of neutrophil adherence and MPO-deposition at the luminal side of cerebrovasculature might support this concept.

On the other hand, most importantly, MPO deposition at the vascular wall appears to be a prerequisite for the formation of highly reactive species at the BBB. This is based on the following considerations: First, systemic LPS is a powerful inducer of non-phagocytic NAD(P)H oxidase system and xanthine oxidase in the vasculature capable of generating high levels of $O_2^{\cdot -}$ in the proximity of deposited MPO. Second, this $O_2^{\cdot -}$ is rapidly dismutated to H_2O_2, the rate-limitating substrate for MPO-catalyzed HOCl formation (Brandes et al. 1999, Javesghani et al. 2003, Qin Z. et al. 2008). Third, since LPS was reported as a potent inducer of the iNOS system in BMVEC (Singh A. K. et al. 2007) it is likely that the tremendous (60-fold) induction of iNOS expression after 6 h in our *in vivo* mouse model is associated with overshooting NO generation at the BBB.

Our studies could unambiguously demonstrate - by detection of 3-nitrotyrosine (NO_2Tyr) epitopes along cerebral vessels - that LPS treatment is accompanied by extensive nitrosative stress. Since RNS were shown to be able to induce oxidation and nitration of lipids one may speculate about a crucial role of nitrosative stress in plasmalogen loss during neuroinflammation (Rubbo et al. 2009). Generally, Tyr-nitration has been attributed to formation of ONO_2^-, as the generation of NO and $O_2^{\cdot -}$ are characteristic features at sites of inflammation (Pacher et al. 2007). However, this view has changed given to the *in vivo* observation that MPO-dependent protein nitration, basically via the one-electron oxidation of NO_2^- and subsequent formation of $NO_2^{\cdot}$, accounted for the majority of nitrotyrosine formed (Brennan et al. 2002). Due to the approx. 1000-fold higher Cl^- (~140 mM) concentrations as compared to NO_2^- (~100-

200 µM) it is reasonable to assume that HOCl formation is favored over $NO_2^{\cdot}$ formation (Lau and Baldus 2006). This is further supported by the finding that NO_2^- is a poor substrate for MPO (van Dalen et al. 2000)

Further *in vitro* experiments aimed to simulate the impact of externalized MPO on BBB integrity under conditions comparable to the cerebrovasculature caused by LPS exposure. These experiments revealed that barrier disrupting properties of H_2O_2 (originally formed by activated neutrophils or by BMVEC itself) are significantly enhanced by the presence of MPO. Attenuation of barrier breakdown by methionine confirmed our hypothesis that MPO deposition induces BMVEC dysfunction via generation of more potent reactive species, most likely HOCl. HOCl, supplied either directly or produced by the MPO-H_2O_2-Cl^- system, is known to be much more effective than H_2O_2 in altering cell shape, electrical resistance, and protein permeability of endothelial cells (Ochoa et al. 1997). Indeed, additional *in vitro* experiments with exogenously added reagent HOCl identified the MPO-H_2O_2-Cl^- system as a potential key mediator of BBB dysfunction under inflammatory conditions.

On the whole, our data indicate that the BBB represents a major target for RCS-mediated attack during endotoxemia. Nevertheless, it is important to note that MPO was also detected basolateral to the endothelium, a finding in line with others (Baldus et al. 2001) that suggests MPO export to brain parenchyma. Although not fully understood at the moment, it is possible that positively charged MPO is co-transported with negatively charged serum albumin across the endothelium by means of caveolae-dependent transcytosis (Tiruppathi et al. 2004). However, this assumption has two important implications to our study. On the one hand it raises the question about transcytosis of the MPO-albumin complex across the BBB since cationized albumin but not native albumin undergoes absorptive-mediated endocytosis (Thole et al. 2002). On the other hand, the concept of MPO transcytosis suggests that activation of peripheral neutrophils and concomitant MPO import across the BBB could contribute to chlorinative stress also in deeper regions of brain parenchyma.

5. The Role α-Chloro Fatty Aldehydes in RCS-mediated BBB Dysfunction

Ether-phospholipids, particularly plasmalogens, represent a major phospholipid class in endothelial cells contributing to about 35 to 50 mol% of PE and 3 to 9 mol% of PC. Furthermore, these contents seem to be relatively conserved in endothelial cells derived from several arteries and veins as well as from brain capillaries (Murphy E. J. et al. 1992, Selivonchick and Roots 1977, Takamura et al. 1990). Significantly reduced plasmalogen contents of endothelial cells were found during several adverse conditions (Collado et al. 2003, Meyer and McHowat 2007). Interestingly, as indicated by a loss of unsaturated FAs of ethanolamine plasmalogens, the cerebrovasculature is significantly more affected by the aging process as compared to brain parenchyma (Williams W. M. and Rapoport 1993). However, plasmalogen damage in the aging brain was suggested to be causally linked to lipid peroxidation and oxidative stress due to a dramatic increase of alpha-hydroxy aldehydes (Weisser et al. 1997).

Above-mentioned evidence implicates that neutrophil- or glia-derived MPO might be capable to oxidatively target the endogenous plasmalogen pool of the cerebrovasculature, thereby generating chlorinated lipids including 2-ClHDA. In accordance to experiments with HCAEC performed by Ford and coworkers, we could detect high plasmalogen concentrations in BMVEC. Moreover, this pool was quantitatively consumed by HOCl and maximal modification rates (between 25-50% of total plasmalogens) were observed even at concentrations, which were already shown to occur under pathophysiological conditions (Messner et al. 2006, Yap et al. 2007). This is of biological significance based on two considerations: pPE are enriched in lipid raft domains, which are structural determinants for junctional positioning at the BBB (Dodelet-Devillers et al. 2009b, Pike et al. 2002). Thus, plasmalogen modification by HOCl is likely to interfere with BBB function. On the other hand, HOCl modification of cerebrovascular plasmalogens results in the formation of considerable amounts of α-ClFALDs (~6 µg or ~200 nmol/10^6 cells).

Considering proinflammatory properties α-ClFALDs (Ford 2010), they represent intriguing candidate molecules that could contribute to BBB dysfunction (de Boer and Gaillard 2006). Therefore, further experiments were designed to corroborate this hypothesis by means of accepted *in vitro* and *in vivo* BBB models. Our studies revealed that low micromolar concentrations (*in vitro*: 5 µM; *in vivo*: 25 µM) of exogenous 2-ClHDA were sufficient to cause significant breakdown of barrier function. This discovery is of biological importance since these concentrations are present *in vivo*. This is further substantiated by the fact that 50-100 µM HOCl is sufficient to generate 2-ClHDA in concentrations (5

μM or 20 nmol/10^6 cells in ECIS wells) that induce barrier dysfunction. In addition, *in vitro* experiments with reagent NaOCl demonstrated that 2-ClHDA is 20 to 50- fold more effective than the strong oxidant itself indicating an extremely high potential of α-ClFALDs to mediate BBB dysfunction.

6. What Are The Key Properties determining the Deleterious Effects of α-ClFALDs towards BMVEC function?

Above-mentioned evidence implicates α-ClFALDs as potential contributors to BBB dysfunction during neurodegeneration. Due to this important finding subsequent studies were designed to characterize the impact of exogenously added 2-ClHDA on key BMVEC properties including junctional architecture, cell viability, mitochondrial function, and induction of apoptosis.

6.1. *2-ClHDA: Precursor of a Variety of Chlorinated Effectors*

During the first set of experiments we could demonstrate a clear divergence between the stability of 2-ClHDA in the cell-free system of blood plasma (τ/2: 32 h) and in the presence of endothelial cells (BMVEC, τ/2:120 min; mouse circulation, τ/2: 40 s). This was most probably the result of metabolism supporting data of Ford and coworkers showing the presence of 2-ClHA but not of 2-ClHDA in plasma of sendai virus-infected mice (Anbukumar et al. 2010).

In subsequent *in vitro* experiments we have compared the loss of 2-ClHDA from the medium and synthesis of chlorinated metabolites by BMVEC. These experiments revealed that approx. 7% of exogenously added 2-ClHDA was recovered in association with cells and further 14% and 4% were recovered as 2-ClHOH and 2-ClHA, respectively, resulting in a recovery rate of ≈ 25%. In addition, approx. 30% of total, cell-associated 2-ClHA was recovered in association with the polar BMVEC lipid pool. Intracellular reduction or oxidation of 2-ClHDA is a rather rapid process reaching maximum conversion at approx. 100 min. These data is reminiscent of what was described for HCAEC by Wildsmith and colleagues (Wildsmith et al. 2006a), a pathway dependent on fatty aldehyde dehydrogenase (ALDH3A2) activity (Anbukumar et al. 2010). ALDH3A2 deficiency results in Sjogren-Larsson syndrome characterized by ichthyosis, spastic paraplegia and mental retardation, respectively. The pathogenesis of the symptoms is thought to result from abnormal lipid accumulation in the membranes of skin and brain, formation of Schiff base adducts with amine-containing lipids or proteins, or defective eicosanoid turnover (Rizzo 2007). Although we have not analyzed 2-ClHDA

incorporation in the neutral lipid fraction of BMVEC our data suggest a substantial loss of 2-ClHDA. This is not surprising since 2-ClHDA was shown to undergo Schiff base adduct formation with ethanolamine-containing glycerophospholipids and/or the ε-amino group of protein lysine residues (Stadelmann-Ingrand et al. 2004, Wildsmith et al. 2006b). PE and pPE contribute to approx. 60% of the total phospholipid fraction in the brain. pPE are enriched in lipid raft domains (Pike et al. 2002), which are major structural determinants for junctional positioning at the BBB (Dodelet-Devillers et al. 2009a). Thus, pPE and/or PE headgroup modification by 2-ClHDA is likely to interfere with BBB function. A second possibility that contributes to 2-ClHDA loss, that was not addressed during our study, is ω-oxidation of 2-ClHA and subsequent β-oxidation starting at the ω-carboxylic acid function (Brahmbhatt et al. 2010a). Under i*n vivo* conditions this reaction gives rise to 2-chloroadipic acid that is subject to urinary excretion (Brahmbhatt et al. 2010a). Of note, the ω-oxidation pathway is also active in the brain (Alexander et al. 1998) although it is not clear whether brain-derived metabolites accumulate in blood or cerebrospinal fluid. In addition, BMVEC are able to convert 20-hydroxyeicosatetraenoic acid (20-hydroxy-HETE) to 20-carboxy-HETE and chain shortened dicarboxylic acid metabolites indicating that ω-oxidation is also active in the cerebrovasculature (Collins et al. 2005).

6.2. *The Role of Signaling in Barrier Dysfunction*

Our data indicate that exogenously added 2-ClHDA induces the activation of ERK1/2, p38 and JNK1/2 signaling; all of them have been shown to be causally involved in stress-induced BBB dysfunction or BMVEC barrier dysfunction:

ERK1/2-phosphorylation is associated with increased expression of MMP-9 and proteolytic cleavage of TJ during focal cerebral ischemia (Maddahi et al. 2009, Yang Y. et al. 2007b). Fischer and colleagues reported that H_2O_2-induced hyperpermeability of BMVEC was prevented by blocking ERK1/2 activation using MAPKK-specific inhibitor PD98059 (Fischer et al. 2005). Our own data revealed that PD98059-induced ERK1/2-inhibition could provide only transient protection of barrier integrity in the presence of 2-ClHDA. Moreover, immediate response of this enzyme to lipid aldehydes (2-ClHDA: 1 min, 4-HNE: 10 min) most likely identifies ERK1/2 activation as an early effector of carbonyl stress-induced barrier dysfunction in endothelial cells (Usatyuk and Natarajan 2004).

Recently, it was demonstrated that increased transendothelial albumin flux of HUVEC is initiated by activation of p38 due to cell contraction as a result of F-actin stress fibers formation (Chu et al. 2010).

This data support the hypothesis that F-actin reorganization is likely involved the formation of intercellular gaps, which probably represents a key feature of 2-ClHDA induced barrier dysfunction. Moreover, *N*-acyl-dopamines induce COX2 expression in brain endothelial cells - an event closely related to permeability increase (Candelario-Jalil et al. 2007) - by stabilizing mRNA through a p38-dependent pathway. This observation likely links barrier dysfunction and p38 activation to already published data of Ford and coworkers, showing COX2 expression and PGI_2 formation in HCAEC in response to 2-ClHDA and 2-ClHA (Messner et al. 2008a, Navarrete et al. 2010). Moreover, strong induction of p38 during the second phase (after 1 h) of biphasic activation might indicate a dominant role of this signaling event during the executioner phase of apoptosis, as previously demonstrated by cadmium-induced cytotoxicity of BMVEC (Jung et al. 2008).

The complex roles of JNK1/2 for acute brain injury have been investigated in models of subarachnoid hemorrhage and transient focal cerebral ischemia: Inhibition of JNK1/2 resulted in protection against mitochondrial apoptosis by Bax and Bim translocation and diminishing caspase-3/9 activation. Moreover, this inhibition reduced MMP-9 levels and consecutively prevented collagen IV loss in cerebral vessels, and it prevented BBB disruption and a concomitant decrease of edema formation (Gao Y. et al. 2005, Yatsushige et al. 2007). Therefore, activation of the cell death mediator JNK1/2 may be a critical signaling event during the late phase (after 1 h) of 2-ClHDA induced BMVEC barrier dysfunction.

Fischer and colleagues demonstrated that H_2O_2-induced permeability changes of BMVEC correlate with alterations of TJ (occludin, ZO-1, and ZO-2) localization. Interestingly, the treatments of BMVEC with H_2O_2 or 2-ClHDA caused similar cell-morphological alterations: A change from continuous distribution of junction proteins to ‘frizzy-like’ structures on the one hand, and the transformation from spindle to a generally more rounded cell shape on the other hand were identified (Fischer et al. 2005). Frizzy-like junctional architecture could be induced by stress-related TJ assembly, an observation that is in line with our findings of ZO-1 accumulation in the nuclear compartment. Recently, it has been shown in GP8 brain endothelial cells that expression of a ZO-2-variant targeted to the cell nucleus is accompanied by altered gene expression, junctional stability and decreased TEERs (Traweger et al. 2008). However, it was suggested that different types of stress like heat shock, oxidative stress, chemical insults, or impaired cell-cell contacts (wounding) alter ZO protein expression and their subcellular localization. While the nuclear targeting of ZO-1 has been well described, its nuclear functions are less clear (Bauer et al. 2010, Gonzalez-Mariscal et al. 2011). Nevertheless, there are some

studies showing that ZO-1 directly participates in the control of gene expression by interaction with the Y-box transcription factor ZONAB (ZO-1 associated nucleic acid binding protein). To date, convincing experimental evidence suggests that ZO-1/ZONAB is capable of regulating G_1/S-phase transition by two mechanisms: Transcriptional regulation of cell cycle- and DNA replication-factors, and modulation of the nuclear accumulation of cyclin-dependent kinase-4 (CDK4) (Balda et al. 2003, Sourisseau et al. 2006)

Highly reactive 4-hydroxy/oxo/hydroperoxy-alkenals (e.g. 4-HNE, 4-HDDE, 4-OHE, or 4-HPNE) are able to covalently modify cellular components either by Schiff base formation or by Michael-addition (Shimozu et al. 2011, Usatyuk and Natarajan 2011). As other lipid aldehydes, 2-ClHDA is able to form covalent adducts with primary amines of ethanolamine glycerophospholipids and proteins by Schiff base formation (Stadelmann-Ingrand et al. 2004, Wildsmith et al. 2006b). Generally, adduct formation evokes a wide range of pathophysiological responses including cytotoxicity as well as activation of stress signaling pathways and gene expression (Riahi et al. 2010, Usatyuk and Natarajan 2011). However, what sets 2-ClHDA apart from other aldehydes is the presence of a polarizable chlorine residue. The presence of halogen residues in the alkyl chain of FAs was shown to induce significant changes in the physico-chemical properties of these compounds, resulting in altered membrane behavior (Dembitsky and Srebnik 2002). Moreover, there is increasing evidence that halogen residues are able to form non-covalent charge transfer complexes to oxygen, nitrogen, sulfur residues with binding constants well in the range of hydrogen bondings. These properties are gaining increasing attention in drug development as the presence of halogen residues and concomitant halogen bonding can increase target selectivity and affinity. This might be of particular importance for the development of specific kinase inhibitors (Auffinger et al. 2004, Hernandes et al. 2010, Voth and Ho 2007). Whether halogen bonding to vitally important BMVEC proteins (e.g. of TJ or AJ) contributes to the deleterious effects of 2-ClHDA remains to be elucidated.

Several studies demonstrated that halogenated lipids are potent signaling mediators: 2-ClHDA activates COX2 (Messner et al. 2008a) and is a natural inhibitor of eNOS biosynthesis (Marsche et al. 2004). eNOS undergoes palmitoylation by Asp-His-His-Cys motif (DHHC) palmitoyl acyl transferases (PAT) and subsequent targeting to the plasma membrane. Interestingly, the structural analogue of 2-ClHDA and potent inhibitor of protein acylation (Resh 2006), 2-bromopalmitate (2-BrHA) induces missorting of eNOS and impaired NO biosynthesis in further consequence. Whether 2-ClHA (generated from 2-ClHDA) could be responsible for mislocalization of eNOS and impaired NO biosynthesis, in a similar

manner as reported for 2-BrHA, is currently unclear (Fernandez-Hernando et al. 2006). Furthermore, 2-iodohexadecanal (2-IHDA), another structural homolog of 2-ClHDA and major iodolipid in thyroid gland (Pereira et al. 1990), inhibits the biosynthesis of cAMP via adenylyl cyclase (Panneels et al. 1994). Although speculative at the moment 2-ClHDA mediated barrier dysfunction might be a triggered by adenylyl cyclase inhibition since cAMP levels are unequivocally involved in barrier regulation of BMVEC (Deli et al. 2005).

6.3. *The Lipotoxic Potential of Chlorinated Lipids*

With regard to cell viability 2-ClHDA displayed higher cytotoxicity towards BMVEC as compared to structurally related C16-analogues and reagent HOCl. The cytotoxic properties of C16-analogues decreased in the order of 2-ClHDA > HDA > palmitic acid > 2-ClHDA-dma. These observations are in line with previously published data showing a higher biological potency of 2-ClHDA and 2-IHDA compared to their non α-halogenated analogues (Messner et al. 2008a, Thomasz et al. 2010). Nevertheless, the reason for these observations is not yet clear but it might be related to either membrane permeability (the logP value decreases from 2-ClHDA (7.6) > HDA (7.1) > palmitic acid (6.4)) or activation of different signaling pathways (*see chapter 6.2.).*

However, the induction of the apoptotic machinery by 2-ClHDA, as demonstrated by caspase-3 processing, might be a critical event in the scenario of BMVEC death (Broughton et al. 2009). Recently, a strong correlation between the decrease in thyroid weight and the number of glandular epithelial cells in response to 2-IHDA was related to the induction of caspase-3 dependent apoptotic cell death (Thomasz et al. 2010). This is supported by evidence from marine biology demonstrating that halogenated metabolites including halogenated fatty acids serve as an innate chemical defense arsenal (Dembitsky and Srebnik 2002). Many of these halogenated compounds have either antimicrobial activity or, due to their cytotoxic properties, protect marine invertebrates against potential predators. Thus, we hypothesize that formation of 2-ClHDA and derived lipid species during neurodegeneration might play a global role in CNS dysfunction, for example, by affecting other brain-resident cell types like neurons.

It is well established that palmitic acid can induce apoptosis via TLR4-dependent pathways - whether this is also a likely pathway for 2-ClHDA remains to be elucidated. However, in a similar manner as reported for TLR4 activation in an experimental stroke model (Pradillo et al. 2009), 2-ClHDA (and its

metabolite 2-ClHA) was shown to induce COX2 expression in HCAEC (Messner et al. 2008a). In cell viability assays performed during the present study NaOCl displayed an IC_{50} value of approx. 400 µM after 24 h incubation. This is different from what was reported for other types of endothelial cells: In HUVEC 5 to 20 µM HOCl caused growth arrest and approx. 35 µM HOCl resulted in maximal apoptosis (Vissers et al. 1999). However, we have been unable to detect pronounced NaOCl-mediated collapse of the mitochondrial membrane potential (Whiteman et al. 2005) nor we could detect NaOCl-dependent caspase-3 activation as demonstrated in human saphenous vein endothelial cells (Sugiyama et al. 2004).

6.4. *Barrier Dysfunction: Mitochondrial dysfunction, ROS and Apoptosis*

Emerging evidence suggests that mitochondrial dysfunction plays a major role in neurological disorders like e.g. AD, MS, PD, or stroke (Knott et al. 2008). The dynamic nature of mitochondria, characterized by tightly controlled fission and fusion, is an important part of mitochondrial health and function (Campello and Scorrano 2010). Mitochondrial permeability transition pore formation (MTP) associated with collapse of $\Delta\psi m$ as observed during the present study is considered a major contributor to disease progression in neurological disorders (Barrientos et al. 2011). These pathophysiological conditions might have particularly deleterious consequences on the elaborate transport systems at the BBB. BMVEC have an extremely high density of mitochondria, which reflects the energy demand necessary to fuel the elaborately developed (ATP-dependent) transport systems present at either the luminal or abluminal side of the BBB (Zlokovic 2008). During normal oxidative phosphorylation electrons leak out of the electron transport chain, giving rise to the formation of $O_2^{\cdot -}$, an event that might be prevalent at the BBB. $O_2^{\cdot -}$ is generated at both, complex I (NADH dehydrogenase) and complex III (ubiquinone Q-cytochrome b) and alterations in the redox status of these enzyme complexes results in excessive ROS production (Boveris and Chance 1973).

Excess cerebral ROS generation after cerebral ischemia was reported for MCAO (Fraser 2011). ROS generation was mainly detected in BMVEC and smooth muscle cells and it was suggested that the accompanying endothelial permeability is one of the key factors generating the penumbra (the hypoxic but regenerable part of the lesion) around the ischemic core (Fraser 2011). In line with the suggestion that brain endothelial ROS production and BBB dysfunction are closely linked (Pun et al. 2009), Manda and colleagues (Manda et al. 2011) have reported mitochondrial ROS production, MTP formation and compromised barrier function in brain endothelial cells that were subjected to high concentrations of

retroviral drugs. In human BMVEC cultures it was demonstrated that ethanol oxidation to acetic aldehyde by Cyp2E1 results in ROS production, subsequent activation of myosin light chain kinase and an increase in endothelial permeability (Haorah et al. 2005).

Of note, the time scale of collapse of $\Delta\psi m$, ROS formation and caspase-3 activation as observed here closely coincides with barrier dysfunction of BMVEC. The time scale of barrier opening by 2-ClHDA is comparable to what was reported for 4-HNE (Mertsch et al. 2001), a prototypic, AA-derived lipid peroxidation product. Whether or not covalent adduct formation between 2-ClHDA and TJ-associated proteins contribute to barrier dysfunction is subject to further studies.

7. The Role of Phloretin during LPS-induced Neuroinflammation

Increasing evidence suggests that flavonoids and non-flavonoid polyphenols - ubiquitously present in fruits, vegetables and spices - have beneficial effects in a variety neurodegenerative disorders including BBB dysfunction (Darvesh et al. 2010). However, the *in vivo* relevance of these compounds as well as their precise molecular actions in biological systems are under intense investigation.

To date, potential mechanisms of action so far include: i) non specific actions, based on chemical features common to most polyphenols, e.g. the presence of a phenol group to scavenge free radicals; and ii) specific mechanisms; based on particular structural and conformational characteristics of select polyphenols and the biological target, e.g. proteins, or defined membrane domains (Fraga et al. 2010, Galleano et al. 2010). For example, the chalcone-type polyphenol phloretin was shown to reduce the dipole membrane potential of the BBB (Cattelotte et al. 2009), to inhibit glucose transport across the BBB (Betz et al. 1976) and to prevent TNFα-stimulated upregulation of VCAM-1, ICAM-1 and E-selectin in HUVEC (Stangl et al. 2005). Furthermore, phloretin was found to protect against cisplatin-induced apoptosis (Choi B. M. et al. 2011), to act as a PGF2α antagonist in astrocytes (Kitanaka et al. 1993) and to regulate the activity of several enzymes including 5'-iodothyronine deiodinase (Morreale de Escobar et al. 1994), PKC/D1 (Gschwendt et al. 1996, Kern et al. 2007), glycogen synthase kinase-3β (Kern et al. 2006), and tyrosine kinases (Yang E. B. et al. 2001).

A large body of evidence addressing the beneficial effects of dietary phloretin comes from *in vitro* experiments or animal models. For *in vivo* applicability in the human system the question of bioavailability arises. The absorption process of polyphenols is complex as these compounds are subject to multiple hydrolysis/conjugation steps in the small intestine, colon, and the liver (Crozier et al.

2010, Gutierrez-Merino et al. 2011). For example, phloretin administration as the aglycone or as the glucoside: 85-95% of the circulating forms are conjugated metabolites of phloretin, predominantly phloretin-2′-*O*-glucuronide (Marks et al. 2009), the result of phlorizidin hydrolysis and further metabolism of phloretin at the small intestine during absorption. However, high-dose intake of approx. 90 mg phlorizidin/kg body weight, which accounts for about 4.5 kg apples or 200 g apple peels, resulted in phloretin metabolite plasma concentration of approx. 70 μmol/L. These findings indicate that high dose supplementation with phloretin results therapeutically useful plasma levels in the medium micromolar range (Crespy et al. 2001a, Crespy et al. 2001b, Escarpa and Gonzalez 1998)

One of the major findings obtained during the present study is a potent rescue capacity of phloretin towards primary and secondary MPO product-mediated BMVEC cell death. In accordance to previously published data showing cytoprotective effects of phloridzin against a variety of oxidants (Choi J. M. et al. 2007b), our studies could also reveal the aglycone as a potent oxidant scavenger, that efficiently protect BMVEC against HOCl-induced cytotoxicity. Observed rescue was most probably due to formation of stable mono- and dichlorinated compounds as already reported for genistein or daidzein. Notably, chemically synthesized 3'-chlorogenistein and 3'-chlorodaidzein increased the ability to inhibit copper-dependent oxidative modification of LDL strengthening the concept of polyphenols as critical modulators at sites of inflammation (Boersma et al. 1999, Patel et al. 2003).

Phloretin is a non-specific fatty acid uptake inhibitor at the BBB (Mitchell R. W. et al. 2009) and we hypothesized that it could also interfere with 2-ClHDA uptake by BMVEC thereby attenuating adverse effects. Indeed, among seven different polyphenols investigated, only phloretin was able to interfere with 2-ClHDA-mediated cytotoxicity and barrier dysfunction. In line with our preliminary hypothesis phloretin inhibited cellular uptake of 2-ClHDA. However, also 2-ClHDA concentrations in the cellular supernatant were significantly lower as compared to incubations performed in the absence of phloretin. This suggested that phloretin is able to form covalent adducts with the chlorinated aldehyde. High resolution mass spectrometric analyses revealed covalent trapping of the model compound 2-chloroheptanal by the phloroglucinol residue of phloretin.

This discovery would be in line with two reports that demonstrated that phloretin acts as a ‘sacrificial nucleophil’ in preventing the formation of advanced glycation products between model compounds and unsaturated aldehydes (4-HNE and acrolein (Zhu et al. 2009)) or reactive dicarbonyl species (methylglyoxal and glyoxal, respectively (Shao et al. 2008)). Both studies indicated that the two unsubstituted carbons at the A ring, positions 3 and/or 5, are the major active sites of chalcone type

compounds for trapping mentioned carbonyl species. In the case of α,β-unsaturated carbonyl species, C-3 and/or C-5 of phloretin likely undergo Michael addition in an initial step. This is followed by nucleophilic attack of the terminal aldehyde carbon by nearby hydroxyl groups (C-2 and/or C-4) leading to the formation of cyclic hemiacetal(s) as more stable final products (Shao et al. 2008, Zhu et al. 2009). However, experiments performed during the present study suggest a different trapping mechanism. Although speculative at the moment, 2-ClHDA might form covalent adducts comparable to a Williamson ether synthesis reaction. This assumption is supported by studies demonstrating selective Zn-catalyzed mono-, di-, or tri-*O*-alkylation of phloroglucinol or base-catalyzed bimolecular nucleophilic substitution (S_N2) reaction of 2-chloro propionic acid with phenols (Aikins et al. 2005, Paul and Gupta 2004).

Quantum mechanical calculations revealed that the 2,4-dihydroxyacetophenone group represents the pharmacophore group in phloretin (Bentes et al. 2011). Another report suggested that (in a peroxynitrite scavenging system) the pharmacophore of phloretin consists of the 2,6-dihydroxyacetophenone group (Rezk et al. 2002). This aspect is strengthened by findings of the present study demonstrating that the glucoside of phloretin, phloridzin, was without effect on BMVEC viability, suggesting that glucosylation of the hydroxyl group at position 2 might prevent 2-ClHDA trapping.

Therefore, it is likely that the primary circulating metabolite phloretin-2′-*O*-glucuronide might also be inactive (Marks et al. 2009). However, flavonoid aglycones are assumed to emerge at the target site under oxidative stress, due to inflammation-dependent release of β-glucuronidase from stimulated neutrophils, as demonstrated in rats after systemic LPS administration (Shimoi et al. 2001, Terao et al. 2011). Moreover, there is clear evidence that flavonoids are able to traverse the BBB according to their logP values and that polar glucuronides of naringenin and hesperetin are actively metabolized by BMVEC (Youdim et al. 2003). Phloretin is more lipophilic than naringenin (logP: 2.05 vs. 1.63) and it may permeate lipid bilayers (Verkman and Solomon 1982). Therefore, it is likely that this flavonoid also exerts neuroprotective effects in brain parenchyma via transcellular BBB passage. Nevertheless, some restriction of entry caused by efflux transporters may be present for certain flavonoids: In contrast to naringenin, quercetin was found to be a substrate for P-gp (Youdim et al. 2004), however, phloretin efflux at the BBB remains elusive at the moment.

VIII. CONCLUDING REMARKS

Persistent and self-propelling neuroinflammation can be considered as a key marker of chronic and acute neurodegenerative disorders (Glass et al. 2010, Teeling and Perry 2009), a scenario where oxidative stress and lipids are causally involved (Di Paolo and Kim 2011, Frisardi et al. 2011, Valko et al. 2010). There is emerging evidence that aberrant metabolism of cholesterol, sphingolipids, and plasmalogens are associated with neuropathological conditions (Farooqui et al. 2007, Hartmann et al. 2007, Jeitner et al. 2011). In line, decreased plasmalogen contents were reported for several neuropathological conditions including Alzheimer disease (Ginsberg et al. 1995, Goodenowe et al. 2007), Gaucher disease (Moraitou et al. 2008), Down syndrome (Murphy E. J. et al. 2000), or experimental autoimmune encephalomyelitis (Singh I. et al. 2004), consequently, a close relation between plasmalogens levels and the extent of neuroinflammation appears reasonable.

This thesis was driven by the hypothesis that through its unique properties the brain plasmalogen fraction might not only serve as a target for inflammation-dependent degradation ('consequence of neuroinflammation') but also as a precursor for potent effectors in disease-amplifying signaling cascades ('cause of neuroinflammation').

Using a rodent model for acute neuroinflammation we were able to provide a potential framework, where, after elicitation of the systemic inflammatory response and propagation to the central nervous system, MPO-derived chlorinating species could oxidatively damage brain plasmalogens thus exacerbating neuropathological conditions. This finding supports the theory that MPO-mediated chlorinative stress is involved in the pathology of neurodegeneration and it is in line with a number of basic research and clinical case-control association studies of -463G/A promoter polymorphism showing a relationship between MPO expression and the risk for neurodegenerative diseases (Crawford et al. 2001, Maki et al. 2009, Nagra et al. 1997).

In line with previous work by Ford and coworkers, we could demonstrate that the vinyl-ether bond of mouse brain plasmalogens is a preferred target for RCS-mediated lipid modification resulting in the substantial formation of two compound classes with proinflammatory properties: α-chloro fatty aldehydes and the corresponding remnant *sn*-1 lysophospholipids (Ford 2010). Nevertheless, the contribution of MPO-dependent modification to the overall loss of cerebral plasmalogens was small.

However, our data were obtained in a rodent system of neuroinflammation, therefore, the extent of HOCl-modification might be an underestimation in extrapolating these data to the human system as MPO protein content of rodent neutrophils is 10-fold less compared to human cells (Klebanoff 2005, Podrez et al. 2000). This assumption raises the possibility that plasmalogen degradation products might accumulate in considerable amounts within the CSF of patients suffering from neurodegeneration. Regardless to the type of patients disease (MS, bacterial meningitis, etc.) we were not able to detect α-ClFALDs in CSF (data not shown). However, biomarkers of oxidative stress are labile and short-lived in body fluids, thus, chemically and metabolically stable biomarkers are needed for accurate tracking (Galasko and Montine 2010). Accordingly, we assume that 2-ClHDA-derived metabolites, especially the stable, water-soluble 2-chloro adipic acid (Anbukumar et al. 2010), might accumulate in the CSF of those patients, likely representing novel biomarkers for MPO activation in the CNS.

Immunohistological studies could identify the cerebrovasculature as a major site of accumulation of active MPO. Results of the present study demonstrate that activation of the neutrophil MPO-H_2O_2-Cl^- system induce the formation of 2-ClHDA, a compound with deleterious effects on BMVEC function. Our data clearly identified 2-ClHDA as a more potent effector of BBB dysfunction than the oxidant HOCl. At the level of BMVEC, the loss of BBB integrity was mainly attributable to the ability of 2-ClHDA to induce the apoptotic machinery and intracellular signaling cascades involved in junctional opening (Fisher 2008, Krizbai and Deli 2003). This aspect is of high pathophysiological relevance given that BBB breakdown is one of the most important inducers/amplifiers of neurodegeneration and it reflects the high pro-inflammatory potential of α-ClFALDs as observed by others (Messner et al. 2008a, Thukkani et al. 2005, Zlokovic 2008). Therefore, it has to be kept in mind that α-ClFALDs might also induce neurodegeneration directly by exerting lipotoxicity to neurons.

Metabolism of 2-ClHDA results in the formation of a plethora of chlorinated lipid species, thus a complex cellular response is likely to occur. Although we got deeper insight into the pathophysiological mechanisms of 2-ClHDA in the cerebrovasculature, the molecular targets of MPO-derived chlorinated lipid species and the activated upstream signaling cascades remain still unidentified. In fact, this is an obvious challenge for future investigations.

Activation of plasmalogen-selective PLA_2 induces the loss plasmalogen, an inflammatory event that is likely associated with BBB dysfunction (Farooqui 2010, Fukumoto et al. 2010). However, with the discovery and the characterization of the HOCl-derived modification product 2-ClHDA we identified MPO activation as novel mechanistic link between plasmalogen loss and BBB dysfunction.

In the etiology of neurodegeneration a dual role of plasmalogens is likely: i) On the one hand plasmalogens are essential for normal CNS function (Gorgas et al. 2006). Independent of the mechanism of plasmalogen loss, i.e. impaired synthesis or increased degradation/modification, the outcome for nervous system function is dismal. Therefore, this project raises new fundamental questions about the role of chlorinative/oxidative/nitrosative stress in a decline of cognitive function, sickness behavior and mood disorders - as seen in patients suffering from neurodegenerative diseases, systemic infection, or cancer (Dantzer et al. 2008, Gorgas et al. 2006) - and the development of pharmaceutical drugs with beneficial effects by maintaining plasmalogen homeostasis. ii) On the other hand plasmalogens are precursors of bioactive lipids with potent signaling activities. Increased activity of the PLA_2 superfamily and the MPO-H_2O_2-halide system induce the mobilization of powerful lipid mediators including leukotriens, prostaglandins (Ong et al. 2010) and α-ClFALDs through enzymatic or oxidative degradation of acyl-/alkenyl-residues, thus favoring neuroinflammation, oxidative stress and neurodegeneration.

Non-specific PLA_2 inhibitors were reported to ameliorate Aβ-induced neurotoxicity in a mouse model for AD (Sanchez-Mejia et al. 2008), to protect neurons in the MPTP-induced model of Parkinsonism (Tariq et al. 2001), and to delay the onset and progression of EAE by reducing inflammation, axonal damage and severity of EAE (Kalyvas and David 2004).

There is increasing interest in the development of MPO inhibitors, however, at the present time the available compounds are of limited pharmacological usefulness (Choi D. K. et al. 2010, Malle et al. 2007, Soubhye et al. 2010). With the discovery of α-ClFALDs we found a vasoactive downstream effector of MPO activation. Since the protection of the BBB has the potential to delay or prevent the development of chronic neurodegeneration (Abbott et al. 2006), the formation and action of 2-ClHDA might represent a novel therapeutical target to ameliorate the pathogenesis of neurodegenerative disorders.

Flavonoids comprise the most common group of polyphenolic compounds in the human diet and there is accumulating evidence of beneficial effects in a multitude of diseases including cardiovascular disease, cancer and neurodegenerative disorders (Vafeiadou et al. 2007). Recently, much attention has been paid to their antioxidant capacity, however, flavonoids are also suggested as potent suppressors of oxidative/chlorinative stress (Gutierrez-Merino et al. 2011) through modulation of leukocyte recruitment (Stangl et al. 2005), and inhibition of oxidant producing enzymes like e.g. endothelial NADPH oxidase (Steffen et al. 2008), MPO (Shiba et al. 2008), NOS (Roh et al. 2011), and/or

proinflammatory signaling pathways (Williams R. J. et al. 2004). Our finding that phloretin alleviates 2-ClHDA-induced barrier dysfunction by covalent trapping, further supports the concept of dietary benefits to MPO-mediated chlorinative stress in CNS and opens potentially new pharmacotherapeutical strategies to interfere aldehyde-mediated BBB dysfunction (Adibhatla et al. 2006, Darvesh et al. 2010).

IX. SUPPLEMENTARY DATA

TABLE I: Percentage composition of C57BL/6 brain glycerophospholipids

Brain lipids were extracted and analyzed by FT-ICR-MS as described in Materials and Methods. Results shown are mean ± SD from three different brains.

Phosphatidylcholine

Species	m/z	m/z (+ H^+)	Mean	SD
30:0	705.53	706.54	0.28%	0.05%
32:0	733.56	734.57	17.04%	2.58%
32:1	731.55	732.55	1.23%	0.22%
34:0	761.59	762.60	4.63%	0.74%
34:1	759.58	760.59	37.56%	5.84%
34:2	757.56	758.57	0.81%	0.13%
34:3	755.55	756.55	0.16%	0.01%
36:0	789.62	790.63	0.09%	0.01%
36:1	787.61	788.62	13.56%	2.34%
36:2	785.59	786.60	2.92%	0.53%
36:3	783.58	784.59	0.09%	0.00%
36:4	781.56	782.57	5.07%	0.75%
38:1	815.64	816.65	0.68%	0.17%
38:2	813.62	814.63	0.50%	0.10%
38:4	809.59	810.60	4.83%	0.69%
38:5	807.58	808.59	1.64%	0.35%
38:6	805.56	806.57	4.29%	0.70%
38:7	803.55	804.55	0.10%	0.01%
40:1	843.67	844.68	0.16%	0.04%
40:2	841.66	842.66	0.16%	0.04%
40:4	837.62	838.63	0.35%	0.05%
40:6	833.59	834.60	2.69%	0.50%
40:7	831.58	832.59	0.88%	0.17%
42:1	871.70	872.71	0.16%	0.05%
42:2	869.69	870.69	0.10%	0.03%
Sum			100.00%	

Plasmenyl Phosphatidylcholine

Species	m/z	m/z (+ H^+)	Mean	SD
32:0	717.57	718.58	8.15%	0.82%
32:1	715.55	716.56	3.08%	0.88%
34:0	745.60	746.61	53.70%	6.07%
34:1	743.58	744.59	11.08%	3.68%
36:0	773.63	774.64	6.54%	0.65%
36:1	771.61	772.62	8.84%	2.16%
36:2	769.60	770.61	4.93%	2.03%
38:1	799.65	800.65	3.01%	0.75%
40:0	829.69	830.70	0.25%	0.11%
40:1	827.68	828.68	0.42%	0.07%
Sum			100.0%	

TABLE II: Percentage composition of C57BL/6 brain glycerophospholipids

Brain lipids were extracted and analyzed by FT-ICR-MS as described in Materials and Methods. Results shown are mean ± SD from three different brains.

Phosphatidylethanolamine

Species	m/z	m/z (+ H^+)	Mean	SD
34:0	719.55	720.55	1.03%	0.18%
34:1	717.53	718.54	2.49%	0.25%
36:0	747.58	748.59	0.98%	0.11%
36:1	745.56	746.57	5.89%	0.53%
36:2	743.55	744.55	3.48%	0.23%
36:4	739.52	740.52	2.01%	0.18%
38:1	773.59	774.60	2.80%	0.53%
38:2	771.58	772.59	0.51%	0.11%
38:4	767.55	768.55	22.34%	2.27%
38:5	765.53	766.54	3.62%	0.23%
38:6	763.52	764.52	8.04%	0.89%
40:1	801.62	802.63	0.45%	0.01%
40:4	795.58	796.59	4.43%	0.60%
40:5	793.56	794.57	0.76%	0.11%
40:6	791.55	792.55	38.69%	3.71%
40:7	789.53	790.54	2.47%	0.20%
Sum			100.00%	

Plasmenyl Phosphatidylethanolamine

Species	m/z	m/z (+ H^+)	Mean	SD
32:0	675.52	676.53	0.04%	0.01%
34:0	703.55	704.56	0.29%	0.02%
34:1	701.54	702.54	5.23%	0.53%
36:1	729.57	730.58	11.28%	1.13%
36:2	727.55	728.56	11.52%	0.88%
36:4	723.52	724.53	1.69%	0.17%
38:0	759.61	760.62	1.73%	0.21%
38:1	757.60	758.61	5.48%	0.77%
38:2	755.58	756.59	6.44%	0.62%
38:4	751.55	752.56	9.83%	0.98%
38:5	749.54	750.54	6.66%	0.58%
38:6	747.52	748.53	8.90%	0.85%
40:1	785.63	786.64	0.31%	0.04%
40:2	783.61	784.62	0.78%	0.09%
40:4	779.58	780.59	5.59%	0.68%
40:6	775.55	776.56	19.81%	1.07%
40:7	773.54	774.54	4.41%	0.35%
Sum			100.0%	

Phosphatidylinositol

Species	m/z	m/z (- H^+)	Mean	SD
34:1	836.54	835.53	11.33%	1.46%
36:0	866.59	865.58	1.79%	0.55%
36:4	858.53	857.52	7.57%	1.32%
38:0	894.62	893.61	2.32%	1.71%
38:4	886.56	885.55	63.09%	8.28%
38:5	884.54	883.53	8.67%	1.06%
38:6	882.53	881.52	1.73%	0.64%
40:6	910.56	909.55	3.30%	0.81%
40:7	908.54	907.53	0.19%	0.02%
Sum			100.00%	

Phosphatidylserine

Species	m/z	m/z (+ H^+)	Mean	SD
34:1	761.52	762.53	0.97%	0.07%
36:1	789.55	790.56	19.36%	1.28%
36:2	787.54	788.54	4.31%	0.43%
38:1	817.58	818.59	2.87%	0.24%
38:4	811.54	812.54	3.20%	0.27%
40:1	845.61	846.62	1.13%	0.29%
40:4	839.57	840.57	3.46%	0.19%
40:5	837.55	838.56	0.97%	0.16%
40:6	835.54	836.54	62.60%	5.22%
40:7	833.52	834.53	1.13%	0.20%
Sum			100.00%	

X. REFERENCES

1. **Aarli JA, Dua T, Janca A, Muscetta A. 2006.** Neurological disorders: public health challenge**.** *WHO Press ISBN 9789241563369.*

2. **Abbott NJ. 1987.** Glia and the Blood-Brain-Barrier. *Nature 325: 195-195.*

3. **Abbott NJ. 2004.** Evidence for bulk flow of brain interstitial fluid: significance for physiology and pathology. *Neurochem Int 45: 545-552.*

4. **Abbott NJ. 2005.** Dynamics of CNS barriers: evolution, differentiation, and modulation. *Cell Mol Neurobiol 25: 5-23.*

5. **Abbott NJ, Ronnback L, Hansson E. 2006.** Astrocyte-endothelial interactions at the blood-brain barrier. *Nat Rev Neurosci 7: 41-53.*

6. **Abbott NJ, Patabendige AA, Dolman DE, Yusof SR, Begley DJ. 2010.** Structure and function of the blood-brain barrier. *Neurobiol Dis 37: 13-25.*

7. **Adam-Vizi V. 2005.** Production of reactive oxygen species in brain mitochondria: contribution by electron transport chain and non-electron transport chain sources. *Antioxid Redox Signal 7: 1140-1149.*

8. **Adibhatla RM, Hatcher JF, Dempsey RJ. 2006.** Lipids and lipidomics in brain injury and diseases. *AAPS J 8: E314-321.*

9. **Aikins JA, et al. 2005.** Synthesis of a peroxime proliferator activated receptor (PPAR) alpha/gamma agonist via stereocontrolled Williamson ether synthesis and stereospecific SN2 reaction of S-2-chloro propionic acid with phenoxides. *J Org Chem 70: 4695-4705.*

10. **Albayrak R, Degirmenci B, Acar M, Haktanir A, Colbay M, Yaman M. 2007.** Doppler sonography evaluation of flow velocity and volume of the extracranial internal carotid and vertebral arteries in healthy adults. *J Clin Ultrasound 35: 27-33.*

11. **Albert CJ, Anbukumar DS, Messner MC, Ford DA. 2009.** Chromatographic methods for the analyses of 2-halofatty aldehydes and chlorohydrin molecular species of lysophosphatidylcholine. *J Chromatogr B Analyt Technol Biomed Life Sci 877: 2768-2777.*

12. **Albert CJ, Crowley JR, Hsu FF, Thukkani AK, Ford DA. 2001.** Reactive chlorinating species produced by myeloperoxidase target the vinyl ether bond of plasmalogens: identification of 2-chlorohexadecanal. *J Biol Chem 276: 23733-23741.*

13. **Alexander JJ, Snyder A, Tonsgard JH. 1998.** Omega-oxidation of monocarboxylic acids in rat brain. *Neurochem Res 23: 227-233.*

14. **Allt G, Lawrenson JG. 2001.** Pericytes: cell biology and pathology. *Cells Tissues Organs 169: 1-11.*

15. **Ames A, 3rd, Wright RL, Kowada M, Thurston JM, Majno G. 1968.** Cerebral ischemia. II. The no-reflow phenomenon. *Am J Pathol 52: 437-453.*

16. **Amor S, Puentes F, Baker D, van der Valk P. 2010.** Inflammation in neurodegenerative diseases. *Immunology 129: 154-169.*

17. **Anbukumar DS, Shornick LP, Albert CJ, Steward MM, Zoeller RA, Neumann WL, Ford DA. 2010.** Chlorinated lipid species in activated human neutrophils: lipid metabolites of 2-chlorohexadecanal. *J Lipid Res 51: 1085-1092.*

18. **Anderson JC, McFarland BC, Gladson CL. 2008.** New molecular targets in angiogenic vessels of glioblastoma tumours. *Expert Rev Mol Med 10: e23.*

19. **Andriopoulou P, Navarro P, Zanetti A, Lampugnani MG, Dejana E. 1999.** Histamine induces tyrosine phosphorylation of endothelial cell-to-cell adherens junctions. *Arterioscler Thromb Vasc Biol 19: 2286-2297.*

20. **Armulik A, Abramsson A, Betsholtz C. 2005.** Endothelial/pericyte interactions. *Circ Res 97: 512-523.*

21. **Armulik A, et al. 2010.** Pericytes regulate the blood-brain barrier. *Nature 468: 557-561.*

22. **Arnhold J, Osipov AN, Spalteholz H, Panasenko OM, Schiller J. 2002.** Formation of lysophospholipids from unsaturated phosphatidylcholines under the influence of hypochlorous acid. *Biochim Biophys Acta 1572: 91-100.*

23. **Attwell D, Buchan AM, Charpak S, Lauritzen M, Macvicar BA, Newman EA. 2010.** Glial and neuronal control of brain blood flow. *Nature 468: 232-243.*

24. **Auffinger P, Hays FA, Westhof E, Ho PS. 2004.** Halogen bonds in biological molecules. *Proc Natl Acad Sci U S A 101: 16789-16794.*

25. **Baars BJ, Gage NM. 2010.** Cognition, brain, and consciousness: introduction to cognitive neuroscience - 2nd ed. *Elsevier ISBN 9780123750709.*

26. **Bajramovic JJ. 2011.** Regulation of innate immune responses in the central nervous system. *CNS Neurol Disord Drug Targets 10: 4-24.*

27. **Balda MS, Matter K. 2009.** Tight junctions and the regulation of gene expression. *Biochim Biophys Acta 1788: 761-767.*

28. **Balda MS, Garrett MD, Matter K. 2003.** The ZO-1-associated Y-box factor ZONAB regulates epithelial cell proliferation and cell density. *J Cell Biol 160: 423-432.*

29. **Baldus S, et al. 2001.** Endothelial transcytosis of myeloperoxidase confers specificity to vascular ECM proteins as targets of tyrosine nitration. *J Clin Invest 108: 1759-1770.*

30. **Ballard C, Gauthier S, Corbett A, Brayne C, Aarsland D, Jones E. 2011.** Alzheimer's disease. *Lancet 377: 1019-1031.*

31. **Bandyopadhyay U, Das D, Banerjee RK. 1999.** Reactive oxygen species: Oxidative damage and pathogenesis. *Current Science 77: 658-666.*

32. **Banks WA, Robinson SM. 2010.** Minimal penetration of lipopolysaccharide across the murine blood-brain barrier. *Brain Behav Immun 24: 102-109.*

33. **Banks WA, Erickson MA. 2010.** The blood-brain barrier and immune function and dysfunction. *Neurobiol Dis 37: 26-32.*

34. **Barker RA, Barasi S, Neal MJ. 1999.** Neuroscience at a Glance. *Blackwell Science Ltd. ISBN: 0865428727.*

35. **Barnham KJ, Masters CL, Bush AI. 2004**. Neurodegenerative diseases and oxidative stress. *Nat Rev Drug Discov 3: 205-214.*

36. **Barrientos SA, Martinez NW, Yoo S, Jara JS, Zamorano S, Hetz C, Twiss JL, Alvarez J, Court FA. 2011.** Axonal degeneration is mediated by the mitochondrial permeability transition pore. *J Neurosci 31: 966-978.*

37. **Bauer H, Zweimueller-Mayer J, Steinbacher P, Lametschwandtner A, Bauer HC. 2010.** The dual role of zonula occludens (ZO) proteins. *J Biomed Biotechnol 2010: 402593.*

38. **Bazan NG. 2003.** Synaptic lipid signaling: significance of polyunsaturated fatty acids and platelet-activating factor. *J Lipid Res 44: 2221-2233.*

39. **Bazan NG. 2005**. Lipid signaling in neural plasticity, brain repair, and neuroprotection. *Mol Neurobiol 32: 89-103.*

40. **Bazzoni G, Dejana E. 2004.** Endothelial cell-to-cell junctions: molecular organization and role in vascular homeostasis. *Physiol Rev 84: 869-901.*

41. **Beal MF. 2001**. Experimental models of Parkinson's disease. *Nat Rev Neurosci 2: 325-334.*

42. **Bedner E, Li X, Gorczyca W, Melamed MR, Darzynkiewicz Z. 1999.** Analysis of apoptosis by laser scanning cytometry. *Cytometry 35: 181-195.*

43. **Bentes AL, Borges RS, Monteiro WR, de Macedo LG, Alves CN. 2011.** Structure of dihydrochalcones and related derivatives and their scavenging and antioxidant activity against oxygen and nitrogen radical species. *Molecules 16: 1749-1760.*

44. **Bergt C, Reicher H, Malle E, Sattler W. 1999.** Hypochlorite modification of high density lipoprotein: effects on cholesterol efflux from J774 macrophages. *FEBS Lett 452: 295-300.*

45. **Bergt C, Oettl K, Keller W, Andreae F, Leis HJ, Malle E, Sattler W. 2000.** Reagent or myeloperoxidase-generated hypochlorite affects discrete regions in lipid-free and lipid-associated human apolipoprotein A-I. *Biochem J 346 Pt 2: 345-354.*

46. **Bernas T, Dobrucki J. 2002.** Mitochondrial and nonmitochondrial reduction of MTT: interaction of MTT with TMRE, JC-1, and NAO mitochondrial fluorescent probes. *Cytometry 47: 236-242.*

47. **Bernhart E, et al. 2010.** Lysophosphatidic acid receptor activation affects the C13NJ microglia cell line proteome leading to alterations in glycolysis, motility, and cytoskeletal architecture. *Proteomics 10: 141-158.*

48. **Bertram L, Tanzi RE. 2005.** The genetic epidemiology of neurodegenerative disease. *J Clin Invest 115: 1449-1457.*

49. **Betz AL, Gilboe DD, Drewes LR. 1976.** The characteristics of glucose transport across the blood brain barrier and its relation to cerebral glucose metabolism. *Adv Exp Med Biol 69: 133-149.*

50. **Betz AL, Firth JA, Goldstein GW. 1980.** Polarity of the blood-brain barrier: distribution of enzymes between the luminal and antiluminal membranes of brain capillary endothelial cells. *Brain Res 192: 17-28.*

51. **Bianca VD, Dusi S, Bianchini E, Dal Pra I, Rossi F. 1999.** beta-amyloid activates the O-2 forming NADPH oxidase in microglia, monocytes, and neutrophils. A possible inflammatory mechanism of neuronal damage in Alzheimer's disease. *J Biol Chem 274: 15493-15499.*

52. **Binsack R, Boersma BJ, Patel RP, Kirk M, White CR, Darley-Usmar V, Barnes S, Zhou F, Parks DA. 2001.** Enhanced antioxidant activity after chlorination of quercetin by hypochlorous acid. *Alcohol Clin Exp Res 25: 434-443.*

53. **Bleul CC, Fuhlbrigge RC, Casasnovas JM, Aiuti A, Springer TA. 1996.** A highly efficacious lymphocyte chemoattractant, stromal cell-derived factor 1 (SDF-1). *J Exp Med 184: 1101-1109.*

54. **Block ML, Zecca L, Hong JS. 2007.** Microglia-mediated neurotoxicity: uncovering the molecular mechanisms. *Nat Rev Neurosci 8: 57-69.*

55. **Boersma BJ, Patel RP, Kirk M, Jackson PL, Muccio D, Darley-Usmar VM, Barnes S. 1999.** Chlorination and nitration of soy isoflavones. *Arch Biochem Biophys 368: 265-275.*

56. **Boersma BJ, Patel RP, Botting N, White CR, Parks D, Barnes S, Darley-Usmar VM. 2001.** Formation of novel bioactive metabolites from the reactions of pro-inflammatory oxidants with polyphenolics. *Biofactors 15: 79-81.*

57. **Bohatschek M, Werner A, Raivich G. 2001.** Systemic LPS injection leads to granulocyte influx into normal and injured brain: effects of ICAM-1 deficiency. *Exp Neurol 172: 137-152.*

58. **Bornemann KD, Staufenbiel M. 2000.** Transgenic mouse models of Alzheimer's disease. *Ann N Y Acad Sci 908: 260-266.*

59. **Bourre JM. 2006a.** Effects of nutrients (in food) on the structure and function of the nervous system: update on dietary requirements for brain. Part 2 : macronutrients. *J Nutr Health Aging 10: 386-399.*

60. **Bourre JM. 2006b.** Effects of nutrients (in food) on the structure and function of the nervous system: update on dietary requirements for brain. Part 1: micronutrients. *J Nutr Health Aging 10: 377-385.*

61. **Boveris A, Chance B. 1973.** The mitochondrial generation of hydrogen peroxide. General properties and effect of hyperbaric oxygen. *Biochem J 134: 707-716.*

62. **Boyer J, Liu RH. 2004.** Apple phytochemicals and their health benefits. *Nutr J 3: 5.*

63. **Brahmbhatt VV, Albert CJ, Anbukumar DS, Cunningham BA, Neumann WL, Ford DA. 2010a.** {omega}-Oxidation of {alpha}-chlorinated fatty acids: Identification of {alpha}-chlorinated dicarboxylic acids. *J Biol Chem.*

64. **Brahmbhatt VV, Albert CJ, Anbukumar DS, Cunningham BA, Neumann WL, Ford DA. 2010b.** {Omega}-oxidation of {alpha}-chlorinated fatty acids: identification of {alpha}-chlorinated dicarboxylic acids. *J Biol Chem 285: 41255-41269.*

65. **Brandes RP, Koddenberg G, Gwinner W, Kim DY, Kruse HJ, Busse R, Mugge A. 1999.** Role of increased production of superoxide anions by NAD(P)H oxidase and xanthine oxidase in prolonged endotoxemia. *Hypertension 33: 1243-1249.*

66. **Breckwoldt MO, Chen JW, Stangenberg L, Aikawa E, Rodriguez E, Qiu S, Moskowitz MA, Weissleder R. 2008.** Tracking the inflammatory response in stroke in vivo by sensing the enzyme myeloperoxidase. *Proc Natl Acad Sci U S A 105: 18584-18589.*

67. **Brennan ML, et al. 2002.** A tale of two controversies: defining both the role of peroxidases in nitrotyrosine formation in vivo using eosinophil peroxidase and myeloperoxidase-deficient mice, and the nature of peroxidase-generated reactive nitrogen species. *J Biol Chem 277: 17415-17427.*

68. **Brightman MW, Reese TS. 1969.** Junctions between intimately apposed cell membranes in the vertebrate brain. *J Cell Biol 40: 648-677.*

69. **Brinkmann V, Zychlinsky A. 2007.** Beneficial suicide: why neutrophils die to make NETs. *Nat Rev Microbiol 5: 577-582.*

70. **Brinkmann V, Reichard U, Goosmann C, Fauler B, Uhlemann Y, Weiss DS, Weinrauch Y, Zychlinsky A. 2004.** Neutrophil extracellular traps kill bacteria. *Science 303: 1532-1535.*

71. **Broughton BR, Reutens DC, Sobey CG. 2009.** Apoptotic mechanisms after cerebral ischemia. *Stroke 40: e331-339.*

72. **Brown AG. 2001.** Nerve cells and nervous systems: An introduction to neuroscience - 2nd edition. *Springer ISBN: 3540760903.*

73. **Brown PD, Davies SL, Speake T, Millar ID. 2004.** Molecular mechanisms of cerebrospinal fluid production. *Neuroscience 129: 957-970.*

74. **Bundgaard M, Abbott NJ. 2008.** All vertebrates started out with a glial blood-brain barrier 4-500 million years ago. *Glia 56: 699-708.*

75. **Campello S, Scorrano L. 2010.** Mitochondrial shape changes: orchestrating cell pathophysiology. *EMBO Rep 11: 678-684.*

76. **Candelario-Jalil E, Taheri S, Yang Y, Sood R, Grossetete M, Estrada EY, Fiebich BL, Rosenberg GA. 2007.** Cyclooxygenase inhibition limits blood-brain barrier disruption following intracerebral injection of tumor necrosis factor-alpha in the rat. *Journal of Pharmacology and Experimental Therapeutics 323: 488-498.*

77. **Cardona AE, Li M, Liu L, Savarin C, Ransohoff RM. 2008.** Chemokines in and out of the central nervous system: much more than chemotaxis and inflammation. *J Leukoc Biol 84: 587-594.*

78. **Cardoso FL, Brites D, Brito MA. 2010.** Looking at the blood-brain barrier: molecular anatomy and possible investigation approaches. *Brain Res Rev 64: 328-363.*

79. **Carlson T, Kroenke M, Rao P, Lane TE, Segal B. 2008.** The Th17-ELR+ CXC chemokine pathway is essential for the development of central nervous system autoimmune disease. *J Exp Med 205: 811-823.*

80. **Carmeliet P, et al. 1999.** Targeted deficiency or cytosolic truncation of the VE-cadherin gene in mice impairs VEGF-mediated endothelial survival and angiogenesis. *Cell 98: 147-157.*

81. **Carr AC, van den Berg JJ, Winterbourn CC. 1998.** Differential reactivities of hypochlorous and hypobromous acids with purified Escherichia coli phospholipid: formation of haloamines and halohydrins. *Biochim Biophys Acta 1392: 254-264.*

82. **Carr AC, Vissers MC, Domigan NM, Winterbourn CC. 1997a.** Modification of red cell membrane lipids by hypochlorous acid and haemolysis by preformed lipid chlorohydrins. *Redox Rep 3: 263-271.*

83. **Carr AC, Winterbourn CC, Blunt JW, Phillips AJ, Abell AD. 1997b.** Nuclear magnetic resonance characterization of 6 alpha-chloro-5 beta-cholestane-3 beta,5-diol formed from the reaction of hypochlorous acid with cholesterol. *Lipids 32: 363-367.*

84. **Carvey PM, Hendey B, Monahan AJ. 2009.** The blood-brain barrier in neurodegenerative disease: a rhetorical perspective. *J Neurochem 111: 291-314.*

85. **Cattelotte J, Tournier N, Rizzo-Padoin N, Schinkel AH, Scherrmann JM, Cisternino S. 2009.** Changes in dipole membrane potential at the mouse blood-brain barrier enhance the transport of 99mTechnetium Sestamibi more than inhibiting Abcb1, Abcc1, or Abcg2. *J Neurochem 108: 767-775.*

86. **Cernak I, Vink R, Zapple DN, Cruz MI, Ahmed F, Chang T, Fricke ST, Faden AI. 2004.** The pathobiology of moderate diffuse traumatic brain injury as identified using a new experimental model of injury in rats. *Neurobiol Dis 17: 29-43.*

87. **Charo IF, Ransohoff RM. 2006.** The many roles of chemokines and chemokine receptors in inflammation. *N Engl J Med 354: 610-621.*

88. **Chen-Quay SC, Eiting KT, Li AW, Lamharzi N, Quay SC. 2009.** Identification of tight junction modulating lipids. *J Pharm Sci 98: 606-619.*

89. **Choi BM, Chen XY, Gao SS, Zhu R, Kim BR. 2011.** Anti-apoptotic effect of phloretin on cisplatin-induced apoptosis in HEI-OC1 auditory cells. *Pharmacol Rep 63: 708-716.*

90. **Choi DK, Koppula S, Choi M, Suk K. 2010.** Recent developments in the inhibitors of neuroinflammation and neurodegeneration: inflammatory oxidative enzymes as a drug target. *Expert Opin Ther Pat 20: 1531-1546.*

91. **Choi DK, et al. 2005.** Ablation of the inflammatory enzyme myeloperoxidase mitigates features of Parkinson's disease in mice. *J Neurosci 25: 6594-6600.*

92. **Choi JJ, Choi J, Kang CD, Chen X, Wu CF, Ko KH, Kim WK. 2007a.** Hydrogen peroxide induces the death of astrocytes through the down-regulation of the constitutive nuclear factor-kappaB activity. *Free Radic Res 41: 555-562.*

93. **Choi JM, Yoon BS, Lee SK, Hwang JK, Ryang R. 2007b.** Antioxidant properties of neohesperidin dihydrochalcone: inhibition of hypochlorous acid-induced DNA strand breakage, protein degradation, and cell death. *Biol Pharm Bull 30: 324-330.*

94. **Chu ZG, Zhang JP, Song HP, Hu JY, Zhang Q, Xiang F, Huang YS. 2010.** p38 MAP kinase mediates burn serum-induced endothelial barrier dysfunction: involvement of F-actin rearrangement and L-caldesmon phosphorylation. *Shock 34: 222-228.*

95. **Cimini A, Bernardo A, Cifone MG, Di Marzio L, Di Loreto S. 2003.** TNFalpha downregulates PPARdelta expression in oligodendrocyte progenitor cells: implications for demyelinating diseases. *Glia 41: 3-14.*

96. **Cirrito JR, et al. 2005.** P-glycoprotein deficiency at the blood-brain barrier increases amyloid-beta deposition in an Alzheimer disease mouse model. *J Clin Invest 115: 3285-3290.*

97. **Clark SR, et al. 2007.** Platelet TLR4 activates neutrophil extracellular traps to ensnare bacteria in septic blood. *Nat Med 13: 463-469.*

98. **Claude P. 1978.** Morphological factors influencing transepithelial permeability: a model for the resistance of the zonula occludens. *J Membr Biol 39: 219-232.*

99. **Coisne C, Engelhardt B. 2011.** Tight Junctions in Brain Barriers during CNS Inflammation. *Antioxid Redox Signal.*

100. **Colgan OC, Collins NT, Ferguson G, Murphy RP, Birney YA, Cahill PA, Cummins PM. 2008**. Influence of basolateral condition on the regulation of brain microvascular endothelial tight junction properties and barrier function. *Brain Res 1193: 84-92.*

101. **Collado MP, Latorre E, Fernandez I, Aragones MD, Catalan RE. 2003.** Endothelin-1 decreases ethanolamine plasmalogen levels and evokes PAF production in brain microvessels. *Microvasc Res 66: 197-203.*

102. **Collins XH, et al. 2005.** Omega-oxidation of 20-hydroxyeicosatetraenoic acid (20-HETE) in cerebral microvascular smooth muscle and endothelium by alcohol dehydrogenase 4. *J Biol Chem 280: 33157-33164.*

103. **Compston A, Sawcer S. 2002.** Genetic analysis of multiple sclerosis. *Curr Neurol Neurosci Rep 2: 259-266.*

104. **Corada M, et al. 1999.** Vascular endothelial-cadherin is an important determinant of microvascular integrity in vivo. *Proc Natl Acad Sci U S A 96: 9815-9820.*

105. **Cowburn AS, Condliffe AM, Farahi N, Summers C, Chilvers ER. 2008.** Advances in neutrophil biology: clinical implications. *Chest 134: 606-612.*

106. **Crawford FC, Freeman MJ, Schinka JA, Morris MD, Abdullah LI, Richards D, Sevush S, Duara R, Mullan MJ. 2001.** Association between Alzheimer's disease and a functional polymorphism in the Myeloperoxidase gene. *Exp Neurol 167: 456-459.*

107. **Crespy V, Morand C, Besson C, Manach C, Demigne C, Remesy C. 2001a.** Comparison of the intestinal absorption of quercetin, phloretin and their glucosides in rats. *J Nutr 131: 2109-2114.*

108. **Crespy V, Aprikian O, Morand C, Besson C, Manach C, Demigne C, Remesy C. 2001b.** Bioavailability of phloretin and phloridzin in rats. *J Nutr 131: 3227-3230.*

109. **Crozier A, Del Rio D, Clifford MN. 2010.** Bioavailability of dietary flavonoids and phenolic compounds. *Mol Aspects Med 31: 446-467.*

110. **Curnutte JT, Whitten DM, Babior BM. 1974.** Defective superoxide production by granulocytes from patients with chronic granulomatous disease. *N Engl J Med 290: 593-597.*

111. **Curtis MP, Hicks AJ, Neidigh JW. 2011.** Kinetics of 3-chlorotyrosine formation and loss due to hypochlorous acid and chloramines. *Chem Res Toxicol 24: 418-428.*

112. **Dale DC, Boxer L, Liles WC. 2008.** The phagocytes: neutrophils and monocytes. *Blood 112: 935-945.*

113. **Dantzer R, O'Connor JC, Freund GG, Johnson RW, Kelley KW. 2008.** From inflammation to sickness and depression: when the immune system subjugates the brain. *Nat Rev Neurosci 9: 46-56.*

114. **Darvesh AS, Carroll RT, Bishayee A, Geldenhuys WJ, Van der Schyf CJ. 2010.** Oxidative stress and Alzheimer's disease: dietary polyphenols as potential therapeutic agents. *Expert Rev Neurother 10: 729-745.*

115. **Davies MJ. 2011.** Myeloperoxidase-derived oxidation: mechanisms of biological damage and its prevention. *J Clin Biochem Nutr 48: 8-19.*

116. **Davies MJ, Hawkins CL, Pattison DI, Rees MD. 2008.** Mammalian heme peroxidases: from molecular mechanisms to health implications. *Antioxid Redox Signal 10: 1199-1234.*

117. **Davson H, Oldendorf WH. 1967.** Symposium on membrane transport. Transport in the central nervous system. *Proc R Soc Med 60: 326-329.*

118. **de Boer AG, Gaillard PJ. 2006.** Blood-brain barrier dysfunction and recovery. *J Neural Transm 113: 455-462.*

119. **Dejana E, Lampugnani MG, Martinez-Estrada O, Bazzoni G. 2000.** The molecular organization of endothelial junctions and their functional role in vascular morphogenesis and permeability. *Int J Dev Biol 44: 743-748.*

120. **del Zoppo GJ. 2010.** The neurovascular unit in the setting of stroke. *J Intern Med 267: 156-171.*

121. **Deli MA, Abraham CS, Kataoka Y, Niwa M. 2005.** Permeability studies on in vitro blood-brain barrier models: physiology, pathology, and pharmacology. *Cell Mol Neurobiol 25: 59-127.*

122. **Dembitsky VM, Srebnik M. 2002.** Natural halogenated fatty acids: their analogues and derivatives. *Prog Lipid Res 41: 315-367.*

123. **Dermietzel R, Spray DC, Nedergaard M. 2006** Blood-Brain Barriers: From Ontogeny to Artificial Interfaces. *WILEY-VCH ISBN: 3527310886.*

124. **Dever G, Stewart LJ, Pitt AR, Spickett CM. 2003.** Phospholipid chlorohydrins cause ATP depletion and toxicity in human myeloid cells. *FEBS Lett 540: 245-250.*

125. **Dever G, Wainwright CL, Kennedy S, Spickett CM. 2006.** Fatty acid and phospholipid chlorohydrins cause cell stress and endothelial adhesion. *Acta Biochim Pol 53: 761-768.*

126. **Di Paolo G, Kim TW. 2011.** Linking lipids to Alzheimer's disease: cholesterol and beyond. *Nat Rev Neurosci 12: 284-296.*

127. **Didier N, Romero IA, Creminon C, Wijkhuisen A, Grassi J, Mabondzo A. 2003.** Secretion of interleukin-1beta by astrocytes mediates endothelin-1 and tumour necrosis factor-alpha effects on human brain microvascular endothelial cell permeability. J Neurochem 86: 246-254.

128. **Dietrich JB. 2004.** Endothelial cells of the blood-brain barrier: a target for glucocorticoids and estrogens? Front Biosci 9: 684-693.

129. **DiStasi MR, Ley K. 2009.** Opening the flood-gates: how neutrophil-endothelial interactions regulate permeability. *Trends Immunol 30: 547-556.*

130. **Dodelet-Devillers A, Cayrol R, van Horssen J, Haqqani AS, de Vries HE, Engelhardt B, Greenwood J, Prat A. 2009a.** Functions of lipid raft membrane microdomains at the blood-brain barrier. *J Mol Med 87: 765-774.*

131. **Dodelet-Devillers A, Cayrol R, van Horssen J, Haqqani AS, de Vries HE, Engelhardt B, Greenwood J, Prat A. 2009b.** Functions of lipid raft membrane microdomains at the blood-brain barrier. *J Mol Med (Berl) 87: 765-774.*

132. **Dohrmann GJ. 1970.** The choroid plexus: a historical review. *Brain Research 18: 197-218.*

133. **Dolphin D, Forman A, Borg DC, Fajer J, Felton RH. 1971.** Compounds I of catalase and horse radish peroxidase: pi-cation radicals. *Proc Natl Acad Sci U S A 68: 614-618.*

134. **Douglas PM, Dillin A. 2010.** Protein homeostasis and aging in neurodegeneration. *J Cell Biol 190: 719-729.*

135. **Drake CT, Iadecola C. 2007.** The role of neuronal signaling in controlling cerebral blood flow. *Brain Lang 102: 141-152.*

136. **Ehrenkranz JR, Lewis NG, Kahn CR, Roth J. 2005.** Phlorizin: a review. Diabetes Metab Res Rev 21: 31-38.

137. **Engelhardt B, Sorokin L. 2009.** The blood-brain and the blood-cerebrospinal fluid barriers: function and dysfunction. *Semin Immunopathol 31: 497-511.*

138. **Engelhardt B, Coisne C. 2011.** Fluids and barriers of the CNS establish immune privilege by confining immune surveillance to a two-walled castle moat surrounding the CNS castle. *Fluids Barriers CNS 8: 4.*

139. **Engelmann B. 2004**. Plasmalogens: targets for oxidants and major lipophilic antioxidants. *Biochem Soc Trans 32: 147-150.*

140. **Escarpa A, Gonzalez MC. 1998.** High-performance liquid chromatography with diode-array detection for the determination of phenolic compounds in peel and pulp from different apple varieties. *J Chromatogr A 823: 331-337.*

141. **Eyster KM. 2007.** The membrane and lipids as integral participants in signal transduction: lipid signal transduction for the non-lipid biochemist. *Adv Physiol Educ 31: 5-16.*

142. **Fabian TM, Walker SE. 1982.** Stability of sodium hypochlorite solutions. *Am J Hosp Pharm 39: 1016-1017.*

143. **Fahy E, Subramaniam S, Murphy RC, Nishijima M, Raetz CR, Shimizu T, Spener F, van Meer G, Wakelam MJ, Dennis EA. 2009.** Update of the LIPID MAPS comprehensive classification system for lipids. *J Lipid Res 50 Suppl: S9-14.*

144. **Fahy E, et al. 2005.** A comprehensive classification system for lipids. *J Lipid Res 46: 839-861.*

145. **Fang W, Geng X, Deng Y, Li Y, Shang E, Cen J, Lv P. 2011.** Platelet activating factor induces blood brain barrier permeability alteration in vitro. *J Neuroimmunol 230: 42-47.*

146. **Faraci FM. 2006.** Reactive oxygen species: influence on cerebral vascular tone. *J Appl Physiol 100: 739-743.*

147. **Farooqui AA. 2010.** Studies on plasmalogen-selective phospholipase A2 in brain. *Mol Neurobiol 41: 267-273.*

148. **Farooqui AA, Horrocks LA. 2001a.** Plasmalogens: workhorse lipids of membranes in normal and injured neurons and glia. *Neuroscientist 7: 232-245.*

149. **Farooqui AA, Horrocks LA. 2001b.** Plasmalogens, phospholipase A2, and docosahexaenoic acid turnover in brain tissue. *J Mol Neurosci 16: 263-272; discussion 279-284.*

150. **Farooqui AA, Horrocks LA. 2007.** Glycerophospholipids in Brain: Phospholipases A2 in Neurological Disorders. *Springer ISBN: 9780387366029.*

151. **Farooqui AA, Ong WY, Horrocks LA. 2006.** Inhibitors of brain phospholipase A2 activity: their neuropharmacological effects and therapeutic importance for the treatment of neurologic disorders. *Pharmacol Rev 58: 591-620.*

152. **Farooqui AA, Horrocks LA, Farooqui T. 2007.** Modulation of inflammation in brain: a matter of fat. *J Neurochem 101: 577-599.*

153. **Farooqui AA, Ong WY, Farooqui T. 2010.** Lipid mediators in the nucleus: Their potential contribution to Alzheimer's disease. *Biochim Biophys Acta 1801: 906-916.*

154. **Felde R, Spiteller G. 1995.** Plasmalogen oxidation in human serum lipoproteins. *Chem Phys Lipids 76: 259-267.*

155. **Feng D, Nagy JA, Pyne K, Dvorak HF, Dvorak AM. 1998.** Neutrophils emigrate from venules by a transendothelial cell pathway in response to FMLP. *J Exp Med 187: 903-915.*

156. **Fernandez-Hernando C, Fukata M, Bernatchez PN, Fukata Y, Lin MI, Bredt DS, Sessa WC. 2006.** Identification of Golgi-localized acyl transferases that palmitoylate and regulate endothelial nitric oxide synthase. *J Cell Biol 174: 369-377.*

157. **Fernandez-Novoa L, Cacabelos R. 2001.** Histamine function in brain disorders. *Behav Brain Res 124: 213-233.*

158. **Ferrari CC, Tarelli R. 2011.** Parkinson's disease and systemic inflammation. *Parkinsons Dis 2011: 436813.*

159. **Ferri CP, et al. 2005.** Global prevalence of dementia: a Delphi consensus study. *Lancet 366: 2112-2117.*

160. **Firuzi O, Mladenka P, Petrucci R, Marrosu G, Saso L. 2004.** Hypochlorite scavenging activity of flavonoids. *J Pharm Pharmacol 56: 801-807.*

161. **Fischer S, Wiesnet M, Renz D, Schaper W. 2005.** H2O2 induces paracellular permeability of porcine brain-derived microvascular endothelial cells by activation of the p44/42 MAP kinase pathway. *Eur J Cell Biol 84: 687-697.*

162. **Fischer S, Clauss M, Wiesnet M, Renz D, Schaper W, Karliczek GF. 1999.** Hypoxia induces permeability in brain microvessel endothelial cells via VEGF and NO. *Am J Physiol 276: C812-820.*

163. **Fisher M. 2008.** Injuries to the vascular endothelium: vascular wall and endothelial dysfunction. *Rev Neurol Dis 5 Suppl 1: S4-11.*

164. **Flemmig J, Arnhold J. 2010.** Interaction of hypochlorous acid and myeloperoxidase with phosphatidylserine in the presence of ammonium ions. *J Inorg Biochem 104: 759-764.*

165. **Flemmig J, Spalteholz H, Schubert K, Meier S, Arnhold J. 2009.** Modification of phosphatidylserine by hypochlorous acid. *Chem Phys Lipids 161: 44-50.*

166. **Folch J, Lees M, Sloane Stanley GH. 1957.** A simple method for the isolation and purification of total lipides from animal tissues. *J Biol Chem 226: 497-509.*

167. **Ford DA. 2010.** Lipid oxidation by hypochlorous acid: chlorinated lipids in atherosclerosis and myocardial ischemia. *Clin Lipidol 5: 835-852.*

168. **Forman MS, Trojanowski JQ, Lee VM. 2004.** Neurodegenerative diseases: a decade of discoveries paves the way for therapeutic breakthroughs. *Nat Med 10: 1055-1063.*

169. **Forster C. 2008.** Tight junctions and the modulation of barrier function in disease. *Histochem Cell Biol 130: 55-70.*

170. **Forster C, Burek M, Romero IA, Weksler B, Couraud PO, Drenckhahn D. 2008.** Differential effects of hydrocortisone and TNFalpha on tight junction proteins in an in vitro model of the human blood-brain barrier. *J Physiol 586: 1937-1949.*

171. **Forster C, Silwedel C, Golenhofen N, Burek M, Kietz S, Mankertz J, Drenckhahn D. 2005.** Occludin as direct target for glucocorticoid-induced improvement of blood-brain barrier properties in a murine in vitro system. *J Physiol 565: 475-486.*

172. **Fraga CG, Galleano M, Verstraeten SV, Oteiza PI. 2010.** Basic biochemical mechanisms behind the health benefits of polyphenols. *Mol Aspects Med 31: 435-445.*

173. **Frank-Cannon TC, Alto LT, McAlpine FE, Tansey MG. 2009.** Does neuroinflammation fan the flame in neurodegenerative diseases? *Mol Neurodegener 4: 47.*

174. **Fraser PA. 2011.** The role of free radical generation in increasing cerebrovascular permeability. *Free Radic Biol Med.*

175. **Frisardi V, Panza F, Seripa D, Farooqui T, Farooqui AA. 2011.** Glycerophospholipids and glycerophospholipid-derived lipid mediators: A complex meshwork in Alzheimer's disease pathology. *Prog Lipid Res 50: 313-330.*

176. **Fruhwirth GO, Loidl A, Hermetter A. 2007.** Oxidized phospholipids: from molecular properties to disease. *Biochim Biophys Acta 1772: 718-736.*

177. **Fukumoto K, Takagi N, Yamamoto R, Moriyama Y, Takeo S, Tanonaka K. 2010.** Prostanoid EP1 receptor antagonist reduces blood-brain barrier leakage after cerebral ischemia. *Eur J Pharmacol 640: 82-86.*

178. **Furey ML. 2011.** The prominent role of stimulus processing: cholinergic function and dysfunction in cognition. *Curr Opin Neurol 24: 364-370.*

179. **Galasko D, Montine TJ. 2010.** Biomarkers of oxidative damage and inflammation in Alzheimer's disease. *Biomark Med 4: 27-36.*

180. **Galea I, Bechmann I, Perry VH. 2007.** What is immune privilege (not)? *Trends Immunol 28: 12-18.*

181. **Galleano M, Verstraeten SV, Oteiza PI, Fraga CG. 2010.** Antioxidant actions of flavonoids: thermodynamic and kinetic analysis. *Arch Biochem Biophys 501: 23-30.*

182. **Gao HM, Hong JS. 2008.** Why neurodegenerative diseases are progressive: uncontrolled inflammation drives disease progression. *Trends Immunol 29: 357-365.*

183. **Gao HM, Liu B, Zhang W, Hong JS. 2003.** Critical role of microglial NADPH oxidase-derived free radicals in the in vitro MPTP model of Parkinson's disease. *FASEB J 17: 1954-1956.*

184. **Gao HM, Jiang J, Wilson B, Zhang W, Hong JS, Liu B. 2002.** Microglial activation-mediated delayed and progressive degeneration of rat nigral dopaminergic neurons: relevance to Parkinson's disease. *J Neurochem 81: 1285-1297.*

185. **Gao Y, Signore AP, Yin W, Cao G, Yin XM, Sun F, Luo Y, Graham SH, Chen J. 2005.** Neuroprotection against focal ischemic brain injury by inhibition of c-Jun N-terminal kinase and attenuation of the mitochondrial apoptosis-signaling pathway. *J Cereb Blood Flow Metab 25: 694-712.*

186. **Gibbons HM, Dragunow M. 2006.** Microglia induce neural cell death via a proximity-dependent mechanism involving nitric oxide. *Brain Res 1084: 1-15.*

187. **Ginsberg L, Rafique S, Xuereb JH, Rapoport SI, Gershfeld NL. 1995.** Disease and anatomic specificity of ethanolamine plasmalogen deficiency in Alzheimer's disease brain. *Brain Res 698: 223-226.*

188. **Girouard H, Iadecola C. 2006.** Neurovascular coupling in the normal brain and in hypertension, stroke, and Alzheimer disease. *J Appl Physiol 100: 328-335.*

189. **Glaser PE, Gross RW. 1995.** Rapid plasmenylethanolamine-selective fusion of membrane bilayers catalyzed by an isoform of glyceraldehyde-3-phosphate dehydrogenase: discrimination between glycolytic and fusogenic roles of individual isoforms. *Biochemistry 34: 12193-12203.*

190. **Glass CK, Saijo K, Winner B, Marchetto MC, Gage FH. 2010.** Mechanisms underlying inflammation in neurodegeneration. *Cell 140: 918-934.*

191. **Godbout JP, Chen J, Abraham J, Richwine AF, Berg BM, Kelley KW, Johnson RW. 2005.** Exaggerated neuroinflammation and sickness behavior in aged mice following activation of the peripheral innate immune system. *FASEB J 19: 1329-1331.*

192. **Goldblum SE, et al. 2011.** The active Zot domain (aa 288-293) increases ZO-1 and myosin 1C serine/threonine phosphorylation, alters interaction between ZO-1 and its binding partners, and induces tight junction disassembly through proteinase activated receptor 2 activation. *FASEB J 25: 144-158.*

193. **Gonsiorek W, et al. 2007.** Pharmacological characterization of Sch527123, a potent allosteric CXCR1/CXCR2 antagonist. *J Pharmacol Exp Ther 322: 477-485.*

194. **Gonzalez-Mariscal L, Tapia R, Chamorro D. 2008.** Crosstalk of tight junction components with signaling pathways. *Biochim Biophys Acta 1778: 729-756.*

195. **Gonzalez-Mariscal L, Quiros M, Diaz-Coranguez M. 2011.** ZO Proteins and Redox-Dependent Processes. *Antioxid Redox Signal 15: 1235-1253.*

196. **Gonzalez-Mariscal L, Tapia R, Huerta M, Lopez-Bayghen E. 2009.** The tight junction protein ZO-2 blocks cell cycle progression and inhibits cyclin D1 expression. *Ann N Y Acad Sci 1165: 121-125.*

197. **Goodenowe DB, et al. 2007.** Peripheral ethanolamine plasmalogen deficiency: a logical causative factor in Alzheimer's disease and dementia. *J Lipid Res 48: 2485-2498.*

198. **Gorgas K, Teigler A, Komljenovic D, Just WW. 2006.** The ether lipid-deficient mouse: tracking down plasmalogen functions. *Biochim Biophys Acta 1763: 1511-1526.*

199. **Goti D, Balazs Z, Panzenboeck U, Hrzenjak A, Reicher H, Wagner E, Zechner R, Malle E, Sattler W. 2002.** Effects of lipoprotein lipase on uptake and transcytosis of low density lipoprotein (LDL) and LDL-associated alpha-tocopherol in a porcine in vitro blood-brain barrier model. *J Biol Chem 277: 28537-28544.*

200. **Graeber MB. 2010.** Changing face of microglia. *Science 330: 783-788.*

201. **Graham SM, McCullough LD, Murphy SJ. 2004.** Animal models of ischemic stroke: balancing experimental aims and animal care. *Comp Med 54: 486-496.*

202. **Grammas P, Martinez J, Miller B. 2011.** Cerebral microvascular endothelium and the pathogenesis of neurodegenerative diseases. *Expert Rev Mol Med 13: e19.*

203. **Green PS, Mendez AJ, Jacob JS, Crowley JR, Growdon W, Hyman BT, Heinecke JW. 2004.** Neuronal expression of myeloperoxidase is increased in Alzheimer's disease. *J Neurochem 90: 724-733.*

204. **Greenwood J, Heasman SJ, Alvarez JI, Prat A, Lyck R, Engelhardt B. 2011.** Review: leucocyte-endothelial cell crosstalk at the blood-brain barrier: a prerequisite for successful immune cell entry to the brain. *Neuropathol Appl Neurobiol 37: 24-39.*

205. **Grone HJ, Grone EF, Malle E. 2002.** Immunohistochemical detection of hypochlorite-modified proteins in glomeruli of human membranous glomerulonephritis. *Lab Invest 82: 5-14.*

206. **Gschwendt M, Dieterich S, Rennecke J, Kittstein W, Mueller HJ, Johannes FJ. 1996.** Inhibition of protein kinase C mu by various inhibitors. Differentiation from protein kinase c isoenzymes. *FEBS Lett 392: 77-80.*

207. **Gupta AK, Joshi MB, Philippova M, Erne P, Hasler P, Hahn S, Resink TJ. 2010.** Activated endothelial cells induce neutrophil extracellular traps and are susceptible to NETosis-mediated cell death. *FEBS Lett 584: 3193-3197.*

208. **Gutierrez-Merino C, Lopez-Sanchez C, Lagoa R, Samhan-Arias AK, Bueno C, Garcia-Martinez V. 2011.** Neuroprotective actions of flavonoids. *Curr Med Chem 18: 1195-1212.*

209. **Haass C. 2010.** Initiation and propagation of neurodegeneration. *Nat Med 16: 1201-1204.*

210. **Haley PJ. 2003.** Species differences in the structure and function of the immune system. *Toxicology 188: 49-71.*

211. **Halliwell B. 2001.** Role of free radicals in the neurodegenerative diseases: therapeutic implications for antioxidant treatment. *Drugs Aging 18: 685-716.*

212. **Halliwell B. 2006.** Oxidative stress and neurodegeneration: where are we now? *J Neurochem 97: 1634-1658.*

213. **Halliwell B, Whiteman M. 2004.** Measuring reactive species and oxidative damage in vivo and in cell culture: how should you do it and what do the results mean? *Br J Pharmacol 142: 231-255.*

214. **Hamilton NB, Attwell D, Hall CN. 2010.** Pericyte-mediated regulation of capillary diameter: a component of neurovascular coupling in health and disease. *Front Neuroenergetics 2.*

215. **Hampton MB, Kettle AJ, Winterbourn CC. 1998.** Inside the neutrophil phagosome: oxidants, myeloperoxidase, and bacterial killing. *Blood 92: 3007-3017.*

216. **Han X. 2005.** Lipid alterations in the earliest clinically recognizable stage of Alzheimer's disease: implication of the role of lipids in the pathogenesis of Alzheimer's disease. *Curr Alzheimer Res 2: 65-77.*

217. **Han X, Holtzman DM, McKeel DW, Jr. 2001.** Plasmalogen deficiency in early Alzheimer's disease subjects and in animal models: molecular characterization using electrospray ionization mass spectrometry. *J Neurochem 77: 1168-1180.*

218. **Han XL, Gross RW. 1990.** Plasmenylcholine and phosphatidylcholine membrane bilayers possess distinct conformational motifs. *Biochemistry 29: 4992-4996.*

219. **Handa O, Naito Y, Yoshikawa T. 2010.** Helicobacter pylori: a ROS-inducing bacterial species in the stomach. *Inflamm Res 59: 997-1003.*

220. **Hanisch UK, Kettenmann H. 2007.** Microglia: active sensor and versatile effector cells in the normal and pathologic brain. *Nat Neurosci 10: 1387-1394.*

221. **Hannun YA. 1996.** Functions of ceramide in coordinating cellular responses to stress. *Science 274: 1855-1859.*

222. **Haorah J, Knipe B, Leibhart J, Ghorpade A, Persidsky Y. 2005.** Alcohol-induced oxidative stress in brain endothelial cells causes blood-brain barrier dysfunction. *J Leukoc Biol 78: 1223-1232.*

223. **Harke N, Leers J, Kietz S, Drenckhahn D, Forster C. 2008.** Glucocorticoids regulate the human occludin gene through a single imperfect palindromic glucocorticoid response element. *Mol Cell Endocrinol 295: 39-47.*

224. **Hartmann T, Kuchenbecker J, Grimm MO. 2007.** Alzheimer's disease: the lipid connection. *J Neurochem 103 Suppl 1: 159-170.*

225. **Harukuni I, Bhardwaj A. 2006.** Mechanisms of brain injury after global cerebral ischemia. *Neurol Clin 24: 1-21.*

226. **Hawkins BT, Davis TP. 2005.** The blood-brain barrier/neurovascular unit in health and disease. *Pharmacol Rev 57: 173-185.*

227. **Hawkins BT, Egleton RD. 2006.** Fluorescence imaging of blood-brain barrier disruption. *J Neurosci Methods 151: 262-267.*

228. **Hawkins CL. 2009.** The role of hypothiocyanous acid (HOSCN) in biological systems. *Free Radic Res 43: 1147-1158.*

229. **Hawkins CL, Pattison DI, Davies MJ. 2003.** Hypochlorite-induced oxidation of amino acids, peptides and proteins. *Amino Acids 25: 259-274.*

230. **Hawkins RA, O'Kane RL, Simpson IA, Vina JR. 2006.** Structure of the blood-brain barrier and its role in the transport of amino acids. *J Nutr 136: 218S-226S.*

231. **Hazell LJ, Arnold L, Flowers D, Waeg G, Malle E, Stocker R. 1996.** Presence of hypochlorite-modified proteins in human atherosclerotic lesions. *J Clin Invest 97: 1535-1544.*

232. **Hazen SL, Hsu FF, Mueller DM, Crowley JR, Heinecke JW. 1996.** Human neutrophils employ chlorine gas as an oxidant during phagocytosis. *J Clin Invest 98: 1283-1289.*

233. **He P. 2010.** Leucocyte/endothelium interactions and microvessel permeability: coupled or uncoupled? *Cardiovasc Res 87: 281-290.*

234. **Henderson JP, Byun J, Heinecke JW. 1999.** Molecular chlorine generated by the myeloperoxidase-hydrogen peroxide-chloride system of phagocytes produces 5-chlorocytosine in bacterial RNA. *J Biol Chem 274: 33440-33448.*

235. **Hernandes MZ, Cavalcanti SM, Moreira DR, de Azevedo Junior WF, Leite AC. 2010.** Halogen atoms in the modern medicinal chemistry: hints for the drug design. *Curr Drug Targets 11: 303-314.*

236. **Herrmann W, Obeid R. 2011.** Biomarkers of neurodegenerative diseases. *Clin Chem Lab Med 49: 343-344.*

237. **Holman DW, Klein RS, Ransohoff RM. 2011.** The blood-brain barrier, chemokines and multiple sclerosis. *Biochim Biophys Acta 1812: 220-230.*

238. **Horrocks LA, Farooqui AA, Ong WY. 2006.** Inhibitors of brain phospholipase A(2) activity: Their neuropharmacological effects and therapeutic importance for the treatment of neurologic disorders. *Pharmacological Reviews 58: 591-620.*

239. **Huber JD, Egleton RD, Davis TP. 2001.** Molecular physiology and pathophysiology of tight junctions in the blood-brain barrier. *Trends Neurosci 24: 719-725.*

240. **Hulshoff Pol HE, Schnack HG, Bertens MG, van Haren NE, van der Tweel I, Staal WG, Baare WF, Kahn RS. 2002.** Volume changes in gray matter in patients with schizophrenia. *Am J Psychiatry 159: 244-250.*

241. **Iadecola C. 2004.** Neurovascular regulation in the normal brain and in Alzheimer's disease. *Nat Rev Neurosci 5: 347-360.*

242. **Iadecola C. 2010.** The overlap between neurodegenerative and vascular factors in the pathogenesis of dementia. *Acta Neuropathol 120: 287-296.*

243. **Inglis VI, Jones MP, Tse AD, Easton AS. 2004.** Neutrophils both reduce and increase permeability in a cell culture model of the blood-brain barrier. *Brain Res 998: 218-229.*

244. **Ingrand SS, Wahl A, Favreliere S, Barbot F, Tallineau C. 2000.** Quantification of long-chain aldehydes by gas chromatography coupled to mass spectrometry as a tool for simultaneous measurement of plasmalogens and their aldehydic breakdown products. *Anal Biochem 280: 65-72.*

245. **Javesghani D, Hussain SN, Scheidel J, Quinn MT, Magder SA. 2003.** Superoxide production in the vasculature of lipopolysaccharide-treated rats and pigs. *Shock 19: 486-493.*

246. **Jeitner TM, Voloshyna I, Reiss AB. 2011.** Oxysterol derivatives of cholesterol in neurodegenerative disorders. *Curr Med Chem 18: 1515-1525.*

247. **Jensen MD, Sheng W, Simonyi A, Johnson GS, Sun AY, Sun GY. 2009.** Involvement of oxidative pathways in cytokine-induced secretory phospholipase A2-IIA in astrocytes. *Neurochem Int 55: 362-368.*

248. **Jerlich A, Fritz G, Kharrazi H, Hammel M, Tschabuschnig S, Glatter O, Schaur RJ. 2000.** Comparison of HOCl traps with myeloperoxidase inhibitors in prevention of low density lipoprotein oxidation. *Biochim Biophys Acta 1481: 109-118.*

249. **Ji KA, Yang MS, Jeong HK, Min KJ, Kang SH, Jou I, Joe EH. 2007.** Resident microglia die and infiltrated neutrophils and monocytes become major inflammatory cells in lipopolysaccharide-injected brain. *Glia 55: 1577-1588.*

250. **Jin AY, Tuor UI, Rushforth D, Kaur J, Muller RN, Petterson JL, Boutry S, Barber PA. 2010.** Reduced blood brain barrier breakdown in P-selectin deficient mice following transient ischemic stroke: a future therapeutic target for treatment of stroke. *BMC Neurosci 11: 12.*

251. **Johanson CE, Duncan JA, 3rd, Klinge PM, Brinker T, Stopa EG, Silverberg GD. 2008.** Multiplicity of cerebrospinal fluid functions: New challenges in health and disease. *Cerebrospinal Fluid Res 5: 10.*

252. **Johnson AC, Mc NA, Rossiter RJ. 1949.** Chemical studies of peripheral nerve during Wallerian degeneration; lipids. *Biochem J 45: 500-508.*

253. **Jung YS, Jeong EM, Park EK, Kim YM, Sohn S, Lee SH, Baik EJ, Moon CH. 2008.** Cadmium induces apoptotic cell death through p38 MAPK in brain microvessel endothelial cells. *Eur J Pharmacol 578: 11-18.*

254. **Kahle K, Kraus M, Richling E. 2005.** Polyphenol profiles of apple juices. *Mol Nutr Food Res 49: 797-806.*

255. **Kahles T, Luedike P, Endres M, Galla HJ, Steinmetz H, Busse R, Neumann-Haefelin T, Brandes RP. 2007.** NADPH oxidase plays a central role in blood-brain barrier damage in experimental stroke. *Stroke 38: 3000-3006.*

256. **Kallmann BA, Wagner S, Hummel V, Buttmann M, Bayas A, Tonn JC, Rieckmann P. 2002.** Characteristic gene expression profile of primary human cerebral endothelial cells. *FASEB J 16: 589-591.*

257. **Kalyvas A, David S. 2004.** Cytosolic phospholipase A2 plays a key role in the pathogenesis of multiple sclerosis-like disease. *Neuron 41: 323-335.*

258. **Kantari C, Pederzoli-Ribeil M, Witko-Sarsat V. 2008.** The role of neutrophils and monocytes in innate immunity. *Contrib Microbiol 15: 118-146.*

259. **Kassner A, Roberts TP, Moran B, Silver FL, Mikulis DJ. 2009.** Recombinant tissue plasminogen activator increases blood-brain barrier disruption in acute ischemic stroke: an MR imaging permeability study. *AJNR Am J Neuroradiol 30: 1864-1869.*

260. **Katsuno T, et al. 2008.** Deficiency of zonula occludens-1 causes embryonic lethal phenotype associated with defected yolk sac angiogenesis and apoptosis of embryonic cells. *Mol Biol Cell 19: 2465-2475.*

261. **Kawai Y, Kiyokawa H, Kimura Y, Kato Y, Tsuchiya K, Terao J. 2006.** Hypochlorous acid-derived modification of phospholipids: characterization of aminophospholipids as regulatory molecules for lipid peroxidation. *Biochemistry 45: 14201-14211.*

262. **Kern M, Pahlke G, Ngiewih Y, Marko D. 2006.** Modulation of key elements of the Wnt pathway by apple polyphenols. *J Agric Food Chem 54: 7041-7046.*

263. **Kern M, Pahlke G, Balavenkatraman KK, Bohmer FD, Marko D. 2007.** Apple polyphenols affect protein kinase C activity and the onset of apoptosis in human colon carcinoma cells. *J Agric Food Chem 55: 4999-5006.*

264. **Kilic T, Akakin A. 2008.** Anatomy of cerebral veins and sinuses. *Front Neurol Neurosci 23: 4-15.*

265. **Kim JH, Park JA, Lee SW, Kim WJ, Yu YS, Kim KW. 2006.** Blood-neural barrier: intercellular communication at glio-vascular interface. *J Biochem Mol Biol 39: 339-345.*

266. **Kitanaka J, Ishibashi T, Baba A. 1993.** Phloretin as an antagonist of prostaglandin F2 alpha receptor in cultured rat astrocytes. *J Neurochem 60: 704-708.*

267. **Klebanoff SJ. 2005.** Myeloperoxidase: friend and foe. *J Leukoc Biol 77: 598-625.*

268. **Klinke A, et al. 2011.** Myeloperoxidase attracts neutrophils by physical forces. *Blood 117: 1350-1358.*

269. **Knott AB, Bossy-Wetzel E. 2009.** Nitric oxide in health and disease of the nervous system. *Antioxid Redox Signal 11: 541-554.*

270. **Knott AB, Perkins G, Schwarzenbacher R, Bossy-Wetzel E. 2008.** Mitochondrial fragmentation in neurodegeneration. *Nat Rev Neurosci 9: 505-518.*

271. **Korade Z, Kenworthy AK. 2008.** Lipid rafts, cholesterol, and the brain. *Neuropharmacology 55: 1265-1273.*

272. **Kratzer I, et al. 2007.** Apolipoprotein A-I coating of protamine-oligonucleotide nanoparticles increases particle uptake and transcytosis in an in vitro model of the blood-brain barrier. *J Control Release 117: 301-311.*

273. **Krizbai IA, Deli MA. 2003.** Signalling pathways regulating the tight junction permeability in the blood-brain barrier. *Cell Mol Biol (Noisy-le-grand) 49: 23-31.*

274. **Krohn M, et al. 2011.** Cerebral amyloid-beta proteostasis is regulated by the membrane transport protein ABCC1 in mice. *J Clin Invest.*

275. **Kukreja RC, Kontos HA, Hess ML, Ellis EF. 1986.** PGH synthase and lipoxygenase generate superoxide in the presence of NADH or NADPH. *Circ Res 59: 612-619.*

276. **Lacy P. 2006.** Mechanisms of degranulation in neutrophils. *Allergy Asthma Clin Immunol 2: 98-108.*

277. **Landar A, Zmijewski JW, Dickinson DA, Le Goffe C, Johnson MS, Milne GL, Zanoni G, Vidari G, Morrow JD, Darley-Usmar VM. 2006.** Interaction of electrophilic lipid oxidation products with mitochondria in endothelial cells and formation of reactive oxygen species. *Am J Physiol Heart Circ Physiol 290: H1777-1787.*

278. **Lang AE. 2010.** Clinical trials of disease-modifying therapies for neurodegenerative diseases: the challenges and the future. *Nat Med 16: 1223-1226.*

279. **Langston JW, Ballard PA, Jr. 1983.** Parkinson's disease in a chemist working with 1-methyl-4-phenyl-1,2,5,6-tetrahydropyridine. *N Engl J Med 309: 310.*

280. **Lankalapalli RS, Eckelkamp JT, Sircar D, Ford DA, Subbaiah PV, Bittman R. 2009.** Synthesis and antioxidant properties of an unnatural plasmalogen analogue bearing a trans O-vinyl ether linkage. *Org Lett 11: 2784-2787.*

281. **Lansbury PT, Jr. 2004.** Back to the future: the 'old-fashioned' way to new medications for neurodegeneration. *Nat Med 10 Suppl: S51-57.*

282. **Larochelle C, Alvarez JI, Prat A. 2011.** How do immune cells overcome the blood-brain barrier in multiple sclerosis? *FEBS Lett.*

283. **Lau D, Baldus S. 2006.** Myeloperoxidase and its contributory role in inflammatory vascular disease. *Pharmacol Ther 111: 16-26.*

284. **Lau D, et al. 2005.** Myeloperoxidase mediates neutrophil activation by association with CD11b/CD18 integrins. *Proc Natl Acad Sci U S A 102: 431-436.*

285. **Lawson LJ, Perry VH, Dri P, Gordon S. 1990.** Heterogeneity in the distribution and morphology of microglia in the normal adult mouse brain. *Neuroscience 39: 151-170.*

286. **Lee WL, Harrison RE, Grinstein S. 2003.** Phagocytosis by neutrophils. *Microbes Infect 5: 1299-1306.*

287. **Lefkowitz DL, Lefkowitz SS. 2008.** Microglia and myeloperoxidase: a deadly partnership in neurodegenerative disease. *Free Radic Biol Med 45: 726-731.*

288. **Lehmann K, Muller JP, Schlott B, Skroblin P, Barz D, Norgauer J, Wetzker R. 2009.** PI3Kgamma controls oxidative bursts in neutrophils via interactions with PKCalpha and p47phox. *Biochem J 419: 603-610.*

289. **Leskovjan AC, Kretlow A, Miller LM. 2010.** Fourier transform infrared imaging showing reduced unsaturated lipid content in the hippocampus of a mouse model of Alzheimer's disease. *Anal Chem 82: 2711-2716.*

290. **Lessig J, Fuchs B. 2009.** Plasmalogens in biological systems: their role in oxidative processes in biological membranes, their contribution to pathological processes and aging and plasmalogen analysis. *Curr Med Chem 16: 2021-2041.*

291. **Lessig J, Fuchs B. 2010.** HOCl-mediated glycerophosphocholine and glycerophosphoethanolamine generation from plasmalogens in phospholipid mixtures. *Lipids 45: 37-51.*

292. **Lessig J, Schiller J, Arnhold J, Fuchs B. 2007.** Hypochlorous acid-mediated generation of glycerophosphocholine from unsaturated plasmalogen glycerophosphocholine lipids. *J Lipid Res 48: 1316-1324.*

293. **Li JM, Shah AM. 2003.** ROS generation by nonphagocytic NADPH oxidase: potential relevance in diabetic nephropathy. *J Am Soc Nephrol 14: S221-226.*

294. **Li Q, Zhang Q, Wang C, Liu X, Li N, Li J. 2009.** Disruption of tight junctions during polymicrobial sepsis in vivo. *J Pathol 218: 210-221.*

295. **Lievano S, Alarcon L, Chavez-Munguia B, Gonzalez-Mariscal L. 2006.** Endothelia of term human placentae display diminished expression of tight junction proteins during preeclampsia. *Cell Tissue Res 324: 433-448.*

296. **Linder ME. 2008.** Neuroscience: greasy proteins of the neuron. *Nature 456: 887-888.*

297. **Lingwood D, Simons K. 2010.** Lipid rafts as a membrane-organizing principle. *Science 327: 46-50.*

298. **Lipinski CA, Lombardo F, Dominy BW, Feeney PJ. 2001.** Experimental and computational approaches to estimate solubility and permeability in drug discovery and development settings. *Adv Drug Deliv Rev 46: 3-26.*

299. **Liu Y, Qin L, Wilson B, Wu X, Qian L, Granholm AC, Crews FT, Hong JS. 2008**. Endotoxin induces a delayed loss of TH-IR neurons in substantia nigra and motor behavioral deficits. *Neurotoxicology 29: 864-870.*

300. **Lo EH, Dalkara T, Moskowitz MA. 2003.** Mechanisms, challenges and opportunities in stroke. *Nat Rev Neurosci 4: 399-415.*

301. **Lohner K. 1996.** Is the high propensity of ethanolamine plasmalogens to form non-lamellar lipid structures manifested in the properties of biomembranes? *Chem Phys Lipids 81: 167-184.*

302. **Loidl-Stahlhofen A, Hannemann K, Felde R, Spiteller G. 1995.** Epoxidation of plasmalogens: source for long-chain alpha-hydroxyaldehydes in subcellular fractions of bovine liver. *Biochem J 309 (Pt 3): 807-812.*

303. **Lok J, Gupta P, Guo S, Kim WJ, Whalen MJ, van Leyen K, Lo EH. 2007.** Cell-cell signaling in the neurovascular unit. *Neurochem Res 32: 2032-2045.*

304. **Luiken JJ, van Nieuwenhoven FA, America G, van der Vusse GJ, Glatz JF. 1997.** Uptake and metabolism of palmitate by isolated cardiac myocytes from adult rats: involvement of sarcolemmal proteins. *J Lipid Res 38: 745-758.*

305. **Lynch MA. 2009.** The multifaceted profile of activated microglia. *Mol Neurobiol 40: 139-156.*

306. **Madamanchi NR, Vendrov A, Runge MS. 2005.** Oxidative stress and vascular disease. *Arterioscler Thromb Vasc Biol 25: 29-38.*

307. **Maddahi A, Chen Q, Edvinsson L. 2009.** Enhanced cerebrovascular expression of matrix metalloproteinase-9 and tissue inhibitor of metalloproteinase-1 via the MEK/ERK pathway during cerebral ischemia in the rat. *BMC Neurosci 10: 56.*

308. **Maderna P, Godson C. 2003.** Phagocytosis of apoptotic cells and the resolution of inflammation. *Biochim Biophys Acta 1639: 141-151.*

309. **Magistretti PJ, Pellerin L. 1996.** Cellular bases of brain energy metabolism and their relevance to functional brain imaging: evidence for a prominent role of astrocytes. *Cereb Cortex 6: 50-61.*

310. **Maki RA, Tyurin VA, Lyon RC, Hamilton RL, DeKosky ST, Kagan VE, Reynolds WF. 2009.** Aberrant expression of myeloperoxidase in astrocytes promotes phospholipid oxidation and memory deficits in a mouse model of Alzheimer disease. *J Biol Chem 284: 3158-3169.*

311. **Malle E, Marsche G, Arnhold J, Davies MJ. 2006a.** Modification of low-density lipoprotein by myeloperoxidase-derived oxidants and reagent hypochlorous acid. *Biochim Biophys Acta 1761: 392-415.*

312. **Malle E, Marsche G, Panzenboeck U, Sattler W. 2006b.** Myeloperoxidase-mediated oxidation of high-density lipoproteins: fingerprints of newly recognized potential proatherogenic lipoproteins. *Arch Biochem Biophys 445: 245-255.*

313. **Malle E, Furtmuller PG, Sattler W, Obinger C. 2007.** Myeloperoxidase: a target for new drug development? *Br J Pharmacol 152: 838-854.*

314. **Malle E, Waeg G, Schreiber R, Grone EF, Sattler W, Grone HJ. 2000.** Immunohistochemical evidence for the myeloperoxidase/H2O2/halide system in human atherosclerotic lesions: colocalization of myeloperoxidase and hypochlorite-modified proteins. *Eur J Biochem 267: 4495-4503.*

315. **Man S, Ubogu EE, Ransohoff RM. 2007.** Inflammatory cell migration into the central nervous system: a few new twists on an old tale. *Brain Pathol 17: 243-250.*

316. **Manda KR, Banerjee A, Banks WA, Ercal N. 2011.** Highly active antiretroviral therapy drug combination induces oxidative stress and mitochondrial dysfunction in immortalized human blood-brain barrier endothelial cells. *Free Radic Biol Med 50: 801-810.*

317. **Marks SC, Mullen W, Borges G, Crozier A. 2009.** Absorption, metabolism, and excretion of cider dihydrochalcones in healthy humans and subjects with an ileostomy. *J Agric Food Chem 57: 2009-2015.*

318. **Marsche G, Hammer A, Oskolkova O, Kozarsky KF, Sattler W, Malle E. 2002.** Hypochlorite-modified high density lipoprotein, a high affinity ligand to scavenger receptor class B, type I, impairs high density lipoprotein-dependent selective lipid uptake and reverse cholesterol transport. *J Biol Chem 277: 32172-32179.*

319. **Marsche G, Heller R, Fauler G, Kovacevic A, Nuszkowski A, Graier W, Sattler W, Malle E. 2004.** 2-chlorohexadecanal derived from hypochlorite-modified high-density lipoprotein-associated plasmalogen is a natural inhibitor of endothelial nitric oxide biosynthesis. *Arterioscler Thromb Vasc Biol 24: 2302-2306.*

320. **Matsushima K, Terashima Y, Toda E, Shand F, Ueha S. 2011.** Chemokines in inflammatory and immune diseases. *Inflammation and Regeneration 31.*

321. **McCandless EE, Wang Q, Woerner BM, Harper JM, Klein RS. 2006.** CXCL12 limits inflammation by localizing mononuclear infiltrates to the perivascular space during experimental autoimmune encephalomyelitis. *J Immunol 177: 8053-8064.*

322. **McKenna SM, Davies KJ. 1988.** Bacterial killing by phagocytes: potential role(s) of hypochlorous acid and hydrogen peroxide in protein turnover, DNA synthesis, and RNA synthesis. *Basic Life Sci 49: 829-832.*

323. **Mertsch K, Blasig I, Grune T. 2001.** 4-Hydroxynonenal impairs the permeability of an in vitro rat blood-brain barrier. *Neurosci Lett 314: 135-138.*

324. **Messner MC, Albert CJ, Ford DA. 2008a.** 2-Chlorohexadecanal and 2-chlorohexadecanoic acid induce COX-2 expression in human coronary artery endothelial cells. *Lipids 43: 581-588.*

325. **Messner MC, Albert CJ, Hsu FF, Ford DA. 2006.** Selective plasmenylcholine oxidation by hypochlorous acid: formation of lysophosphatidylcholine chlorohydrins. *Chem Phys Lipids 144: 34-44.*

326. **Messner MC, Albert CJ, McHowat J, Ford DA. 2008b.** Identification of lysophosphatidylcholine-chlorohydrin in human atherosclerotic lesions. *Lipids 43: 243-249.*

327. **Meyer MC, McHowat J. 2007.** Calcium-independent phospholipase A2-catalyzed plasmalogen hydrolysis in hypoxic human coronary artery endothelial cells. *Am J Physiol Cell Physiol 292: C251-258.*

328. **Migliore L, Coppede F. 2009.** Environmental-induced oxidative stress in neurodegenerative disorders and aging. *Mutat Res 674: 73-84.*

329. **Miller AK, Alston RL, Corsellis JA. 1980.** Variation with age in the volumes of grey and white matter in the cerebral hemispheres of man: measurements with an image analyser. *Neuropathol Appl Neurobiol 6: 119-132.*

330. **Mitchell RW, Edmundson CL, Miller DW, Hatch GM. 2009.** On the mechanism of oleate transport across human brain microvessel endothelial cells. *J Neurochem 110: 1049-1057.*

331. **Mitchell TW, Buffenstein R, Hulbert AJ. 2007.** Membrane phospholipid composition may contribute to exceptional longevity of the naked mole-rat (Heterocephalus glaber): a comparative study using shotgun lipidomics. *Exp Gerontol 42: 1053-1062.*

332. **Mitra P, Keese CR, Giaever I. 1991.** Electric measurements can be used to monitor the attachment and spreading of cells in tissue culture. Biotechniques 11: 504-510.

333. **Montero-Menei CN, Sindji L, Garcion E, Mege M, Couez D, Gamelin E, Darcy F. 1996.** Early events of the inflammatory reaction induced in rat brain by lipopolysaccharide intracerebral injection: relative contribution of peripheral monocytes and activated microglia. *Brain Res 724: 55-66.*

334. **Moraitou M, Dimitriou E, Zafeiriou D, Reppa C, Marinakis T, Sarafidou J, Michelakakis H. 2008.** Plasmalogen levels in Gaucher disease. *Blood Cells Mol Dis 41: 196-199.*

335. **Morreale de Escobar G, Calvo R, Escobar del Rey F, Obregon MJ. 1994.** Thyroid hormones in tissues from fetal and adult rats. *Endocrinology 134: 2410-2415.*

336. **Morris JC. 1966.** The Acid Ionization Constant of HOCl from 5 to 35°. *J. Phys. Chem. 70: 3763-4102.*

337. **Mosley RL, Benner EJ, Kadiu I, Thomas M, Boska MD, Hasan K, Laurie C, Gendelman HE. 2006.** Neuroinflammation, Oxidative Stress and the Pathogenesis of Parkinson's Disease. *Clin Neurosci Res 6: 261-281.*

338. **Mosser DM, Zhang X. 2008.** Activation of murine macrophages. *Curr Protoc Immunol Chapter 14: Unit 14 12.*

339. **Murphy EJ, Joseph L, Stephens R, Horrocks LA. 1992.** Phospholipid composition of cultured human endothelial cells. *Lipids 27: 150-153.*

340. **Murphy EJ, Stephens R, Jurkowitz-Alexander M, Horrocks LA. 1993.** Acidic hydrolysis of plasmalogens followed by high-performance liquid chromatography. *Lipids 28: 565-568.*

341. **Murphy EJ, Schapiro MB, Rapoport SI, Shetty HU. 2000**. Phospholipid composition and levels are altered in Down syndrome brain. *Brain Res 867: 9-18.*

342. **Murphy RC. 2001.** Free-radical-induced oxidation of arachidonoyl plasmalogen phospholipids: antioxidant mechanism and precursor pathway for bioactive eicosanoids. *Chem Res Toxicol 14: 463-472.*

343. **Nag S, Kapadia A, Stewart DJ. 2011.** Review: molecular pathogenesis of blood-brain barrier breakdown in acute brain injury. *Neuropathol Appl Neurobiol 37: 3-23.*

344. **Nagan N, Zoeller RA. 2001.** Plasmalogens: biosynthesis and functions. *Prog Lipid Res 40: 199-229.*

345. **Nagasawa K, Chiba H, Fujita H, Kojima T, Saito T, Endo T, Sawada N. 2006.** Possible involvement of gap junctions in the barrier function of tight junctions of brain and lung endothelial cells. *J Cell Physiol 208: 123-132.*

346. **Nagra RM, Becher B, Tourtellotte WW, Antel JP, Gold D, Paladino T, Smith RA, Nelson JR, Reynolds WF. 1997.** Immunohistochemical and genetic evidence of myeloperoxidase involvement in multiple sclerosis. *J Neuroimmunol 78: 97-107.*

347. **Nagyoszi P, Wilhelm I, Farkas AE, Fazakas C, Dung NT, Hasko J, Krizbai IA. 2010.** Expression and regulation of toll-like receptors in cerebral endothelial cells. *Neurochem Int 57: 556-564.*

348. **Nakagawa S, Deli MA, Nakao S, Honda M, Hayashi K, Nakaoke R, Kataoka Y, Niwa M. 2007.** Pericytes from brain microvessels strengthen the barrier integrity in primary cultures of rat brain endothelial cells. *Cell Mol Neurobiol 27: 687-694.*

349. **Nakamura Y. 2002.** Regulating factors for microglial activation. *Biol Pharm Bull 25: 945-953.*

350. **Navarrete CM, Perez M, de Vinuesa AG, Collado JA, Fiebich BL, Calzado MA, Munoz E. 2010.** Endogenous N-acyl-dopamines induce COX-2 expression in brain endothelial cells by stabilizing mRNA through a p38 dependent pathway. *Biochem Pharmacol 79: 1805-1814.*

351. **Navarro P, Ruco L, Dejana E. 1998.** Differential localization of VE- and N-cadherins in human endothelial cells: VE-cadherin competes with N-cadherin for junctional localization. *J Cell Biol 140: 1475-1484.*

352. **Nicholls SJ, Hazen SL. 2009.** Myeloperoxidase, modified lipoproteins, and atherogenesis. *J Lipid Res 50 Suppl: S346-351.*

353. **Nimmerjahn A, Kirchhoff F, Helmchen F. 2005.** Resting microglial cells are highly dynamic surveillants of brain parenchyma in vivo. *Science 308: 1314-1318.*

354. **Nitta T, Hata M, Gotoh S, Seo Y, Sasaki H, Hashimoto N, Furuse M, Tsukita S. 2003.** Size-selective loosening of the blood-brain barrier in claudin-5-deficient mice. *J Cell Biol 161: 653-660.*

355. **Nitz T, Eisenblatter T, Psathaki K, Galla HJ. 2003**. Serum-derived factors weaken the barrier properties of cultured porcine brain capillary endothelial cells in vitro. *Brain Res 981: 30-40.*

356. **Novgorodov AS, El-Alwani M, Bielawski J, Obeid LM, Gudz TI. 2007.** Activation of sphingosine-1-phosphate receptor S1P5 inhibits oligodendrocyte progenitor migration. *FASEB J 21: 1503-1514.*

357. **Nussbaum RL, Ellis CE. 2003.** Alzheimer's disease and Parkinson's disease. *N Engl J Med 348: 1356-1364.*

358. **Nusshold C, et al. 2010.** Hypochlorite modification of sphingomyelin generates chlorinated lipid species that induce apoptosis and proteome alterations in dopaminergic PC12 neurons in vitro. *Free Radic Biol Med 48: 1588-1600.*

359. **O'Brien JS, Sampson EL. 1965.** Lipid composition of the normal human brain: gray matter, white matter, and myelin. *J Lipid Res 6: 537-544.*

360. **Oberheim NA, Wang X, Goldman S, Nedergaard M. 2006.** Astrocytic complexity distinguishes the human brain. *Trends Neurosci 29: 547-553.*

361. **Ochoa L, Waypa G, Mahoney JR, Jr., Rodriguez L, Minnear FL. 1997.** Contrasting effects of hypochlorous acid and hydrogen peroxide on endothelial permeability: prevention with cAMP drugs. *Am J Respir Crit Care Med 156: 1247-1255.*

362. **Ong WY, Farooqui T, Farooqui AA. 2010.** Involvement of cytosolic phospholipase A(2), calcium independent phospholipase A(2) and plasmalogen selective phospholipase A(2) in neurodegenerative and neuropsychiatric conditions. *Curr Med Chem 17: 2746-2763.*

363. **Owens T, Bechmann I, Engelhardt B. 2008.** Perivascular spaces and the two steps to neuroinflammation. *J Neuropathol Exp Neurol 67: 1113-1121.*

364. **Pacher P, Beckman JS, Liaudet L. 2007.** Nitric oxide and peroxynitrite in health and disease. *Physiol Rev 87: 315-424.*

365. **Painsipp E, Kofer MJ, Sinner F, Holzer P. 2011.** Prolonged depression-like behavior caused by immune challenge: influence of mouse strain and social environment. *PLoS One 6: e20719.*

366. **Panasenko OM, Spalteholz H, Schiller J, Arnhold J. 2003.** Myeloperoxidase-induced formation of chlorohydrins and lysophospholipids from unsaturated phosphatidylcholines. *Free Radic Biol Med 34: 553-562.*

367. **Panasenko OM, Evgina SA, Aidyraliev RK, Sergienko VI, Vladimirov YA. 1994.** Peroxidation of human blood lipoproteins induced by exogenous hypochlorite or hypochlorite generated in the system of 'myeloperoxidase + H2O2 + Cl-'. *Free Radic Biol Med 16: 143-148.*

368. **Panneels V, Van Sande J, Van den Bergen H, Jacoby C, Braekman JC, Dumont JE, Boeynaems JM. 1994.** Inhibition of human thyroid adenylyl cyclase by 2-iodoaldehydes. *Mol Cell Endocrinol 106: 41-50.*

369. **Panzenboeck U, Raitmayer S, Reicher H, Lindner H, Glatter O, Malle E, Sattler W. 1997.** Effects of reagent and enzymatically generated hypochlorite on physicochemical and metabolic properties of high density lipoproteins. *J Biol Chem 272: 29711-29720.*

370. **Papayannopoulos V, Zychlinsky A. 2009.** NETs: a new strategy for using old weapons. *Trends Immunol 30: 513-521.*

371. **Pardridge WM. 2002.** Drug and gene delivery to the brain: the vascular route. *Neuron 36: 555-558.*

372. **Pardridge WM. 2005.** The blood-brain barrier: bottleneck in brain drug development. *NeuroRx 2: 3-14.*

373. **Pardridge WM. 2007a.** Blood-brain barrier delivery. *Drug Discov Today 12: 54-61.*

374. **Pardridge WM. 2007b.** Drug targeting to the brain. *Pharm Res 24: 1733-1744.*

375. **Patel RP, Boersma BJ, D'Alessandro T, Benton MR, Kirk M, Wilson LS, Prasain J, Botting NP, Barnes S, Darley-Usmar VM. 2003.** Neutrophil myeloperoxidase chlorinates and nitrates soy isoflavones and enhances their antioxidant properties. *Free Radical Biology and Medicine 35: 1417-1430.*

376. **Pattison DI, Davies MJ. 2001.** Absolute rate constants for the reaction of hypochlorous acid with protein side chains and peptide bonds. *Chem Res Toxicol 14: 1453-1464.*

377. **Pattison DI, Davies MJ. 2005.** Kinetic analysis of the role of histidine chloramines in hypochlorous acid mediated protein oxidation. *Biochemistry 44: 7378-7387.*

378. **Pattison DI, Davies MJ. 2006.** Reactions of myeloperoxidase-derived oxidants with biological substrates: gaining chemical insight into human inflammatory diseases. *Curr Med Chem 13: 3271-3290.*

379. **Pattison DI, Hawkins CL, Davies MJ. 2003.** Hypochlorous acid-mediated oxidation of lipid components and antioxidants present in low-density lipoproteins: absolute rate constants, product analysis, and computational modeling. *Chem Res Toxicol 16: 439-449.*

380. **Paul S, Gupta M. 2004.** Zinc-catalyzed Williamson ether synthesis in the absence of base. *Tetrahedron Letters 45: 4.*

381. **Paumen MB, Ishida Y, Muramatsu M, Yamamoto M, Honjo T. 1997.** Inhibition of carnitine palmitoyltransferase I augments sphingolipid synthesis and palmitate-induced apoptosis. *J Biol Chem 272: 3324-3329.*

382. **Peppiatt CM, Howarth C, Mobbs P, Attwell D. 2006.** Bidirectional control of CNS capillary diameter by pericytes. *Nature 443: 700-704.*

383. **Pereira A, Braekman JC, Dumont JE, Boeynaems JM. 1990.** Identification of a major iodolipid from the horse thyroid gland as 2-iodohexadecanal. *J Biol Chem 265: 17018-17025.*

384. **Perez-Sala D. 2007.** Protein isoprenylation in biology and disease: general overview and perspectives from studies with genetically engineered animals. *Front Biosci 12: 4456-4472.*

385. **Perry VH. 2010.** Contribution of systemic inflammation to chronic neurodegeneration. *Acta Neuropathol 120: 277-286.*

386. **Perry VH, Cunningham C, Holmes C. 2007.** Systemic infections and inflammation affect chronic neurodegeneration. *Nat Rev Immunol 7: 161-167.*

387. **Pfaffl MW, Horgan GW, Dempfle L. 2002.** Relative expression software tool (REST) for group-wise comparison and statistical analysis of relative expression results in real-time PCR. *Nucleic Acids Res 30: e36.*

388. **Pike LJ, Han X, Chung KN, Gross RW. 2002.** Lipid rafts are enriched in arachidonic acid and plasmenylethanolamine and their composition is independent of caveolin-1 expression: a quantitative electrospray ionization/mass spectrometric analysis. *Biochemistry 41: 2075-2088.*

389. **Piontek J, Winkler L, Wolburg H, Muller SL, Zuleger N, Piehl C, Wiesner B, Krause G, Blasig IE. 2008.** Formation of tight junction: determinants of homophilic interaction between classic claudins. *FASEB J 22: 146-158.*

390. **Podrez EA, Abu-Soud HM, Hazen SL. 2000.** Myeloperoxidase-generated oxidants and atherosclerosis. *Free Radic Biol Med 28: 1717-1725.*

391. **Poduslo JF, Curran GL, Berg CT. 1994.** Macromolecular permeability across the blood-nerve and blood-brain barriers. *Proc Natl Acad Sci U S A 91: 5705-5709.*

392. **Polazzi E, Monti B. 2010.** Microglia and neuroprotection: from in vitro studies to therapeutic applications. *Prog Neurobiol 92: 293-315.*

393. **Pradillo JM, Fernandez-Lopez D, Garcia-Yebenes I, Sobrado M, Hurtado O, Moro MA, Lizasoain I. 2009.** Toll-like receptor 4 is involved in neuroprotection afforded by ischemic preconditioning. *J Neurochem 109: 287-294.*

394. **Presecki P, Muck-Seler D, Mimica N, Pivac N, Mustapic M, Stipcevic T, Smalc VF. 2011.** Serum lipid levels in patients with Alzheimer's disease. *Coll Antropol 35 Suppl 1: 115-120.*

395. **Prince M, Jackson J. 2009.** *World Alzheimer Report 2009.* www.alz.co.uk/research/files/WorldAlzheimerReport.pdf.

396. **Przedborski S, Jackson-Lewis V, Naini AB, Jakowec M, Petzinger G, Miller R, Akram M. 2001.** The parkinsonian toxin 1-methyl-4-phenyl-1,2,3,6-tetrahydropyridine (MPTP): a technical review of its utility and safety. *J Neurochem 76: 1265-1274.*

397. **Pullar JM, Vissers MC, Winterbourn CC. 2000.** Living with a killer: the effects of hypochlorous acid on mammalian cells. *IUBMB Life 50: 259-266.*

398. **Pun PB, Lu J, Moochhala S. 2009.** Involvement of ROS in BBB dysfunction. *Free Radic Res 43: 348-364.*

399. **Purves D, Augustine GJ, Fitzpatrick D, Katz LC, LaMantia AS, McNamara JO, Williams SM. 2001.** Neuroscience 2th ed. *Sinauer Associates ISBN: 0878937420.*

400. **Qian L, Flood PM, Hong JS. 2010.** Neuroinflammation is a key player in Parkinson's disease and a prime target for therapy. *J Neural Transm 117: 971-979.*

401. **Qin L, Li G, Qian X, Liu Y, Wu X, Liu B, Hong JS, Block ML. 2005.** Interactive role of the toll-like receptor 4 and reactive oxygen species in LPS-induced microglia activation. *Glia 52: 78-84.*

402. **Qin L, Wu X, Block ML, Liu Y, Breese GR, Hong JS, Knapp DJ, Crews FT. 2007.** Systemic LPS causes chronic neuroinflammation and progressive neurodegeneration. *Glia 55: 453-462.*

403. **Qin Z, Reszka KJ, Fukai T, Weintraub NL. 2008.** Extracellular superoxide dismutase (ecSOD) in vascular biology: an update on exogenous gene transfer and endogenous regulators of ecSOD. *Transl Res 151: 68-78.*

404. **Ramirez SH, Fan S, Zhang M, Papugani A, Reichenbach N, Dykstra H, Mercer AJ, Tuma RF, Persidsky Y. 2010.** Inhibition of glycogen synthase kinase 3beta (GSK3beta) decreases inflammatory responses in brain endothelial cells. *Am J Pathol 176: 881-892.*

405. **Ramsauer M, Krause D, Dermietzel R. 2002.** Angiogenesis of the blood-brain barrier in vitro and the function of cerebral pericytes. *FASEB J 16: 1274-1276.*

406. **Ransohoff RM, Kivisakk P, Kidd G. 2003.** Three or more routes for leukocyte migration into the central nervous system. *Nat Rev Immunol 3: 569-581.*

407. **Redzic Z. 2011.** Molecular biology of the blood-brain and the blood-cerebrospinal fluid barriers: similarities and differences. *Fluids Barriers CNS 8: 3.*

408. **Redzic ZB, Preston JE, Duncan JA, Chodobski A, Szmydynger-Chodobska J. 2005.** The choroid plexus-cerebrospinal fluid system: from development to aging. *Curr Top Dev Biol 71: 1-52.*

409. **Rees MD, Kennett EC, Whitelock JM, Davies MJ. 2008.** Oxidative damage to extracellular matrix and its role in human pathologies. *Free Radic Biol Med 44: 1973-2001.*

410. **Reese TS, Karnovsky MJ. 1967.** Fine structural localization of a blood-brain barrier to exogenous peroxidase. *J Cell Biol 34: 207-217.*

411. **Remijsen Q, Vanden Berghe T, Wirawan E, Asselbergh B, Parthoens E, De Rycke R, Noppen S, Delforge M, Willems J, Vandenabeele P. 2011.** Neutrophil extracellular trap cell death requires both autophagy and superoxide generation. *Cell Res 21: 290-304.*

412. **Resh MD. 2006.** Use of analogs and inhibitors to study the functional significance of protein palmitoylation. *Methods 40: 191-197.*

413. **Reynolds WF, Rhees J, Maciejewski D, Paladino T, Sieburg H, Maki RA, Masliah E. 1999.** Myeloperoxidase polymorphism is associated with gender specific risk for Alzheimer's disease. *Exp Neurol 155: 31-41.*

414. **Rezai-Zadeh K, Gate D, Town T. 2009.** CNS infiltration of peripheral immune cells: D-Day for neurodegenerative disease? *J Neuroimmune Pharmacol 4: 462-475.*

415. **Rezk BM, Haenen GR, van der Vijgh WJ, Bast A. 2002.** The antioxidant activity of phloretin: the disclosure of a new antioxidant pharmacophore in flavonoids. *Biochem Biophys Res Commun 295: 9-13.*

416. **Riahi Y, Cohen G, Shamni O, Sasson S. 2010.** Signaling and cytotoxic functions of 4-hydroxyalkenals. *Am J Physiol Endocrinol Metab 299: E879-886.*

417. **Richter G, Schober C, Suss R, Fuchs B, Birkemeyer C, Schiller J. 2008.** Comparison of the positive and negative ion electrospray ionization and matrix-assisted laser desorption ionization-time-of-flight mass spectra of the reaction products of phosphatidylethanolamines and hypochlorous acid. *Anal Biochem 376: 157-159.*

418. **Rite I, Machado A, Cano J, Venero JL. 2007.** Blood-brain barrier disruption induces in vivo degeneration of nigral dopaminergic neurons. *J Neurochem 101: 1567-1582.*

419. **Rizzo WB.** 2007. Sjogren-Larsson syndrome: molecular genetics and biochemical pathogenesis of fatty aldehyde dehydrogenase deficiency. *Mol Genet Metab 90: 1-9.*

420. **Rizzo WB, Carney G. 2005.** Sjogren-Larsson syndrome: diversity of mutations and polymorphisms in the fatty aldehyde dehydrogenase gene (ALDH3A2). *Hum Mutat 26: 1-10.*

421. **Robinson JM. 2009.** Phagocytic leukocytes and reactive oxygen species. *Histochem Cell Biol 131: 465-469.*

422. **Rock RB, Gekker G, Hu S, Sheng WS, Cheeran M, Lokensgard JR, Peterson PK. 2004.** Role of microglia in central nervous system infections. *Clin Microbiol Rev 17: 942-964, table of contents.*

423. **Rodemer C, Thai TP, Brugger B, Gorgas K, Just W. 2003.** Targeted disruption of ether lipid synthesis in mice. *Adv Exp Med Biol 544: 355-368.*

424. **Roh E, Lee HS, Kwak JA, Hong JT, Nam SY, Jung SH, Lee JY, Kim ND, Han SB, Kim Y. 2011.** MD-2 as the target of nonlipid chalcone in the inhibition of endotoxin LPS-induced TLR4 activity. *J Infect Dis 203: 1012-1020.*

425. **Rohatgi T, Sedehizade F, Reymann KG, Reiser G. 2004.** Protease-activated receptors in neuronal development, neurodegeneration, and neuroprotection: thrombin as signaling molecule in the brain. *Neuroscientist 10: 501-512.*

426. **Ropper AH. 2006.** Selective treatment of multiple sclerosis. *N Engl J Med 354: 965-967.*

427. **Rosenberg GA. 2009.** Matrix metalloproteinases and their multiple roles in neurodegenerative diseases. *Lancet Neurol 8: 205-216.*

428. Rubbo H, Trostchansky A, O'Donnell VB. 2009. Peroxynitrite-mediated lipid oxidation and nitration: mechanisms and consequences. *Arch Biochem Biophys 484: 167-172.*

429. **Rydell-Tormanen K, Uller L, Erjefalt JS. 2006.** Neutrophil cannibalism--a back up when the macrophage clearance system is insufficient. *Respir Res 7: 143.*

430. **Saitou M, Furuse M, Sasaki H, Schulzke JD, Fromm M, Takano H, Noda T, Tsukita S. 2000.** Complex phenotype of mice lacking occludin, a component of tight junction strands. *Mol Biol Cell 11: 4131-4142.*

431. **Salat DH, Kaye JA, Janowsky JS. 1999.** Prefrontal gray and white matter volumes in healthy aging and Alzheimer disease. *Arch Neurol 56: 338-344.*

432. **Sanchez-Mejia RO, et al. 2008.** Phospholipase A2 reduction ameliorates cognitive deficits in a mouse model of Alzheimer's disease. *Nat Neurosci 11: 1311-1318.*

433. **Sanfilipo MP, Benedict RH, Weinstock-Guttman B, Bakshi R. 2006.** Gray and white matter brain atrophy and neuropsychological impairment in multiple sclerosis. *Neurology 66: 685-692.*

434. **Sang N, Chen C. 2006.** Lipid signaling and synaptic plasticity. *Neuroscientist 12: 425-434.*

435. **Sastry PS. 1985**. Lipids of nervous tissue: composition and metabolism. *Prog Lipid Res 24: 69-176.*

436. **Saunders NR, Ek CJ, Habgood MD, Dziegielewska KM. 2008.** Barriers in the brain: a renaissance? *Trends Neurosci 31: 279-286.*

437. **Sayre LM, Perry G, Smith MA. 2008.** Oxidative stress and neurotoxicity. *Chem Res Toxicol 21: 172-188.*

438. **Schneiter R, et al. 1999.** Electrospray ionization tandem mass spectrometry (ESI-MS/MS) analysis of the lipid molecular species composition of yeast subcellular membranes reveals acyl chain-based sorting/remodeling of distinct molecular species en route to the plasma membrane. *J Cell Biol 146: 741-754.*

439. **Schratl P, Sturm EM, Royer JF, Sturm GJ, Lippe IT, Peskar BA, Heinemann A. 2006.** Hierarchy of eosinophil chemoattractants: role of p38 mitogen-activated protein kinase. *Eur J Immunol 36: 2401-2409.*

440. **Schulze C, Firth JA. 1993.** Immunohistochemical localization of adherens junction components in blood-brain barrier microvessels of the rat. *J Cell Sci 104 (Pt 3): 773-782.*

441. **Seabrook TJ, Littlewood-Evans A, Brinkmann V, Pollinger B, Schnell C, Hiestand PC. 2010.** Angiogenesis is present in experimental autoimmune encephalomyelitis and pro-angiogenic factors are increased in multiple sclerosis lesions. *J Neuroinflammation 7: 95.*

442. **Seehusen DA, Reeves MM, Fomin DA. 2003.** Cerebrospinal fluid analysis. *Am Fam Physician 68: 1103-1108.*

443. **Segal BH, Leto TL, Gallin JI, Malech HL, Holland SM. 2000.** Genetic, biochemical, and clinical features of chronic granulomatous disease. *Medicine (Baltimore) 79: 170-200.*

444. **Selivonchick DP, Roots BI. 1977.** Lipid and fatty acyl composition of rat brain capillary endothelia isolated by a new technique. *Lipids 12: 165-169.*

445. **Selvakumar P, Pasha MK, Ashakumary L, Dimmock JR, Sharma RK. 2002**. Myristoyl-CoA:protein N-myristoyltransferase: a novel molecular approach for cancer therapy (Review). *Int J Mol Med 10: 493-500.*

446. **Semmler A, Hermann S, Mormann F, Weberpals M, Paxian SA, Okulla T, Schafers M, Kummer MP, Klockgether T, Heneka MT. 2008.** Sepsis causes neuroinflammation and concomitant decrease of cerebral metabolism. *J Neuroinflammation 5: 38.*

447. **Shaftel SS, Carlson TJ, Olschowka JA, Kyrkanides S, Matousek SB, O'Banion MK. 2007.** Chronic interleukin-1beta expression in mouse brain leads to leukocyte infiltration and neutrophil-independent blood brain barrier permeability without overt neurodegeneration. *J Neurosci 27: 9301-9309.*

448. **Shao X, Bai N, He K, Ho CT, Yang CS, Sang S. 2008.** Apple polyphenols, phloretin and phloridzin: new trapping agents of reactive dicarbonyl species. *Chem Res Toxicol 21: 2042-2050.*

449. **Shepherd GM. 1994.** Neurobiology. *Oxford University Press ISBN: 9780390850751.*

450. **Shiba Y, et al. 2008.** Flavonoids as substrates and inhibitors of myeloperoxidase: molecular actions of aglycone and metabolites. *Chem Res Toxicol 21: 1600-1609.*

451. **Shimoi K, Saka N, Nozawa R, Sato M, Amano I, Nakayama T, Kinae N. 2001.** Deglucuronidation of a flavonoid, luteolin monoglucuronide, during inflammation. *Drug Metab Dispos 29: 1521-1524.*

452. **Shimozu Y, Hirano K, Shibata T, Shibata N, Uchida K. 2011.** 4-Hydroperoxy-2-nonenal Is Not Just an Intermediate but a Reactive Molecule That Covalently Modifies Proteins to Generate Unique Intramolecular Oxidation Products. *J Biol Chem 286: 29313-29324.*

453. **Shiu C, Barbier E, Di Cello F, Choi HJ, Stins M. 2007.** HIV-1 gp120 as well as alcohol affect blood-brain barrier permeability and stress fiber formation: involvement of reactive oxygen species. *Alcohol Clin Exp Res 31: 130-137.*

454. **Sicard KM, Fisher M. 2009.** Animal models of focal brain ischemia. *Exp Transl Stroke Med 1: 7.*

455. **Siddharthan V, Kim YV, Liu S, Kim KS. 2007.** Human astrocytes/astrocyte-conditioned medium and shear stress enhance the barrier properties of human brain microvascular endothelial cells. *Brain Res 1147: 39-50.*

456. **Siegel G, Albers WR, Brady S, D. P. 2006.** Basic Neurochemistry: Molecular, Cellular and Medical Aspects 7th ed. *Elsevier ISBN: 9780120883974.*

457. **Silva MT. 2010.** Neutrophils and macrophages work in concert as inducers and effectors of adaptive immunity against extracellular and intracellular microbial pathogens. *J Leukoc Biol 87: 805-813.*

458. **Singh AK, Jiang Y, Gupta S. 2007**. Effects of bacterial toxins on endothelial tight junction in vitro: a mechanism-based investigation. *Toxicol Mech Methods 17: 331-347.*

459. **Singh I, Paintlia AS, Khan M, Stanislaus R, Paintlia MK, Haq E, Singh AK, Contreras MA. 2004.** Impaired peroxisomal function in the central nervous system with inflammatory disease of experimental autoimmune encephalomyelitis animals and protection by lovastatin treatment. *Brain Res 1022: 1-11.*

460. **Skaff O, Pattison DI, Davies MJ. 2008.** The vinyl ether linkages of plasmalogens are favored targets for myeloperoxidase-derived oxidants: a kinetic study. *Biochemistry 47: 8237-8245.*

461. **Smith JA. 1994.** Neutrophils, host defense, and inflammation: a double-edged sword. *J Leukoc Biol 56: 672-686.*

462. **Smith JC, Hou W, Whitehead SN, Ethier M, Bennett SA, Figeys D. 2008.** Identification of lysophosphatidylcholine (LPC) and platelet activating factor (PAF) from PC12 cells and mouse cortex using liquid chromatography/multi-stage mass spectrometry (LC/MS3). *Rapid Commun Mass Spectrom 22: 3579-3587.*

463. **Sonnino S, Prinetti A. 2010.** Lipids and membrane lateral organization. *Front Physiol 1: 153*.

464. **Soubhye J, et al. 2010.** Structure-based design, synthesis, and pharmacological evaluation of 3-(aminoalkyl)-5-fluoroindoles as myeloperoxidase inhibitors. *J Med Chem 53: 8747-8759.*

465. **Sourisseau T, Georgiadis A, Tsapara A, Ali RR, Pestell R, Matter K, Balda MS. 2006.** Regulation of PCNA and cyclin D1 expression and epithelial morphogenesis by the ZO-1-regulated transcription factor ZONAB/DbpA. *Mol Cell Biol 26: 2387-2398.*

466. **Spector AA, Yorek MA. 1985.** Membrane lipid composition and cellular function. *J Lipid Res 26: 1015-1035.*

467. **Spickett CM. 2007.** Chlorinated lipids and fatty acids: an emerging role in pathology. *Pharmacol Ther 115: 400-409.*

468. **Sprague AH, Khalil RA. 2009.** Inflammatory cytokines in vascular dysfunction and vascular disease. *Biochem Pharmacol 78: 539-552.*

469. S**riram S, Steiner I. 2005.** Experimental allergic encephalomyelitis: a misleading model of multiple sclerosis. *Ann Neurol 58: 939-945.*

470. **Stadelmann-Ingrand S, Pontcharraud R, Fauconneau B. 2004.** Evidence for the reactivity of fatty aldehydes released from oxidized plasmalogens with phosphatidylethanolamine to form Schiff base adducts in rat brain homogenates. *Chem Phys Lipids 131: 93-105.*

471. **Stamatovic SM, Dimitrijevic OB, Keep RF, Andjelkovic AV. 2006.** Protein kinase Calpha-RhoA cross-talk in CCL2-induced alterations in brain endothelial permeability. *J Biol Chem 281: 8379-8388.*

472. **Stangl V, Lorenz M, Ludwig A, Grimbo N, Guether C, Sanad W, Ziemer S, Martus P, Baumann G, Stangl K. 2005.** The flavonoid phloretin suppresses stimulated expression of endothelial adhesion molecules and reduces activation of human platelets. *J Nutr 135: 172-178.*

473. **Stanimirovic D, Satoh K. 2000.** Inflammatory mediators of cerebral endothelium: a role in ischemic brain inflammation. *Brain Pathol 10: 113-126.*

474. **Stanzione P, Tropepi D. 2011.** Drugs and clinical trials in neurodegenerative diseases. *Ann Ist Super Sanita 47: 49-54.*

475. **Steffen Y, Gruber C, Schewe T, Sies H. 2008**. Mono-O-methylated flavanols and other flavonoids as inhibitors of endothelial NADPH oxidase. *Arch Biochem Biophys 469: 209-219.*

476. **Stevens CL, Farkas E, Gillis B. 1954.** Epoxyethers. VII. Reaction of α-Haloaldehydes with Base. *Journal of the American Chemical Society 76: 2695-2698.*

477. **Stevenson BR, Anderson JM, Braun ID, Mooseker MS. 1989.** Phosphorylation of the tight-junction protein ZO-1 in two strains of Madin-Darby canine kidney cells which differ in transepithelial resistance. *Biochem J 263: 597-599.*

478. **Stoffers D, Sheldon S, Kuperman JM, Goldstein J, Corey-Bloom J, Aron AR. 2010.** Contrasting gray and white matter changes in preclinical Huntington disease: an MRI study. *Neurology 74: 1208-1216.*

479. **Stolp HB, Dziegielewska KM. 2009.** Review: Role of developmental inflammation and blood-brain barrier dysfunction in neurodevelopmental and neurodegenerative diseases. *Neuropathol Appl Neurobiol 35: 132-146.*

480. **Stolp HB, Dziegielewska KM, Ek CJ, Potter AM, Saunders NR. 2005.** Long-term changes in blood-brain barrier permeability and white matter following prolonged systemic inflammation in early development in the rat. *Eur J Neurosci 22: 2805-2816.*

481. **Sugiyama S, Kugiyama K, Aikawa M, Nakamura S, Ogawa H, Libby P. 2004.** Hypochlorous acid, a macrophage product, induces endothelial apoptosis and tissue factor expression: involvement of myeloperoxidase-mediated oxidant in plaque erosion and thrombogenesis. *Arterioscler Thromb Vasc Biol 24: 1309-1314.*

482. **Swanson LW. 1995.** Mapping the human brain: past, present, and future. *Trends Neurosci 18: 471-474.*

483. **Taguchi R, Ishikawa M. 2010.** Precise and global identification of phospholipid molecular species by an Orbitrap mass spectrometer and automated search engine Lipid Search. *J Chromatogr A 1217: 4229-4239.*

484. **Taguchi R, Ishikawa M. 2010** Precise and global identification of phospholipid molecular species by an Orbitrap mass spectrometer and automated search engine Lipid Search. *J Chromatogr A 1217: 4229-4239.*

485. **Takamura H, Kasai H, Arita H, Kito M. 1990.** Phospholipid molecular species in human umbilical artery and vein endothelial cells. *J Lipid Res 31: 709-717.*

486. **Takano T, Tian GF, Peng W, Lou N, Libionka W, Han X, Nedergaard M. 2006.** Astrocyte-mediated control of cerebral blood flow. *Nat Neurosci 9: 260-267.*

487. **Takasato Y, Rapoport SI, Smith QR. 1984.** An in situ brain perfusion technique to study cerebrovascular transport in the rat. *Am J Physiol 247: H484-493.*

488. **Tambuyzer BR, Ponsaerts P, Nouwen EJ. 2009.** Microglia: gatekeepers of central nervous system immunology. *J Leukoc Biol 85: 352-370.*

489. **Tapia R, Huerta M, Islas S, Avila-Flores A, Lopez-Bayghen E, Weiske J, Huber O, Gonzalez-Mariscal L. 2009.** Zona occludens-2 inhibits cyclin D1 expression and cell proliferation and exhibits changes in localization along the cell cycle. *Mol Biol Cell 20: 1102-1117.*

490. **Tariq M, Khan HA, Al Moutaery K, Al Deeb S. 2001.** Protective effect of quinacrine on striatal dopamine levels in 6-OHDA and MPTP models of Parkinsonism in rodents. *Brain Res Bull 54: 77-82.*

491. **Teeling JL, Perry VH. 2009.** Systemic infection and inflammation in acute CNS injury and chronic neurodegeneration: underlying mechanisms. *Neuroscience 158: 1062-1073.*

492. **Terao J, Murota K, Kawai Y. 2011.** Conjugated quercetin glucuronides as bioactive metabolites and precursors of aglycone in vivo. *Food Funct 2: 11-17.*

493. **Terry SJ, Zihni C, Elbediwy A, Vitiello E, Leefa Chong San IV, Balda MS, Matter K. 2011.** Spatially restricted activation of RhoA signalling at epithelial junctions by p114RhoGEF drives junction formation and morphogenesis. *Nat Cell Biol 13: 159-166.*

494. **Tewes BJ, Galla HJ. 2001.** Lipid polarity in brain capillary endothelial cells. *Endothelium 8: 207-220.*

495. **Theoharides TC. 2009.** Luteolin as a therapeutic option for multiple sclerosis. *J Neuroinflammation 6: 29.*

496. **Thole M, Nobmann S, Huwyler J, Bartmann A, Fricker G. 2002.** Uptake of cationzied albumin coupled liposomes by cultured porcine brain microvessel endothelial cells and intact brain capillaries. *J Drug Target 10: 337-344.*

497. **Thomasz L, Oglio R, Rivandeira DT, Dagrosa MA, Jahn G, Pignataro OP, Sartorio G, Pisarev MA, Juvenal GJ. 2010.** Inhibition of goiter growth and of cyclic AMP formation in rat thyroid by 2-iodohexadecanal. *Mol Cell Endocrinol 317: 141-147.*

498. **Thompson PM, et al. 2003.** Dynamics of gray matter loss in Alzheimer's disease. *J Neurosci 23: 994-1005.*

499. **Thukkani AK, Martinson BD, Albert CJ, Vogler GA, Ford DA. 2005.** Neutrophil-mediated accumulation of 2-ClHDA during myocardial infarction: 2-ClHDA-mediated myocardial injury. *Am J Physiol Heart Circ Physiol 288: H2955-2964.*

500. **Thukkani AK, Hsu FF, Crowley JR, Wysolmerski RB, Albert CJ, Ford DA. 2002.** Reactive chlorinating species produced during neutrophil activation target tissue plasmalogens: production of the chemoattractant, 2-chlorohexadecanal. *J Biol Chem 277: 3842-3849.*

501. **Thukkani AK, McHowat J, Hsu FF, Brennan ML, Hazen SL, Ford DA. 2003a.** Identification of alpha-chloro fatty aldehydes and unsaturated lysophosphatidylcholine molecular species in human atherosclerotic lesions. *Circulation 108: 3128-3133.*

502. **Thukkani AK, Albert CJ, Wildsmith KR, Messner MC, Martinson BD, Hsu FF, Ford DA. 2003b.** Myeloperoxidase-derived reactive chlorinating species from human monocytes target plasmalogens in low density lipoprotein. *J Biol Chem 278: 36365-36372.*

503. **Tiruppathi C, Naqvi T, Wu Y, Vogel SM, Minshall RD, Malik AB. 2004.** Albumin mediates the transcytosis of myeloperoxidase by means of caveolae in endothelial cells. *Proc Natl Acad Sci U S A 101: 7699-7704.*

504. **Traweger A, Lehner C, Farkas A, Krizbai IA, Tempfer H, Klement E, Guenther B, Bauer HC, Bauer H. 2008.** Nuclear Zonula occludens-2 alters gene expression and junctional stability in epithelial and endothelial cells. *Differentiation 76: 99-106.*

505. **Tsui-Pierchala BA, Encinas M, Milbrandt J, Johnson EM, Jr. 2002.** Lipid rafts in neuronal signaling and function. *Trends Neurosci 25: 412-417.*

506. **Tsukita S, Furuse M, Itoh M. 2001.** Multifunctional strands in tight junctions. *Nat Rev Mol Cell Biol 2: 285-293.*

507. **Ubogu EE, Cossoy MB, Ransohoff RM. 2006.** The expression and function of chemokines involved in CNS inflammation. *Trends Pharmacol Sci 27: 48-55.*

508. **Usatyuk PV, Natarajan V. 2004.** Role of mitogen-activated protein kinases in 4-hydroxy-2-nonenal-induced actin remodeling and barrier function in endothelial cells. *J Biol Chem 279: 11789-11797.*

509. **Usatyuk PV, Natarajan V. 2011.** Hydroxyalkenals and oxidized phospholipids modulation of endothelial cytoskeleton, focal adhesion and adherens junction proteins in regulating endothelial barrier function. *Microvasc Res.*

510. **Usatyuk PV, Parinandi NL, Natarajan V. 2006.** Redox regulation of 4-hydroxy-2-nonenal-mediated endothelial barrier dysfunction by focal adhesion, adherens, and tight junction proteins. *J Biol Chem 281: 35554-35566.*

511. **Vafeiadou K, Vauzour D, Spencer JP. 2007.** Neuroinflammation and its modulation by flavonoids. Endocr Metab Immune Disord Drug Targets 7: 211-224.

512. **Valko M, Jomova K, Vondrakova D, Lawson M. 2010.** Metals, oxidative stress and neurodegenerative disorders. *Molecular and Cellular Biochemistry 345: 91-104.*

513. **van Dalen CJ, Winterbourn CC, Senthilmohan R, Kettle AJ. 2000.** Nitrite as a substrate and inhibitor of myeloperoxidase. Implications for nitration and hypochlorous acid production at sites of inflammation. *J Biol Chem 275: 11638-11644.*

514. **van der Veen BS, de Winther MP, Heeringa P. 2009.** Myeloperoxidase: molecular mechanisms of action and their relevance to human health and disease. *Antioxid Redox Signal 11: 2899-2937.*

515. **van Pee KH, Dong C, Flecks S, Naismith J, Patallo EP, Wage T. 2006.** Biological halogenation has moved far beyond haloperoxidases. *Adv Appl Microbiol 59: 127-157.*

516. **Verkman AS, Solomon AK. 1982.** A Stepwise Mechanism for the Permeation of Phloretin through a Lipid Bilayer. *Journal of General Physiology 80: 557-581.*

517. **Viani P, Zini I, Cervato G, Biagini G, Agnati LF, Cestaro B. 1995.** Effect of endothelin-1 induced ischemia on peroxidative damage and membrane properties in rat striatum synaptosomes. *Neurochem Res 20: 689-695.*

518. **Vissers MC, Pullar JM, Hampton MB. 1999.** Hypochlorous acid causes caspase activation and apoptosis or growth arrest in human endothelial cells. *Biochem J 344 Pt 2: 443-449.*

519. **Volterra A, Meldolesi J. 2005.** Astrocytes, from brain glue to communication elements: the revolution continues. *Nat Rev Neurosci 6: 626-640.*

520. **von Tell D, Armulik A, Betsholtz C. 2006.** Pericytes and vascular stability. *Exp Cell Res 312: 623-629.*

521. **von Wedel-Parlow M, Schrot S, Lemmen J, Treeratanapiboon L, Wegener J, Galla HJ. 2011.** Neutrophils cross the BBB primarily on transcellular pathways: an in vitro study. *Brain Res 1367: 62-76.*

522. **Voth AR, Ho PS. 2007.** The role of halogen bonding in inhibitor recognition and binding by protein kinases. *Curr Top Med Chem 7: 1336-1348.*

523. **Votyakova TV, Reynolds IJ. 2001.** DeltaPsi(m)-Dependent and -independent production of reactive oxygen species by rat brain mitochondria. *J Neurochem 79: 266-277.*

524. **Wake H, Moorhouse AJ, Jinno S, Kohsaka S, Nabekura J. 2009.** Resting microglia directly monitor the functional state of synapses in vivo and determine the fate of ischemic terminals. *J Neurosci 29: 3974-3980.*

525. **Wallner S, Schmitz G. 2011.** Plasmalogens the neglected regulatory and scavenging lipid species. *Chem Phys Lipids.*

526. **Walter L, Neumann H. 2009.** Role of microglia in neuronal degeneration and regeneration. *Semin Immunopathol 31: 513-525.*

527. **Wang ML, Huang XJ, Fang SH, Yuan YM, Zhang WP, Lu YB, Ding Q, Wei EQ. 2006.** Leukotriene D4 induces brain edema and enhances CysLT2 receptor-mediated aquaporin 4 expression. *Biochem Biophys Res Commun 350: 399-404.*

528. **Wang W, Dentler WL, Borchardt RT. 2001.** VEGF increases BMEC monolayer permeability by affecting occludin expression and tight junction assembly. *Am J Physiol Heart Circ Physiol 280: H434-440.*

529. **Weiss SJ. 1989.** Tissue destruction by neutrophils. *N Engl J Med 320: 365-376.*

530. **Weisser M, Spiteller G. 1996.** Increase of aldehydic compounds derived from plasmalogens in the brain of aged cattle. *Chem Phys Lipids 82: 173-178.*

531. **Weisser M, Vieth M, Stolte M, Riederer P, Pfeuffer R, Leblhuber F, Spiteller G. 1997.** Dramatic increase of alpha-hydroxyaldehydes derived from plasmalogens in the aged human brain. *Chem Phys Lipids 90: 135-142.*

532. **Westerlund M, Belin AC, Anvret A, Hakansson A, Nissbrandt H, Lind C, Sydow O, Olson L, Galter D. 2009.** Association of a polymorphism in the ABCB1 gene with Parkinson's disease. *Parkinsonism Relat Disord 15: 422-424.*

533. **Whiteman M, Rose P, Siau JL, Cheung NS, Tan GS, Halliwell B, Armstrong JS. 2005.** Hypochlorous acid-mediated mitochondrial dysfunction and apoptosis in human hepatoma HepG2 and human fetal liver cells: role of mitochondrial permeability transition. *Free Radic Biol Med 38: 1571-1584.*

534. **Whitton PS. 2007.** Inflammation as a causative factor in the aetiology of Parkinson's disease. *Br J Pharmacol 150: 963-976.*

535. **WHO. 2002.** Active ageing: A policy framework. Second United Nations World Assembly, Madrid, Spain http://whqlibdoc.who.int/hq/2002/WHO_NMH_NPH_02.8.pdf.

536. **Wildsmith KR, Albert CJ, Anbukumar DS, Ford DA. 2006a.** Metabolism of myeloperoxidase-derived 2-chlorohexadecanal. *J Biol Chem 281: 16849-16860.*

537. **Wildsmith KR, Albert CJ, Hsu FF, Kao JL, Ford DA. 2006b.** Myeloperoxidase-derived 2-chlorohexadecanal forms Schiff bases with primary amines of ethanolamine glycerophospholipids and lysine. *Chem Phys Lipids 139: 157-170.*

538. **Wilkinson BL, Landreth GE. 2006.** The microglial NADPH oxidase complex as a source of oxidative stress in Alzheimer's disease. *J Neuroinflammation 3: 30.*

539. **Williams RJ, Spencer JP, Rice-Evans C. 2004.** Flavonoids: antioxidants or signalling molecules? *Free Radic Biol Med 36: 838-849.*

540. **Williams WM, Rapoport SI. 1993.** Altered composition of cerebral microvessel membrane phosphoglycerides from senescent mouse. *J Neurochem 61: 1843-1849.*

541. **Winterbourn CC, van den Berg JJ, Roitman E, Kuypers FA. 1992.** Chlorohydrin formation from unsaturated fatty acids reacted with hypochlorous acid. *Arch Biochem Biophys 296: 547-555.*

542. **Winterbourn CC, Hampton MB, Livesey JH, Kettle AJ. 2006.** Modeling the reactions of superoxide and myeloperoxidase in the neutrophil phagosome: implications for microbial killing. *J Biol Chem 281: 39860-39869.*

543. **Wolburg H, Lippoldt A. 2002.** Tight junctions of the blood-brain barrier: development, composition and regulation. *Vascul Pharmacol 38: 323-337.*

544. **Wolburg H, Wolburg-Buchholz K, Engelhardt B. 2005.** Diapedesis of mononuclear cells across cerebral venules during experimental autoimmune encephalomyelitis leaves tight junctions intact. *Acta Neuropathol 109: 181-190.*

545. **Wolburg H, Noell S, Mack A, Wolburg-Buchholz K, Fallier-Becker P. 2009.** Brain endothelial cells and the glio-vascular complex. *Cell Tissue Res 335: 75-96.*

546. **Wood PL, Mankidy R, Ritchie S, Heath D, Wood JA, Flax J, Goodenowe DB. 2010.** Circulating plasmalogen levels and Alzheimer Disease Assessment Scale-Cognitive scores in Alzheimer patients. *J Psychiatry Neurosci 35: 59-62.*

547. **Wymann MP, Schneiter R. 2008.** Lipid signalling in disease. Nat Rev Mol Cell Biol 9: 162-176.

548. **Wyss-Coray T, Mucke L. 2002.** Inflammation in neurodegenerative disease--a double-edged sword. *Neuron 35: 419-432.*

549. **Yang EB, Guo YJ, Zhang K, Chen YZ, Mack P. 2001.** Inhibition of epidermal growth factor receptor tyrosine kinase by chalcone derivatives. *Biochim Biophys Acta 1550: 144-152.*

550. **Yang K, Zhao Z, Gross RW, Han X. 2007a.** Shotgun lipidomics identifies a paired rule for the presence of isomeric ether phospholipid molecular species. *PLoS One 2: e1368.*

551. **Yang Y, Estrada EY, Thompson JF, Liu W, Rosenberg GA. 2007b.** Matrix metalloproteinase-mediated disruption of tight junction proteins in cerebral vessels is reversed by synthetic matrix metalloproteinase inhibitor in focal ischemia in rat. *J Cereb Blood Flow Metab 27: 697-709.*

552. **Yap YW, Whiteman M, Cheung NS. 2007.** Chlorinative stress: an under appreciated mediator of neurodegeneration? *Cell Signal 19: 219-228.*

553. **Yap YW, Whiteman M, Bay BH, Li Y, Sheu FS, Qi RZ, Tan CH, Cheung NS. 2006.** Hypochlorous acid induces apoptosis of cultured cortical neurons through activation of calpains and rupture of lysosomes. *J Neurochem 98: 1597-1609.*

554. **Yatsushige H, Ostrowski RP, Tsubokawa T, Colohan A, Zhang JH. 2007.** Role of c-Jun N-terminal kinase in early brain injury after subarachnoid hemorrhage. *J Neurosci Res 85: 1436-1448.*

555. **Youdim KA, Qaiser MZ, Begley DJ, Rice-Evans CA, Abbott NJ. 2004.** Flavonoid permeability across an in situ model of the blood-brain barrier. *Free Radic Biol Med 36: 592-604.*

556. **Youdim KA, Dobbie MS, Kuhnle G, Proteggente AR, Abbott NJ, Rice-Evans C. 2003.** Interaction between flavonoids and the blood-brain barrier: in vitro studies. *J Neurochem 85: 180-192.*

557. **Zhang F, Shi JS, Zhou H, Wilson B, Hong JS, Gao HM. 2010a.** Resveratrol protects dopamine neurons against lipopolysaccharide-induced neurotoxicity through its anti-inflammatory actions. *Mol Pharmacol 78: 466-477.*

558. **Zhang S, Liu Y, Zhao Z, Xue Y. 2010b.** Effects of green tea polyphenols on caveolin-1 of microvessel fragments in rats with cerebral ischemia. *Neurol Res 32: 963-970.*

559. **Zhang SX. 1998.** An atlas of histology. *Springer ISBN: 0387949542.*

560. **Zhang Z, Artelt M, Burnet M, Trautmann K, Schluesener HJ. 2006.** Early infiltration of CD8+ macrophages/microglia to lesions of rat traumatic brain injury. *Neuroscience 141: 637-644.*

561. **Zhou H, Andonegui G, Wong CH, Kubes P. 2009.** Role of endothelial TLR4 for neutrophil recruitment into central nervous system microvessels in systemic inflammation. *J Immunol 183: 5244-5250.*

562. **Zhou H, Lapointe BM, Clark SR, Zbytnuik L, Kubes P. 2006.** A requirement for microglial TLR4 in leukocyte recruitment into brain in response to lipopolysaccharide. *J Immunol 177: 8103-8110.*

563. **Zhu Q, Zheng ZP, Cheng KW, Wu JJ, Zhang S, Tang YS, Sze KH, Chen J, Chen F, Wang M. 2009.** Natural polyphenols as direct trapping agents of lipid peroxidation-derived acrolein and 4-hydroxy-trans-2-nonenal. *Chem Res Toxicol 22: 1721-1727.*

564. **Zigmond MJ, Bloom FE, Landis SC, Roberts JL, Squire LR. 1999.** Fundamental Neuroscience. *Academic Press ISBN: 0127808701.*

565. **Zlokovic BV. 2008.** The blood-brain barrier in health and chronic neurodegenerative disorders. *Neuron 57: 178-201.*

566. **Zlokovic BV. 2010.** Neurodegeneration and the neurovascular unit. Nat Med 16: 1370-1371.

567. **Zlokovic BV, Apuzzo ML. 1998.** Strategies to circumvent vascular barriers of the central nervous system. *Neurosurgery 43: 877-878.*

568. **Zonta M, Angulo MC, Gobbo S, Rosengarten B, Hossmann KA, Pozzan T, Carmignoto G. 2003.** Neuron-to-astrocyte signaling is central to the dynamic control of brain microcirculation. *Nat Neurosci 6: 43-50.*